

THE UNIVERSITY OF MANITOBA

CREEP BEHAVIOUR OF FROZEN SALINE SILT UNDER
ISOTROPIC COMPRESSION

BY

EDWARD O.F. YONG

A THESIS

SUBMITTED TO THE FACULTY OF GRADUATE STUDIES
IN PARTIAL FULFILLMENT OF THE REQUIREMENT FOR THE DEGREE OF
MASTER OF SCIENCE

DEPARTMENT OF CIVIL ENGINEERING

WINNIPEG, MANITOBA

MAY 1983

CREEP BEHAVIOUR OF FROZEN SALINE SILT UNDER
ISOTROPIC COMPRESSION

BY

EDWARD O.F. YONG

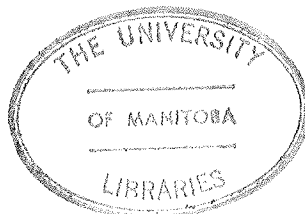
A thesis submitted to the Faculty of Graduate Studies of
the University of Manitoba in partial fulfillment of the requirements
of the degree of

MASTER OF SCIENCE

© 1983

Permission has been granted to the LIBRARY OF THE UNIVER-
SITY OF MANITOBA to lend or sell copies of this thesis, to
the NATIONAL LIBRARY OF CANADA to microfilm this
thesis and to lend or sell copies of the film, and UNIVERSITY
MICROFILMS to publish an abstract of this thesis.

The author reserves other publication rights, and neither the
thesis nor extensive extracts from it may be printed or other-
wise reproduced without the author's written permission.



ABSTRACT

The objective of this study described herein was to determine the creep behaviour of frozen soil, similar to that found in the Beaufort sea, under isotropic compression. This thesis includes the evolution, distribution and properties of the permafrost in the Beaufort Sea, and a review of existing creep constitutive equations. The validity of these constitutive equations were carefully examined.

Using the method of sample preparation and laboratory testing equipment outlined in this thesis, four three-inch diameter specimens were prepared and tested. Isotropic compression creep tests were conducted on four samples with pore-fluid salinity of about 60 ppt. Multi-step loading cell pressures of 70 and 140 kpa. were applied to soil samples at three test temperatures (-15°C , -10°C and -5°C). Two single-step loading tests using stress increments of 350 and 700 kpa. were also carried out.

From the test results, it was found that the sample underwent attenuating creep under isotropic compression. About 70 % of the total volume change occurred within the first four hours after stress application. About 50 % of the volume change was not recovered upon unloading. A history of loading and recovery had a strain hardening effect on the frozen soil. The saline frozen soil was non-ice-bonded at -5°C , but

its response to isotropic compression did not seem to be qualitatively different from the ice-bonded.

ACKNOWLEDGMENT

I am sincerely indebted to Dr.L.Domaschuk for his patience,enthusiasm, guidance and continued support in the preparation of this thesis.

I am also indebted to Dr.C-S.Man for his assistance and helpful discussion to make this thesis possible.

Special thanks to Dr.D.H.Shields for his assistance and encouragement during the early phase.

The author wishes to thank Mr.E.Lemke, Mr.N.Piamsalee, Mr.G.Tays, Mr.J.Clark and Mr.S.Meyerhoff of the technical staff of Civil Engineering Department,for their assistance during the experimental investigation.

I also wish to thank Mr.K.M.Ang for his helping in computer programming.

The author also wishes to thank Mr.B.Kjartanson and Mr.R.Kenyon, who never missed a day,shared his frustration and lifted his spirit, and for their enthusiasm in reviewing this thesis.

I also wish to thank Mr.K.V.Lew,for all the years of his support and friendships.

The author also wishes to thank all his colleagues for helping him through the difficult time and sharing with him the good time.

Financial assistance, in the form of support from NSERC grant 311-2720-19 is also acknowledged.

Lastly, the author is deeply indebted to his mother, Madam C.M.Chin, who has been a constant source of support and encouragement.

TABLE OF CONTENTS

	PAGE
ABSTRACT -----	i
ACKNOWLEDGEMENTS -----	iii
TABLE OF CONTENTS -----	v
LIST OF SYMBOLS -----	viii
LIST OF TABLES -----	xi
LIST OF FIGURES -----	xii

CHAPTER	PAGE
1 INTRODUCTION	1
1.1 GENERAL -----	1
1.2 SCOPE OF STUDY -----	2
2 BEAUFORT SEA PERMAFROST EVOLUTION	4
2.1 INTRODUCTION -----	4
2.2 SEA ICE -----	5
2.3 SEAFLOOR GEOMORPHOLOGY -----	7
2.4 SURFICIAL SEDIMENTS -----	11
2.5 SEA LEVELS -----	19
2.6 SEABOTTOM SALINITY AND TEMPERATURES ---	21
3 DISTRIBUTION OF SEABOTTOM PERMAFROST IN THE SOUTHERN BEAUFORT SEA	24
3.1 INTRODUCTION -----	24
3.2 SEISMIC INTERPRETATION OF SEABOTTOM PERMAFROST IN THE BEAUFORT SEA -----	25
3.3 OFFSHORE DRILLING IN THE BEAUFORT SEA -	32

	3.3.1 A.P.O.A. DRILLING -----	32
	3.3.2 IMPERIAL OIL LTD. DRILLING -----	32
	3.3.3 G.S.C. DRILLING IN KUGMALLIT BAY-	33
	3.3.4 G.S.C. DRILLING IN MACKENZIE	
	DELTA -----	34
	3.3.5 PRUDHOE BAY DRILLING -----	35
4	CREEP OF FROZEN SOILS	47
	4.1 INTRODUCTION -----	47
	4.2 COMPOSITION OF FROZEN SOIL -----	48
	4.3 CLASSIFICATION OF FROZEN SOILS -----	49
	4.4 DEFORMATION BEHAVIOUR OF FROZEN SOILS	
	UNDER CONSTANT LOAD -----	52
	4.5 THE CONSTITUTIVE EQUATIONS OF FROZEN	
	SOILS -----	57
5	TESTING PROGRAM	68
	5.1 INTRODUCTION -----	68
	5.2 SAMPLE PREPARATION -----	71
	5.2.1 METHOD OF SAMPLE PREPARATION ----	71
	5.3 TESTING EQUIPMENT -----	79
	5.4 SAMPLE TRIMMING AND BUILDING-IN	
	PROCEDURES -----	83
	5.5 TESTING PROCEDURE -----	86
	5.6 TEST RESULTS -----	90
	5.6.1 EFFECT OF STRESS REPETITION -----	91
	5.6.2 EFFECT OF TEMPERATURE -----	92
	5.6.3 EFFECT OF STRESS INCREMENT -----	93
	5.6.4 CREEP ANALYSIS -----	93

5.6.5 BULK MODULUS ANALYSIS -----	96
6 CONCLUSIONS AND SUGGESTIONS FOR FURTHER RESEARCH	112
6.1 CONCLUSIONS -----	112
6.2 RECOMMENDATION FOR FURTHER RESEARCH ---	114
BIBLIOGRAPHY -----	116
APPENDIX I ISOTROPIC COMPRESSION TEST RESULTS ---	123
APPENDIX II CALIBRATION OF VOLUME CHANGE MEASUREMENTS DEVICE -----	136
APPENDIX III TRIAXIAL CELL AND VOLUME CHANGE MEASUREMENT DEVICE -----	160
APPENDIX IV PLEXIGLASS SPLIT MOULD -----	177
APPENDIX V PROGRAMME LISTING FOR HYPERBOLIC REGRESSION ANALYSIS -----	185
APPENDIX VI PROGRAMME LISTING FOR LINEAR REGRESSION ANALYSIS -----	201

LIST OF SYMBOLS

- α = material constant
- C_{∞} = temperature dependent adhesion at $t=\infty$
- ϕ_{∞} = internal friction angle at $t=\infty$
- ϕ = internal friction angle
- $\theta_c = 1^{\circ} C$
- ϵ = total strain
- ϵ_0 = instantaneous strain
- ϵ_1 = primary creep strain
- ϵ_2 = secondary creep strain
- ϵ_3 = tertiary creep strain
- ϵ_v = volumetric strain
- ϵ_v^{∞} = ultimate volumetric strain
- ϵ_v^i = incremental volumetric strain
- $\dot{\epsilon}$ = strain rate
- $\dot{\epsilon}_v$ = volumetric strain rate
- $\dot{\epsilon}_i$ = initial creep rate
- $\dot{\epsilon}_c$ = arbitrary strain rate
- $\dot{\epsilon}_{ij}^{(c)}$ = creep rate tensor = time rate of infinitesimal strain tensor
- $\dot{\epsilon}_e$ = equivalent strain rate tensor
- δ_{ij} = kroneckor delta
- $\delta = \arctan (a_1 / z)$
- σ_{ij} = stress tensor
- σ_e = equivalent stress tensor
- σ_c = temperature dependent uniaxial creep parameter

σ_m = mean normal stress
 $\sigma_1 - \sigma_3$ = principal stress difference
 S_{ij} = deviatoric stress tensor
 J_2^S = second deviatoric stress invariant
 J_3^S = third deviatoric stress invariant
 \dot{J}_2^E = second deviatoric strain-rate invariant
 \dot{J}_3^E = third deviatoric strain-rate invariant
A = temperature dependent deformation modulus
B = temperature experimental parameter
 E_k = triaxial modulus
 $K(t)$ = time dependent bulk modulus
 K_∞ = ultimate secant bulk modulus
K = bulk modulus
J = temperature dependent experimental parameter
M = experimental parameter
N = experimental parameter
R = universal gas constant
S = material constant
T = absolute temperature
U = activation energy
 $V(0)$ = original volume of the sample
 $V(0^-)$ = volume of sample just before the increment of
stress
 $V(t)$ = volume of sample at time t
 V_∞ = volume at the end of each stress increment
W = temperature exponent
a = initial tangent

a_1 = radius of circular area

b = reciprocal of the ultimate value of

m = experimental creep exponent

n = creep exponent

p = uniform circular distributed load

r = ratio between uniaxial compression and tension
creep strength

t = elapsed time

w_z = displacement in z-direction

z = depth

LIST OF TABLES

TABLE	PAGE
4.1 FROZEN SOIL CLASSIFICATION SYSTEM -----	50
4.2 CLASSIFICATION OF FROZEN SOILS (U.S.S.R) ---	51
5.1 SAMPLE DETAILS -----	89
5.2 DETAILS OF VOLUME CHANGE AND RECOVERY -----	88
5.3 HYPERBOLIC FUNCTION PARAMETERS -----	99
5.4 VALUES OF LONG-TERM BULK MODULUS -----	100

LIST OF FIGURES

FIGURE	PAGE
2.3.1 SEABOTTOM BATHYMETRY IN THE BEAUFORT SEA --	9
2.3.2 BOTTOM SCOURING BY ICE PROJECTIONS ON THE CONTINENTAL SHELF -----	10
2.4.1 THE DISTRIBUTION OF MAIN SEDIMENT TYPES ON THE BEAUFORT SHELF -----	14
2.4.2 THE DISTRIBUTION OF GRAVEL -----	15
2.4.3 THE DISTRIBUTION OF SAND -----	16
2.4.4 THE DISTRIBUTION OF SILT -----	17
2.4.5 THE DISTRIBUTION OF CLAY -----	18
2.5.1 SEA LEVEL HISTORY OF THE BEAUFORT SHELF ---	20
2.6.1 SUMMER AND WINTER SEABOTTOM WATER TEMPERATURES IN THE SOUTHERN BEAUFORT SEA -	22
2.6.2 SUMMER AND WINTER SEABOTTOM WATER SALINITIES IN THE SOUTHERN BEAUFORT SEA -----	23
3.2.1 AN INTERPRETATION OF THE OCCURRENCE OF SUB- SEABOTTOM ICE-BONDED PERMAFROST FROM INDUSTRY SEISMIC RECORDS -----	28
3.2.2 DISTRIBUTION AND DEPTH TO THE TOP OF THE LOWER THIN DISCONTINUOUS HIGH-VELOCITY LAYER -----	29
3.2.3 DISTRIBUTION AND DEPTH TO THE TOP OF THE LOWER THICK CONTINUOUS HIGH-VELOCITY LAYER -	30
3.2.4 DISTRIBUTION OF ANOMALOUS VELOCITY WHICH ARE HIGHER THAN EXPECTED FOR UNCONSOLIDATED SATURATED SEDIMENTS -----	31

3.3.1	LOCATION OF A.P.O.A. SHALLOW DRILLHOLES	----	36
3.3.2	A COMPILATION OF DRILLING RESULTS FROM A.P.O.A. REPORT #3 FOR THE HOLES ENCOUNTERING PERMAFROST	-----	37
3.3.3	GENERALIZED GEOLOGY AND CRYSTAL CABLE VELOCITY LOG FROM I.O.E. HOOPER NAKTAK	-----	38
3.3.4	GENERALIZED GEOLOGY AND CRYSTAL CABLE VELOCITY LOG FROM I.O.E. IMMERK B-48	-----	39
3.3.5	LOCATION OF THE TWO PROPOSED DRILLING SITES-		40
3.3.6	GENERALIZED GEOLOGICAL LOG FROM TINGMIARK DRILL SITE	-----	41
3.3.7	LOCATION OF G.S.C. DRILLHOLES IN KUGMALLIT BAY	-----	42
3.3.8	LITHOLOGICAL DESCRIPTION OF G.S.C. KUGMALLIT BAY DRILLHOLES	-----	43
3.3.9	LOCATION OF G.S.C. DRILLHOLES IN MACKENZIE DELTA	-----	44
3.3.10	DESCRIPTION OF MACKENZIE DELTA DRILLHOLES	--	45
3.3.11	LOCATION OF DRILLHOLES AND SEISMIC INTERPRETATION IN THE SOUTHERN BEAUFORT SEA-		46
4.4.1	TYPICAL CREEP CURVE OF FROZEN SOILS UNDER CONSTANT STRESS	-----	52
4.4.2	GROUP OF CREEP CURVES FOR VARIOUS CONSTANT LOAD	-----	55
4.4.3	CONTINUOUS STRENGTH CURVE	-----	56
4.5.1	EFFECT OF CONFINING PRESSURE ON CREEP STRAIN	-----	62

4.5.2	MOHR CIRCLE FAILURE ENVELOPE AT EACH GIVEN TIME TO FAILURE -----	62
5.2.1	GRAIN SIZE DISTRIBUTION CURVE -----	75
5.2.2	PLEXIGLASS SPLIT MOULD -----	76
5.2.3	SAMPLE SATURATION SYSTEM -----	77
5.2.4	FREEZING OF SPECIMEN -----	78
5.3.1	TRIAxIAL APPARATUS ASSEMBLY -----	81
5.6.1	THE VOLUMETRIC STRAIN-TIME GRAPHS OF THE MULTI-STEP TESTS ON SAMPLE A02 -----	101
5.6.2	THE VOLUMETRIC STRAIN-TIME GRAPHS OF THE SINGLE-STEP LOADING TESTS -----	102
5.6.3	THE VOLUMETRIC STRAIN-TIME GRAPHS OF THE MULTI-STEP TEST ON SAMPLE A06 -----	103
5.6.4	THE INCREMENTAL VOLUMETRIC STRAIN-TIME GRAPHS OF THE FIRST-STEP OF MULTI-STEP LOADING TESTS ON SAMPLE A02 -----	104
5.6.5	THE INCREMENTAL VOLUMETRIC STRAIN-TIME GRAPHS OF THE NTH-STEP OF THE MULTI-STEP LOADING TESTS ON SAMPLE A02 -----	105
5.6.6	HYPERBOLIC CURVE FITTING OF SINGLE-STEP LOADING TEST DATA ON SAMPLE A07 AND A08 -----	106
5.6.7	THE CREEP RATE-TIME GRAPHS OF SINGLE-STEP LOADING TESTS ON SAMPLE A07 AND A08 -----	107
5.6.8	THE CREEP RATE-TIME GRAPHS OF FIRST-STEP OF MULTI-STEP LOADING TESTS ON SAMPLE A02 AND A06 -----	108
5.6.9	THE LONG-TERM BULK MODULUS VS.TIME AT -15°C-	109

5.6.10	THE ULTIMATE VOLUMETRIC STRAIN VS.ISOTROPIC STRESS FOR THE MULTI-STEP TESTS -----	110
5.6.11	ULTIMATE SECANT BULK MODULUS VS.ISOTROPIC STRESS AT -15 °C -----	111
I.1	THE INCREMENTAL VOLUMETRIC STRAIN VERSUS TIME FOR THE 1ST,2ND AND 3RD STRESS INCREMENTS ON SAMPLE A0215 -----	124
I.2	THE INCREMENTAL VOLUMETRIC STRAIN VERSUS TIME FOR THE 4TH,5TH AND 6TH STRESS INCREMENTS ON SAMPLE A0215 -----	125
I.3	THE INCREMENTAL VOLUMETRIC STRAIN VERSUS TIME FOR THE 7TH,8TH AND 9TH STRESS INCREMENTS ON SAMPLE A0215 -----	126
I.4	THE INCREMENTAL VOLUMETRIC STRAIN VERSUS TIME FOR THE 2ND AND 4TH STRESS INCREMENTS ON SAMPLE A0210 -----	127
I.5	THE INCREMENTAL VOLUMETRIC STRAIN VERSUS TIME FOR THE 5TH,6TH AND 7TH STRESS INCREMENTS ON SAMPLE A0210 -----	128
I.6	THE INCREMENTAL VOLUMETRIC STRAIN VERSUS TIME FOR THE 8TH,9TH AND 10TH STRESS INCREMENTS ON SAMPLE A0210 -----	129
I.7	THE INCREMENTAL VOLUMETRIC STRAIN VERSUS TIME FOR THE 3RD,4TH,5TH AND 6TH STRESS INCREMENTS ON SAMPLE A0205 -----	130
I.8	THE INCREMENTAL VOLUMETRIC STRAIN VERSUS TIME FOR THE 9TH AND 7TH STRESS	

	INCREMENTS ON SAMPLE A0205 -----	131
I.9	THE INCREMENTAL VOLUMETRIC STRAIN VERSUS TIME FOR THE 8TH AND 10TH STRESS INCREMENTS ON SAMPLE A0205 -----	132
I.10	THE INCREMENTAL VOLUMETRIC STRAIN VERSUS TIME FOR THE 1ST AND 2ND STRESS INCREMENTS ON SAMPLE A0615 -----	133
I.11	THE INCREMENTAL VOLUMETRIC STRAIN VERSUS TIME FOR THE 3RD STRESS INCREMENTS ON SAMPLE A0615 -----	134
I.12	THE INCREMENTAL VOLUMETRIC STRAIN VERSUS TIME FOR THE 4TH AND 5TH STRESS INCREMENTS ON SAMPLE A0615 -----	135

CHAPTER 1

INTRODUCTION

1.1 GENERAL

In the last decade, the Beaufort Sea has become of great interest to the petroleum companies and the Canadian government, because of the large deposits of oil and natural gases discovered beneath the seabottom. During this decade offshore artificial islands were built in shallow water, not deeper than 30m., to facilitate exploration on the Beaufort Sea continental shelf. These artificial islands, for oil discovery and production purposes, rest on either ice-bonded or non-ice-bonded permafrost in the Beaufort Sea.

Frozen soil in thermal equilibrium provides an excellent foundation. However, if the permafrost is in thermal non-equilibrium or thawing condition, there will be a reduction in bearing strength, especially in ice-rich permafrost. Moreover, the ice-rich permafrost does creep even if they are held at a fixed temperature, and it creep even more when subjected to stress. This may cause large settlements and instability of the structures. Creep behaviour of frozen soils is important in designing structures on the permafrost. The amount of creep which occurs in permafrost during the service life of the structures depends on the state of stress, the properties of the permafrost and the thermal conditions.

In the Beaufort Sea, the offshore permafrost temperatures range from 0 °C to -5°C. The pore-fluid salinities of offshore permafrost are relatively higher than the onshore permafrost, and vary with soil conditions. The artificial islands constructed on the permafrost may or may not perform satisfactorily as the strength and deformation of the permafrost respond to the changes in time and thermal domain.

The geotechnical group at the University of Manitoba is currently engaged in a research program to study the long-term multiaxial creep behaviour of relatively warm saline frozen soils which simulate those beneath the Beaufort Sea. The present study is only a part of this broader investigation.

1.2 SCOPE OF STUDY

Isotropic compression tests were conducted on prepared frozen saline sandy silt. Most of the samples were tested at a relative low temperature (-15°C) and higher salinities (60 ppt) than the permafrost present in the Beaufort seabottom. The data generated from these tests is to be used for viscoelastic modelling and for pseudo-elastic modelling in Domaschuk's method of estimating settlement of artificial islands.

A brief review of the conditions of Beaufort Sea permafrost evolution and the Beaufort Sea permafrost distribution are presented in chapter 2 and chapter 3.

Chapter 4 presents a brief review of deformation behaviour of frozen soils and the existing constitutive relationships for creep in frozen soils. This is followed by examining the validity of the hypothesis commonly used on multiaxial creep of frozen soils.

Chapter 5 presents the testing program which includes the sample preparation, testing equipment and the test results of the isotropic compression tests. Conclusions of the study and future research recommendation are presented in chapter 6.

CHAPTER 2

BEAUFORT SEA PERMAFROST EVOLUTION

2.1 INTRODUCTION

Permafrost is known to occur onshore and offshore. The aggradation of permafrost occurs typically by freezing downward from the ground surface under cold surface conditions. The permafrost now located under the seabottom (For example Arctic ocean, Beaufort Sea) is the result of ocean transgression (Mackay, 1972; Hunter et al, 1976).

Extensive permafrost has been encountered offshore in the Beaufort Sea, and its existence has been confirmed by numerous investigators (Mackay, 1972; Judge, 1974; Hunter et al, 1976; Osterkamp et al, 1976, 1982; Morack et al, 1982; Macaulay et al, 1982). Much of the offshore permafrost in the Beaufort Sea is relict in nature. Investigations to date indicate the permafrost present in the Beaufort seabed is either degrading or aggrading, due to the presence of positive or negative seabottom temperatures.

The thickness of inland permafrost is controlled by the thermal properties of the soil, ground surface temperatures, vegetation cover, albedo, geothermal heat flow and the time of exposure to the cold surface conditions (Brown, 1973). To determine the evolution and thickness of offshore permafrost more complexities must be taken into ac-

count, such as the variation of soil conditions, sea water temperature, sea water salinity, geomorphology, the fluctuation of ocean water level and ice conditions.

The following sections outline the above complexities which influence the evolution of the subsea permafrost in the Beaufort Sea (Mackay, 1972; Judge, 1974; Markham, 1976; Hunter et al, 1976; Milne et al, 1977; Pelletier, 1979).

2.2 SEA ICE

The ice conditions are a major factor in determining the aggradation and degradation of existing offshore permafrost in the Beaufort Sea. Permafrost is sometimes encountered at shallow depths below the seabottom in the Beaufort Sea shelf, where the ice-cover extends to the sea bed during the winter. The permafrost table degrades sharply where there is a relatively warm, saline thick layer of unfrozen sea water between the ice cover and the sea bed. Extensive ice studies have been carried out in the southern Beaufort Sea by several researchers (Mackay, 1972; Markham, 1976; Milne et al, 1977; pelletier, 1979).

The ice existing in the southern continental margin of the Beaufort Sea during the winter may be divided into three zones:

1. The offshore polar pack.

This ice is mainly old ice, continuous and is usually three to four metres thick. Its near shore

boundary usually lays over the 500 m. isobath near the edge of the continental shelf.

2. The shore-fast ice.

This ice lays along the coast, and it generally extends seaward to the 25m. isobath. It has an average thickness of two metres.

3. The multi-year ice

This ice lays between the zones of the polar pack and the shore-fast ice. It covers approximately seven-eighths of the sea surface and has a thickness of one to two metres.

The multi-year ice is highly irregular, heavily ridged, highly unstable and during winter may even develop leads (Anonymous, 1970; Markham, 1976; Milne et al, 1977; Pelletier, 1979).

In the summer, ice conditions in the southern Beaufort Sea vary from year to year. The beginning of break-up could be as early as March in a "light-ice" year. The ice break-up along the coast becomes significant in mid-July. During the melting period in August, the coastal shore-fast ice gradually moves seaward with the polar pack and retreats 180 km. off the Canadian coast. The retreat of the polar pack also depends on the direction of the winds. A strong northwesterly wind would drive the polar pack shoreward. Freeze-up in the Beaufort sea usually occurs in the second week of October, but it may vary from late September to early November, depending on the boundary of the polar pack ice.

The seabottom temperature is directly related to the ice conditions in the Beaufort Sea. The boundary of warmer seabottom temperature (above 0 C) depends on the boundary of the retreat of the polar pack ice. The seabottom permafrost degradation or aggradation depends on the period of positive or negative temperature present on the seabottom. For example, an early break up of ice and a late freeze up in the Beaufort Sea, means a longer period of positive temperature may exist at the seabottom, which may cause degradation of seabottom permafrost. The winter and summer seabottom temperature will be given in a later section.

2.3 SEAFLOOR GEOMORPHOLOGY

The bathymetry of the continental shelf and slope of southeastern Beaufort Sea has been studied extensively by the Geological Survey of Canada and other researchers (Shearer et al, 1971; Pelletier and Shearer, 1972). As mentioned by these researchers, three distinct physiographic features are present on the floor of the Beaufort Sea (Figure 2.3.1 from Canadian hydrographic charts). These features, as described by Hunter et al (1976), Pelletier et al (1979), are as follows:

1. Continental shelf.

A wide gentle slope which extends approximately 100 km. off the Yukon coast to a depth of 100 m..

2. Continental slope.

A steeply falling slope extends from the 100 m. isobath towards the Canada basin to a depth of 2000 m.. The Canada basin is approximately 500 km. offshore.

3. Mackenzie Canyon.

This V-shape canyon transects the steeply falling slope of the Canada basin and continental shelf slope. The headward portion of this canyon, lays immediately adjacent to the Mackenzie Bay, to the 500 m. isobath is approximately 120 km..

Other geomorphological features present on the seafloor of the Beaufort Sea are submarine pingos (Shearer et al, 1971) and grooves (Pelletier and Shearer, 1972). The submarine pingos occur primarily on the outer shelf, east of the Mackenzie canyon in water depths of about 11 m. Some of these ice-cored, conical pingos are 300 m. in diameter at the base and 20 m. to 50 m. in height. This type of pingo commonly has been breached by expansion within the pingo. Pingos found in the inshore area were thought to be formed on land and may have been eroded and submerged recently by the rising sea level. The submarine pingo swarms are related to the distribution of seabottom permafrost. As pointed out by Hunter et al, (1976), the discontinuous ice-bonded permafrost is associated with the submarine pingos.

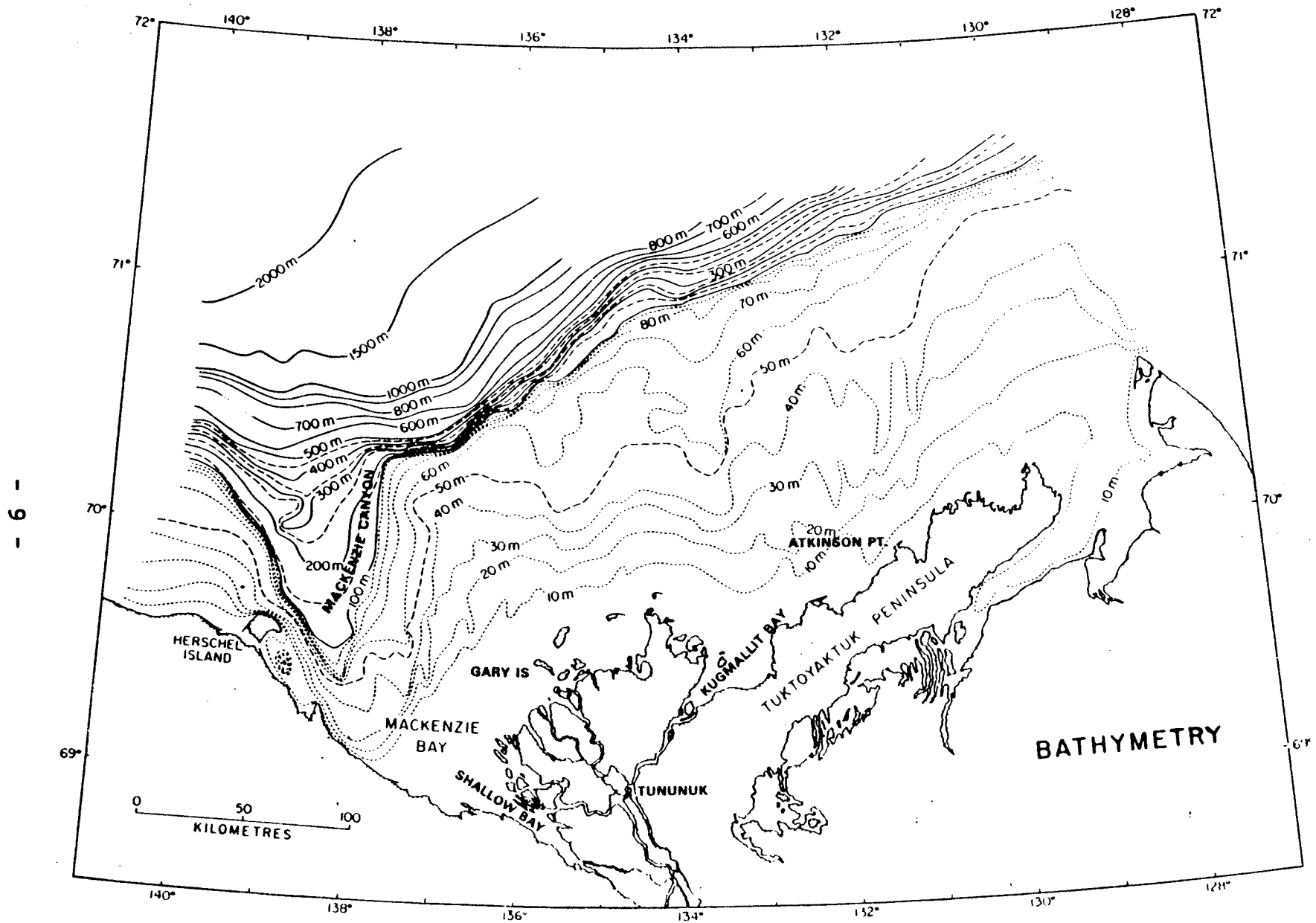


Fig. 2.3.1 Seabottom bathymetry in the Beaufort Sea
(after Pelletier, 1975) .

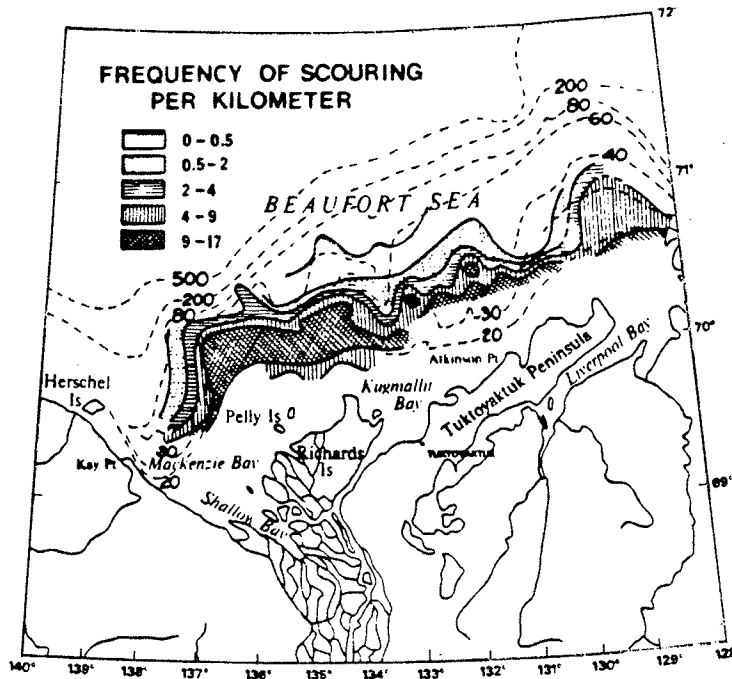


Fig. 2.3.2 Bottom scouring by ice projections on the continental shelf. Shaded areas depict the number of scours per km. measure perpendicular to the depth contours. Depths are in meters. (after Milne et al, 1976).

Grooves are present over a large area on the seafloor. These features were probably produced by ice scouring and occur at depths between 10 and 50 m.. They are generally linear features and have steeply dipping walls. These grooves are approximately 0.5 m. to 10 m. deep and oriented southeasterly. The grooves are more frequent and not as deep at shallow depths. Grooves discovered at depths of about 50 m.were thought to be relict (Lewis,1975). These grooves may have some relations to the degradation of permafrost in the inshore area. Figure 2.3.2 shows the bottom scouring by sub-sea ice projections on the continental shelf.

2.4 SURFICIAL SEDIMENTS

The late to early Holocene sediments in the continental shelf of the Beaufort sea consist mainly of clay and silt,with some gravel and sand. Pelletier (1979) reported on the distribution of all classes of sediments as shown in Figure 2.4.1. The sand and gravel occur on the Beaufort Sea shelf west of Herschel Island,along the coast and in the Mackenzie Delta. They are also found in the isolated area across the eastern portion of the shelf. Silt occurs in a zone which varies in width from 50 km. to 100 km.and extends across the eastern portion of the shelf. It also occurs in the inshore region beyond the sands and extends to 10 m isobath. Clay and silt cover the remainder of the shelf and eastern portion of Beaufort Sea.

Pelletier et al (1979) summarized all available data on the classes of sediments as follows:

1. Gravel distribution (Figure 2.4.2) .

The greatest concentration of gravel generally occurs in the area northwest of Herschel Island and isolated areas in the extreme eastern end of the shelf (Rodeick,1974; Lewis et al,1975; Pelletier et al, 1979).

2. Sand distribution (Figure 2.4.3) .

Sand is more widespread than gravel,with major deposits occurring in the area west of Herschel island. Other deposits lay along the coastal zones and eastern portion of the shelf. In the central part of the shelf and the Mackenzie Canyon,sand deposits comprise less than 1 % of the seabottom sediments. Over the area of inlets and bays the sands are mainly covered by mud (Lewis et al,1974, 1976; Pelletier et al,1979).

3. Silt distribution (Figure 2.4.4) .

Silt is predominant in the Mackenzie Bay and the coastal areas. Other concentrations are in eastern part of the shelf. In the remaining area silt constitutes less than 40 % of the bottom sediments (Lewis et al,1974,1975; Pelletier et al,1979).

4. Clay distribution (Figure 2.4.5) .

Clay is present over the entire shelf, but its greatest concentration is in the Mackenzie Canyon and the central part of the shelf, east of the Mackenzie Canyon. Its occurrence generally decreases in a shoreward direction (Pelletier et al, 1979). Clay mineral composition of the clay size fraction (less than 2 microns) of the Beaufort Sea shelf sediments consist of Illite, and minor amounts of Smectite, Kaolinite and Chlorite (Naidu et al, 1974) .

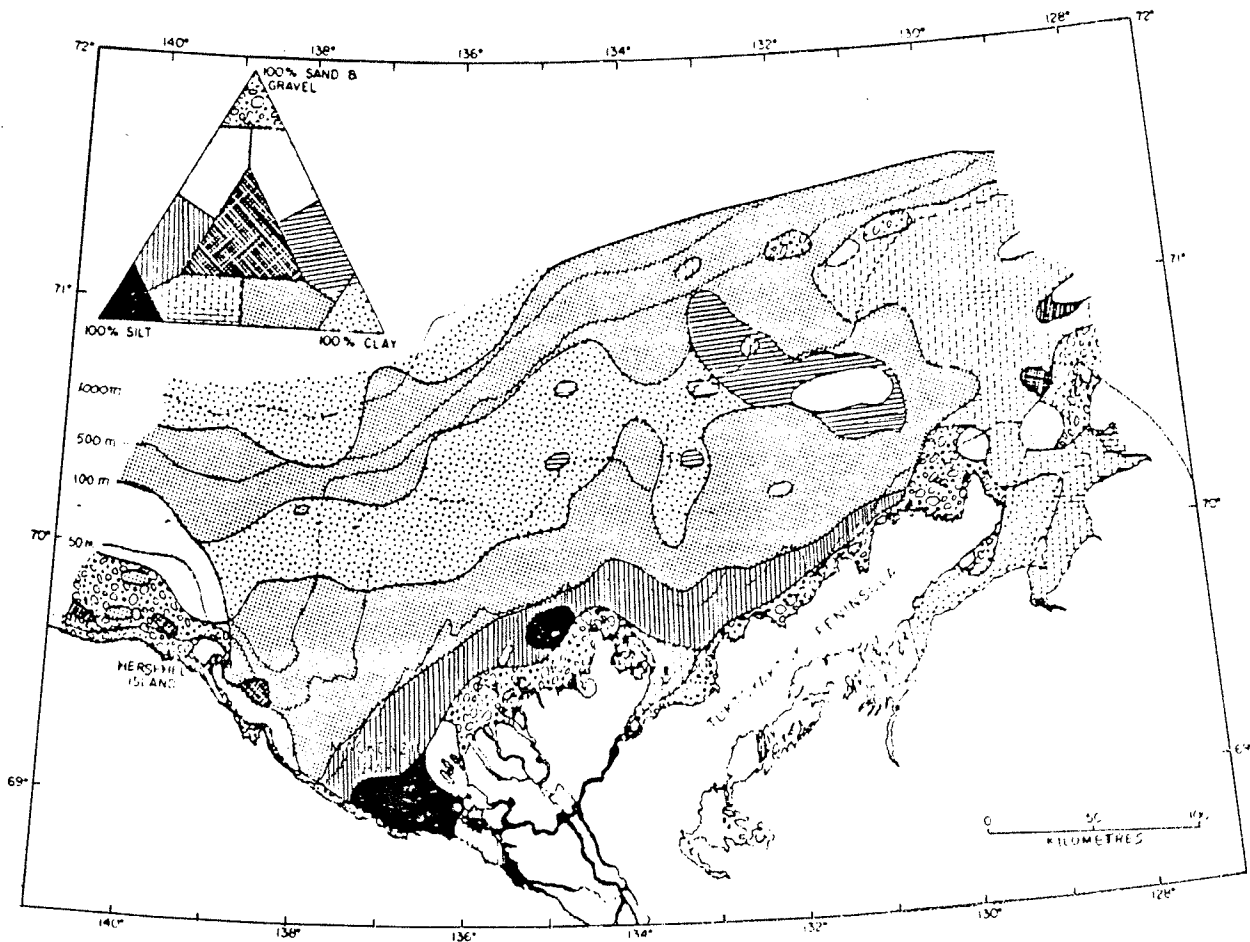


Fig.2.4.1 The distribution of main sediment types on the Beaufort shelf. The ternary textural diagram of main sediment types is after shepard,1954. (after Pelletier,1979).

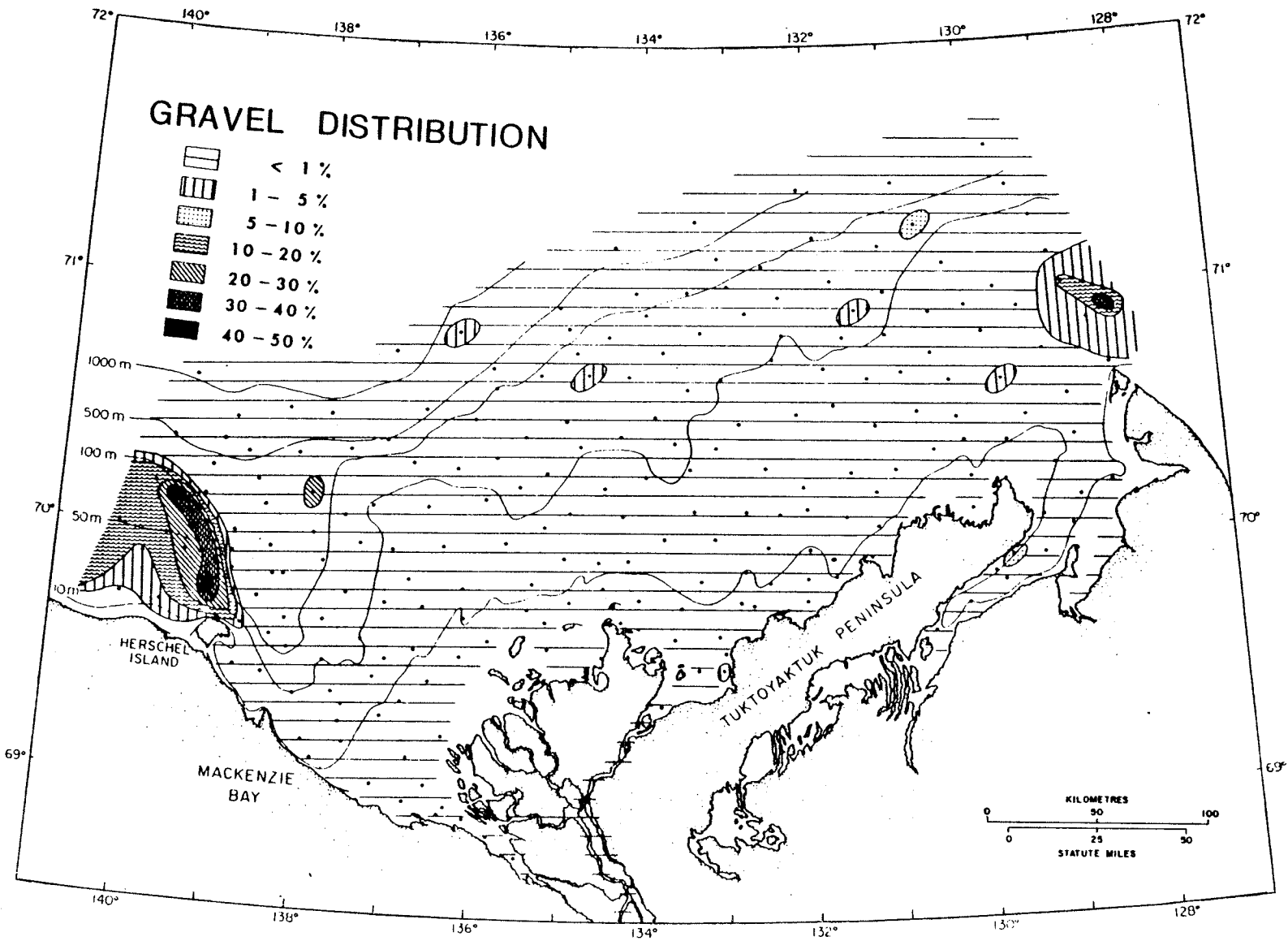


Fig.2.4.2 The distribution of gravel.
(after Pelletier, 1979).

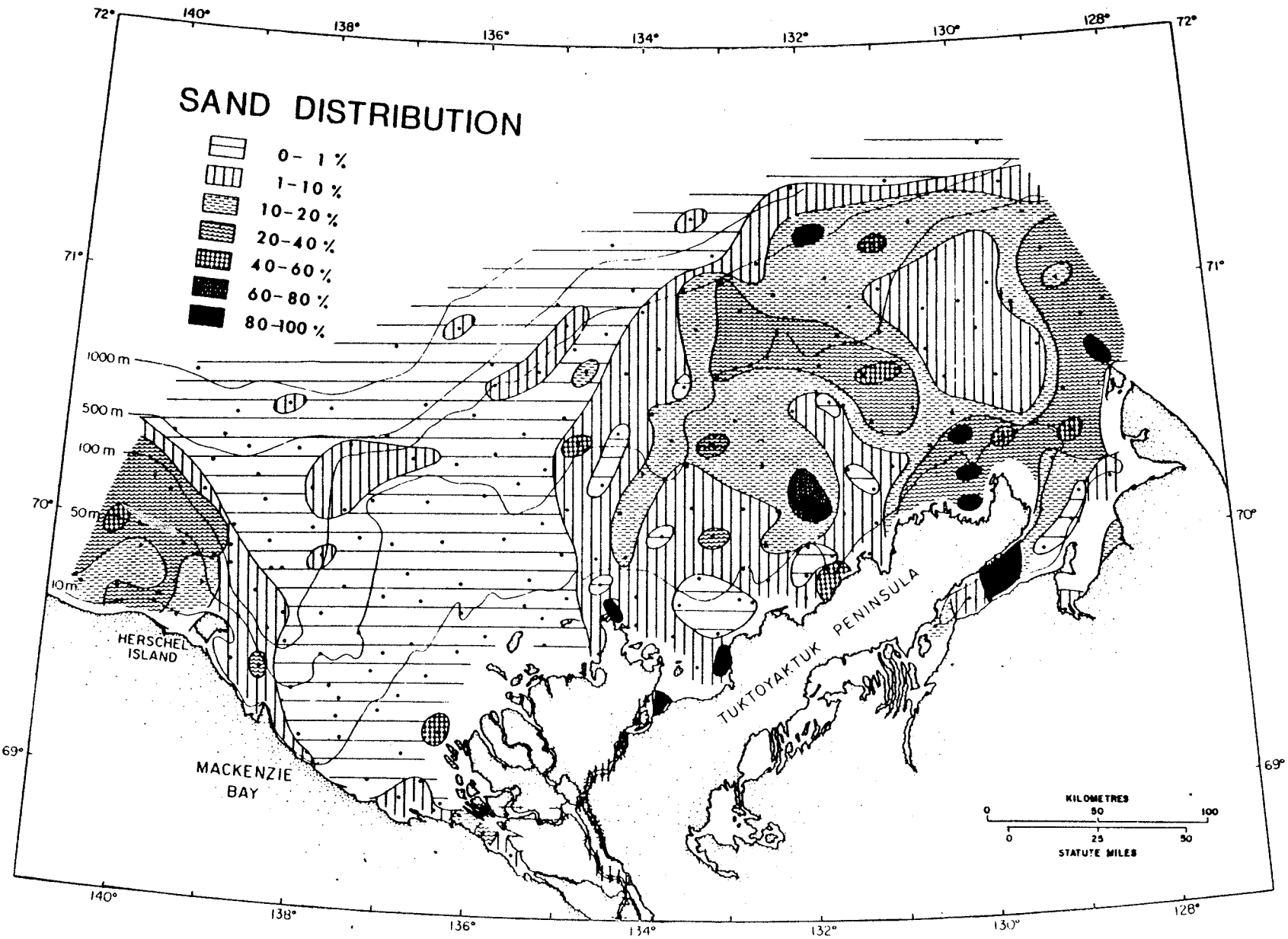


Fig.2.4.3 The distribution of sand.
(after Pelletier,1979).

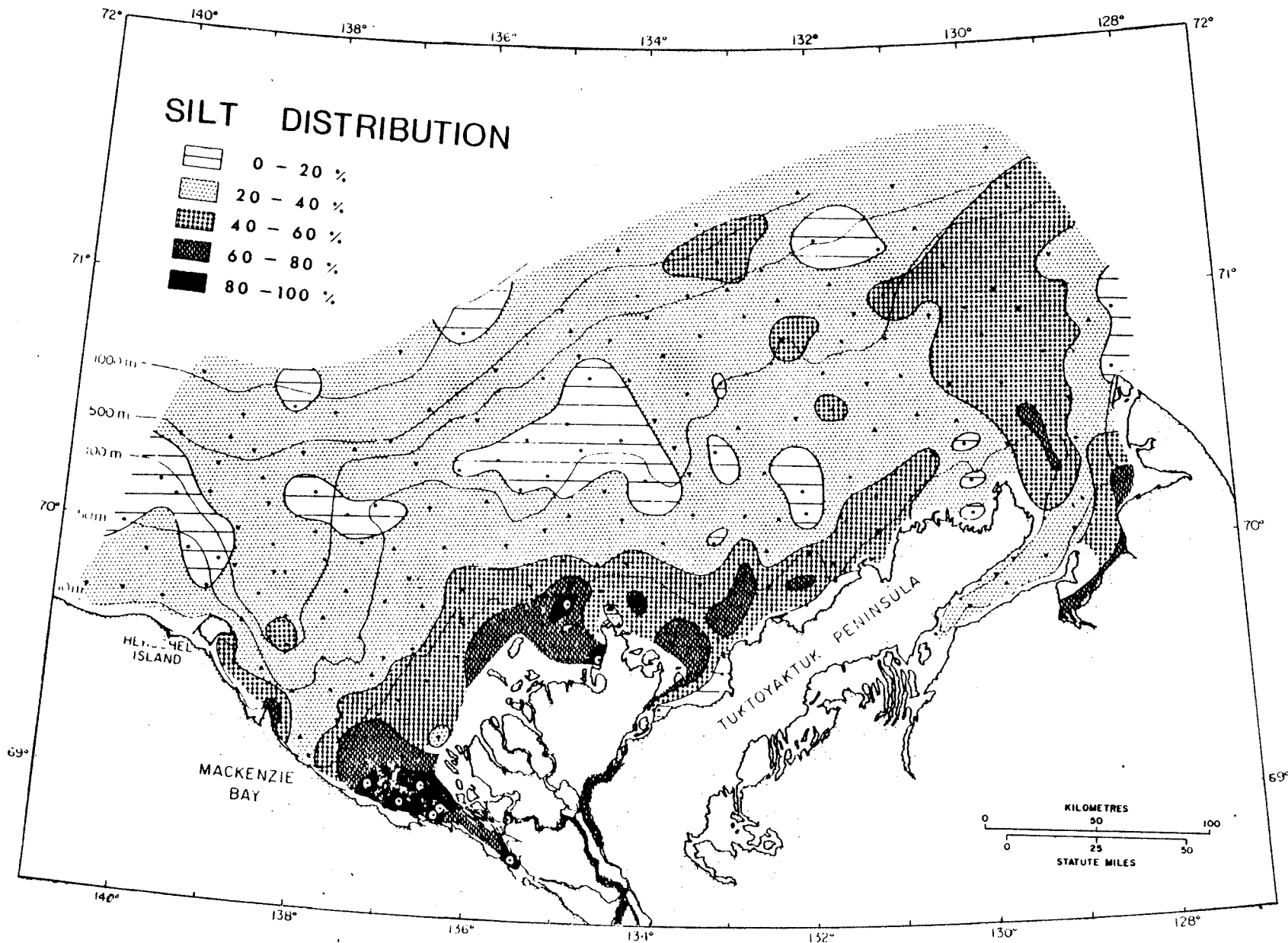


Fig.2.4.4 The distribution of silt (after Pelletier, 1979).

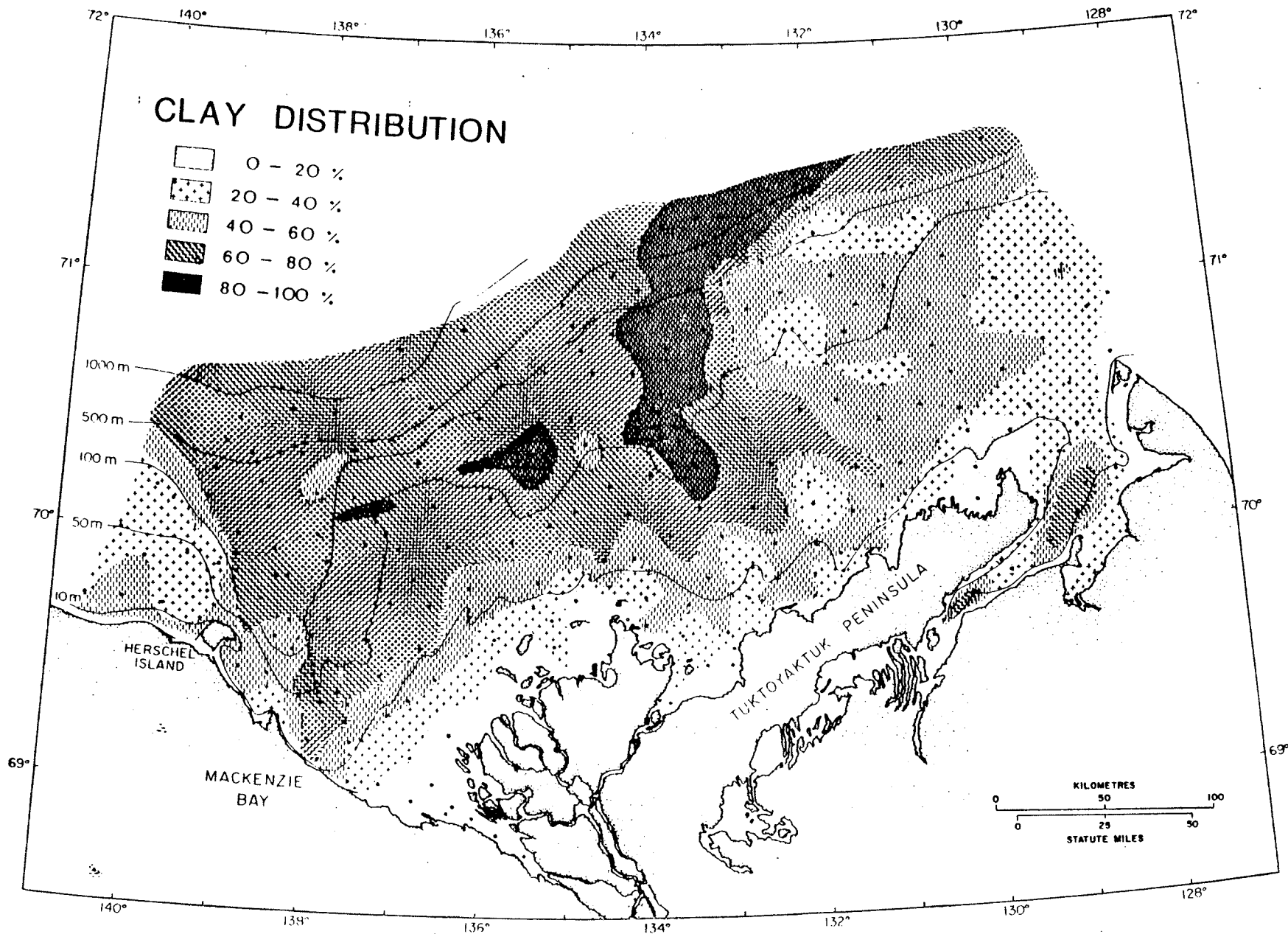


Fig.2.4.5 The distribution of clay
(after Pelletier, 1979).

2.5 SEA LEVELS

The sea-level of the Beaufort Sea has changed dramatically in the past. Muller-Beck (1966) and Milliman and Emery (1968) reported that the mean sea-level in the Beaufort Sea, between 17000 and 7000 B.P., rose by approximately 130 m due to the melting of the Wisconsin continental glaciers. In highly glaciated areas the sea-level was strongly influenced by isotatic rebound. In such areas the sea level came up during early Holocene and dropped down in late Holocene (Figure 2.5.1) (Hunter et al, 1976; Pelletier et al, 1979).

Change in sea-level results in period of emergence and submergence of the Beaufort Sea shelf. About 17000 years ago, the Beaufort Sea and the Mackenzie Delta area were exposed to sub-zero temperature and permafrost aggradation occurred. Since then the sea-level has been rising, and 3000 to 4000 years ago, the permafrost was submerged under relatively warm, sea water rather than being exposed to the cold air temperature conditions (Mackay et al, 1972).

- 20 -

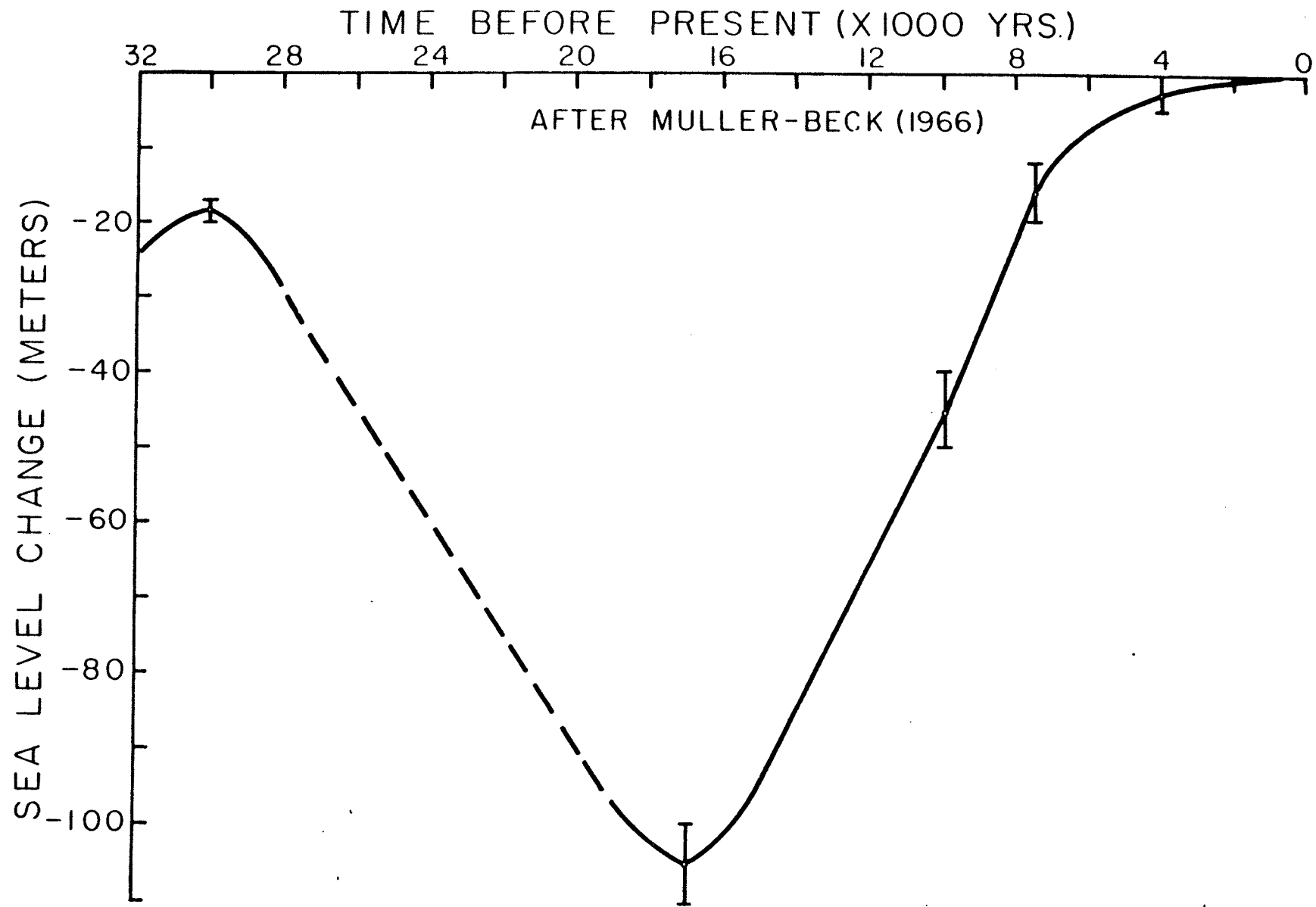


Fig.2.5.1 Sea level history of the Beaufort Sea shelf (after Mackay,1972).

2.6 SEABOTTOM SALINITY AND TEMPERATURE

The seabottom water temperature and salinity of the Beaufort Sea have been studied extensively. Vilks (1973) and Vilks et al (1979) have gathered all the available information on the offshore water mass structure. They reported on summer and winter relationships between temperature and depths, as well as between salinity and depths, over the Continental shelf and slope. The mean annual seabottom 0°C isotherm lays between the shoreline and a water depth of 20 m. . The winter and summer 0°C isotherm lie along the edge of the Beaufort Sea shelf (Figure 2.6.1) . The distribution of winter and summer salinities are shown in Figure 2.6.2 (Vilks, 1972; Hunter et al, 1976; Vilks, 1979) . The average salinity in the shelf area is typically about 30 ppt, but the salinity of the unfrozen sea water is higher in the winter due to salt rejection when the ice is formed.

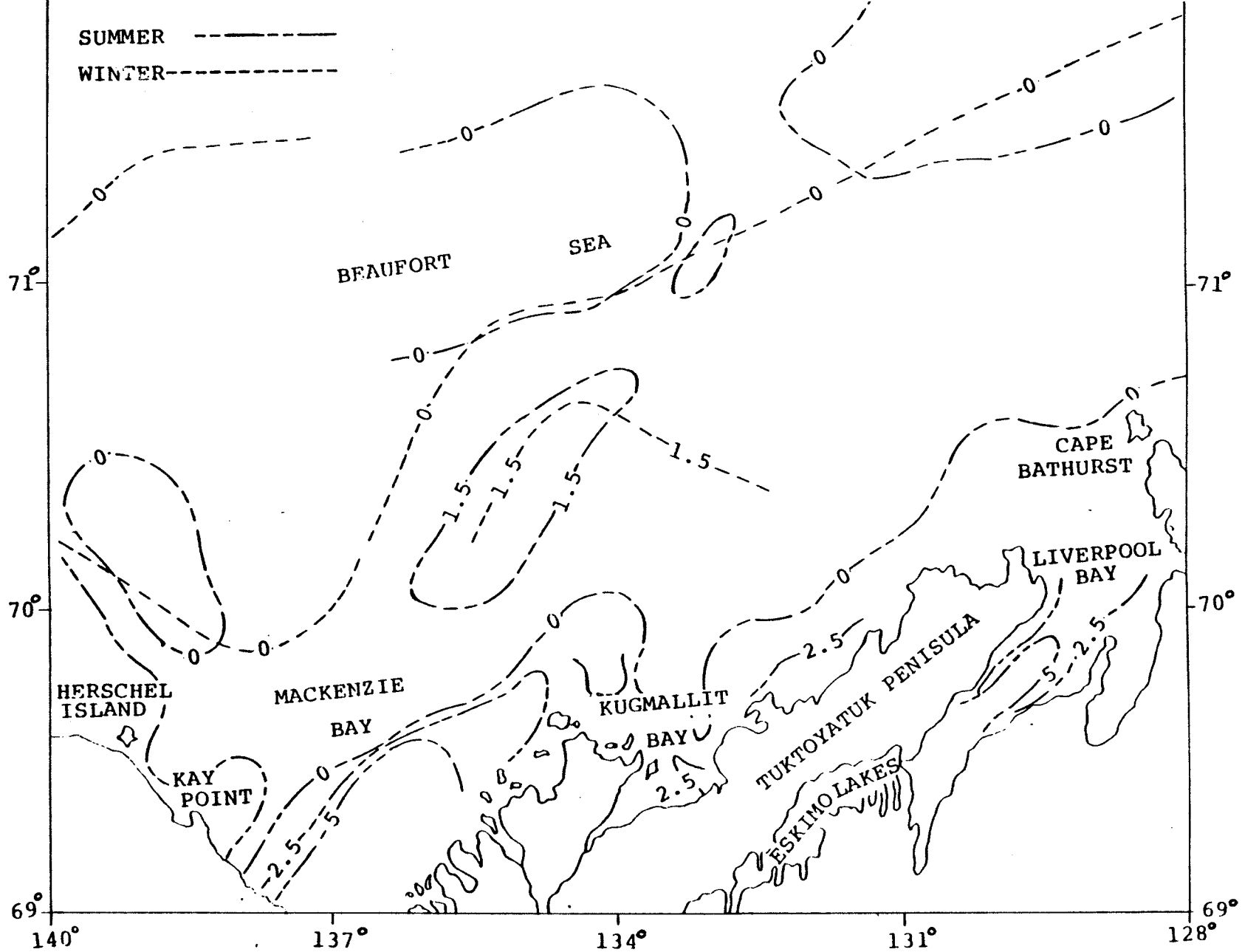


Fig. 2.6.1 Summer and winter bottom water temperatures in the southern Beaufort Sea. (temperature contours in °C). (after Hunter et al, 1976).

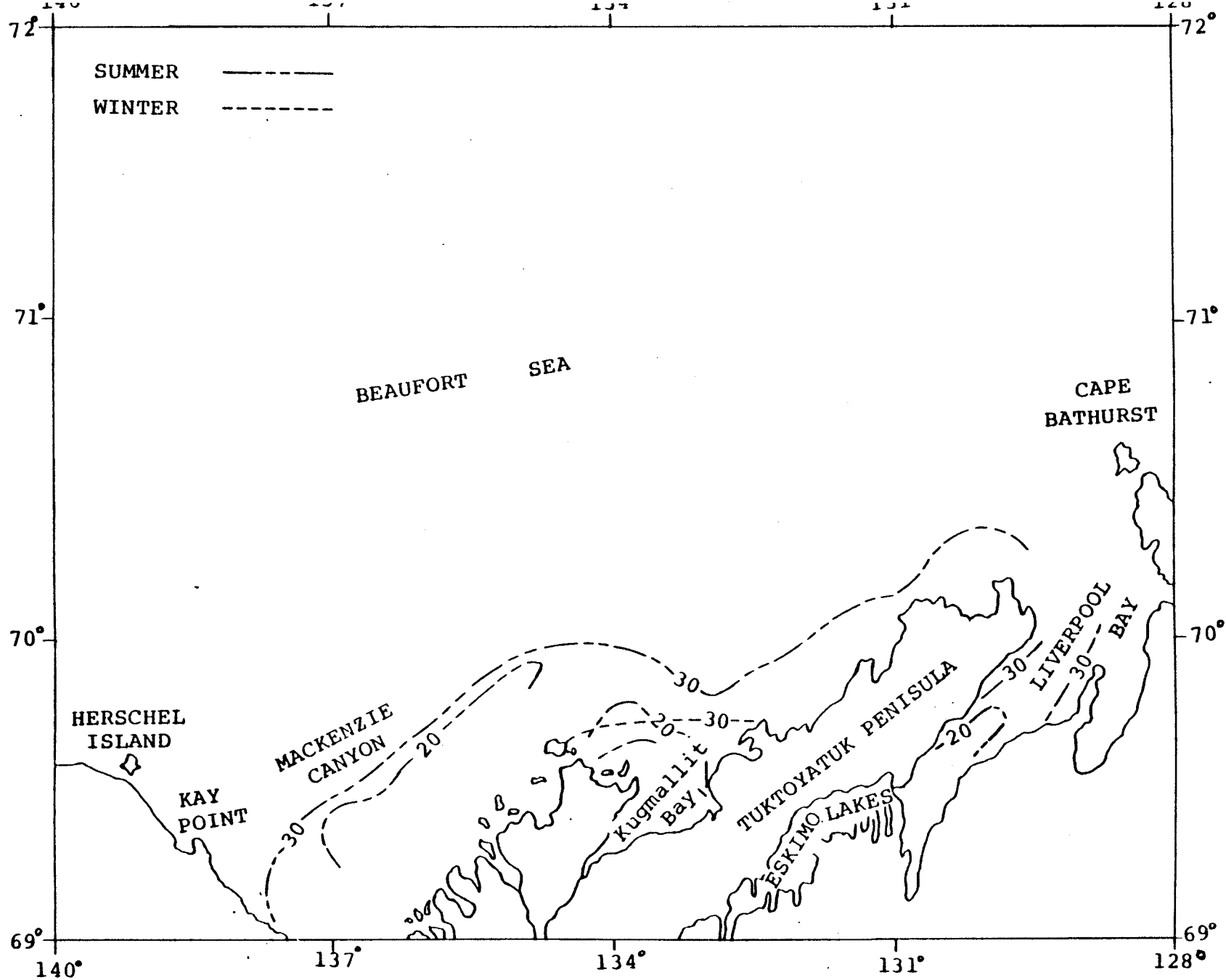


Fig.2.6.2 Summer and winter bottom water salinities in the southern Beaufort Sea.
 (salinity contours in parts per thousand.)
 (after Hunter et al,1976).

CHAPTER 3

DISTRIBUTION OF SEABOTTOM PERMAFROST IN THE SOUTHERN BEAUFORT SEA

3.1 INTRODUCTION

In the last decade, several research programs have been carried out in the Beaufort Sea shelf area. The main objectives of these programs were to study and map the permafrost underlying the Beaufort Sea shelf. Two different methods have been used in those studies, namely:

1. Seismic refraction method (Hunter et al, 1976; Morack et al, 1982) .
2. The offshore drilling method (Golden et al, 1970; Hunter et al, 1976; Judge et al, 1976; Osterkamp et al, 1982; King et al, 1982).

The results from the above two methods suggest that the occurrence and distribution of offshore permafrost in the Beaufort Sea is variable. The suggested distribution of seabottom permafrost from seismic data interpretation and offshore drilling in the southern Beaufort Sea shelf is discussed in this chapter.

3.2 SEISMIC INTERPRETATION OF SEABOTTOM PERMAFROST IN THE BEAUFORT SEA

The seismic method used in the mapping of offshore permafrost has its limitations. It is only successfully used in areas of coarse-grained, ice-saturated sediments or areas where substantial ice lensing occurs in fine-grained sediments. For fine-grained seabottom materials, such as clays and silts, at marginally permafrost temperature (-1°C) with a high salinity and absence of ice lensing, the seismic method can not distinguish the frozen state of these materials (Hunter et al, 1976).

From the seismic interpretation, as reported by Hunter et al, (1976) (Figures 3.2.1 and 3.2.4), three permafrost zones were delineated and described as follows:

1. The continuous ice-bonded permafrost zone.

These ice-bonded sediments are confined to the eastern portion of the southern Beaufort Sea shelf (east of Richard Island). In this zone, the coarse-grained seabottom materials are dominant and abundance of fresh water has been available to form the inter-granular ice. The seabottom topography is much more rugged in this zone. The rugged topography apparent in inshore regions may be due to either the differential degradational rates resulting from river channel development at lower sea levels, or the complex distribution of grain-size and pore-water sa-

linity in the sediments. From the seismic interpretation, Hunter et al (1976) suggested that there are at least two "seismic" layers existing in the ice-bonded permafrost zone. The upper layer occurs in the surficial 60 to 100 m., and the lower layer has been determined to be in the range of 120 to 250 m. deep. The location of the interpreted upper and lower "seismic" layers are shown in the Figures 3.2.2 and 3.2.3.

2. The discontinuous ice-bonded permafrost zone.

This type of permafrost lays between the ice-bonded and non ice-bonded permafrost zones. It may have been partially ice-bonded clays and silts. The submarine pingo swarms are associated with the discontinuous ice-bonded permafrost zone.

3. The non ice-bonded permafrost zone.

The non ice-bonded sediments occur in the western portion of the southern Beaufort Sea shelf (west of Richard Island). Most of the upper 100 metres of the seabottom materials are fine-grained clays and silts. The fine-grained seabottom materials increase in the thickness towards the west. There are no indications of ice-bonding in the sediments from seismic interpretations, but seabottom temperature data suggests that permafrost conditions exist (Figure 3.2.4). The thick, fine-grained materials probably may also be found in the seabottom north of Cape Dalhousie.

The report by Hunter et al (1976) also pointed out several outstanding features concerning the distribution of permafrost in the southern Beaufort sea shelf. These features are as follows:

1. No evidence of ice-bonded permafrost has been found in water depths in excess of 90 m..
2. No ice-bonded permafrost occurs in the offshore region with water depths greater than 20 m. west of the N-S line at approximately 135 W longitude.
3. There are no correlation between interpreted boundaries and major bottom features (e.g. Mackenzie Canyon).
4. Permafrost is aggrading downwards from the seafloor in the offshore and is degrading in the inshore region.

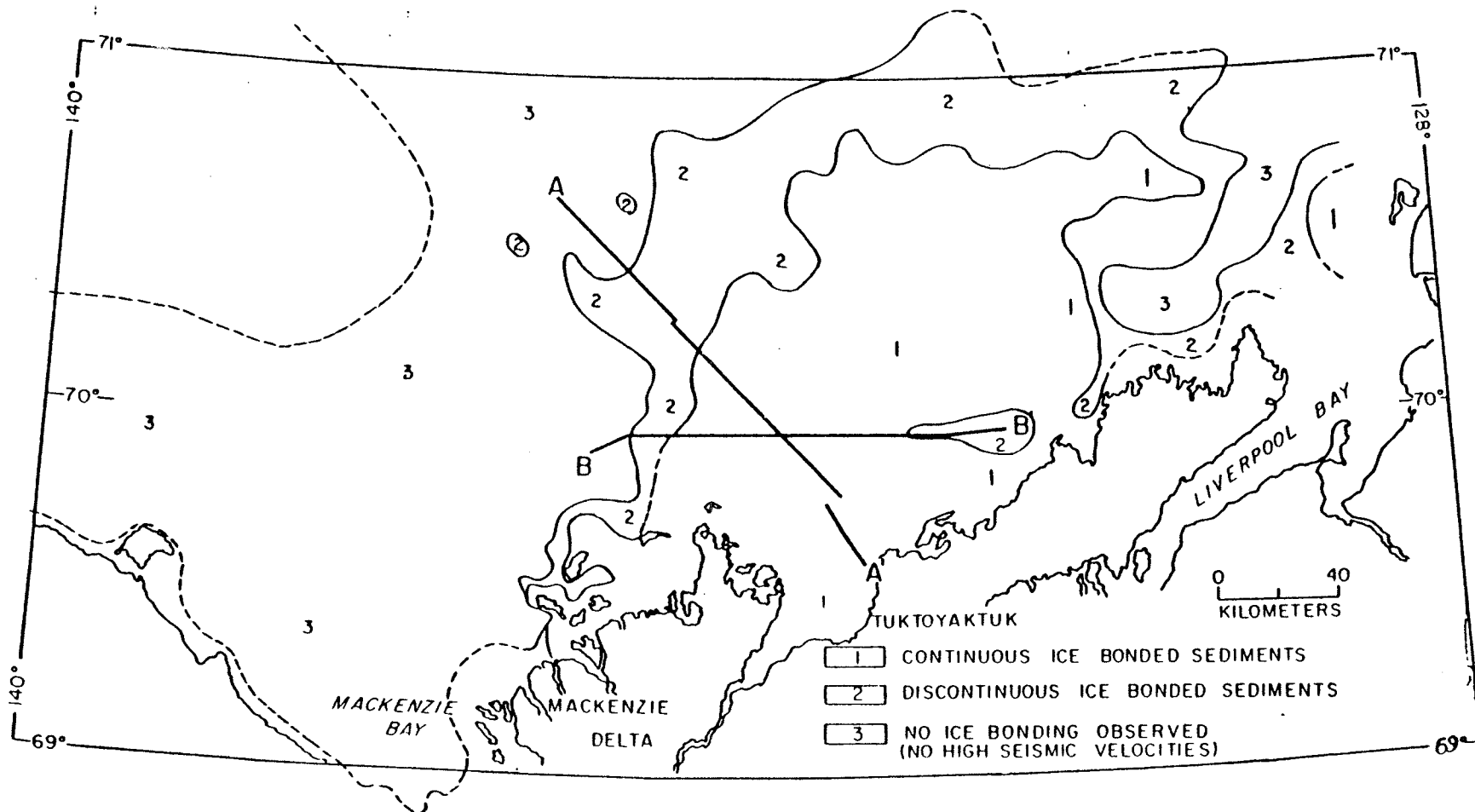


Fig.3.2.1 An interpretation of the occurrence of sub-seabottom ice-bonded permafrost from industry seismic records. (after Hunter et al,1976)

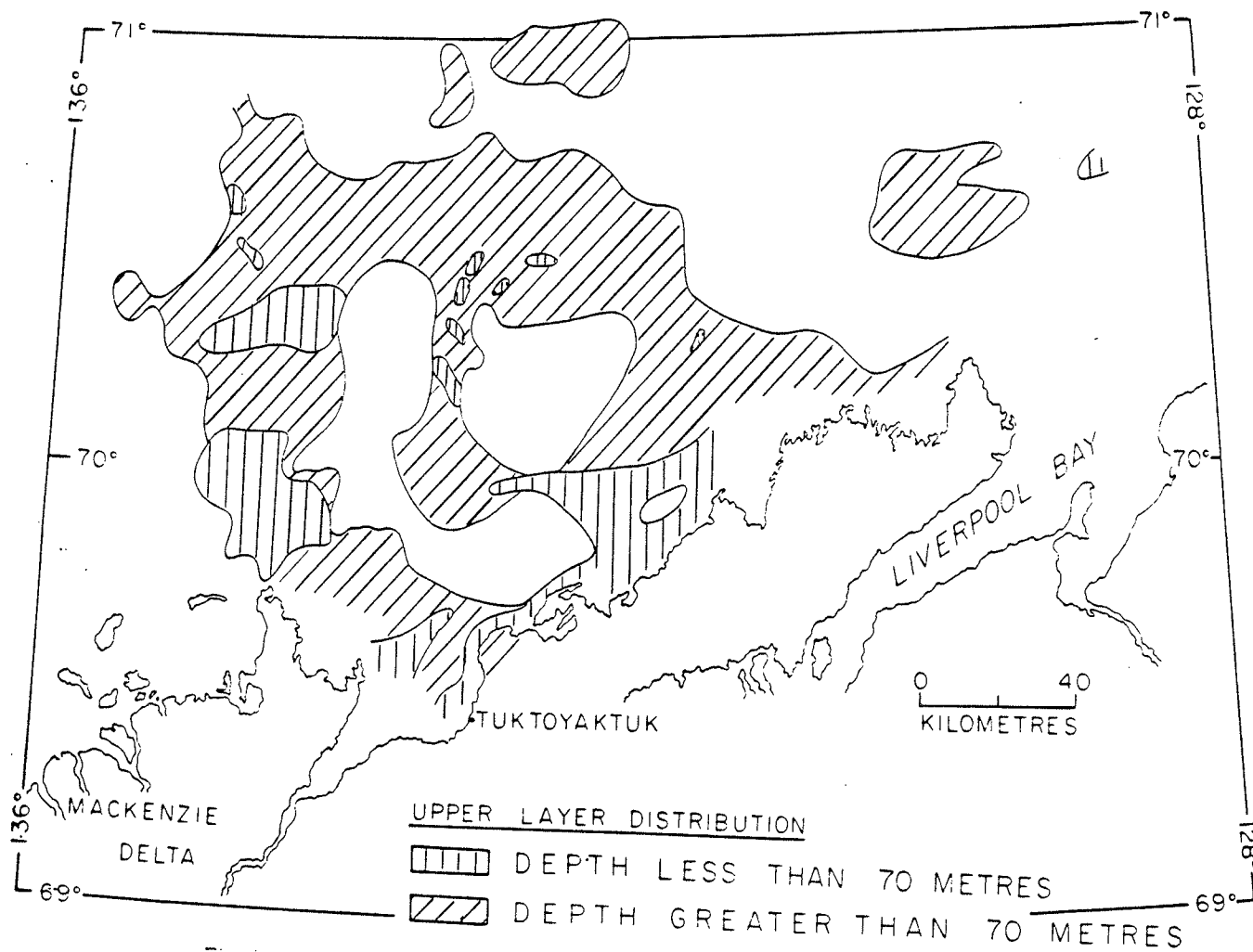


Fig.3.2.2 Distribution and depth to the top of the upper thin discontinuous high-velocity layer.
(after Hunter et al,1978)

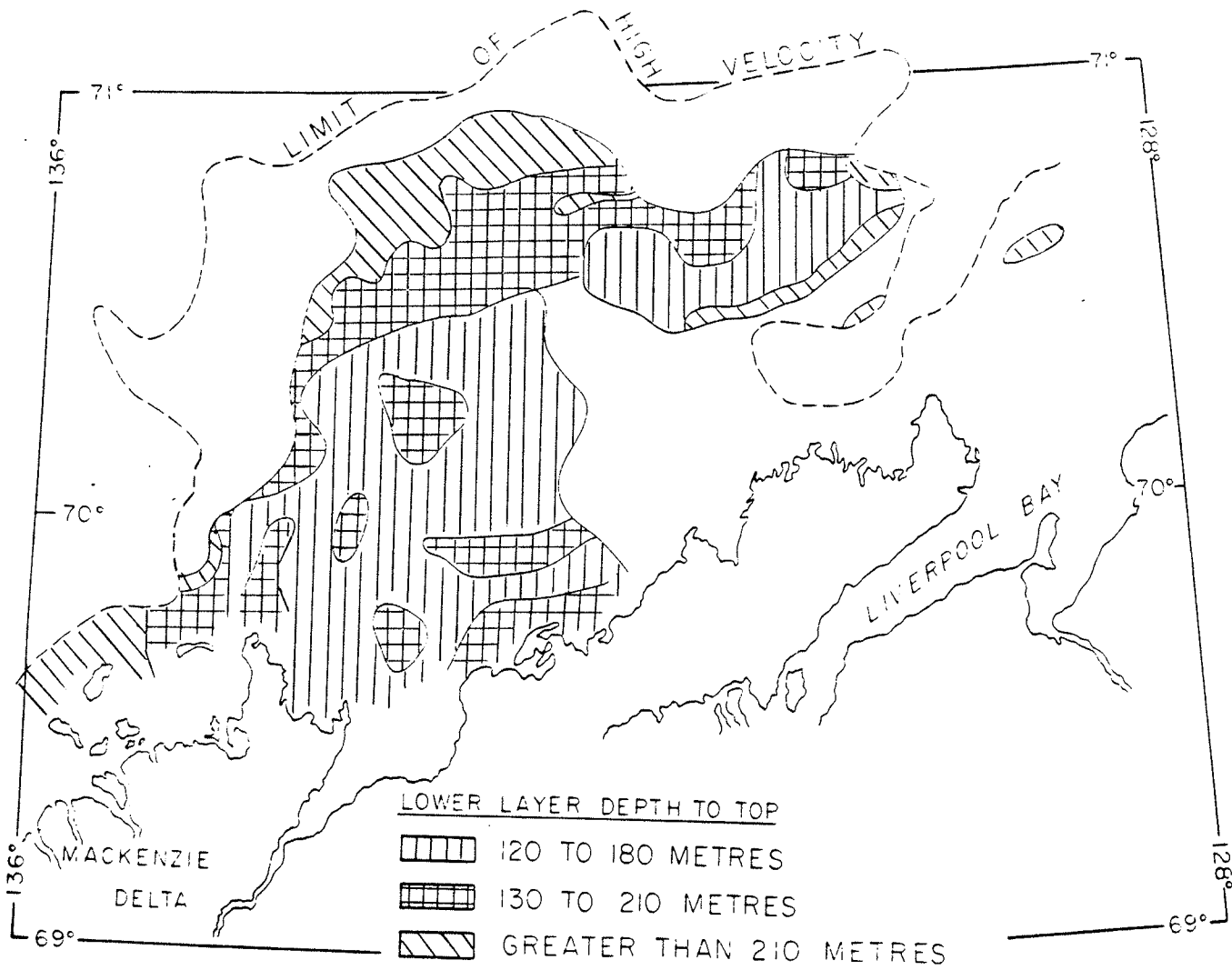


Fig.3.2.3 Distribution and depth to the top of the lower thick continuous high-velocity layer. (after Hunter et al,1978)

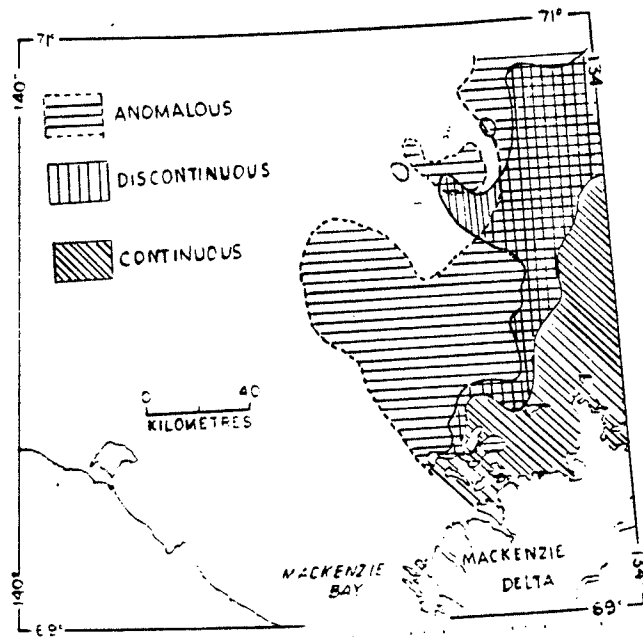


Fig.3.2.4 Distribution of anomalous velocity which are higher than expected for unconsolidated sediments but lower than expected for ice-saturated sediments. (after Hunter et al,1978)

3.3 OFFSHORE DRILLING IN THE BEAUFORT SEA

Numerous exploration wells have been drilled in the shoreline area and in the shallow waters offshore at the sites of artificial islands. The drill logs of most of these holes remain confidential information. However, available information gathered from published reports is presented below.

3.3.1 A.P.O.A. DRILLING

The Arctic Petroleum Operation's Association (A.P.O.A.) shallow water drilling program on the Beaufort Sea shelf is shown in Figure 3.3.1. Figure 3.3.2 details borehole information from the drillholes which encountered permafrost. These results (Figure 3.3.2) indicate that a wide range of frozen soils, such as clay, clayey silt, silty sand, sand and gravel, are present in the shelf of the Beaufort Sea.

3.3.2 IMPERIAL OIL LTD. DRILLING

Two of the Imperial exploration wells which were reported encountered frozen materials. These two wells are Imperial Nuktak P-50 and Imperial Immerk B-48. The Imperial Nuktak P-50 is located at Hopper Island. The material encountered from the surface to a depth of 685 m. was frozen and ice-bonded. The Imperial Immerk B-48 hole is situated between Hopper and Pelly Islands. This well contained ice-bonded materials from 150 m. to 380 m. below the surface. The geology

logs of these two wells are shown in Figures 3.3.4 and 3.3.5 (Hunter et al,1976).

Figures 3.3.6 shows the proposed sites of artificial islands Tingmiark and Kopenoar. Figure 3.3.7 shows the drill log from the proposed site of Tingmiark. Permafrost was encountered from 34 m. to 43 m. below seabottom in the Tingmiark site. The temperature of the sediments at the 60 m. depth was -1.6°C , indicating a total permafrost thickness considerably in excess of that depth, although no further ice-bonded permafrost was encountered. For the Kopenoar drill hole, ice-bonded sediments were encountered immediately below the sea bottom (Hunter et al,1976).

3.3.3 G.S.C. DRILLING IN KUGMALLIT BAY

In 1974, the Geological Survey of Canada (G.S.C.) conducted a drilling program in Kugmallit Bay. Four holes were drilled at the locations shown in Figure 3.3.7. As shown in Figure 3.3.8, the drillholes logs indicate that sand is a dominant material type in the Kugmallit bay. The sand found in Kugmallit bay has an average density of 2.66 g/cm^3 (26.1 KN/m^3). The range of moisture contents of this sand (and gravel) was between 45 to 71 % in the frozen state, and 31 ± 6 % in thawed state. The salinity of the pore fluid of the sand ranges from 2 to 30 parts per thousand (ppt). The clays and silts encountered in this area have an average density of 2.70 g/cm^3 (26.5 KN/m^3). The moisture contents of the

silts and clays were about 50 ± 2 %, and the pore fluid salinities ranged from 6 to 39 ppt. Similar results have also been reported (King et al,1982) for salinities of pore water in subsea samples from the Beaufort Sea. The results, in terms of NaCl, were:

1. Sand : 0.02 --- 0.08 molar (1.2 --- 5 ppt).
2. Silt : 0.13 molar (8 ppt).
3. Clay : 0.3 molar (18 ppt).

Permafrost was detected in holes #1,#2 and #3. However, no permafrost was encountered in hole #4, but the hole temperature suggested the presence of permafrost below 70 m. The permafrost was encountered in holes #1,#2 and #3 at depths of 37 to 40 m., 70 m. and 61 m. respectively (Hunter et al,1976).

3.3.4 G.S.C. DRILLING IN MACKENZIE DELTA

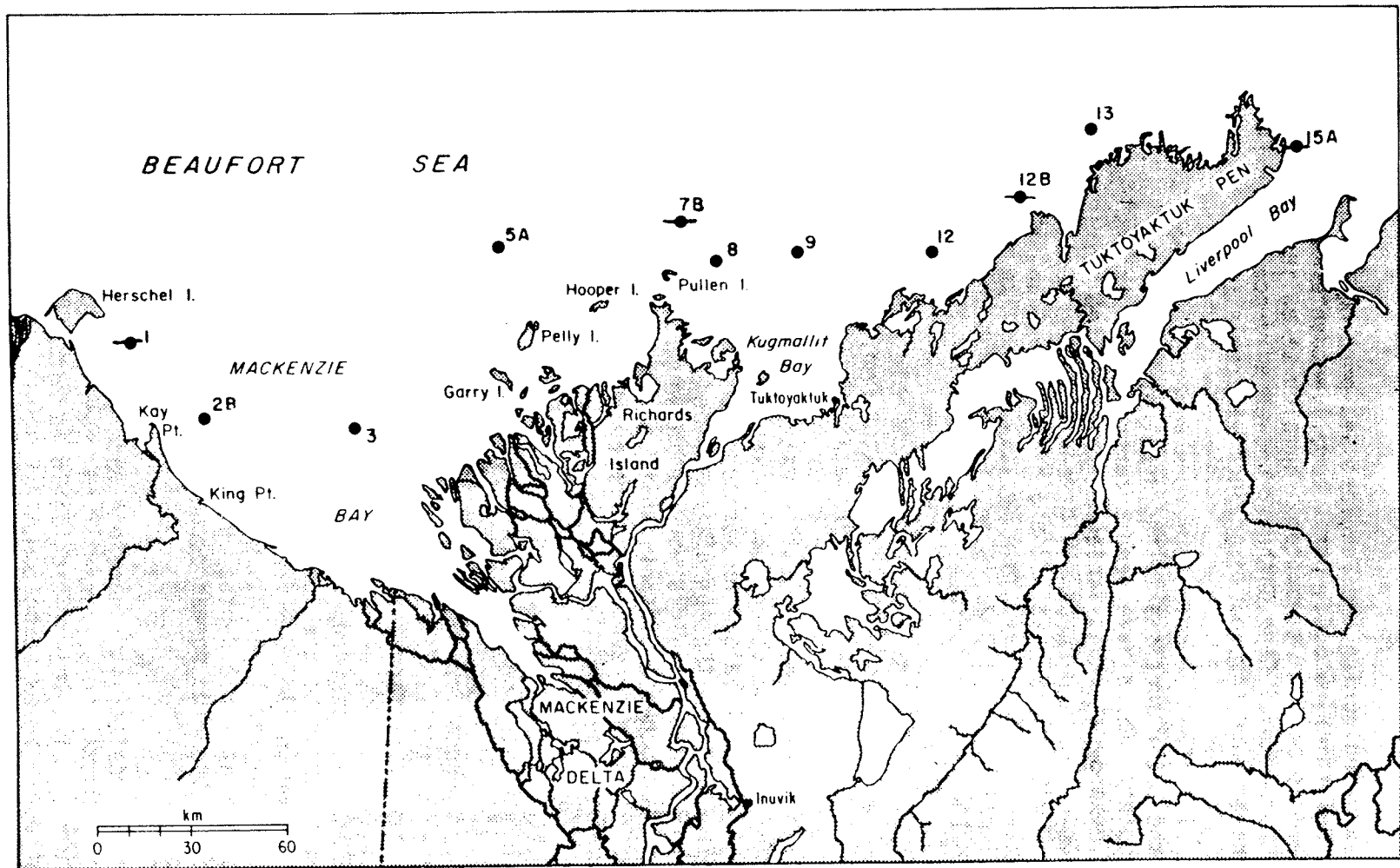
In 1976, five experimental drillholes were drilled into the seabottom of the Beaufort Sea shelf by the G.S.C.. The locations of the five holes are shown in Figure 3.3.9 . Test holes #1 and #2 were drilled in the shallow Mackenzie Bay. Holes #3,#4 and #5 were drilled on an east-west line approximately 32 km. north of Hopper Island perpendicular to a seismic boundary delineated by Hunter et al (1976). The test hole logs are shown in Figure 3.3.10 . Ice-bonded permafrost was encountered in holes #1,#2 and #5. It was detected at depths of 19 m., 27 m. and 45 m. below the water surface in

holes #1, #2 and #5 respectively. Although the ground temperature recorded in these test holes were below 0°C (0 to -2°C), no frozen soils were encountered in holes #3 and #4 to a depth of 30 m. and 60 m. respectively (Judge et al, 1976).

3.3.5 PRUDHOE BAY DRILLING

In the near shore area at Prudhoe Bay the salinity of the thawed layer beneath the sea bed was found to be about 25 ppt higher than the normal sea water. A temperature of -2.4°C corresponding to a salinity of 43 ppt was encountered at the phase boundary between the thawed layer and the ice bearing permafrost (Harrison et al, 1982).

All the available information from the seismic interpretation and offshore drilling programs is shown in Figure 3.3.11. Enough information, however, is not available to form a detailed map of the seabottom permafrost conditions in the Beaufort Sea. The data also indicated that the salinity of some non-ice-bonded, fine-grained permafrost is higher than the normal sea water (for example, 30 to 55 ppt (Harrison et al, 1982)), and this corresponds to a range of freezing point depression of 0°C to -5°C. The ice-bonded, fine-grained or coarse-grained permafrost is related to a lower salinity.



- ENGINEERING BORE HOLES PERMAFROST ENCOUNTERED
- ENGINEERING BORE HOLES PERMAFROST NOT ENCOUNTERED

Fig.3.3.1 Location of A.P.O.A. shallow drillholes.
(after Mackay, 1972)

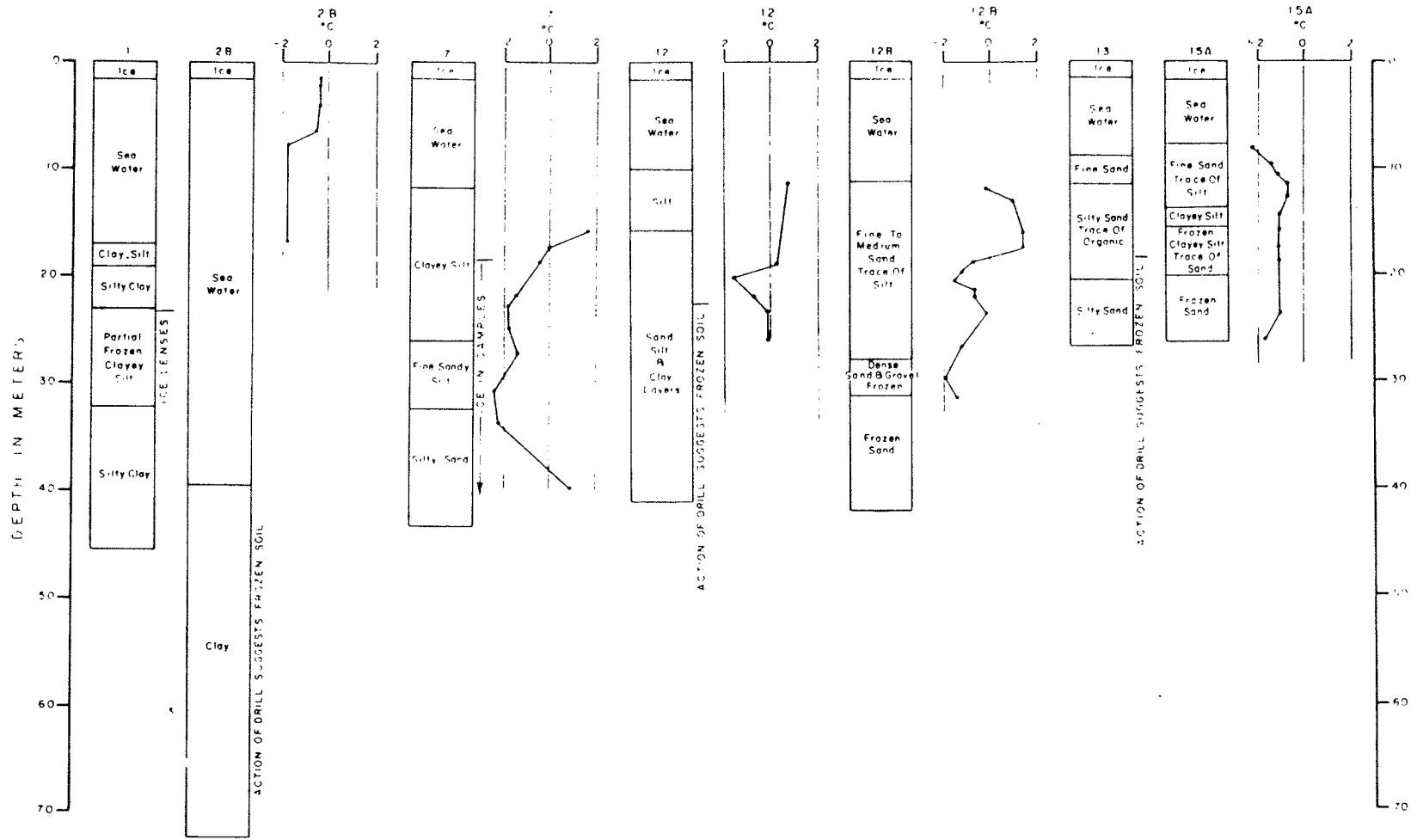


Fig.3.3.2 A compilation of drilling results from A.P.O.A. report #3 for the holes encountering permafrost. Temperature measurements were obtained from samples. (after Hunter et al,1976)

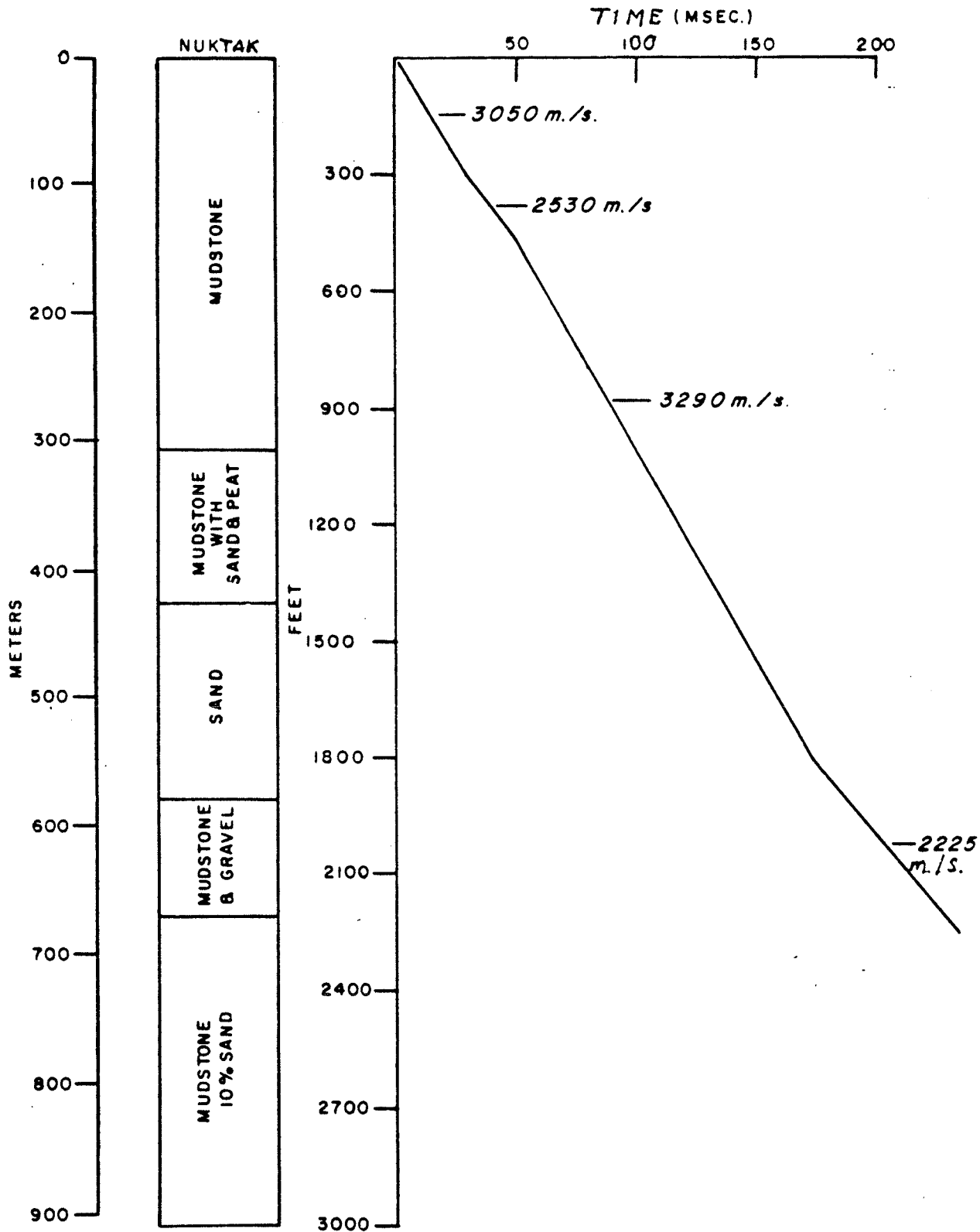


Fig.3.3.3 Generalized geology and crystal cable velocity log from I.O.E. Hooper NAKTAK c-22 (after Hunter et al,1976).

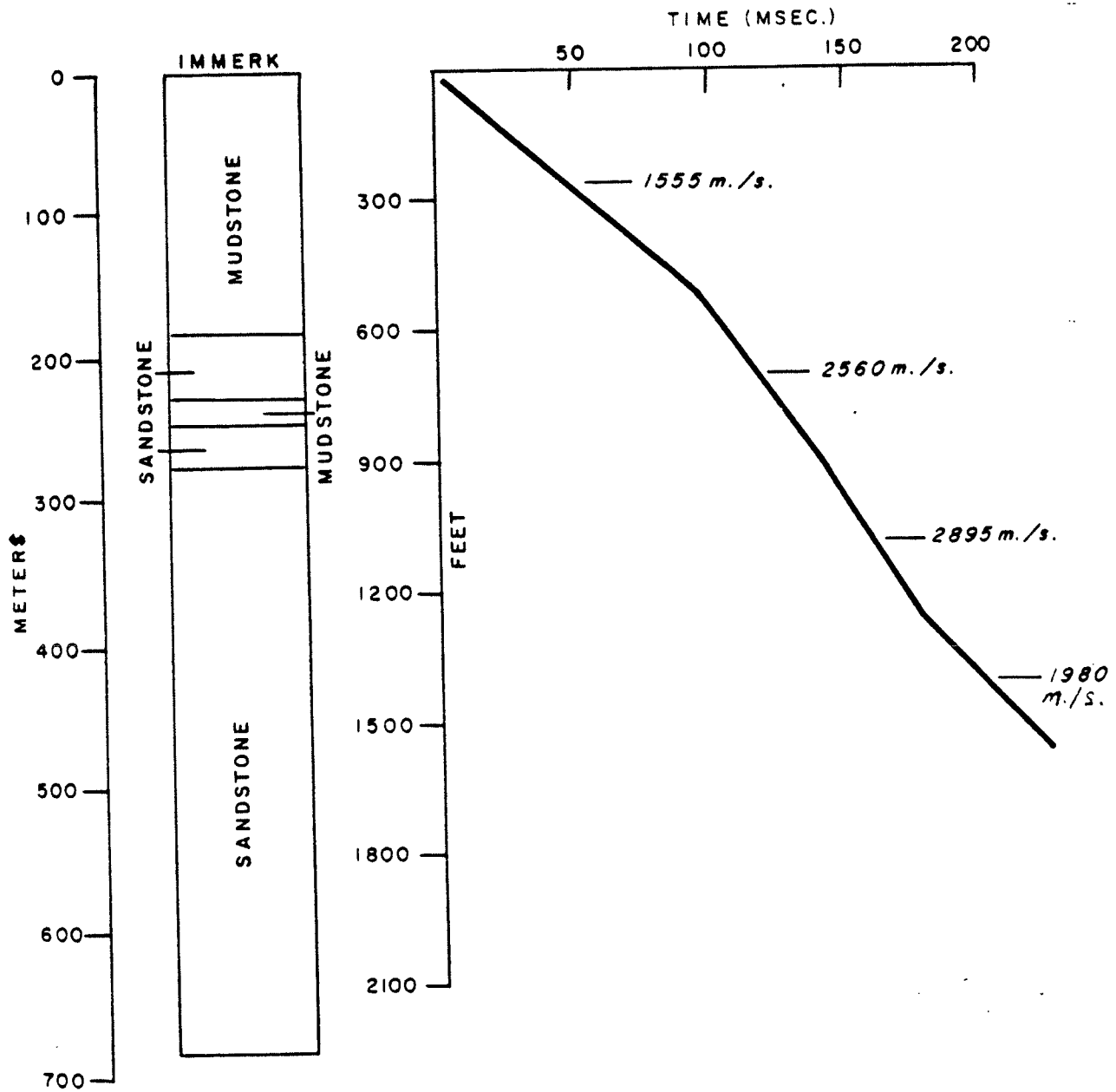


Fig.3.3.4 Generalized geology and crystal cable velocity log from I.O.E. IMMERSK B-48 (after Hunter et al,1976).

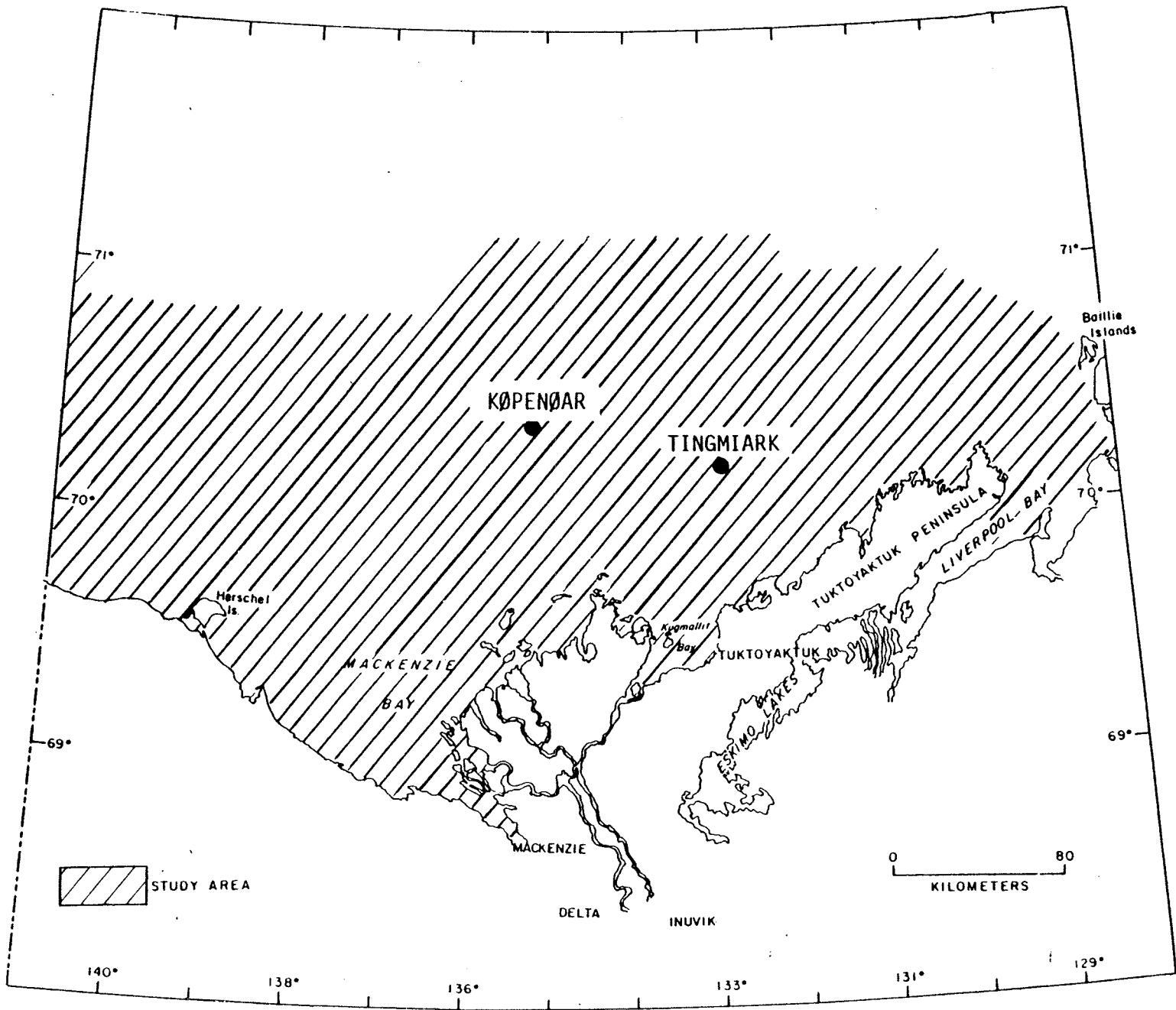


Fig.3.3.5 Location of the two proposed drilling sites.
(after Hunter et al,1976)

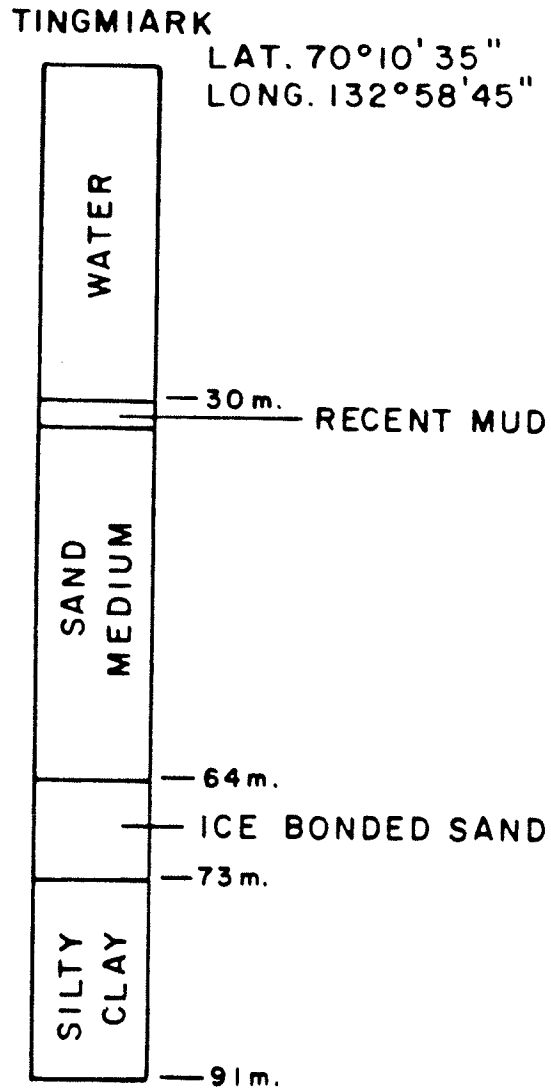
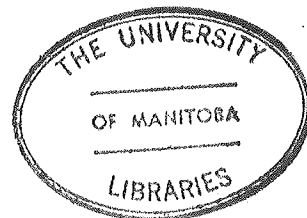


Fig.3.3.6 Generalized geological log from Tingmiark drill site. 80 km. north of Tuktoyuktak. Water depth 30 m. (after Hunter et al,1976)



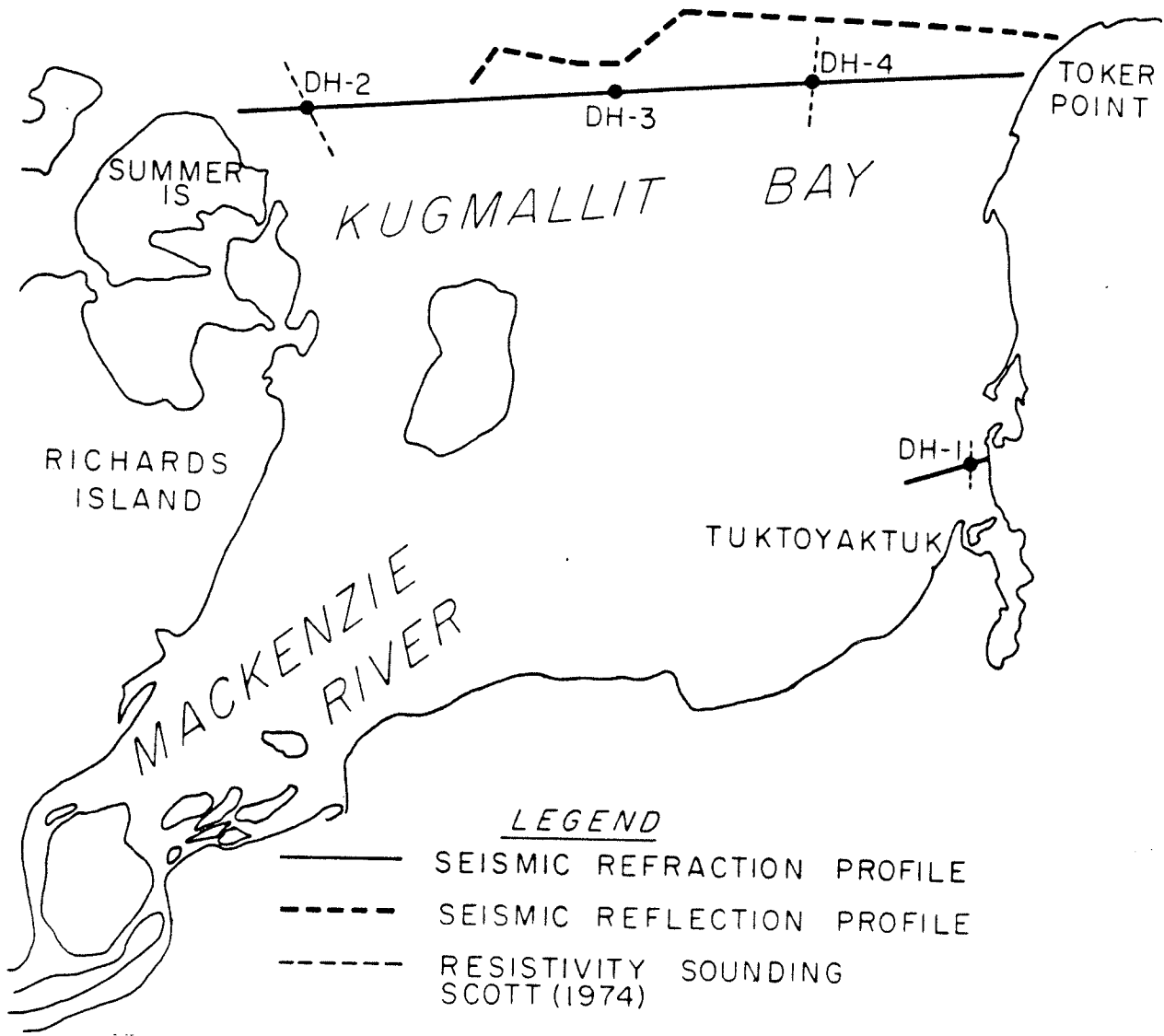
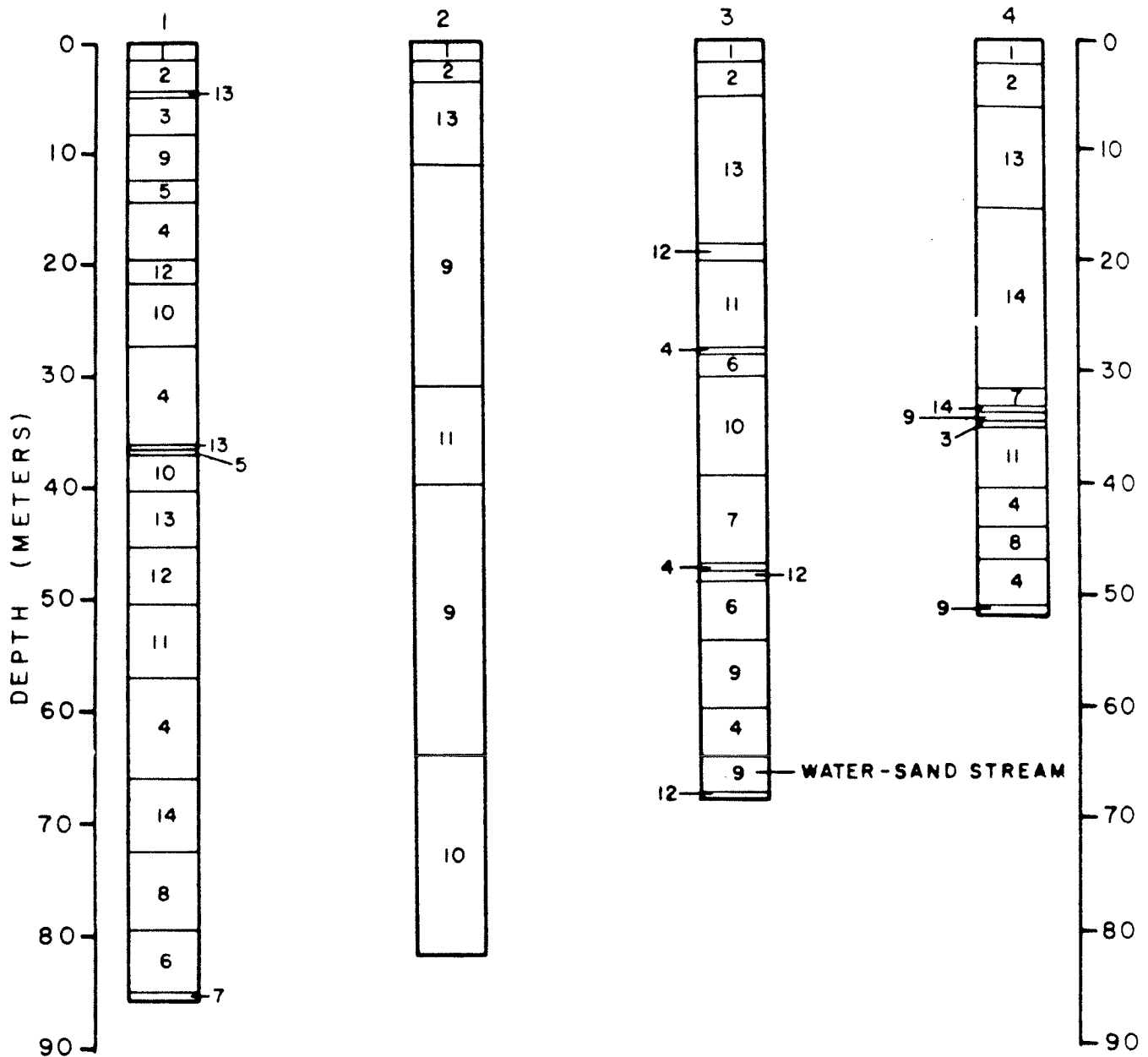


Fig 3.3.7 Location of GSC drillholes in Kugmallit Bay (after Hunter et al, 1976)



LEGEND

- | | | | |
|----------|-----------------|----------------------|------------------------|
| 1 ICE | 4 SAND & GRAVEL | 7 SAND(fine-coarse) | 11 SAND(coarse-medium) |
| 2 WATER | 5 SANDY GRAVEL | 8 SAND(coarse) | 12 SILTY SAND |
| 3 GRAVEL | 6 PEBBLY SAND | 9 SAND(medium) | 13 CLAYEY SILT |
| | | 10 SAND(fine-medium) | 14 SILTY CLAY |

Fig.3.3.8 Lithological description of GSC Kugmallit Bay drillholes. (after Hunter et al,1976).

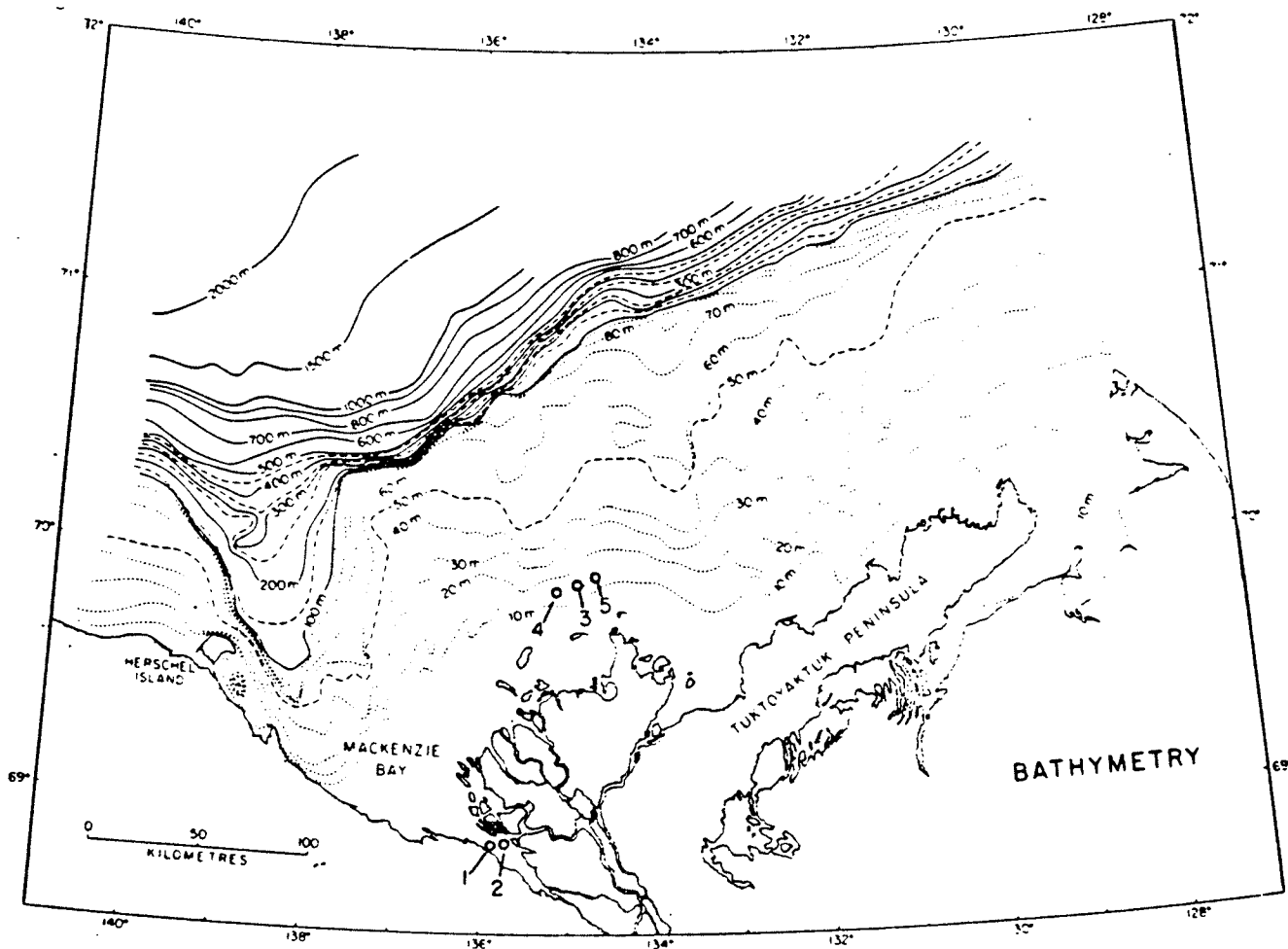


Fig.3.3.9 Location of GSC drillholes in Mackenzie Delta.
(after Judge et al,1976).

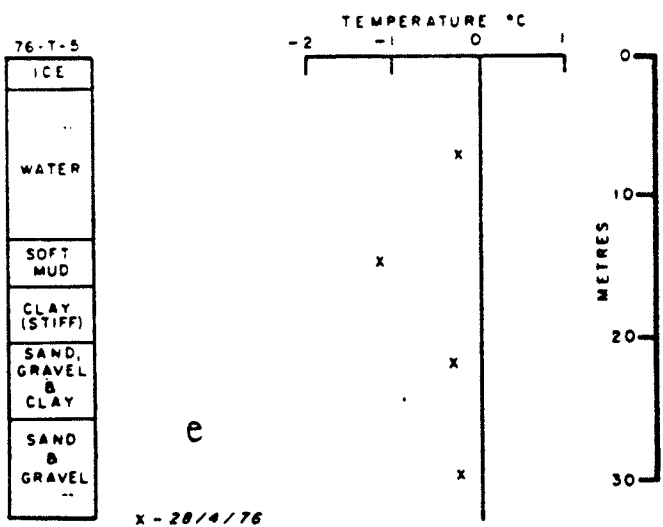
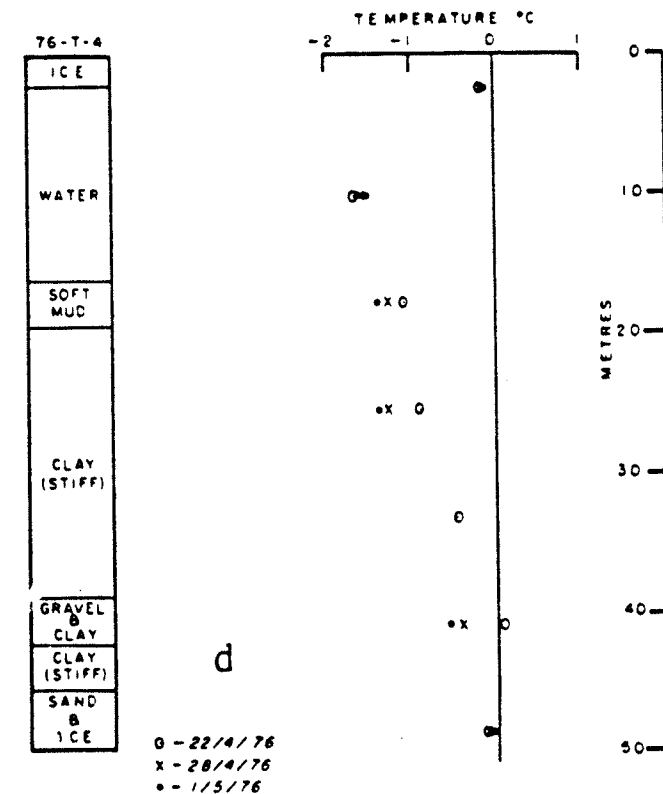
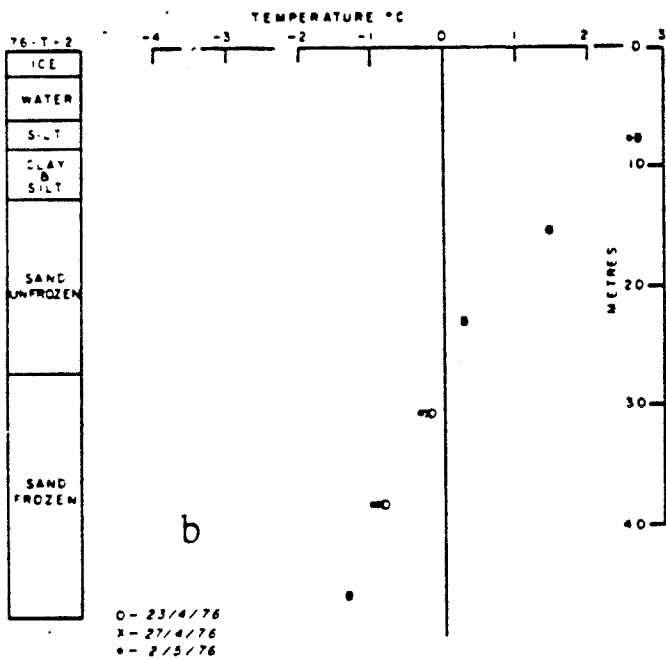
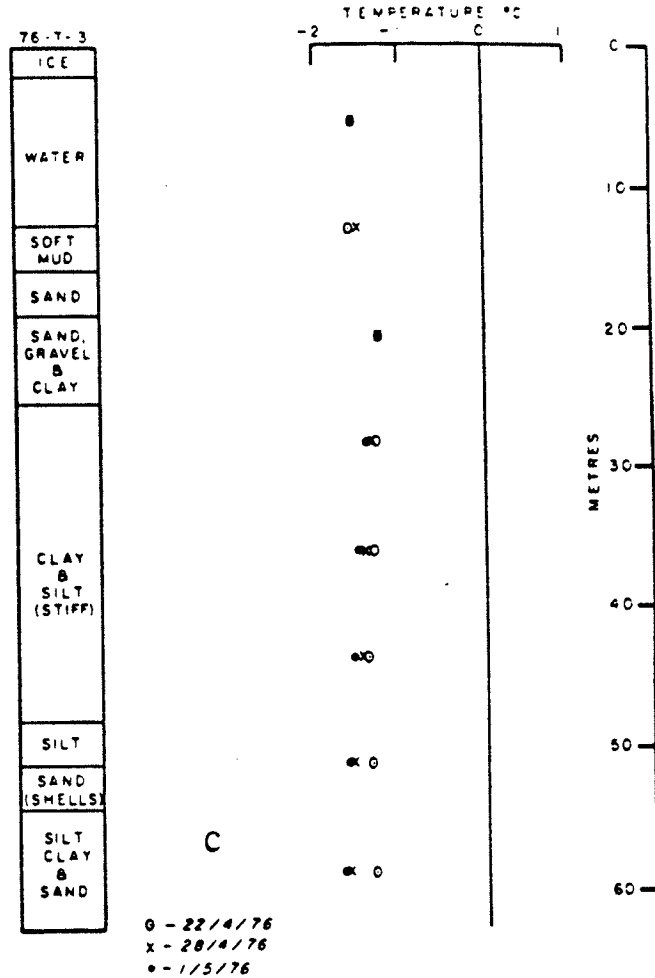
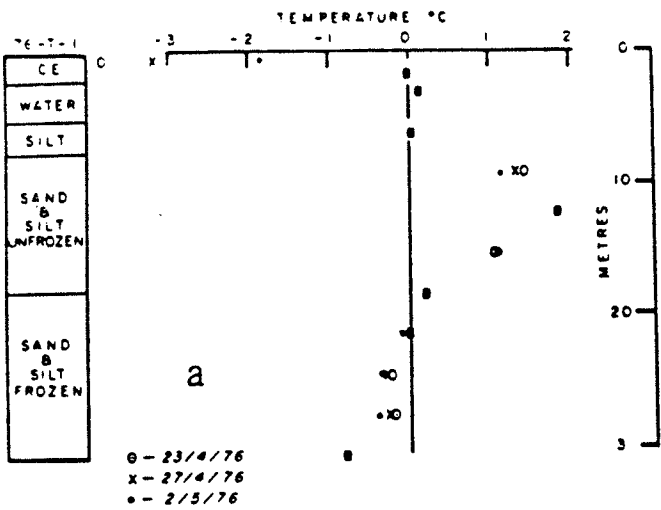


Fig.3.3.10 Description of Mackenzie Delta drillholes. (after Judge et al,1976).

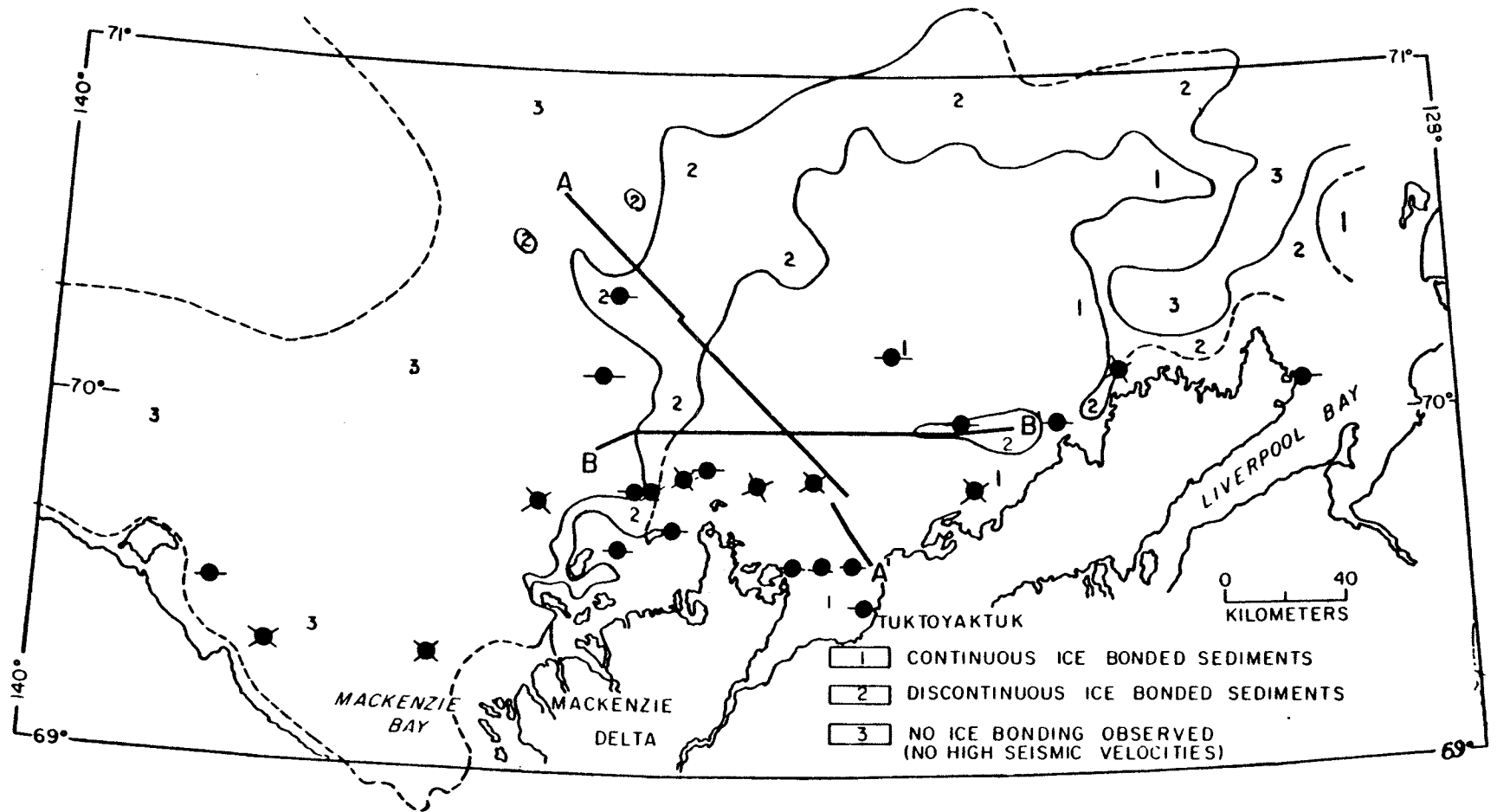


Fig.3.3.11 Location of drillholes and seismic interpretation in the southern Beaufort Sea.

CHAPTER 4

CREEP OF FROZEN SOIL

4.1 INTRODUCTION

In the last three decades, laboratory studies have been carried out to obtain the constitutive relationships in describing the stress-strain-time behaviour of frozen soils (Vyalov, 1962; Andersland and Alnouri, 1970; Ladanyi, 1972; Sayles, 1972; Klein and Jessberger, 1981). Many of the early studies were limited to uniaxial compression tests on frozen soils and ice. The constitutive equations describing the creep behaviour of frozen soil were obtained for uniaxial stress conditions. But these equations were generalized for complex stress conditions, such as triaxial stress state (Vyalov, 1962; Sayles, 1972; Ladanyi, 1972; Klein and Jessberger, 1981). Frozen soils are often assumed to be incompressible. Based on this assumption, the hydrostatic stress should have no influence on the deformation and flow, i.e. no effect on the creep rate. Because of this assumption the creep constitutive equations in the literature often give zero strain when the stress condition is hydrostatic (Ladanyi, 1972; Andersland and Alnouri, 1970; Diekmann and Jessberger, 1982).

In this chapter, different constitutive equations, which describe the deformation behaviour of frozen soil are briefly reviewed.

4.2 COMPOSITION OF FROZEN SOIL

Frozen soil is a four phase system consisting of mineral solid particles, unfrozen water, ice and gases. Each phase plays an important role in the behaviour of the frozen soil.

The shape, size and mineralogical composition of mineral solid particles are the primary factors in a frozen soil. The particle shape and size influence the contact and the surface tension between ice, unfrozen water and particles. The mineralogical composition affects the surface activity such as the exchangeable cation which influences the thickness of the bonded water layer.

There are two states of unfrozen water present in the frozen soil, namely, the strongly-bonded water and the loosely-bonded water. The strongly-bonded water is attached to the solid particles. Interchangeable cations produce an electro-molecular force which suppresses the formation of ice crystals, even at very low temperatures. The strongly-bonded water is surrounded by a layer of loosely-bonded water. Intermolecular forces are also present in this layer. The layer of loosely-bonded water is capable of releasing heat of crystallization (latent heat of fusion) at temperature below 0°C. The amount of unfrozen water present in the frozen soils depends on the pore fluid chemistry, temperature, external pressure, soil type and mineralogy.

Ice, the most important component in the frozen soil, dictates the deformation behaviour of frozen soil. The

time, rate and temperature dependent deformation properties depend on the amount of ice present in the frozen soils. Ice present in the frozen soils is either pore ice or segregated ice or both, and is generally polycrystalline with a hexagonal ring structure. Gas and water vapour, only present in partially saturated frozen soil, influence the water content distribution.

More detailed studies of the composition of frozen soil are given in Morgenstern and Anderson (1973) and Ladanyi (1981).

4.3 CLASSIFICATION OF FROZEN SOIL

There are two different classification systems of frozen soil proposed in the literature. Weaver (1979) proposed a classification of frozen soils based on the ice-grains ratio. This classification system is shown in Table 4.1. Another classification system of frozen soils proposed by Russian Permafrost Construction Standards (U.S.S.R. 1969) is based on the temperature and the type of frozen soils. The temperature and the type of frozen soils reflect the amount of unfrozen water content. This type of frozen soils classification is shown in Table 4.2 .

TABLE 4.1

FROZEN SOIL CLASSIFICATION SYSTEM

(Proposed by Weaver, 1979)

SOIL TYPE	DESCRIPTION
Dirty Ice	<ul style="list-style-type: none"> -- applies to ice that has a low solid concentration -- unit wt. = 0.9 - 1.0 Mg/cu.m -- the soil particles present reduce the average grain size of the ice crystal resulting in higher creep rates than pure ice
Very Dirty Ice	<ul style="list-style-type: none"> -- applies to ice that has medium to high solids concentration -- unit wt. = 0.9 - 1.8 Mg/cu.m -- very little grain to grain contact between soil particles -- lower secondary creep rates than polycrystalline ice because soil impedes dislocation movement
Ice-Poor Frozen Soil	<ul style="list-style-type: none"> -- applies to saturated frozen soil whose deformation patterns are characterized primary creep -- unit wt. = 1.7 - 2.0 Mg/cu.m
Ice-Rich Frozen Soil	<ul style="list-style-type: none"> -- applies to soils that have a continuous network of segregated ice -- the overall creep response is complex and is very sensitive to the reticulate structure of the segregated ice, bulk density grain size and ground temperature

TABLE 4.2

CLASSIFICATION OF FROZEN SOILS

(Russian Permafrost Construction Standards, 1969)

SOIL TYPE	DESCRIPTION
Hard Frozen	-- well cemented ice bonding
	-- low unfrozen water content
	-- for silty sand $T < -0.3^{\circ}\text{C}$
	for sandy loams $T < -0.6^{\circ}\text{C}$
	for clay loams $T < -1.0^{\circ}\text{C}$
	for clay $T < -1.5^{\circ}\text{C}$
Plastic Frozen	-- little cemented ice bonding
	-- large amount of unfrozen water content
	-- for silty sand $T > -0.3^{\circ}\text{C}$
	for sandy loams $T > -0.6^{\circ}\text{C}$
	for clay loams $T > -1.0^{\circ}\text{C}$
	for clay $T > -1.5^{\circ}\text{C}$

4.4 DEFORMATION BEHAVIOUR OF FROZEN SOIL UNDER CONSTANT LOAD

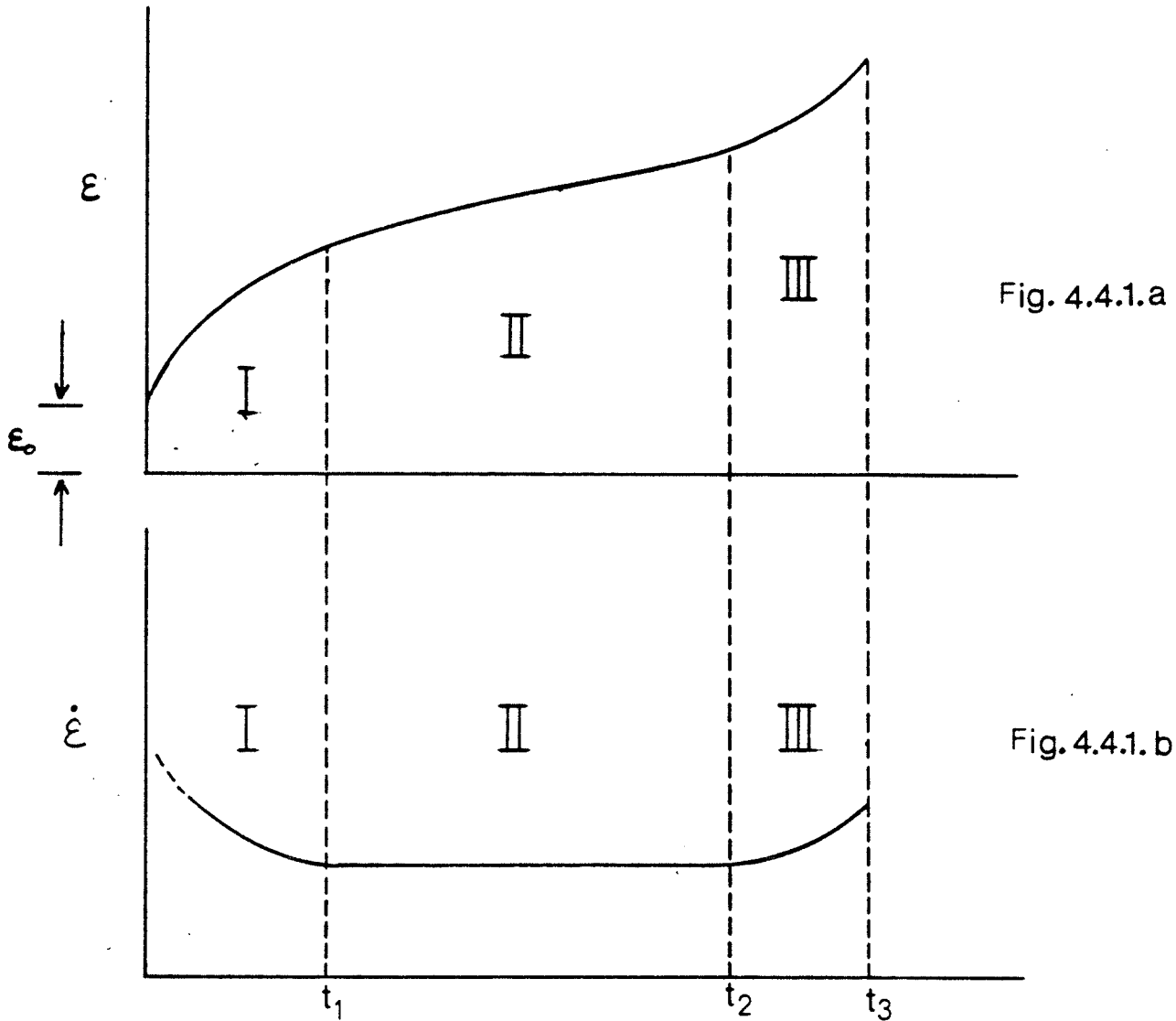


Fig.4.4.1 Typical creep curves of frozen soils under constant stress.
a). the total strain vs.time.
b). the strain rate vs.time.
(after Ladanyi,1972).

A typical creep curve is shown in Figure 4.4.1a, and Figure 4.4.1b shows the relationship between strain rate and time. The total strain is composed of an instantaneous component and a time dependent component, both of which contain reversible and irreversible components. In general, the total strain under a continuous increase of stress (σ) with time (t) and temperature (T) may be written in the form

$$\epsilon = E[\sigma(t), T] + \int_0^t G[\sigma(t), T] dt \quad (4.1)$$

For a constant stress and a constant temperature, the instantaneous component is ($t=0$)

$$E[\sigma, T] = \epsilon_0 \quad (4.2)$$

And the time dependent component or creep component is

$$\int_0^t G[\sigma, T] dt = \int_0^{t_1} \frac{\partial \epsilon_1}{\partial t} dt + \int_{t_1}^{t_2} \frac{\partial \epsilon_2}{\partial t} dt + \int_{t_2}^{t_3} \frac{\partial \epsilon_3}{\partial t} dt \dots \quad (4.3)$$

As shown in Figure 4.4.1, the three time dependent functions in Eqn.(4.3) are :

1. [I] Primary creep whose creep rate decreases with time .
2. [II] Secondary creep whose creep rate is at a minimum .
3. [III] Tertiary creep whose creep rate increases and accelerates, and leads to ultimate failure.

The shape of the creep curve differs with respect to the stress magnitude (Figure 4.4.2) . At a stress level lower than the long-term strength, the strain is damped with time. Nondamped creep results when the stress levels in question exceeds the long-term strength. The higher the applied stress the sooner the failure occurs. The strength which relates the stress with time to failure is shown in Figure 4.4.3 . The strength loses with increasing of load durations. Vyalov (1963) defined the asymptote to the curve as the long-term strength.

The long-term strength of ice is zero. Nondamped creep results at any stress levels above zero. For ice-poor, dense frozen soils, the deformation response is characterized by damped creep. For ice-rich soils, the deformation response is either nondamped and damped dependent upon the ratio of ice to soil solid, as well as the stress magnitude (Vyalov, 1959).

According to Tsytoovich (1975) the application of a constant external load may cause local stress concentration, resulting in plastic flow and melting of ice. As a result of

this, the pressure gradient from the difference of surface tension causes the melted ice to migrate into a lower stress zone, where it again refreezes. Simultaneously, the intermolecular and ice-cementation bonds break down and mineral particles slip. The pressure melting process is accompanied by reorientation of the ice crystal, which tends to orient with their basal plane to the slide direction. This results in a reduction in shearing resistance, i.e., a weakening process. The strengthening process begins at the particles slip, the particles packing becoming denser and the ice-cementation bonds increasing as the melted ice refreezes. Damped creep occurs when the strengthening overcomes weakening, otherwise nondamped creep results.

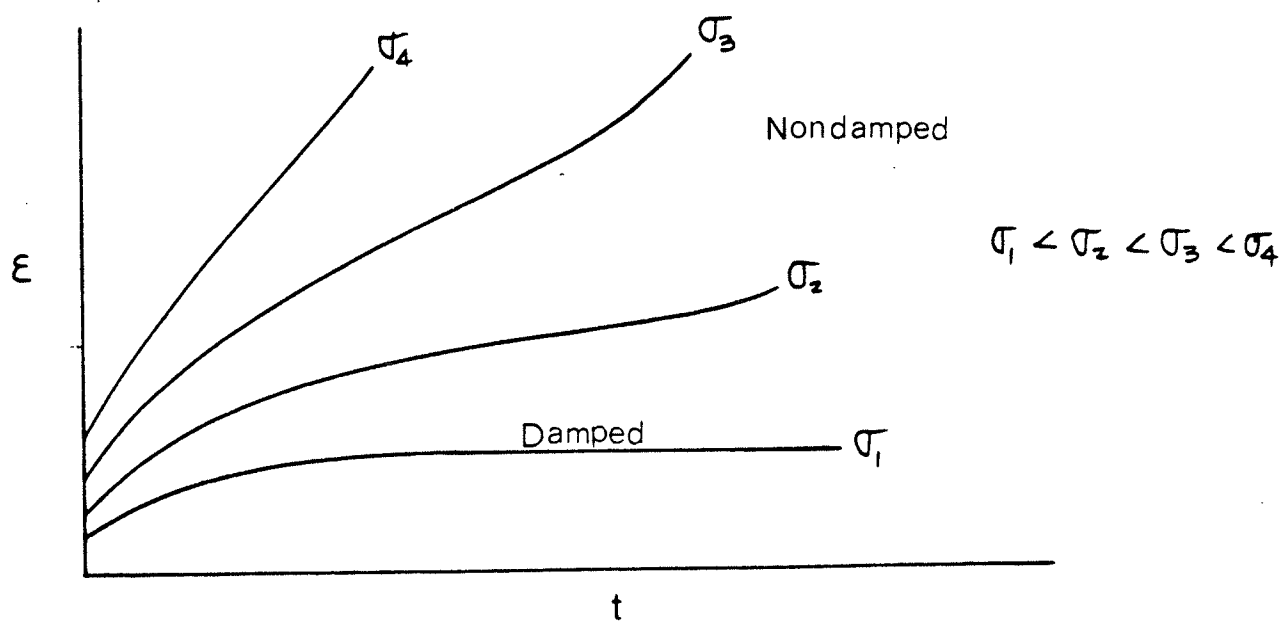


Fig.4.4.2 Group of creep curves for various constant load (after Vyalov, 1963).

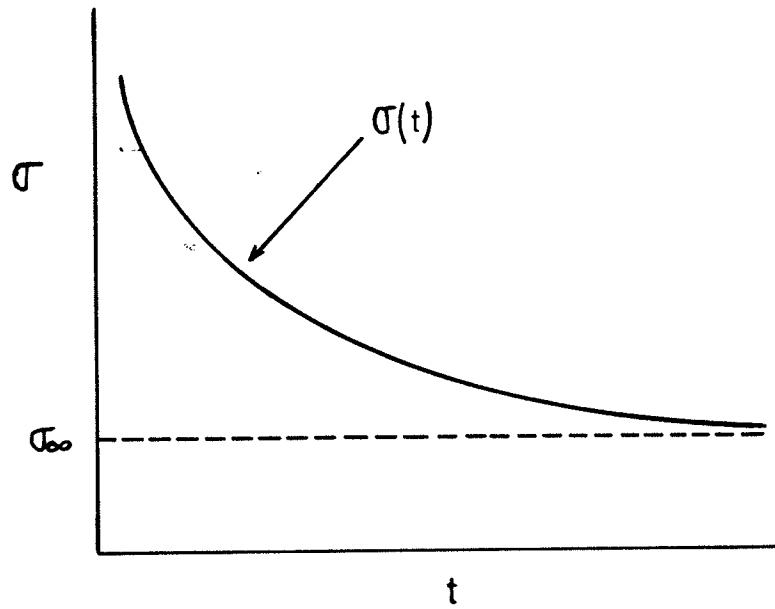


Fig.4.4.3 Continuous strength curve.
(after Vyalov,1963).

4.5 THE CONSTITUTIVE EQUATIONS OF FROZEN SOILS

In the literature, most of the constitutive equations of frozen soils under multiaxial state of stress were derived from the following expression (Odqvist,1966) :

$$\dot{\epsilon}_{ij}^c = F (J_2^s, J_3^s) \cdot S_{ij} \quad (4.4)$$

where

$\dot{\epsilon}_{ij}^c$ = creep rate tensor or
time rate of the infinitesimal
strain tensor

S_{ij} = deviatoric stress tensor
 J_2^S = second deviatoric stress invariant
= $1/2 S_{ij} S_{ij}$
 J_3^S = third deviatoric stress invariant
= $1/3 S_{ij} S_{jk} S_{ki}$

with

$$S_{ij} = \sigma_{ij} - \frac{1}{3} \sigma_{kk} \delta_{ij}$$

where

σ_{ij} = stress tensor

δ_{ij} = kroneckor delta

The basic assumptions used in the derivation of the constitutive equations are :

1. The material is incompressible which implies that no volume change occurs during creep.

2. The hydrostatic stress has no influence on the strain rates.
3. The true elastic deformation is much more smaller than the sum of plastic and creep deformation (Vyalov,1963; Ladanyi,1972).

Multiaxial experimental results are rare and therefore most of the creep equations of complex stress conditions in the literature were formulated using uniaxial creep test data. The constitutive creep equation for frozen soils is commonly represented empirically by a simple power law in the form

$$\dot{\epsilon} = A \sigma^n \quad (4.5)$$

where

$\dot{\epsilon}$ = axial strain rate

A = temperature dependent
deformation modulus

σ = axial stress

n = creep exponent

For multiaxial state of stress conditions, the equation may be written as (Vyalov,1962; Odqvist,1966)

$$\dot{\epsilon}_e = A \sigma_e^n \quad (4.6)$$

where

$$\begin{aligned} \dot{\epsilon}_e &= \text{equivalent strain rate tensor} \\ \sigma_e &= \text{equivalent stress tensor} \end{aligned}$$

The equivalent stress tensor, which is a function of deviatoric stress tensor only, is defined by the square root of the second invariant of deviatoric stress tensor multiplied by a constant. Similarly, the equivalent strain rate tensor, which is a function of shearing deformation only, is defined by the square root of the second invariant of shear strain rate tensor. Several different equivalent stress and strain rate tensors have been used in the literature, such as

		σ_e	$\dot{\epsilon}_e$
Odqvist	(1966)		
Ladanyi	(1972)	$\sqrt{3} \sqrt{J_2^s}$	$\frac{2}{\sqrt{3}} \sqrt{J_2^{\dot{\epsilon}}}$
Vyalov	(1963)		
Jessberger	(1978)	$\sqrt{J_2^s}$	$\sqrt{2} \sqrt{J_2^{\dot{\epsilon}}}$

Due to the stress raised exponentially in the simple power law, the different constants in the equivalent stress and strain rate tensors may result in a nonlinear relationship between stress and strain rate (Roggensack, 1977). The different experimental parameter, A, may be obtained for different equivalent stress and strain rate tensors, but the end result is the same.

Odqvist and Hult (1962) adopted the power law to generalize the creep equation for uniaxial and multiaxial state of stress, of nondamped creep behaviour of metallic materials. Assuming the validity of the Von Mises plasticity rule and the volume constancy for all plastic deformation including the creep deformation, the power law describing the steady state creep is expressed in terms of equivalent strain rate and stress as

$$\dot{\epsilon}_e = \dot{\epsilon}_c (\sigma_e / \sigma_c)^n \quad (4.7)$$

where

$$\sigma_c = \sigma_{cu} = \text{temperature dependent uniaxial creep parameter}$$

For axially symmetric state of stress, the equivalent strain rate becomes

$$\dot{\epsilon}_s = \dot{\epsilon}_c \left[\frac{\sigma_1 - \sigma_3}{\sigma_c} \right] \quad (4.8)$$

where

$$\sigma_1 - \sigma_3 = \text{principal stress difference}$$

The strain rate in Equations 6 and 7 are independent of hydrostatic pressure. The hydrostatic pressures influence not only the peak strength but also the stress-strain-strain rate behaviour in the pre-failure state of unconsolidated frictional earth materials (Vyalov et al,1962; Gorodetsky,1975; Ladanyi,1972) (Figure 4.5.1). The effect of confining pressures on creep and strength on frozen sand has been studied by Sayles (1972) and Alkire and Andersland (1973). Sayles(1972) reported that the creep strain can be reduced by increasing the confining pressure. In the finding of Alkire and Andersland study, they reported that the creep strain rate decreases exponentially with an increase in confining pressures.

Vyalov (1962) proposed that the strength of frozen soils can be represented by a set of failure envelopes of Mohr circles at failure, where each envelope corresponds to a given time to failure (Fig.4.5.2).

The creep strain equation in the pre-failure state as proposed by Vyalov (1978) has taken into the account of the effect of mean normal stress.

$$\epsilon_e = \left[\frac{C_\infty}{B} \right]^{1/m} \left[\frac{\sigma_e t^\alpha}{C_\infty + \sigma_m t \tan \phi_\infty} \right] \quad (4.9)$$

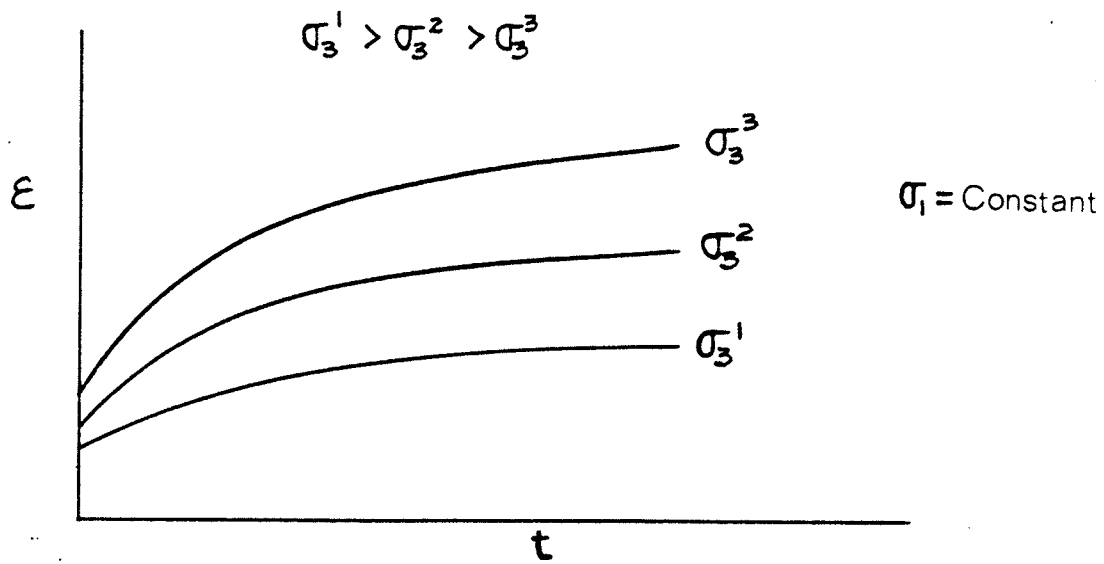


Fig.4.5.1 Effect of confining pressure on creep strain.
 (after Vyalov,1963).

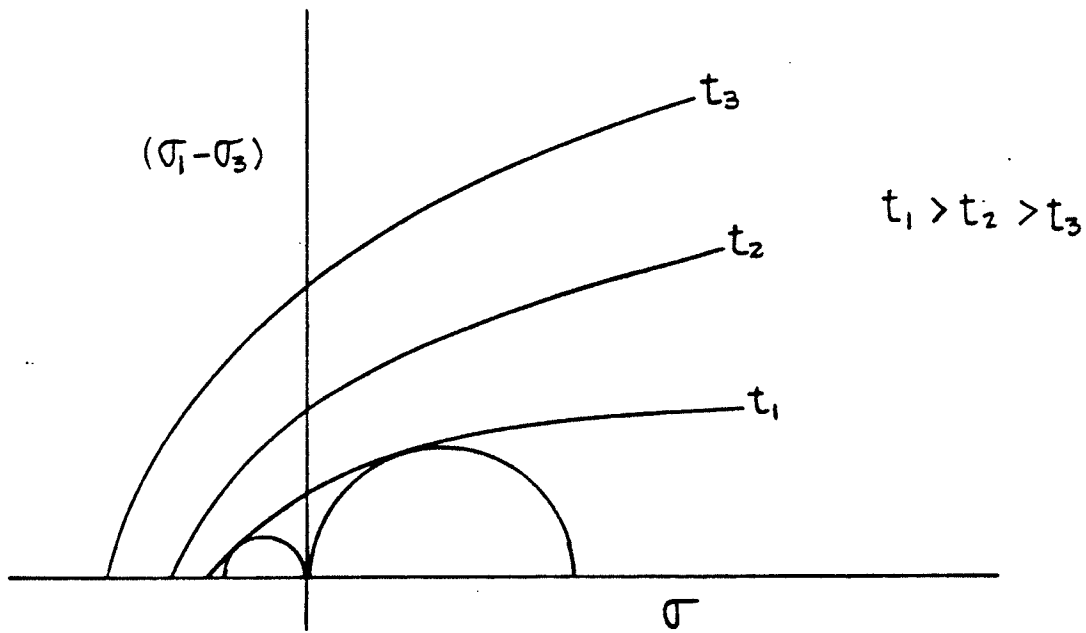


Fig. 4.5.2 Mohr circle failure envelope at each given time to failure.
 (after Vyalov,1963).

where

- C_{∞} = temperature dependent adhesion at $t = \infty$
- ϕ_{∞} = internal friction angle at $t = \infty$
- m = experimental creep exponents
- $B = \omega(1+\theta)^k$ = temperature experimental parameter
- α = material characteristic

For uniaxial state of stress, Equation 6 transforms into

$$\epsilon_e = \left[\frac{\sigma_e t^{\alpha}}{B} \right]^{1/m} \quad (4.10)$$

Ladanyi (1972) modified the equation originally proposed by Vyalov (1962) and Hult (1966) to account for the mean normal stress by using a two or a three parameter failure theory. Assuming the validity of Coulomb-Mohr failure criterion in the pre-failure state. The pre-failure steady state creep rate equation, for axial symmetry condition, was expressed in terms of mean normal stress and principal stress difference as :

$$\dot{\epsilon}(c) = \dot{\epsilon}_c \left[\frac{(f+2) (\sigma_1 - \sigma_3) - 3(f-1) \sigma_m}{3 \sigma_c} \right] \quad (4.11)$$

where

$$\sigma_c = \sigma_{cu} f(\theta)$$

and

$$f(\theta) = \left(1 + \frac{\theta}{\theta_c}\right)^\omega$$

$$f = \frac{1 + \sin \phi}{1 - \sin \phi}$$

$$\sigma_m = \frac{1}{3} (\sigma_1 + \sigma_2 + \sigma_3)$$

$\dot{\epsilon}_c$ = arbitrary strain rate

σ_c = creep modulus for a given $\dot{\epsilon}_c$

ω = temperature exponent

θ_c = 1°C

σ_{cu} = value of σ_c at $\dot{\epsilon}_c$ obtained from
uniaxial compression

Equation 11 assumes full mobilization of internal friction ($f = \text{constant}$) over the whole region of pre-failure state. The assumption leads to a non-zero strain rate at zero stress difference. This implies that the application of equation 8 should be limited either to strains close to failure or to those contained within a narrow range of mobilization of internal friction. The limitation may be overcome by assuming a time dependent internal friction. For frictionless soil, $f = 1$, the equation is the same as equation 5.

For frozen soils with low internal friction, Ladanyi (1972) proposed to use the extended von Mises failure criterion, a three-principal-stress failure criterion, to account for the effect of mean normal stress. For the case of axial symmetry, the steady state strain rate in the pre-failure state is written as

$$\dot{\epsilon}(c) = \dot{\epsilon}_c \left[\frac{(r+1) (\sigma_1 - \sigma_3) - 3 (r-1) \sigma_m}{2 \sigma_c} \right]^n \dots (4.12)$$

where

r = the ratio between uniaxial compression
and tension creep strength

As the same discussion before, equation 12 yields a non-zero strain rate at a zero stress difference with an assumed constant strength ratio r. The limitation may be overcome by assuming the mean normal stress has no effect on the strain rate in the pre-failure state, and only the creep strength is dependent on the mean normal stress.

Andersland and Alnouri (1970) proposed the steady state strain rate equation based on the exponential law to account for the effect of mean normal stress at intermediate or high stress levels. The strain rate equation for axially symmetric state of stress is written as

$$\dot{\epsilon}(c) = \frac{A \exp N (\sigma_1 - \sigma_3)}{F(T) \exp(M\sigma_m)} \quad (4.13)$$

where

A, N and M are experimental parameters and

$F(T) = \exp(L/T)$ and

$L = U/R$

$U =$ activation energy

$T =$ absolute temperature

$R =$ universal gas constant

Again, equation 13 subject to the same limitation as equations 11 and 12, if the creep exponent M is assumed to be constant.

Jessberger and Diekmann (1982) modified the equations originally proposed by Vyalov (1962) to account for the influence of confining pressure. The creep equation for axially symmetric state of stress and isothermal condition is written as

$$\dot{\epsilon}(c) = \left[\frac{\sigma_1 - \sigma_3}{E_k} \right]^\rho \quad \dots\dots\dots (4.14)$$

where

$$E_k = \text{triaxial modulus} \\ = (J \cdot \sigma_3^n \cdot t^s)^{-1/\rho}$$

and

ρ and s are material constants

j and n are temperature dependent parameters.

The creep equations proposed by Vyalov (1962), Ladanyi (1972), Andersland and Alnouri (1970), and Jessberger and Diekmann (1982) give zero strain when the stress is hydrostatic. Some recent studies show that the validity of the assumption of isochoric creep, i.e. no volume change, may have a rather restricted domain.

Baker et al (1981) conducted triaxial compression tests with volume-change measurement on frozen Ottawa sand at -6°C . The finding of the study reported that 2 % volumetric strain developed in the sample when the axial strain was 6.5 %, and this was corresponded to a strain rate of 10^{-4} sec^{-1} . At low strain rate ($< 10^{-6} \text{ sec}^{-1}$), the volume change was negligible.

A separate study by Bragg and Andersland (1982) who conducted constant-stress uniaxial creep tests on frozen sand at -6°C . The axial and volumetric strain were measured during the tests. They found that the volumetric strain developed in the sample was negligible when the axial strain was less than 2 %. But the volumetric strain could approach half the value of the axial strain when the axial strain was above 5 %.

CHAPTER 5

TESTING PROGRAM

5.1 INTRODUCTION

This study is part of a broader investigation by the Geotechnical group at the University of Manitoba into the long-term multiaxial creep behaviour of frozen saline soils that simulate those beneath the Beaufort Sea. The seabottom permafrost in the Beaufort Sea, as mentioned in previous chapters, was either ice-bonded or non ice-bonded saline mixtures of sand, silt or clay. Because of the prohibitive cost of sampling the seabottom permafrost, artificially prepared samples were used in the first stage of the research program. Uniform sandy silt was used, and the properties were somewhat similar to sediments which have been encountered in the Beaufort seabottom. Isotropic compression tests with volume-change measurements were conducted on the samples. The data was used to model creep behaviour under isotropic compression and to obtain a pseudo-elastic bulk modulus to be used in Domaschuk's method of estimating settlements of artificial islands in the Beaufort Sea. Domaschuk's method is an extension of that which Domaschuk and Valliappan (1975) developed to provide a nonlinear approximate solution to the ultimate settlement of structures on clay. A brief review of Domaschuk's method is given in the following paragraphs.

The constitutive equation for an isotropic linearly elastic solid may be written in terms of the bulk modulus K and shear modulus G as

$$\sigma_{ij} = K \epsilon_{ii} \delta_{ij} + 2G (\epsilon_{ij} - \frac{1}{3} \epsilon_{kk} \delta_{ij}) \dots\dots\dots (a)$$

where

- σ_{ij} = ijth stress component
- ϵ_{ij} = ijth strain component
- δ_{ij} = kronecker delta
- $\frac{1}{3} \epsilon_{ii}$ = mean normal strain component

Similary, displacement equations can also be written in terms of deformation parameters (K and G). For example (Domaschuk and Wade, 1969), the displacement equation of a circular loaded area on soil may be expressed in terms of K and G as

$$W_z = Pa_1 \left[\frac{1}{2G} \sin \delta + \left(\frac{27K^2}{6K+2G} \right) \left(\frac{1-\cos\delta}{\sin\delta} \right) \right] \dots\dots\dots (b)$$

where

- w_z = displacement in z direction
- p = uniform circular distributed load

$$\begin{aligned} z &= \text{depth} \\ a_1 &= \text{radius of circular area} \\ &= \arctan (a_1 / z) \end{aligned}$$

Strictly speaking, Equations (a) and (b) apply only to a linear elastic solid undergoing small deformations. But Domaschuk and Valliappan method stepped beyond the linear elasticity. The deformation parameters (K and G) were no longer taken as constants, but they were stress state and soil properties dependent. This method showed that the linear elasticity approach when combined with the finite element method could be used to provide a nonlinear approximate solution to the ultimate settlement of structures resting on clay. The bulk and shear moduli solutions were obtained independently by drained triaxial compression tests. Isotropic compression tests were used to determine the bulk modulus, and constant-mean-normal stress triaxial compression tests were used to determine the shear modulus. Solutions for these two parameters were developed in terms of soil properties and prevailing state of stress.

In the writer's program, only isotropic compression tests were conducted on the artificially prepared saline samples. Sample preparation, testing equipment, testing procedures and test results are presented in this chapter.

5.2 SAMPLE PREPARATION

In order to investigate the creep behaviour of frozen saline soils under isotropic compression, the prepared samples had to be reproducible. Sample preparation techniques as described by Baker (1976) were adopted in this study. Properties which affect the mechanical behaviour of frozen soils are nonhomogeneity, grain size distribution, moisture content (unfrozen water content and / or ice content), anisotropy, density and chemical content. In the study, the frozen soil specimens were prepared to approximately the same density, salt content and moisture content.

A non-plastic glaciolacustrine silt consisting of 34 % sand, 56 % silt and 10 % clay was used in the study. The grain size distribution is shown in Figure 5.2.1. This silt was classified as highly frost susceptible (Charleson, 1981). The silt has specific gravity of 2.71 and a standard proctor optimum moisture content of 15 %, and a standard proctor density of 18.5 KN/m^3 .

5.2.1 METHOD OF SAMPLE PREPARATION

The method of specimen preparation, which includes compaction, saturation and freezing, is described below:

1. COMPACTION

A plexiglass split mould with two end caps, developed by Baker (1976), was modified for preparation of cylindrical frozen specimens. The

split mould assembly is shown in Figure 5.2.2 and further details are given in Appendix IV. An aluminum cylindrical rod, 32 mm. in diameter and 175 mm. in length, was used as a tamper for compaction of the sample.

The sample consisting of approximately 1500 g. of dry silt, mixed with saline water (water content =15 % and salt content =1.5 % by weight of dry soil), was formed by compacting 25 mm. thick layers in the split mould. Forty drops of the tamper for each layer was necessary to achieve the desired proctor dry density of 16.6 KN/m^3 . The compacted specimens was approximately 76 mm. in diameter and 210 mm. in height. The properties of the specimens after compaction are presented in Table 1 .

2. SATURATION

The compacted specimens were saturated under a 610 mm. head of water. Air in the sample was removed under vacuum. The vacuum was left on for four hours or until a layer of water drawn by vacuum covered the sample. The purpose of using distilled water to saturate the sample was to dilute the pore fluid salinity to about 60 parts per thousand, which is approximately twice as high as normal sea water (30 ppt).

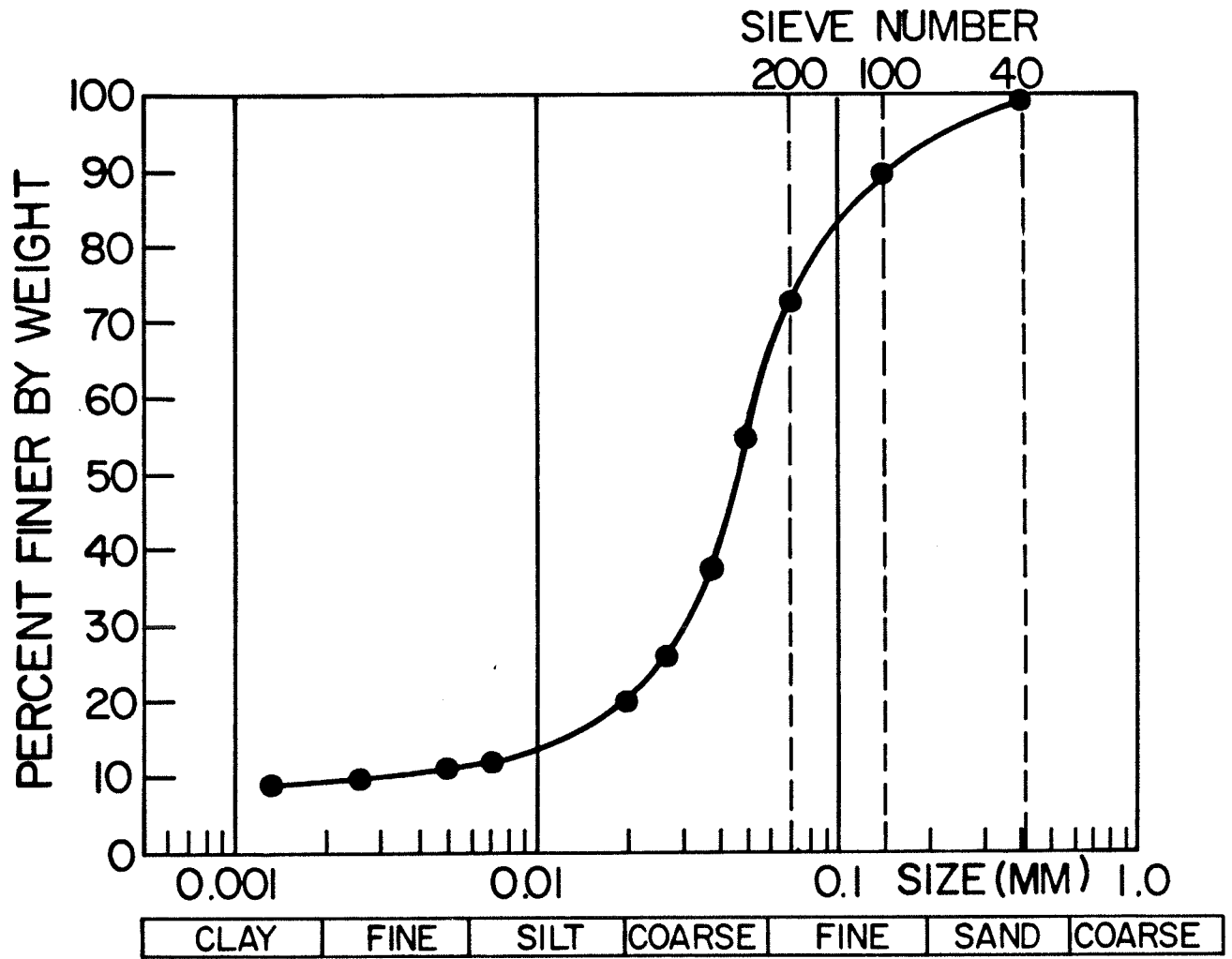
After compaction, a porous stone was placed on top of the compacted specimen. The top end of the split

mould was then tightened by four bolts, and the piston with a plexiglass top cap was lowered and locked to the porous stone. The control valve was opened to allow distilled water to flow into the sample, and a low suction pressure was applied through the top. The saturation system is shown in Figure 5.2.3. The saturation process was completed within a period of 24 hours.

3. FREEZING

All the samples were frozen in the same manner. The split mould with its compacted-saturated specimen was placed in a wooden box. A thin access tube was attached to the hose fixture at the bottom of the mould to allow collection of any water expelled from the sample due to a build up of cryostatic pressure, or to act as free water supplied to the sample during freezing process. The water level was kept the same in the access tube and in the mould to prevent drainage prior to freezing. A heating cable was placed around the mould and the access tube to prevent freezing of water in the tube and to control the temperature around the mould. The temperature of the heating cable was controlled by adjusting the transformer which supplied power to the cable. This allowed control of the rate of freezing of the specimen.

To ensure uniaxial freezing of the specimen, vermiculite was carefully placed around the mould. The top end of the mould, the top cap and the porous stone were removed during freezing (Figure 5.2.4). Freezing of the specimen was carried out in a deep freezer at -25°C . Three thermocouples were placed along the wall of the mould. One was at the bottom of the mould, while the other two were 60 mm. and 120 mm. from the bottom of the mould. Thermocouples were connected to a thermal reader with a read-out accuracy of $\pm 0.3^{\circ}\text{C}$. The rate of freezing of the sample was determined from thermocouples readings. The average freezing rate of the specimen was about 25 mm. per day. After the samples were frozen, they were chilled to one or two degrees Celsius below the proposed test temperature. No ice lens formation was observed in all of the samples with the exception of Sample A06 during freezing, but an increase in volume of specimens occurred due to the phase change.



MIT GRAIN SIZE CLASSIFICATION

Fig.5.2.1 Grain size distribution curve.

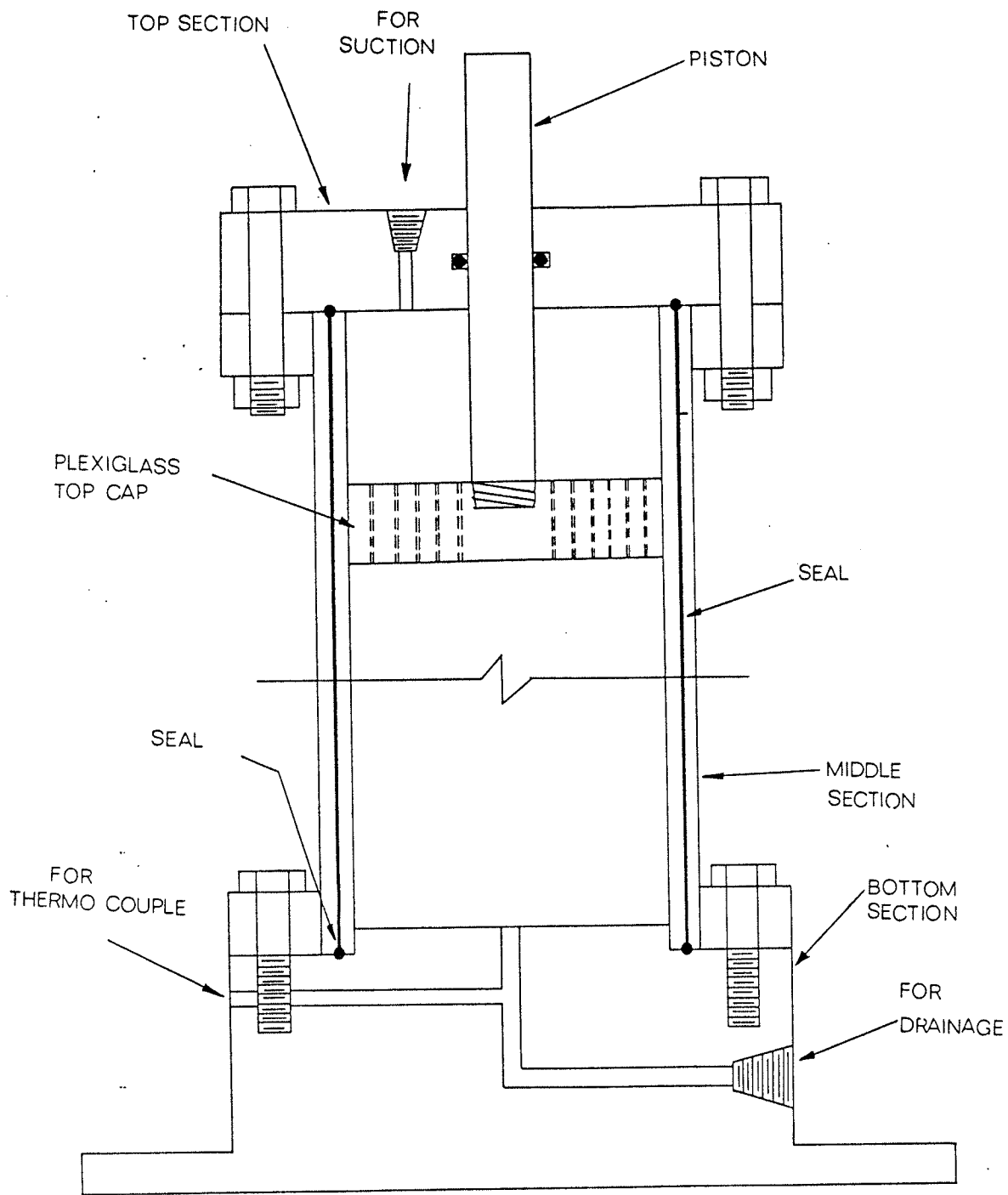


Fig.5.2.2 Plexiglass split mould.

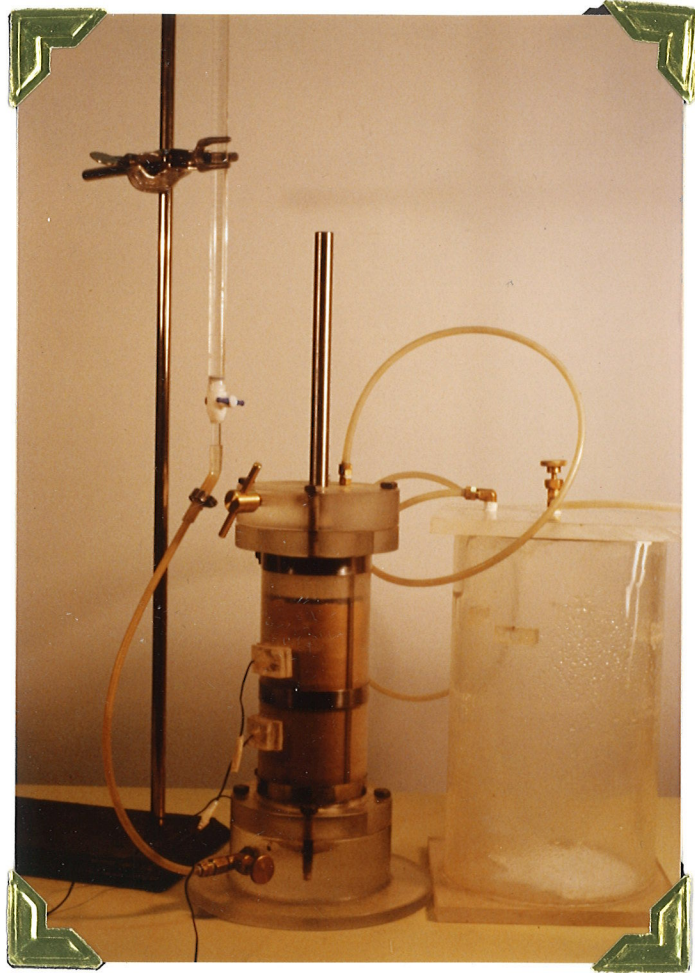


Fig.5.2.3 Sample saturation system.

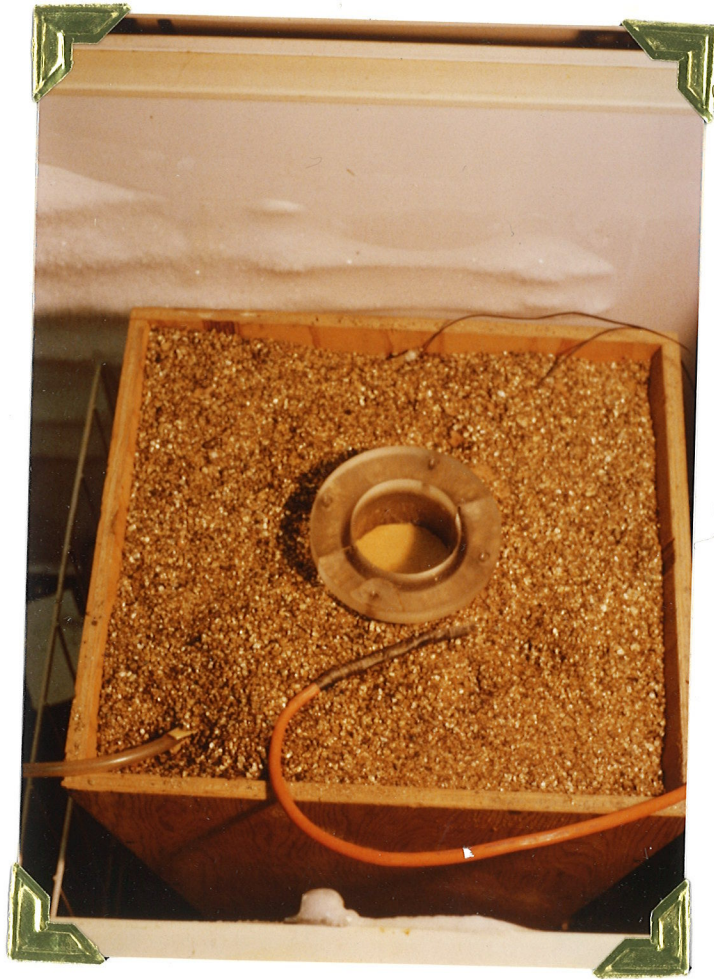


Fig.5.2.4 Freezing of specimen.

5.3 TESTING EQUIPMENT

A double-walled triaxial cell similar to that developed by Mitchell and Burn (1971), and later modified by Baker et al (1981), was used. Further modifications were done in the University of Manitoba, Department of Civil Engineering machine shop to suit this research program. The triaxial testing system is shown in Figure 5.3.1. Details of the design and modifications are given in the Appendix III.

The double-walled triaxial cell used is shown in Figure 5.3.2. No drainage was provided through the pedestal, but three air-dried porous stones were placed on top of the pedestal to collect any drainage. An O-ring provided a seal between the cell base and cylinder, which was clamped to the cell base with six bolts. The inner cylinder was tightened by four steel rods with nuts on top of the cover. To ensure that no leakage occurred, an O-ring seal was placed in between the inner cylinder and top cover, as well as the inner cylinder and cell base. The outer cylinder was installed before the inner cylinder.

During most of the testing, the cell pressure was supplied by an air-line and regulator system. The air-line provided constant pressure up to 700 kpa. Pressures above this were supplied by a tank of dry-pressurized nitrogen gas. The disadvantage of using an air-line was that moisture in the air could freeze and subsequently plug the pipe. Dry air is recommended for future research. The cell pressure was moni-

tored by pressure transducers and a calibrated digital voltmeter (DVM, electrical signal conditional). One pressure transducer was attached to one of the cell drainage leads and the other one was attached to the volume-change measurement device drainage lead. The pressure transducers were calibrated by using a gradual mercury column which, when coupled with the signal conditional DVM, provided an accuracy to within ± 1.0 kpa. . The pressure transducers were calibrated prior to each test.

The volume-change measurement device (VCMD) was designed to measure the volume displacement of the triaxial cell fluid automatically. The antifreeze (ethylene glycol) level in the VCMD was kept at the same level as in the triaxial cell. One direct current displacement transducer (DCDT or LVDT) connected to an Hp digital multimeter was used to measure the plexiglass float movement in the VCMD. The antifreeze used in the testing was compressible and sensitive to temperature. Because pressure and temperature fluctuations caused the fluid and the apparatus to contract or expand, it was necessary to calibrate the glass float movement for each temperature increment. The LVDT calibrations are given in Appendix II.

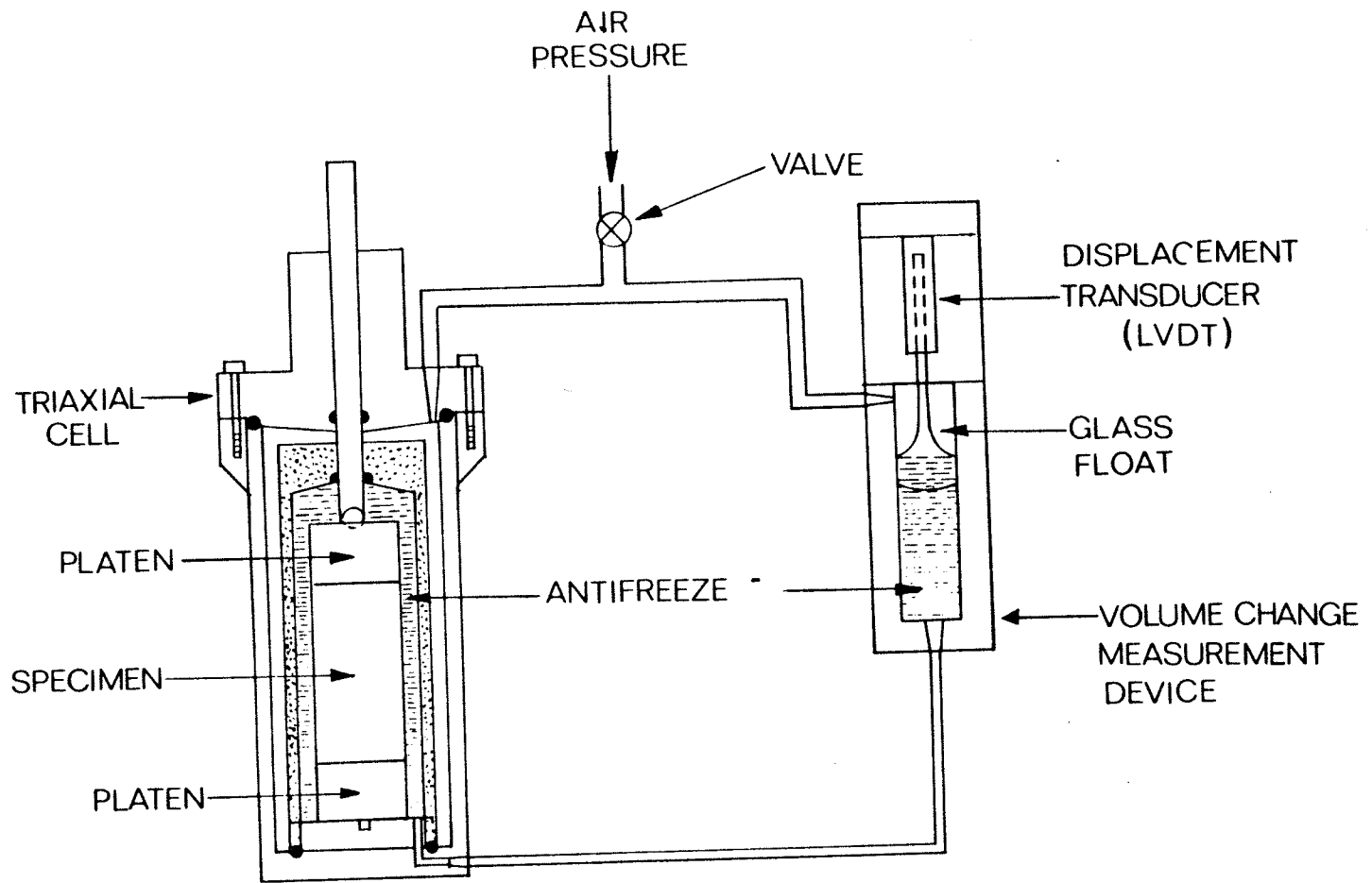
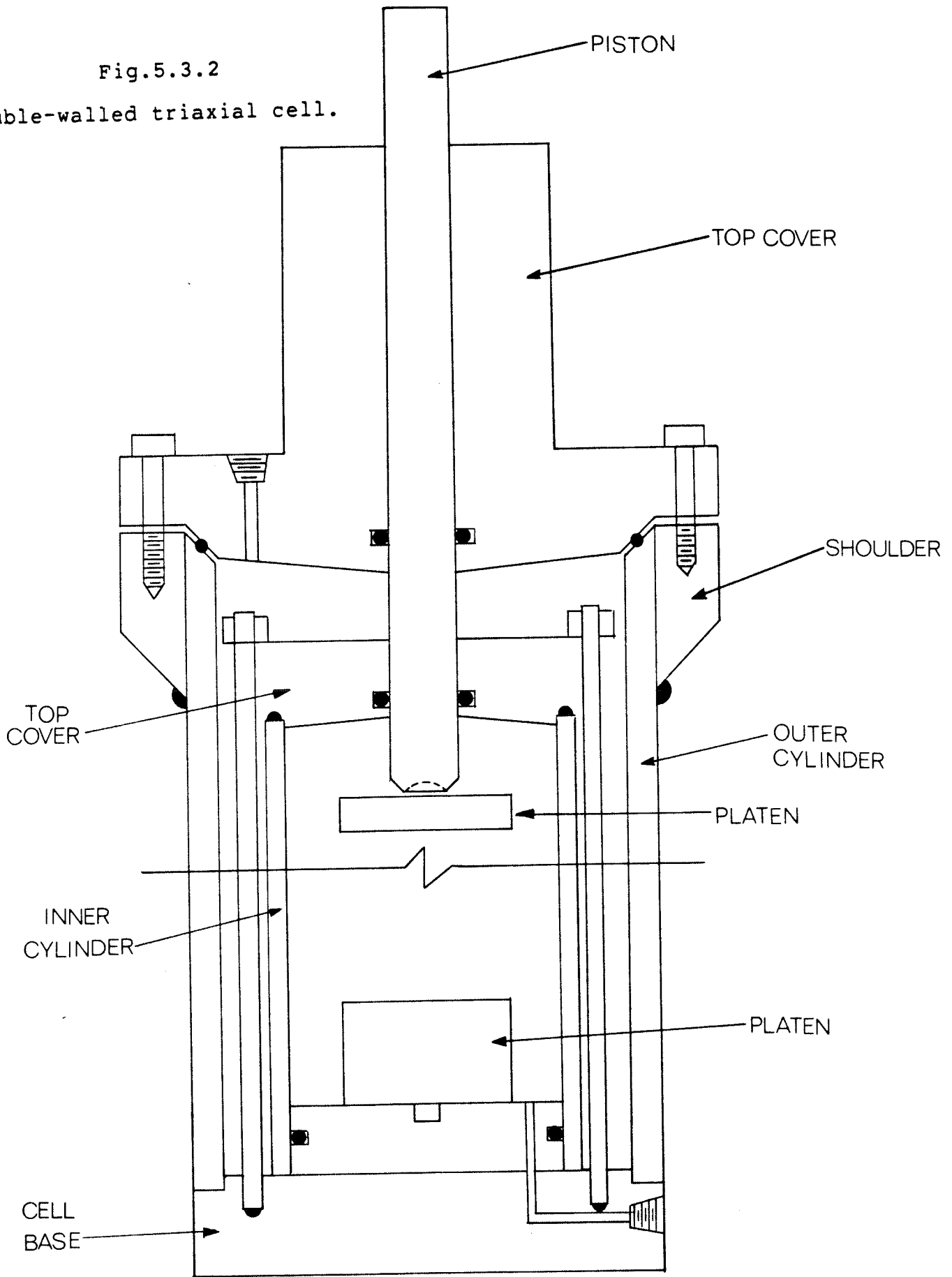


Fig.5.3.1 Triaxial apparatus assembly.

Fig.5.3.2

Double-walled triaxial cell.



5.4 SAMPLE TRIMMING AND BUILDING-IN PROCEDURES

In any laboratory testing program it is important to have a complete set of the necessary equipment prepared in advance. It is especially true in frozen soil testing since the time of sample exposure during trimming and building-in must be kept to a minimum. This section presents the step by step procedures used in equipment preparation, sample trimming and sample building-in.

1. Sample trimming and building-in equipment was assembled.

A) Sample trimming equipment

one hack saw

one steel split mould with 76 mm. inner diameter

and 152 mm. in length

two weighed tares

B) Sample building-in equipment

three 76 mm. diameter porous stones

one 76 mm. diameter rubber membrane (natural)

five 76 mm. diameter rubber O-rings (neoprene)

one 76 mm. diameter steel top cap

one membrane stretcher.

2. The deaired antifreeze was prepared.
3. The top covers of the inner and outer cylinders, the inner cylinder, the piston and the pedestal were removed from the triaxial cell.

4. The deaired antifreeze and all the equipment were kept in the cold room at the test temperature for at least 24 hours prior to sample trimming.
5. A frozen sample was prepared.
6. The frozen sample was placed in the steel split mould and trimmed to the required length.
7. The porous stone was removed from the bottom end of sample.
8. The trimmed sample was removed from steel split mould and wrapped with saran wrap.
9. The sample was left in the freezing chamber for at least an hour to ensure that any thermal disturbance induced by trimming was eliminated. The sample was weighed before building-in.
10. The trimmings were collected for determining the ice content of the sample.
11. Three porous stones were placed on top of pedestal and the trimmed sample with the top cap in place was placed on the pedestal. A layer of lubricant was placed between the top cap and the sample (thickness of lubricant was about 0.5 mm. thick).
12. Five rubber O-rings were put on the bottom half of the membrane stretcher, along with one thin rubber membrane.
13. The membrane stretcher was lowered over the pedestal and the membrane was placed on the sample, with three

O-rings at the bottom just below the porous stones and two O-rings at the top, just above the sample.

14. The outside of the membrane was moistened with anti-freeze to eliminate any entrapped air between the O-rings and membrane.
15. The pedestal, sample and top cap was lowered into the triaxial cell and was properly seated on the base.

Note : Care was taken to ensure that the pedestal, sample and top cap was slowly lowered to the bottom of the cell without dropping.

16. The inner cylinder was lowered onto the cell base.
17. The inner cylinder top-cover was placed on top of the inner cylinder and was tightened with four brass screws.

Note : Care was taken to ensure that the inner cylinder sat properly on the cell base and that the O-ring seal in the top-cover was in proper contact with the inner cylinder, otherwise leaks would occur during testing.

18. The inner cell was filled three-quarters full with deaired antifreeze.
19. The piston was greased with lubricant (silicone oil).
20. Four 30-mm. diameter rubber bushings were placed on the top of outer cylinder and the top-cover of the outer cylinder was put on top of them.

21. A measuring stick was inserted into the piston hole to record the height from the steel ball to the top of the outer cylinder top-cover. This height was marked onto the piston.
22. The piston was inserted into the piston hole to the ball bearing.
23. The rest of the inner cell was filled with antifreeze until the fluid began to flow from the bleed valve.
24. The bleed valve was plugged with a brass nut.
25. The rubber bushings were removed and the top-cover was lowered on top of the outer cylinder and it was tightened with four screws.
26. The volume-change measurement device was filled with deaired antifreeze to the same level as the height of the antifreeze in the triaxial cell.
27. A small amount of pressure, about 7 to 15 kpa., was applied to check for any leakage of system.
28. If no leakage was observed, the sample was ready for the first pressure increment of loading.

5.5 TESTING PROCEDURE

Single-step and multi-step cell pressure increments were applied to the samples at test temperatures of -15°C , -10°C , and -5°C . One Sample, A02, was tested using ten pressure increments of 70 kpa. each while the temperature was held at -15°C . Before the application of each subsequent pressure

increment, the sample was allowed to compress until no further volume change could be measured. After the multi-step test on the sample at -15°C was completed, the pressure was released, and the sample was allowed to recover. Then the test temperature was raised from -15°C to -10°C , and the temperature of the sample was assumed to reach equilibrium after 24 hours. Another multi-step creep test, which followed the procedure of the -15°C test described above, was conducted on Sample A02 at -10°C . By using the same procedure, another multi-step test was repeated on Sample A02 at -5°C .

Another sample, A06, was tested using five pressure increments of 140 kpa. each at the temperature of -15°C . Two additional tests were carried out on two other samples, A07 and A08, using pressure increments of 350 kpa. and 700 kpa. respectively. A simplified numbering system was adopted for identification of each test. The first three digits identify the sample number, and the last three digits identify the temperature and pressure increment of the test. For example, A0215-2 refers to the second pressure increment ($n=2$) of the multi-step test on Sample A02 conducted at -15°C .

In each test the sample properties before and after testing were determined. Hence the amount of unfrozen pore fluid was not determined and the samples were assumed to be totally frozen. All the samples were not at 100 % saturation after freezing. Details of the sample properties before and

after testing are given in Table 5.1, and the details of the volume change and recovery are given in Table 5.2.

Table 5.2
Sample Volume change and Recovery

SAMPLE NO.	V_0 (CC.)	ΔV_{wt} (CC.)	V_{NR} (CC.)	ϵ_V^∞ (%)	ϵ_p (%)
A0215	644.16	28.27	9.39	4.39	1.46
A0210	634.77	15.66	7.64	2.47	1.20
A0205	627.13	15.35		2.45	

V_{NR} = Non recoverable volume change

ϵ_p = Non recoverable part of the ultimate volumetric strain

Table 5.1
Sample Details

	SAMPLE NO.	A0215	A0210	A0205	A0715	A0815	A0615
C O M P A C T E D	W (%)	13.9	—	—	15.1	14.9	14.9
	γ (KN/m)	16.9	—	—	16.4	16.6	16.9
	e	0.59	—	—	0.65	0.62	0.59
	S (%)	64	—	—	63	65	68
	NaCl (ppt)	97	—	—	90	91	92
B E F O R E	W (%)	22.4	—	—	20.8	17.7	18.0
	γ (KN/m)	14.8	14.9	15.0	15.7	16.2	16.5
	e	0.82	0.79	0.77	0.71	0.66	0.63
	S (%)	81	—	—	87	79	84
	NaCl (ppt)	63	—	—	67	78	77
A F T E R	W (%)	—	—	21.7	20.3	17.6	18.0
	γ (KN/m)	—	—	15.6	16.1	16.5	16.8
	e	—	—	0.72	0.66	0.63	0.66
	S (%)	—	—	82	83	76	81

5.6 TEST RESULTS

During the isotropic compression test, the sample volume change was recorded at regular time intervals for each stress increment and was converted to volumetric strain. The volumetric strain at any time t during the stress application was defined as

$$\epsilon_v = - \left[\frac{V(t) - V(0)}{V(0)} \right] \quad (5.1)$$

where

t = time elapsed from time $t = 0$

$V(t)$ = volume of sample at time t

$V(0)$ = original volume of the sample

The ultimate volumetric strain ϵ_v^∞ of a sample was defined as

$$\epsilon_v^\infty = - \left[\frac{V_\infty - V(0)}{V(0)} \right] \quad (5.2)$$

where

V_∞ = the volume at the end of each stress increment

Figure 5.6.1 shows the volumetric strain-time graphs of three multi-step tests on Sample A02 under test temperatures of -15°C , -10°C and -5°C . The start of each stress increment is indicated by an arrow. Samples A07 and A08 were tested at a temperature of -15°C under isotropic stresses of 350 kpa. and 700 kpa. respectively. Figure 5.6.2 shows the volumetric strain-time graphs for Sample A0715, A0815 and the first-step of Sample A0215 which was tested at -15°C . As can be seen from Figures 5.6.1 and 5.6.2, the volumetric strains of the samples were time dependent. For each stress increment most of the volumetric strain occurred within a relatively short period of time following the stress application. This initial deformation may be attributed to the instantaneous compression of the gaseous phase, elastic compression of the solid particles and some particle reorientation.

5.6.1 EFFECT OF STRESS REPETITION

From Figure 5.6.1, it can be seen that the volumetric strains of samples during the second stress increment were generally larger than during the first increment for all three temperatures. Thereafter the volumetric strain per stress increment generally decreased with each stress increment. One exception was the tenth stress increment for Sample A0205.

5.6.2 EFFECT OF TEMPERATURE

Samples tested at temperatures of -15°C and -10°C were ice-bonded and ice-poor. Sample A02 was non ice-bonded when tested under -5°C . Figure 5.6.1 shows that Sample A02 developed much larger volumetric strain at the temperature of -15°C than at the other two warmer temperatures of -10°C and -5°C . The total volumetric strains of Sample A02 when tested at two warmer temperatures (-10°C and -5°C) were about 45 % less than those tested at -15°C . This is contrary to the expectation that the warmer soil would be more compressible. This apparent anomaly is attributed to the fact that Sample A02 had been subjected to a history of loading and recovery before it was tested at the two warmer temperatures. The history of loading has two major effects on the sample, a strain hardening effect and an irrecoverable volume change effect under consolidation. Because of the loading history effect, no definite conclusion could be drawn from the results regarding the influence of temperature on the compressibility of the frozen soil under isotropic compression. For the same reasons no conclusion could be made regarding the difference in the responses of ice-bonded and non ice-bonded materials to isotropic compression. The total volumetric strains of Samples A0215, A0210 and A0205 after the completion of multi-step tests were 4.4 % , 2.47 % and 2.45 % respectively.

5.6.3 EFFECT OF STRESS INCREMENT

A comparison of the three single-step volumetric strain-time curves in Figure 5.6.2 indicates that the sample tested at the lowest stress level (A0215) required less time to achieve complete isotropic compression than the samples (A0715 and A0815) tested at higher stress levels. The magnitude of the volumetric strain varied with the applied pressure. The larger the applied pressure, the larger the volumetric strain.

Figure 5.6.3 shows the volumetric strain of a multi-step test on Sample A06 under a test temperature of -15°C . Five steps of stress increments were applied to the sample, and each stress increment was 140 kpa.. The sample was found to have a 1 mm.thick layer of segregated ice and in this way differed from the other samples. As seen from the figure, a large instantaneous deformation occurred in the first stress increment. The total volumetric strain of Sample A06 was 4.8 percent.

5.6.4 CREEP ANALYSIS

For creep analysis, the volume change was represented by an "incremental volumetric strain". For each stress increment the "incremental volumetric strain" was defined as

$$\epsilon_v^i = - \left[\frac{V(t) - V(0^-)}{V(0^-)} \right] \quad (5.3)$$

where

t = time elapsed since the increment
of stress in question

V(t) = volume of sample at time t

V(0⁻) = volume of sample just before the
increment of stress

The first step incremental volumetric strain of the multi-step test is the same as the volumetric strain defined previously. The incremental volumetric strain-time graphs for the first-step of the multi-step tests at three test temperatures are shown in Figure 5.6.4. The incremental volumetric strain-time graphs of the tenth step (n = 10) at temperature -15°C, the third step (n = 3) at temperature -10°C and the second step (n = 2) at temperature -5°C are shown in Figure 5.6.5 .

The incremental volumetric strain-time test data was fitted by an appropriate hyperbolic function of the form :

$$\epsilon_v^i = \frac{t}{a + bt} \quad (5.4)$$

where

a = initial tangent

b = reciprocal of the ultimate
value of ϵ_v^i

Both 'a' and 'b' were determined empirically for each curve. The hyperbolic function provided a good fit for the data with the exception of the first few hours after the stress application. The long-term deformation was the major concern in this study, and the hyperbolic model was to be considered suitable. Typical hyperbolic curve fittings are shown in Figures 5.6.4, 5.6.5 and 5.6.6 .

The results of the Sample A06 tested at a temperature of -15°C under stress increments of 140 kpa. were not used for comparative purposes, because of the samples high ice-content in relation to the other samples. The test data and incremental volumetric strain-time graphs for Samples A02, A06, A07 and A08 are given in Appendix I.

The incremental volumetric strain-time curves shown in Figures 5.6.4 , 5.6.5 and 5.6.6 indicate that with time the incremental volumetric strain initially decreased at a relatively rapid rate, then the rate of decreasing became very slow and approached zero. The creep rate $\dot{\epsilon}_v$ taken as the derivative of Eqn.(5.4) with respect to time is given by :

$$\dot{\epsilon}_v = \frac{\dot{\epsilon}_i}{(1 + bt \dot{\epsilon}_i)^2} \quad (5.5)$$

where

$$\dot{\epsilon}_i = 1/a = \text{initial creep rate}$$

The initial creep rate and parameters a and b for each curves are given in Table 5.3.

The creep rate-time curves of Sample A0215, A0615, A0715 and A0815 are shown in Figures 5.6.7 and 5.6.8. The creep rate was high right after loading, and decreased sharply as time proceeded. The long term creep rate approached zero for all the stress increments. As indicated from the figures the creep rate varied with applied pressure. The larger the applied pressure, the slower the creep rate would attenuate.

5.6.5 BULK MODULUS ANALYSIS

For the hyperbolic volumetric strain relationship, the time dependent bulk modulus is given as :

$$K(t) = \frac{\sigma_m (a + bt)}{t} \quad (5.6)$$

The values of time dependent bulk modulus computed from Eqn.(5.6) for three single-step tests were plotted against time in Figure 5.6.9. As can be seen from the figure, the bulk modulus decreased sharply in a period of time after loading (t < 30 hours), and became essentially constant . The values of bulk modulus computed from the Eqn.(5.6) for different stress increments and temperatures are given in Table 5.4.

In the previous section, ϵ_v^∞ was defined as the ultimate volumetric strain of the sample under a given increase in mean normal stress. Figure 5.6.10 shows the relationship between the ultimate volumetric strain and isotropic stress for Samples A0215, A0210 and A0205. The ultimate secant bulk modulus K_∞ of the sample in question is defined as

$$K_\infty = \frac{\sigma_m}{\epsilon_v^\infty} \quad (5.7)$$

Figure 5.6.11 shows the relationship of the ultimate bulk modulus with the isotropic stress for Samples A0215, A0715 and A0815. It suggests that the K_∞ of the Sample A0215 is approximately linear with isotropic stress. The K_∞ depends not only the ultimate isotropic stress but also on the loading history. For example, the K_∞ of Sample A0215 at isotropic stress of 350 kpa. depends not only on the additional 70 kpa., but also on that previously applied isotropic stress of 280 kpa. . The comparison of K_∞ on Samples A0215, A0715 and A0815 in Figure 5.6.11 suggests that the single-step loading and multi-step monotonic-increase loading might have approximately the same effect on samples. From the test data, no definite conclusion can be drawn on the effect of single-step and multi-step loading on ultimate secant bulk modulus.

For nonlinear relationship of ultimate strain and isotropic stress, the tangent bulk modulus may be defined as

$$K = \lim_{\Delta \epsilon_v^\infty \rightarrow 0} \frac{\Delta \sigma_m}{\Delta \epsilon_v^\infty} = \frac{d\sigma_m}{d\epsilon_v^\infty} \quad (5.8)$$

From Figure 5.6.13, it shows that the relationship of ultimate volumetric strain with isotropic stress can approximately be represented by two linear sections. This indicates that the tangent bulk modulus is constant when the ultimate isotropic stress is below 210 kpa., and becomes another constant when the isotropic stress exceeds 210 kpa.. Yet, from the test data, no definite conclusion could be drawn for the effect of temperature and stress increment on tangent ultimate bulk modulus.

Table 5.3

Hyperbolic Function Parameters

SAMPLE NO.	A0215			A0210			A0205		
	n	a	b	a	b	a	b		
1	20.2	49.4	1.57	19.6	50.9	2.28	3.1	322.2	2.48
2	19.9	50.2	1.27	16.7	59.7	1.80	60.6	16.5	2.21
3	12.0	83.2	1.64	5.7	175.3	2.44	18.1	55.1	2.74
4	7.5	134.0	7.24	3.3	305.5	9.90	3.6	281.9	4.51
5	11.8	85.0	3.19	1.4	718.3	4.2	3.0	337.6	7.04
6	7.3	137.9	2.54	0.6	1596.	9.45	2.0	513.5	7.51
7	1.9	532.6	2.91	0.5	2209.	5.77	0.4	2412.	9.83
8	3.6	279.4	2.34	0.2	4977.	4.31	0.9	1106.	5.35
9	2.6	387.3	3.92	0.1	6898.	9.84	0.9	1082.	9.10
10	2.3	436.6	3.91	0.4	2391.	4.73	2.2	456.2	2.28

Table 5.3 (Continue)
Hyperbolic Function Parameters

SAMPLE NO.	A0715			A0815		
	n	a	b	a	b	
1	2.9	343.3	0.47	16.6	60.2	0.26
2	3.1	322.2	2.06	4.7	210.9	1.38

Table 5.4
Values of Long-term Bulk Modulus

TEMP.	SAMPLE	ISO.STRESS	K (T>30 hr.)
-15 C	A0815	700 kpa.	20000 kpa.
-15 C	A0715	350 kpa.	20000 kpa.
-15 C	A0215	70 kpa.	11100 kpa.
-10 C	A0210	70 kpa.	16100 kpa.
-5 C	A0205	70 kpa.	17900 kpa.

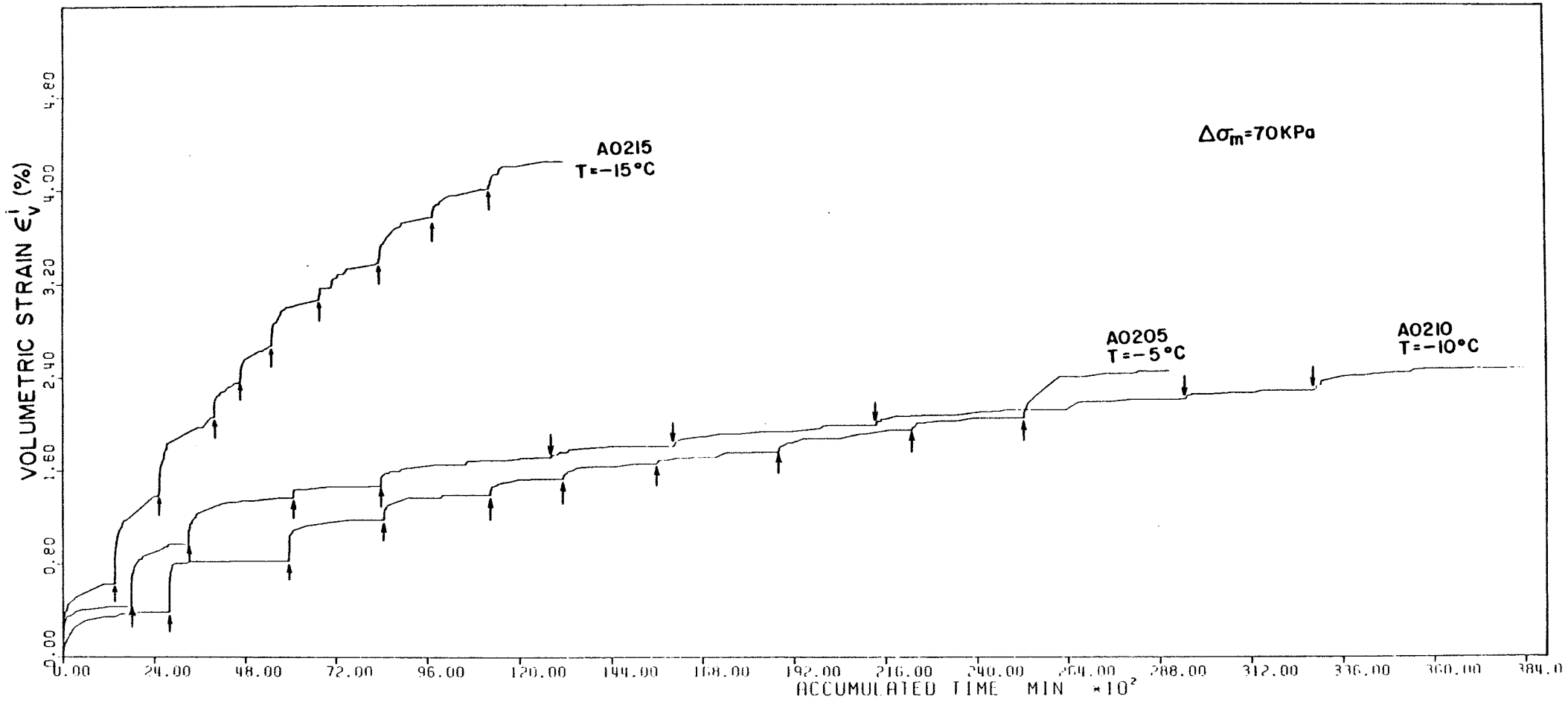


Fig. 5.6.1 The volumetric strain-time graphs of the multi-step tests on sample A02.

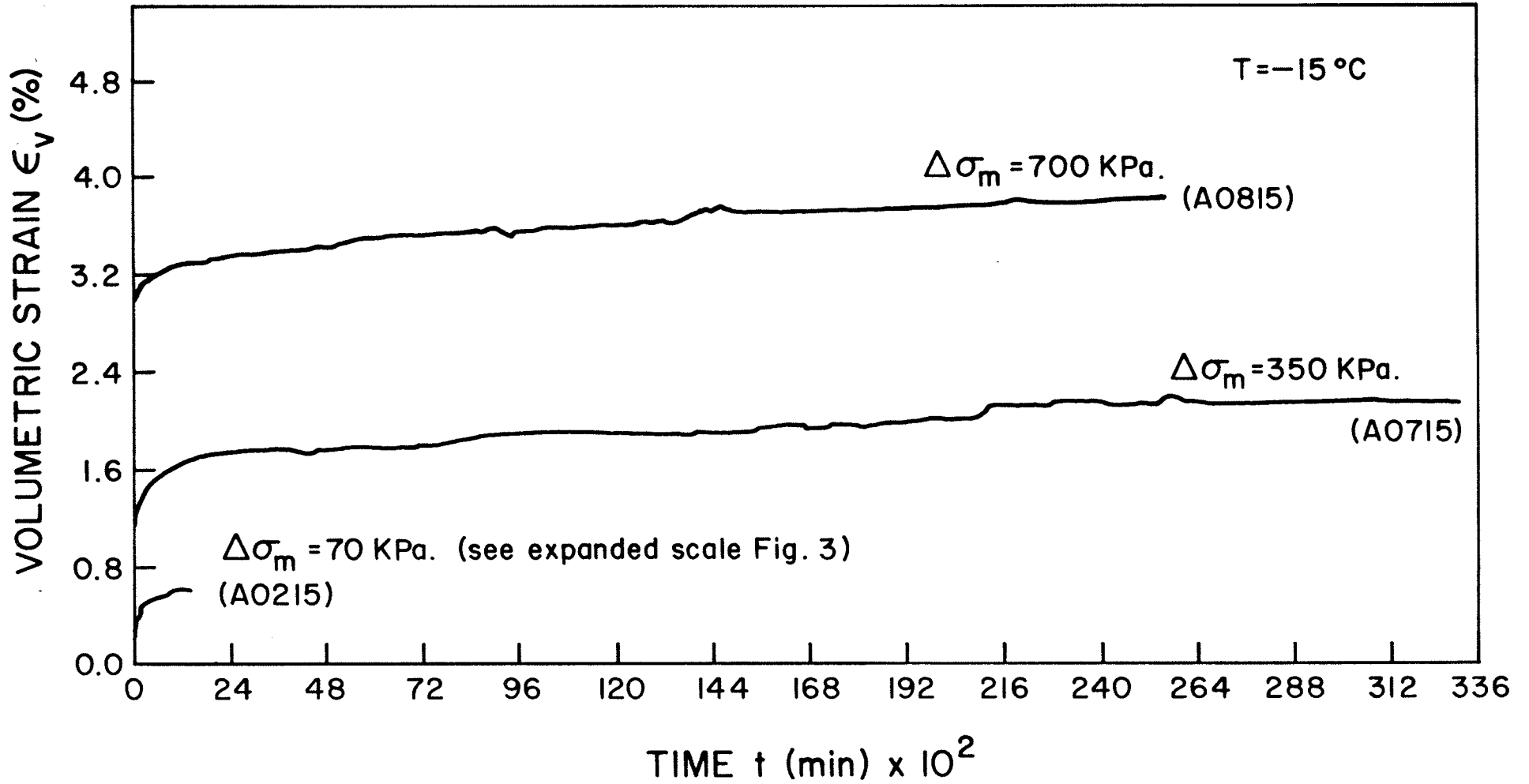
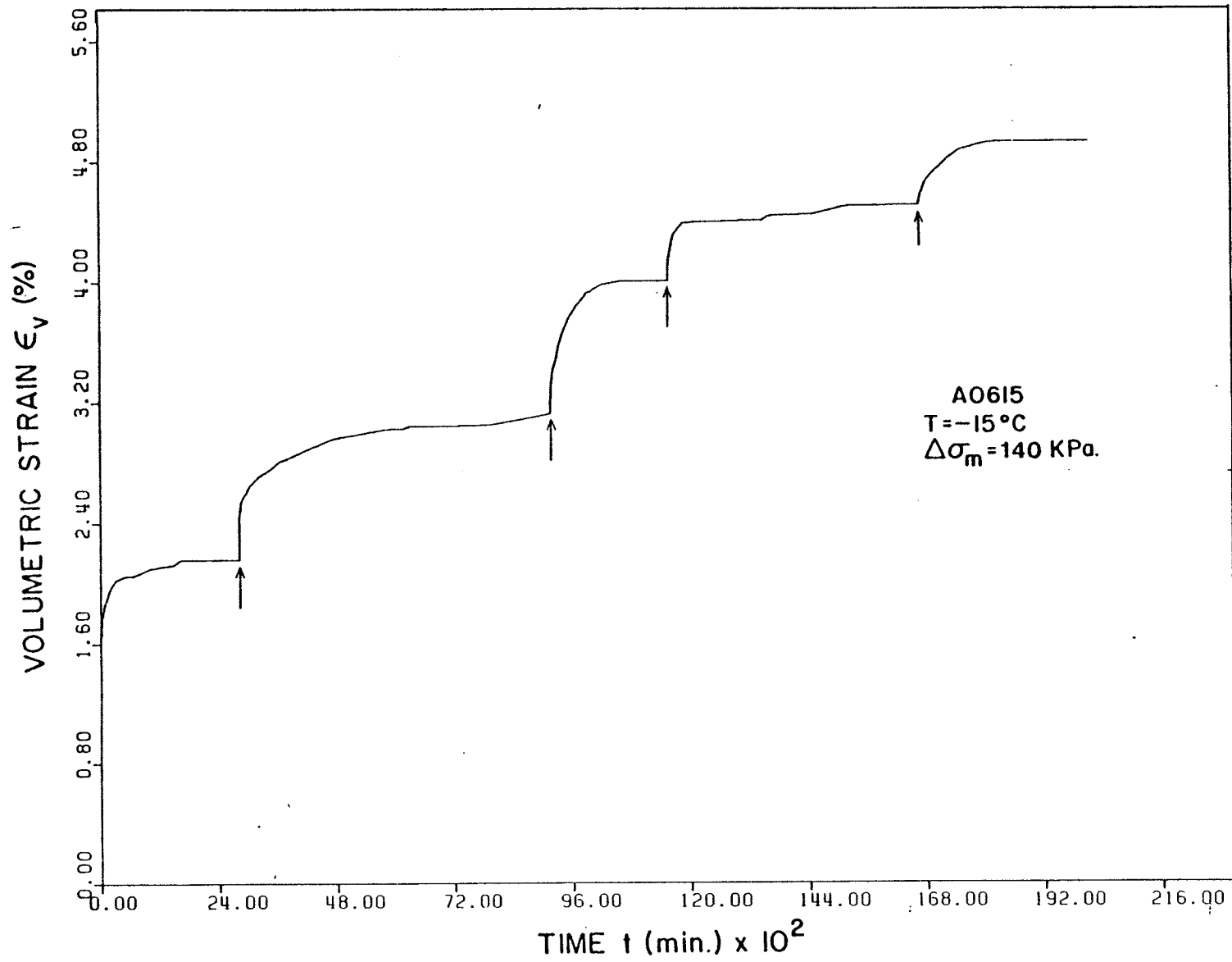


Fig. 5.6.2 The volumetric strain-time graphs of the single-step loading tests.

Fig. 5.6.3 The volumetric strain-time graphs of the multi-step test on sample A06.



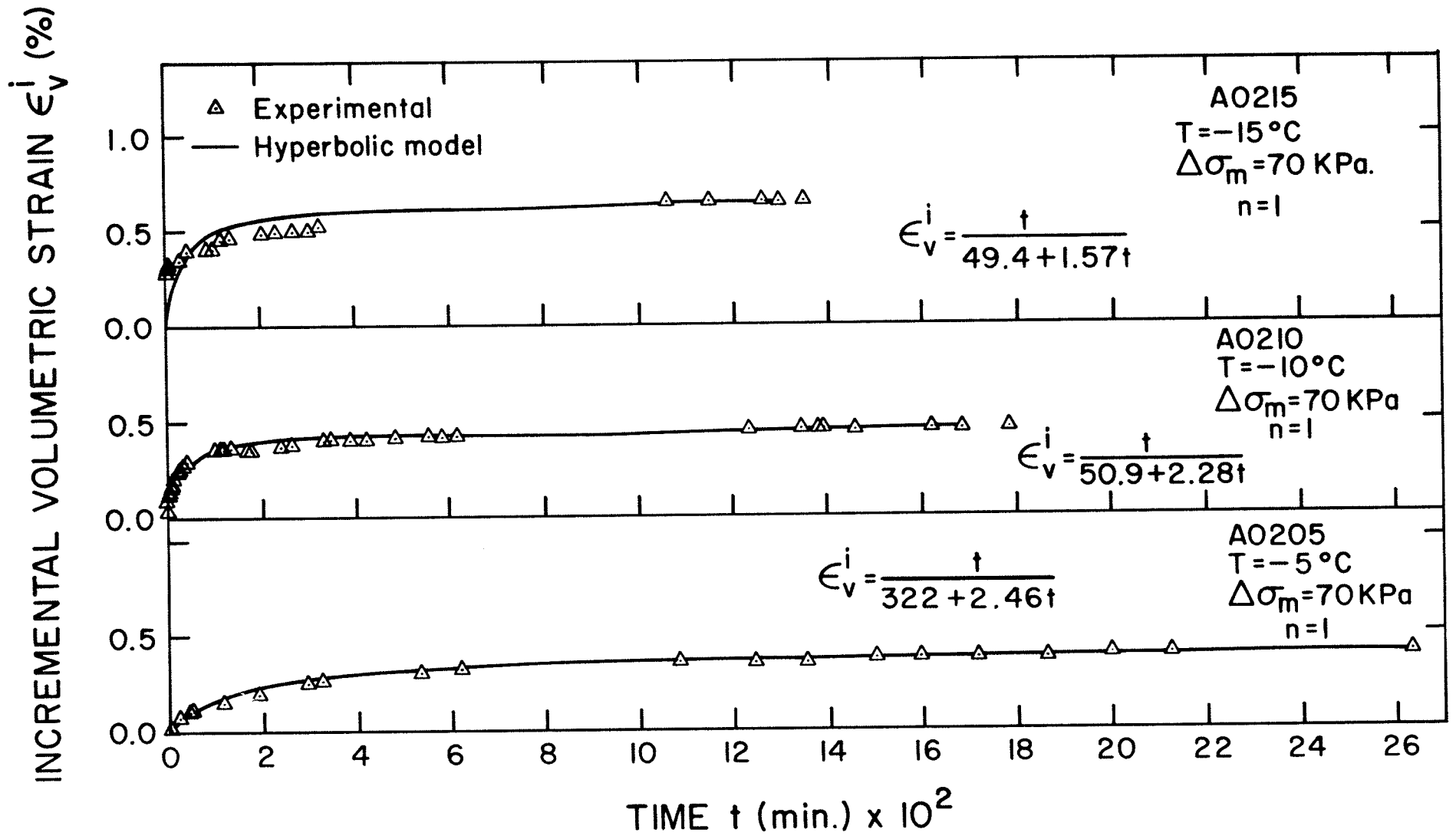


Fig. 5.6.4 The incremental volumetric strain-time graphs of the first-step of multi-step loading tests on sample A02.

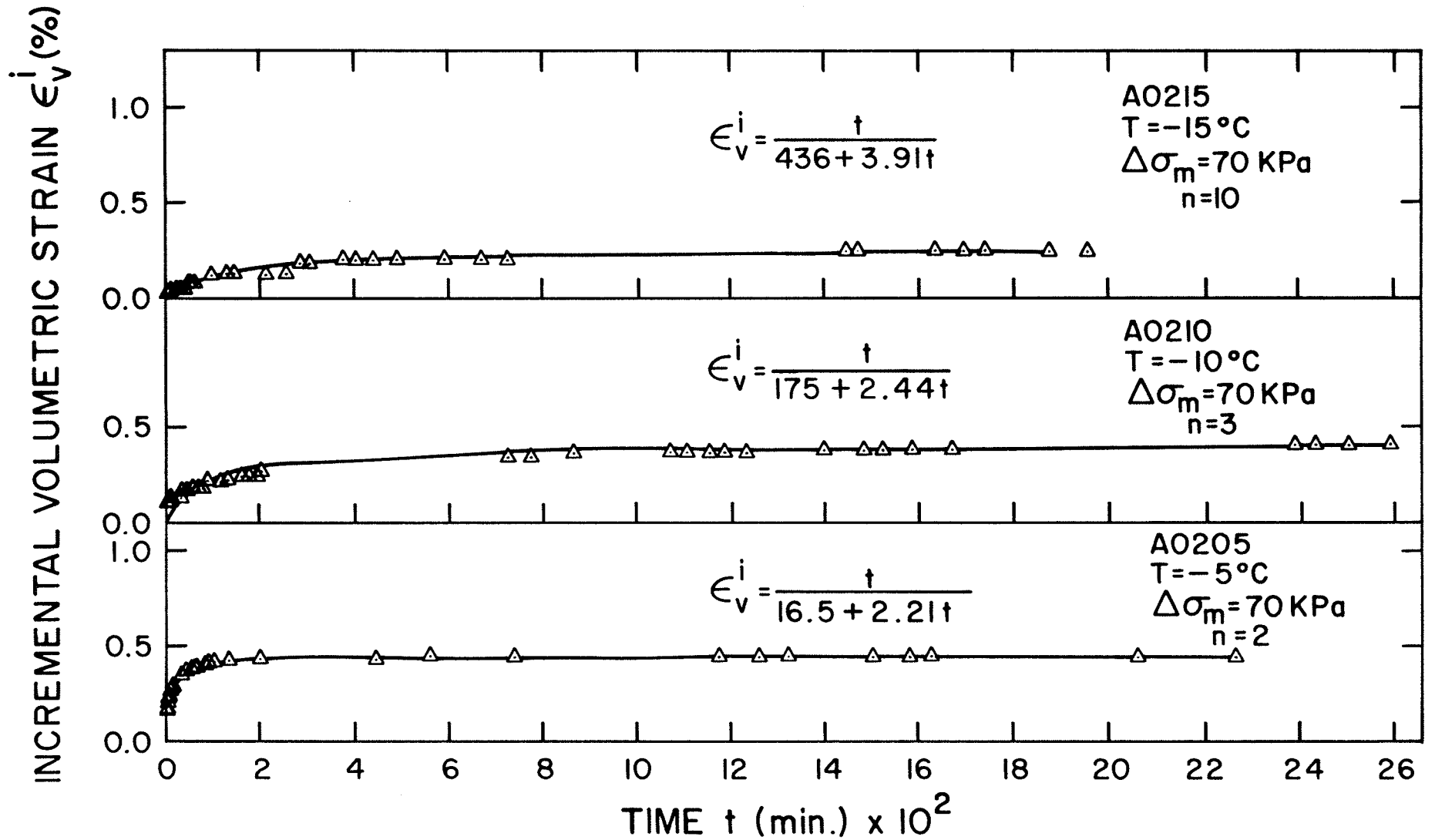


Fig. 5.6.5 The incremental volumetric strain-time graphs of the nth-step of the multi-step loading tests on sample A02.

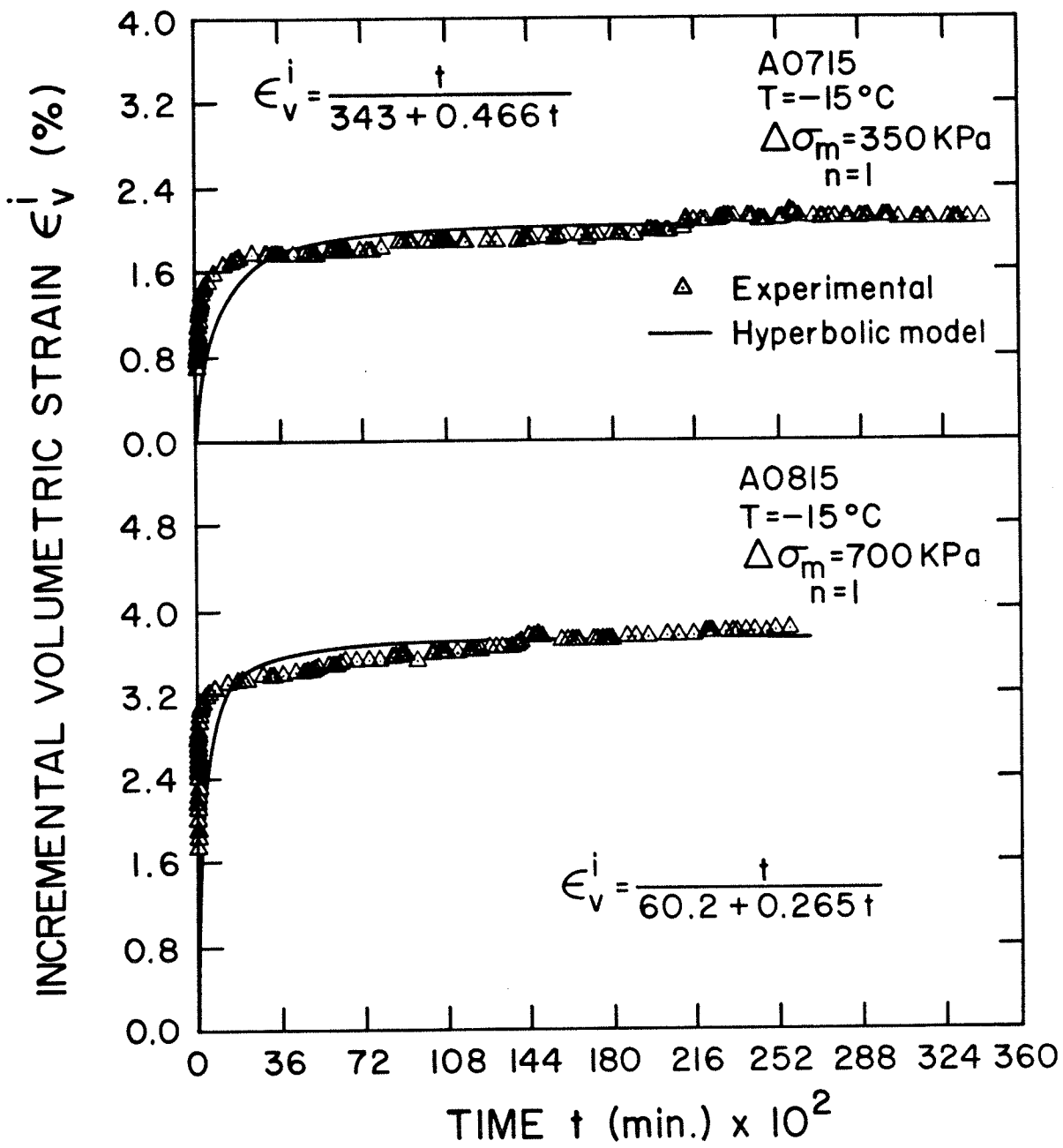


Fig.5.6.6 Hyperbolic curve fitting of single-step loading test data on sample A07 and A08.

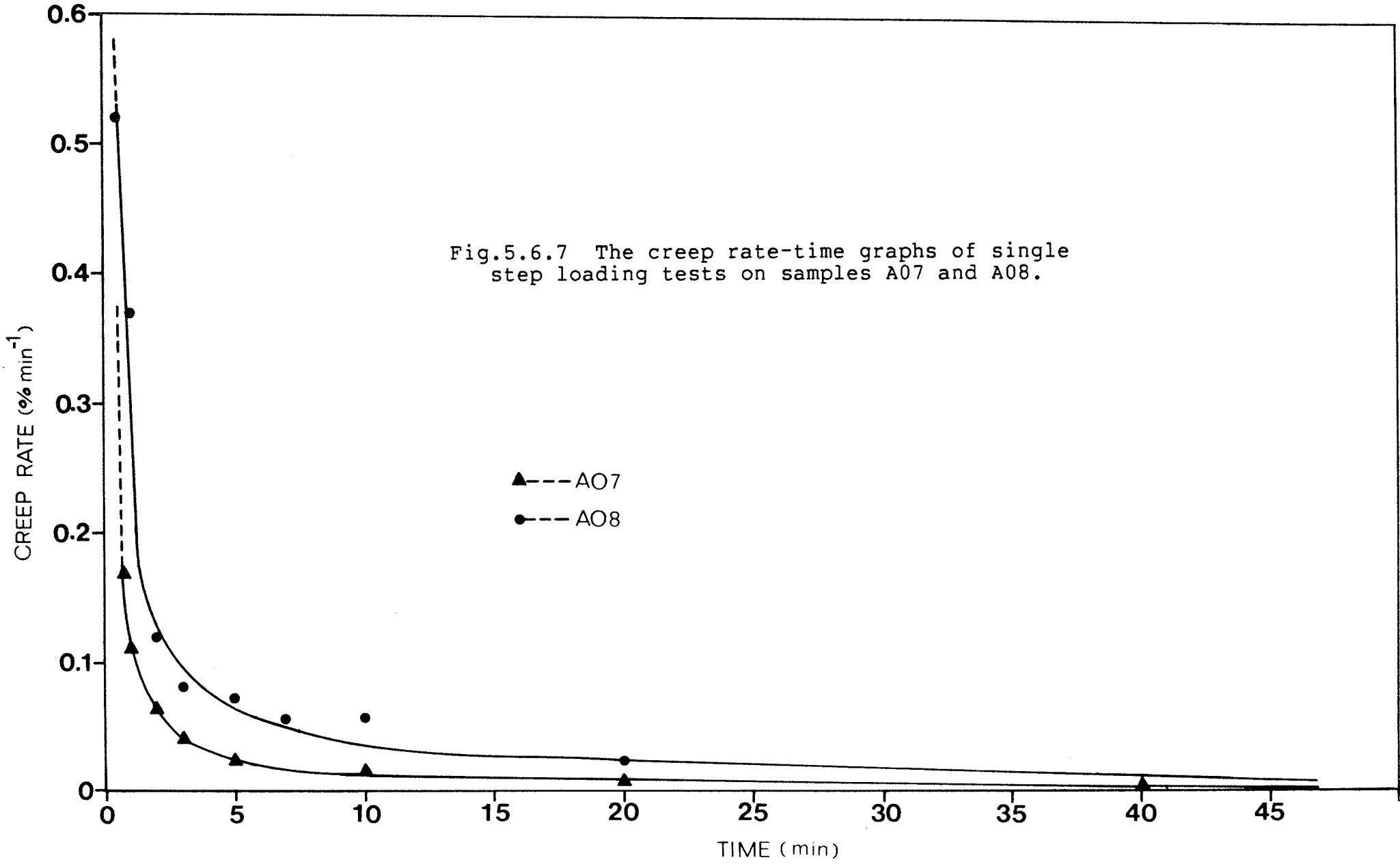
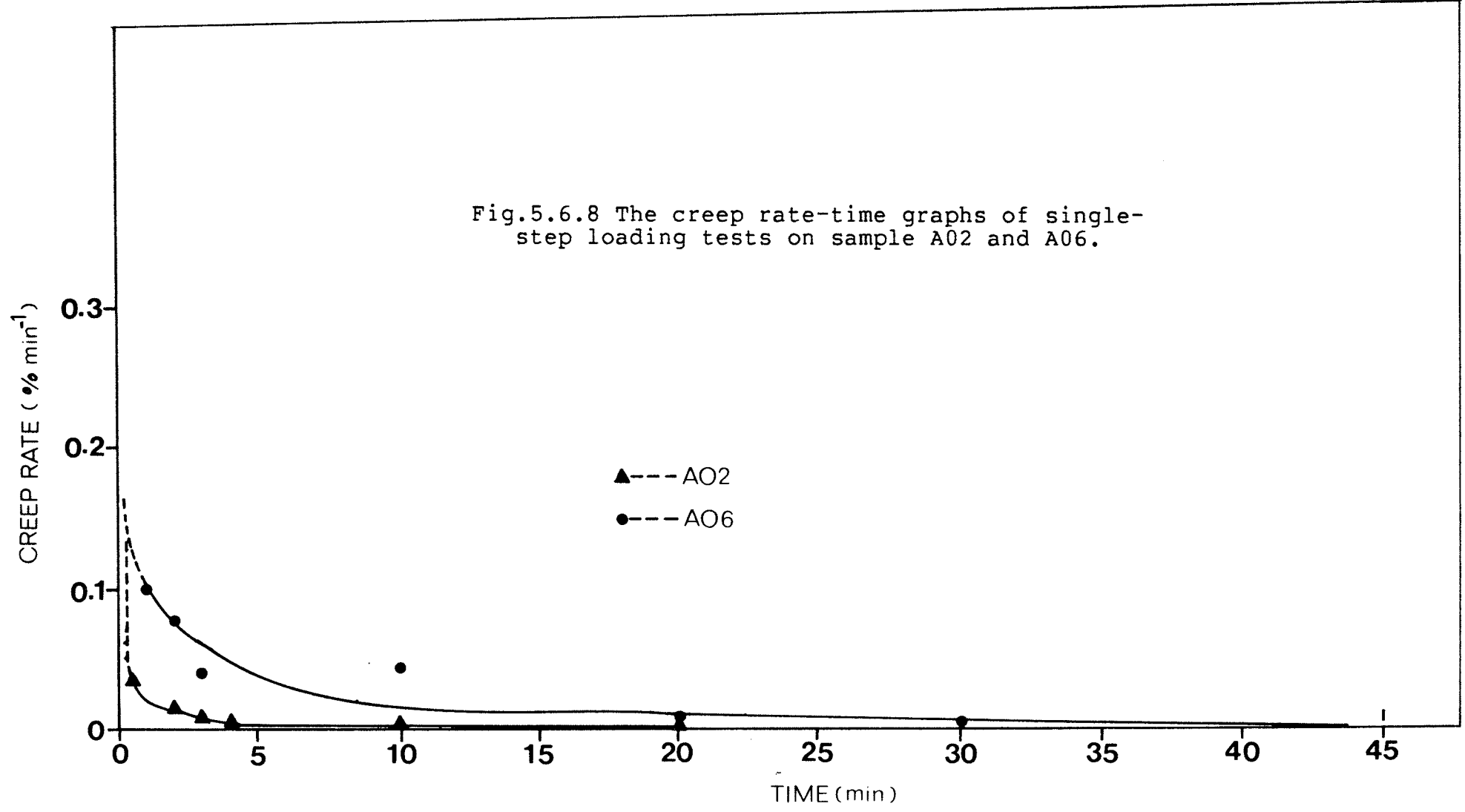


Fig.5.6.8 The creep rate-time graphs of single-step loading tests on sample A02 and A06.



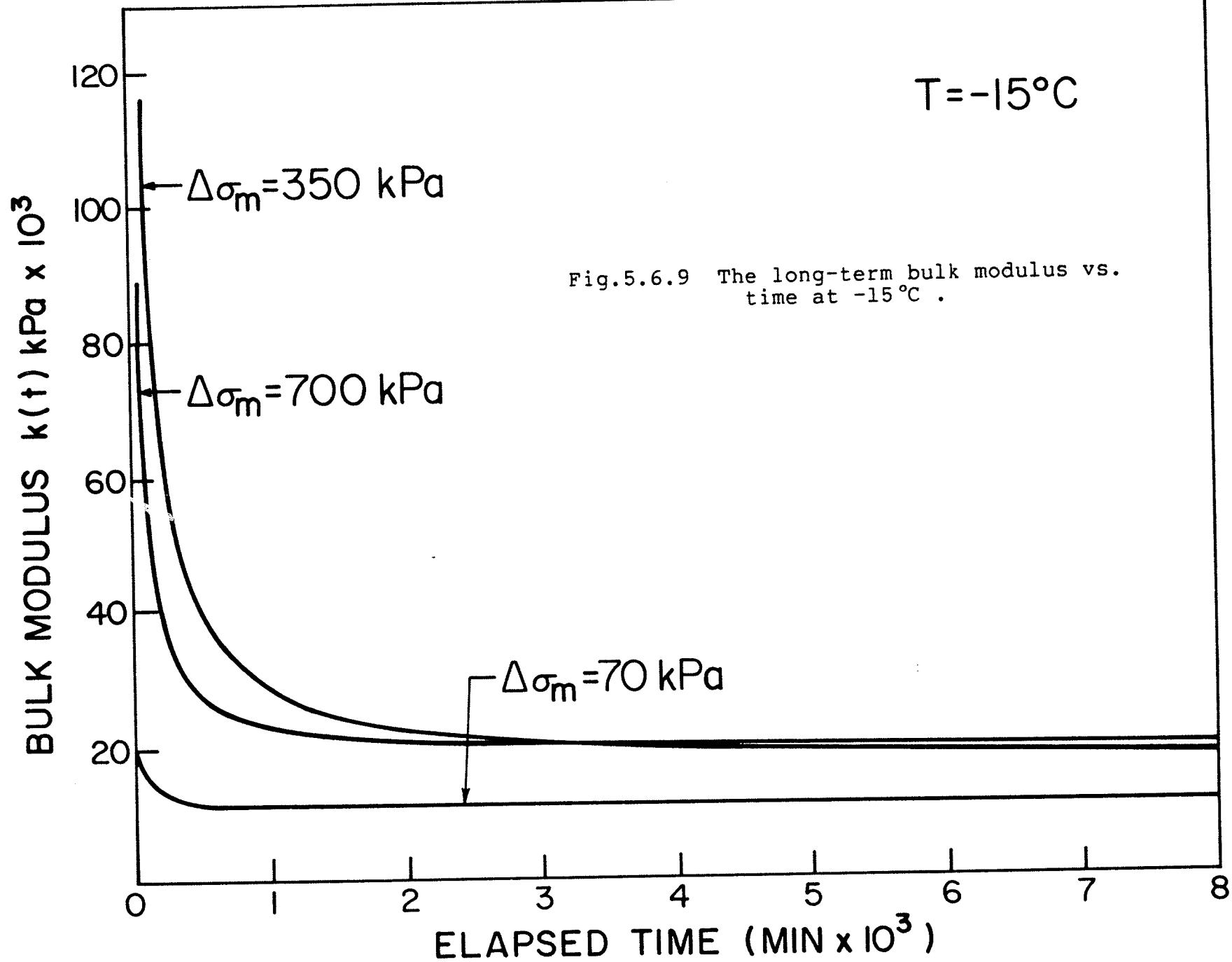


Fig.5.6.9 The long-term bulk modulus vs. time at -15°C .

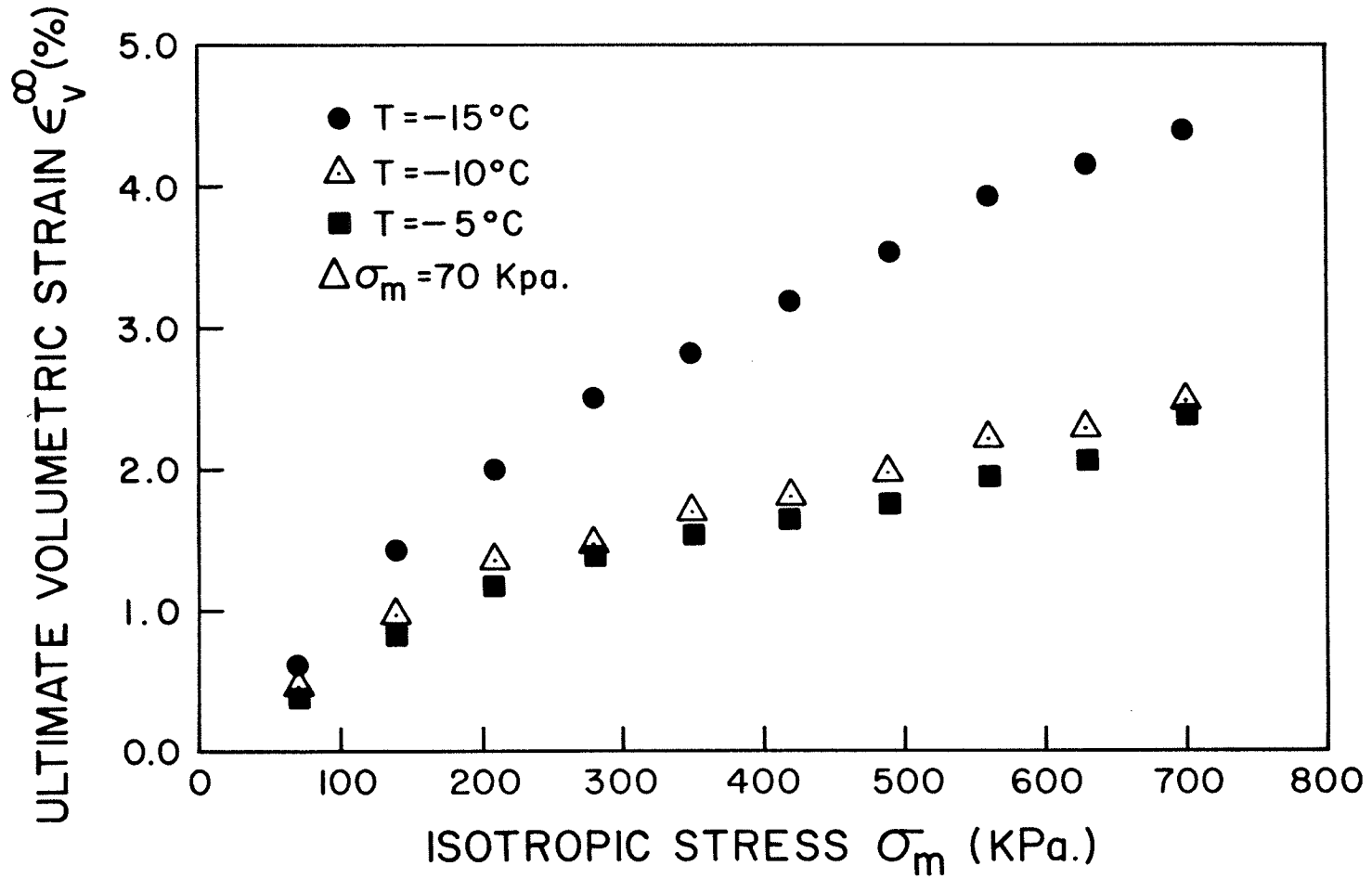


Fig. 5.6.10 The ultimate volumetric strain vs. isotropic stress for the multi-step tests.

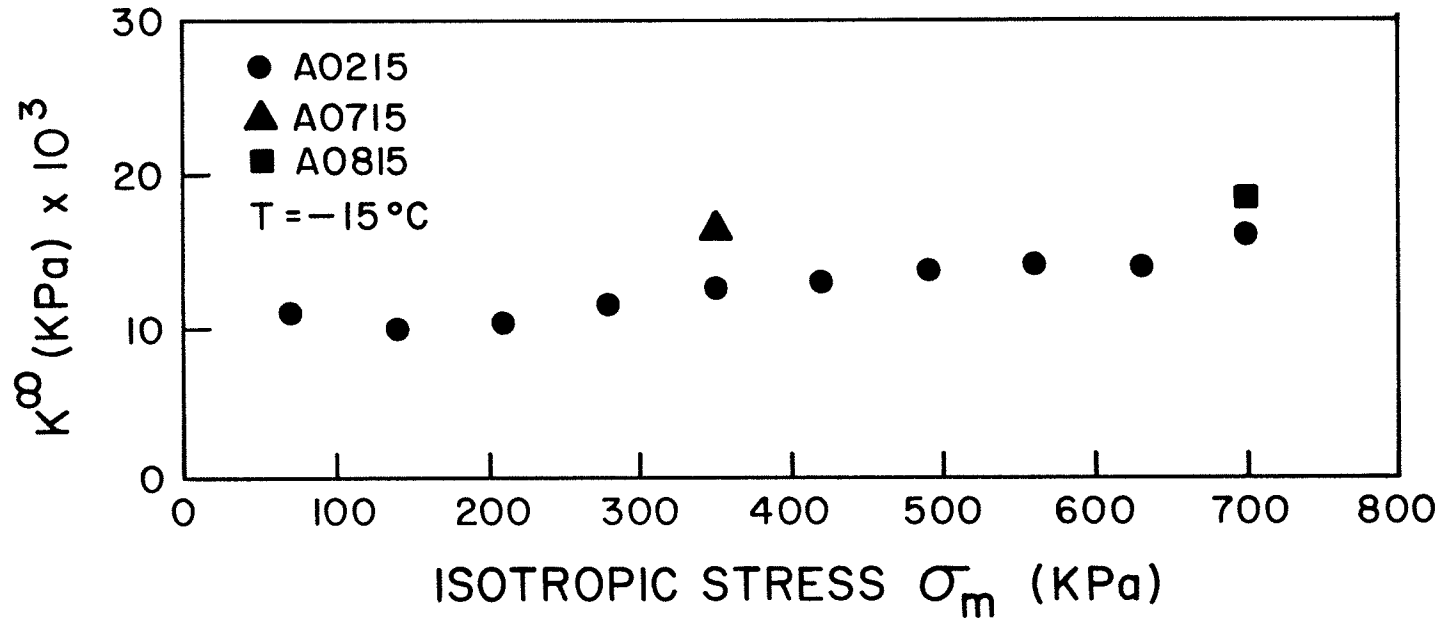


Fig.5.6.11 Ultimate secant bulk modulus vs. isotropic stress at -15°C .

CHAPTER 6

CONCLUSIONS AND SUGGESTIONS FOR FURTHER RESEARCH

6.1 CONCLUSIONS

An experimental study of the creep behaviour of frozen saline silt was carried out. The results of the series of tests cannot be considered definite because of the limited number of samples tested. However, several conclusions can be drawn based on the test results.

1. Each of the frozen saline silt samples underwent attenuating creep when subjected to a constant hydrostatic stress. The creep curve could be approximated by an appropriate hyperbolic function.
2. When an additional hydrostatic stress was superimposed on a sample which had approached equilibrium after creep under an isotropic stress, the sample underwent a new attenuating creep.
3. When the frozen saline silt was allowed to rebound after a history of loading, it ultimately recovered only part of the volume change which occurred during the previous loading. The volume change recovery was generally greater than 50 percent. The test results of Sample A02 showed that up to 50 % of the volume change could remain after recovery. This fact has an important implication for any attempt at viscoelastic modelling. Moreover, a simple nonlinear hereditary-

creep constitutive equation which ties up attenuating creep at constant stress with complete recovery after unloading would be inadequate.

4. A history of loading and recovery had a strain hardening effect on the frozen saline soil.
5. The saline silt was non ice-bonded at -5°C , but its response to isotropic compression did not seem to be qualitatively different than when it was ice-bonded.
6. Unfrozen pore fluid was expelled from the sample under isotropic compression at a low temperature of -15°C . This suggests that in modelling the creep behaviour of frozen saline soils, a quasi one-phase approach might be inadequate; mixture theories should be considered.
7. The long-term pseudo-elastic bulk modulus did not differ substantially from the short-term bulk modulus for a constant stress, but the long-term bulk modulus should be used in designing the structure on permafrost.

6.2 RECOMMENDATION FOR FURTHER RESEARCH

In this study, very limited investigation of creep behaviour of frozen soils was carried out. The following suggestions are made with regard to future studies on creep behaviour of frozen soils.

1. It is suggested that the sample be prepared from a slurry of silt with a water content twice as high as the liquid limit followed by consolidation under a constant load.
2. Further isotropic compression tests on samples with various test temperatures are required to clarify the effect of temperature on the creep behaviour of frozen soils.
3. Thermocouples should be installed inside the triaxial cell to monitor the temperature of the sample during testing.
4. A temperature bath should be used to maintain a constant temperature of the cell fluid during testing in order to eliminate the temperature fluctuations on the sample and cell fluid.
5. In future studies, it is suggested that the amount of salt in the pore fluid be varied to study the effect of pore fluid salinity on the creep behaviour of frozen soils.
6. Further isotropic loading and unloading tests on samples are required to clarify the uncertainties of the recovery of the volume change during unloading.

7. The effect of single-step and multi-step loading on creep behaviour of frozen soils requires further investigation.

REFERENCE

Andersland, O.B. and Alnouri, I., 1970. Time dependent strength behaviour of frozen soils. Proc. ASCE, 96 (SM4), pp. 1249-1265.

Anderson, D.M. and Morgenstern, N.R., 1973. Physics, chemistry and mechanics of frozen ground : A review. In: Permafrost, the North American contribution of the 2nd Int. Conf., Yakutsk, pp 257-288.

Baker, T.H.W., 1976. Preparation of artificially frozen sand specimens. DBR paper No. 682 (NRCC 15349), Ottawa, NRC, Division of Building Research.

Baker, T.H.W., Jones, S.J. and Parameswaran, V.R., 1981. Confined and unconfined compression tests on frozen sands. In : Proc. of the 4th Can. Permafrost Conf., Calgary, 1981, pp 387-393.

Bragg, R.A. and Andersland, O.B., 1981. Strain dependence of Poisson's Ratio for frozen sand. In : Proc. of the 4th Can. Permafrost Conf., Calgary, 1981, pp 365-373.

Brown, R.J.E., 1973. Influence of climatic and terrain factors on ground temperature at three locations in the permafrost region of Canada. North American Contribution to the Second International Conference on Permafrost, pp 27-34.

Charleson, D., 1981. Frost heave study of Lake Agassiz silt. Meng Thesis, Univ. of Manitoba.

Diekmann,N. and Jessberger,H.L.,1982. Creep behaviour and strength of an artificially frozen silt under triaxial stress state. In : Proc. of the 3rd Int. Symposium on Ground Freezing,Hanover, New Hampshire,U.S.A.,1982.

Domaschuk,L. and Valliappan,P.,1975. Nonlinear settlement analysis by finite element. Journal of Geotechnical Engineering Division, ASCE,V.101,pp 601-614.

Golder,Brawner and Associates,1970. Bottom sampling program, Southern Beaufort sea. Arctic Petroleum Operators Association project #3.

Harrison,W.D. and Osterkamp,K.E.,1981. Measurements of the electrical conductivity of interstitial water in subsea Permafrost. In : Proc. of the 4th Can. Permafrost conf.,Calgary,1981,pp 229-237.

Hult,J.A.H.,1966. Creep in Engineering structures. Blaisdell publ. Comp.Waltham,Mass.,p 115.

Hunter,J.A.M.,Judge,A.S.,MacAulay,H.A.,Good,R.L.,Gagne,R.M. and Burns,R.A.,1976. Permafrost and frozen sub-seabottom materials in the Southern Beaufort Sea. Beaufort Sea project, Dept.of the Environment,Technical report No.22.

Hunter,J.A.M.,Neave,K.G.,MacAulay,H.A. and Hobson,G.D.,1978. Interpretation of sub-seabottom permafrost in the Beaufort Sea by seismic methods part 1 Seismic refraction methods. In

: Proc. of 3rd Int. Conf. on Permafrost, Edmonton, 1978, Vol.1 pp 515-521.

Judge, A.S., 1974. The occurrence of offshore permafrost in Northern Canada. In : Proc. of the Symposium on Beaufort Sea coastal and shelf research, A.I.N.A., pp 427-437.

Judge, A.S., MacAulay, H.A. and Hunter, J.A.M., 1976. An application of hydraulic jet drilling techniques to mapping sub-seabottom permafrost. Rep. Activities, Part c, Geol. Surv. Can., Paper 76-1C, Ottawa, Canada.

King, M.S., Pandit, B.I., Hunter, J.A.M. and Gajtani, M., 1981. Some seismic, electrical and thermal properties of sub-seabottom permafrost from the Beaufort Sea. In : Proc. of the 4th Can. Permafrost Conf., Calgary, 1981, pp 268-273.

Klein, J. and Jessberger, H.L., 1979. Creep stress analysis of frozen soils under multiaxial states of stress. Engineering Geology, V.13, pp 353-365.

Ladanyi, B., 1972. An engineering theory of creep of frozen soils. Can. Geot. J., Vol.9, pp 63-80.

Ladanyi, B., 1981. Mechanics of structured media. In: Proc. of the Int. Symposium on the mechanical behaviour of structured media, Ottawa, 1981, pp 203-245.

Lewis, C.P. and McDonald, B.C., 1974. Sediments and sedimentary processes of Western Canadian Beaufort Sea coast. In : Proc.

of the Symposium on Beaufort Sea coastal and shelf research, A.I.N.A., pp 491-493.

Lewis, C.P. and Forbes, D.L., 1976. Beaufort Sea coast sediments and sedimentary processes. Beaufort Sea project, Technical report #24, Dept. of the Environment, Victoria, B.C..

MacAulay, H.A. and Hunter, J.A.M., 1981. Detailed Seismic refraction analysis of ice-bonded permafrost layering in the Canadian Beaufort Sea. In : Proc. of the 4th Can. Permafrost Conf., Calgary, 1981, pp 256-267.

MacKay, J.R., 1972. Offshore permafrost and ground ice, Southern Beaufort Sea. Can. J. Earth Sci. 9, pp 1550-1561.

MacKay, J.R. Rampton, V.N. and Fyles, J.G., 1972. Relict Pleistocene permafrost, Western Arctic, Canada. Science, 176, pp 1321-1323.

Markham, W.E., 1976. Ice climatology in the Beaufort Sea. Beaufort sea project, Dept. of the Environment, Technical report #26.

Milne A.R. and Smiley, B.D., 1976. Offshore drilling for oil in the Beaufort Sea. Beaufort sea project, Dept. of the Environment, Technical report #39.

Mitchell,R.J. and Burn,K.N.,1971. Electrical measurement of changes in the volume of pore water during testing of soil samples. C.G.J.,Vol. 8, pp 341-345.

Morack,J.L. and Rogers,J.C.,1981. Marine Seismic refraction measurements of near-shore subsea permafrost. In : Proc. of the 4th Can. permafrost Conf.,Calgary,1981, pp 256-267.

Muller-beck,H.,1966. Paleohunters in America: Origins and Diffusion. Science, Vol. 152 (3726), pp 1191-1200.

Naidu,A.S. and Mowatt,T.C.,1974. Clay mineralogy and geochemistry of continental shelf sediments of the Beaufort sea. In : Proc. of the Symposium on Beaufort sea coastal shelf research,A.I.N.A.,pp 493-510.

Odquist,F.K.G. and Hult,J.,1962. Creep in metallic material. Spinger,Berlin.

Odquist,F.K.G.,1966. Mathematical theory of creep and creep rupture. Oxford Math. Mono.,Clarendon press,Clarendon, Texas, p 168.

Osterkamp,T.E. and Harrison,W.D.,1976. Subsea permafrost regime at Prudhoe Bay,Alaska. J. Glaciol.,Vol. 19 (81), pp 627-637.

Osterkamp,T.E. and Harrison,W.D.,1981. Temperature measurements in subsea permafrost off the coast of Alaska. In : Proc. of the 4th Can. Permafrost Conf.,Calgary,1981, pp 229-237.

Pelletier, B.R. and Shearer, J.M., 1972. Seabottom scouring in the Beaufort Sea of the Arctic ocean. In : Proc. of the 24th Int. Geol. Congress, Montreal, 1972, section 8 , pp 251-261.

Pelletier, B.R., 1975. Sediment dispersal in the Southern Beaufort Sea. Beaufort Sea project, Dept. of the Environment, Technical report #25a.

Rodeick, C.A., 1974. Marine gravel deposits of the Beaufort Sea. In : Proc. of the Symposium on Beaufort Sea coastal and shelf research, A.I.N.A., pp 511-512.

Roggensack, W.D., 1977. Geotechnical properties of fine-grained permafrost soils. Ph.D. thesis, Univ. of Alberta, Edmonton, p 449.

Sayles, F.H., 1972. Triaxial and creep tests on frozen Ottawa sand. In : Permafrost The North America Contr. to the 2nd Int. Conf., Yakutsk, pp 384-391.

Shearer, J.M., MacNab, R.F., Pelletier, B.R. and Smith, T.B., 1971. Submarine Pingo in the Beaufort Sea. Science, 175 , pp 816-818.

Tsytoich, N.A., 1975. The mechanics of frozen ground. Transl. from Russian by Scripta Technical, McGraw Hill, New York, N.Y., pp 147-157.

Vilks, G., Wagner, F.J.E. and Pelletier, B.R., 1979. The Holocene marine environment of the Beaufort Sea shelf. Geological Survey Bulletin 303.

Vyalov,S.S.,1959. Rheological properties and bearing capacity of frozen soils. Transl. 74,U.S. Army CRREL,Hanover,N.H..

Vyalov,S.S.,1962. The strength and creep of frozen soils and calculations for ice-soil retaining structures. Transl. 76, U.S. Army CRREL,Hanover,N.H..

Vyalov,S.S.,1963. Rheology of frozen soils. In : Proc. NAS. NRC, Int. Permafrost Conf. Purdue Univ.,Lafayette, Indiana, pp 332-339.

Vyalov,S.S., Zaretsky,Yu.K., and Gorodetsky,S.E.,1978. Stability of mine workings in frozen soils. In : Proc. of the 1st Int. Symposium on Ground Freezing,Bochum, 1978, pp 339-351.

Weaver,J.s.,1979. Pile foundations in permafrost. Ph.D. Thesis, Univ. of Alberta,Edmonton, p 225.

APPENDIX I

ISOTROPIC COMPRESSION TEST RESULTS

Figure I.1 The incremental volumetric strain versus time for the 1st, 2nd and 3rd stress increments on Sample A0215.

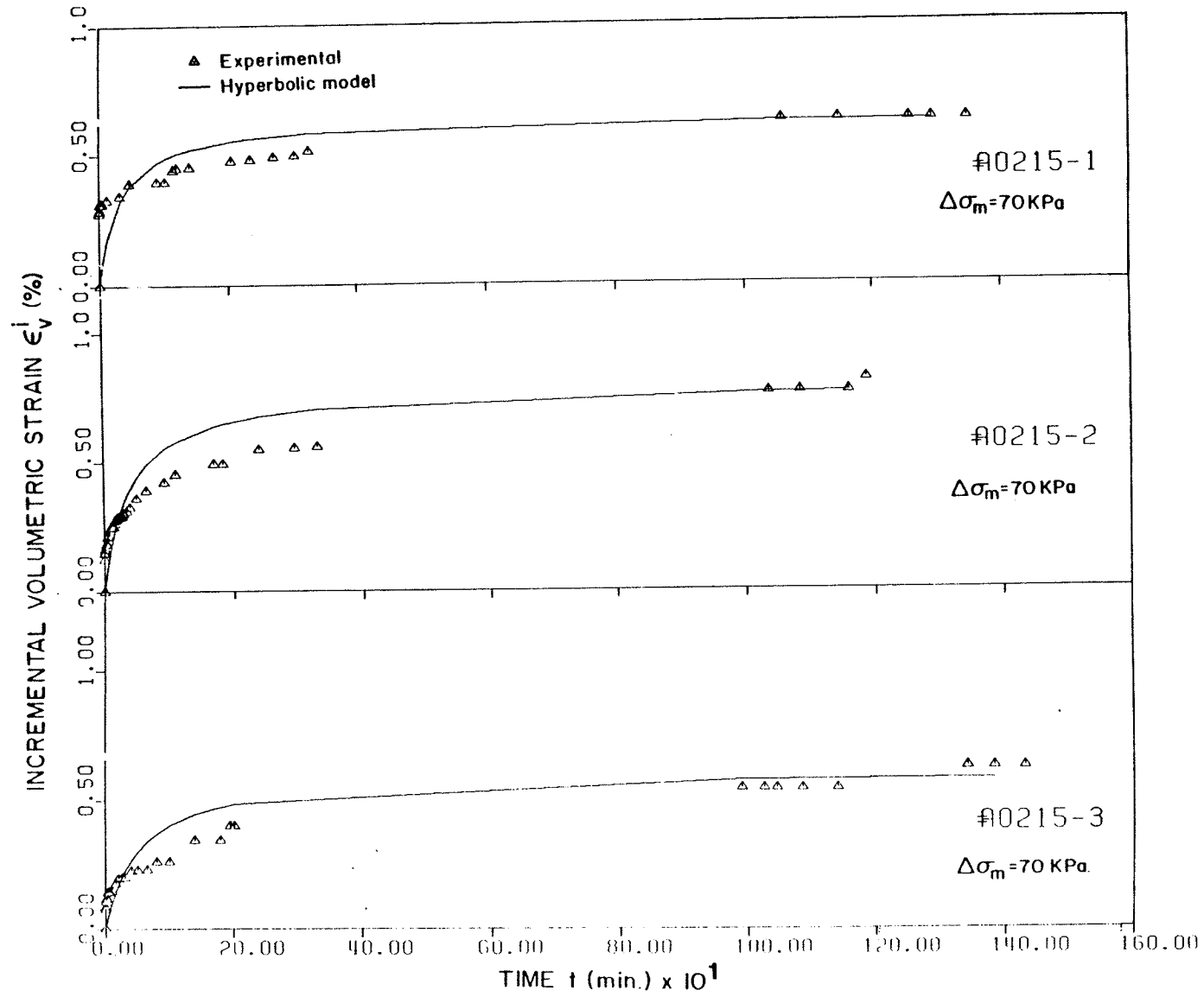


Figure 1.2 The incremental volumetric strain versus time for the 4th,5th and 6th stress increments on Sample A0215.

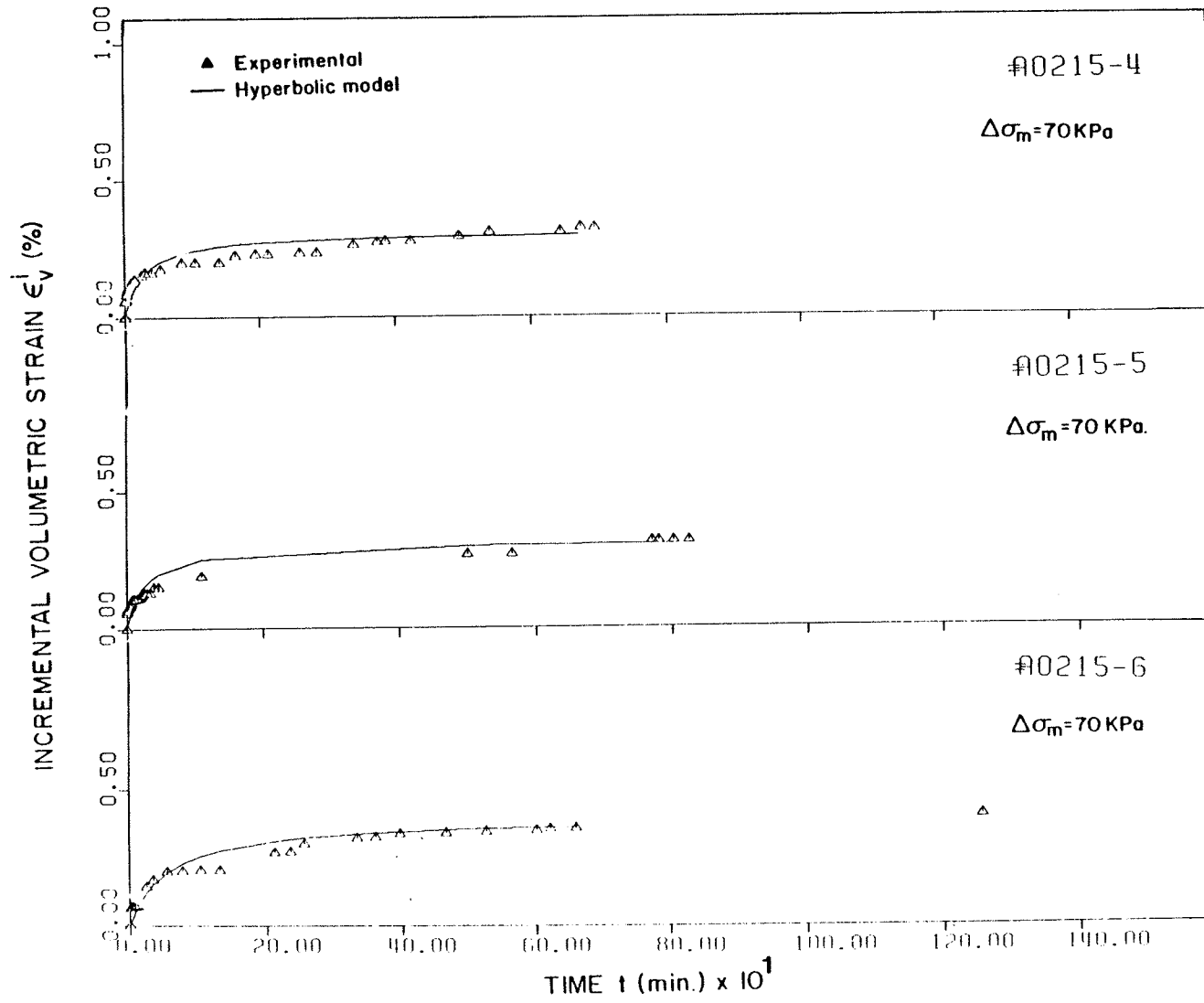


Figure I.3 The incremental volumetric strain versus time for the 7th,8th and 9th stress increments on Sample A0215.

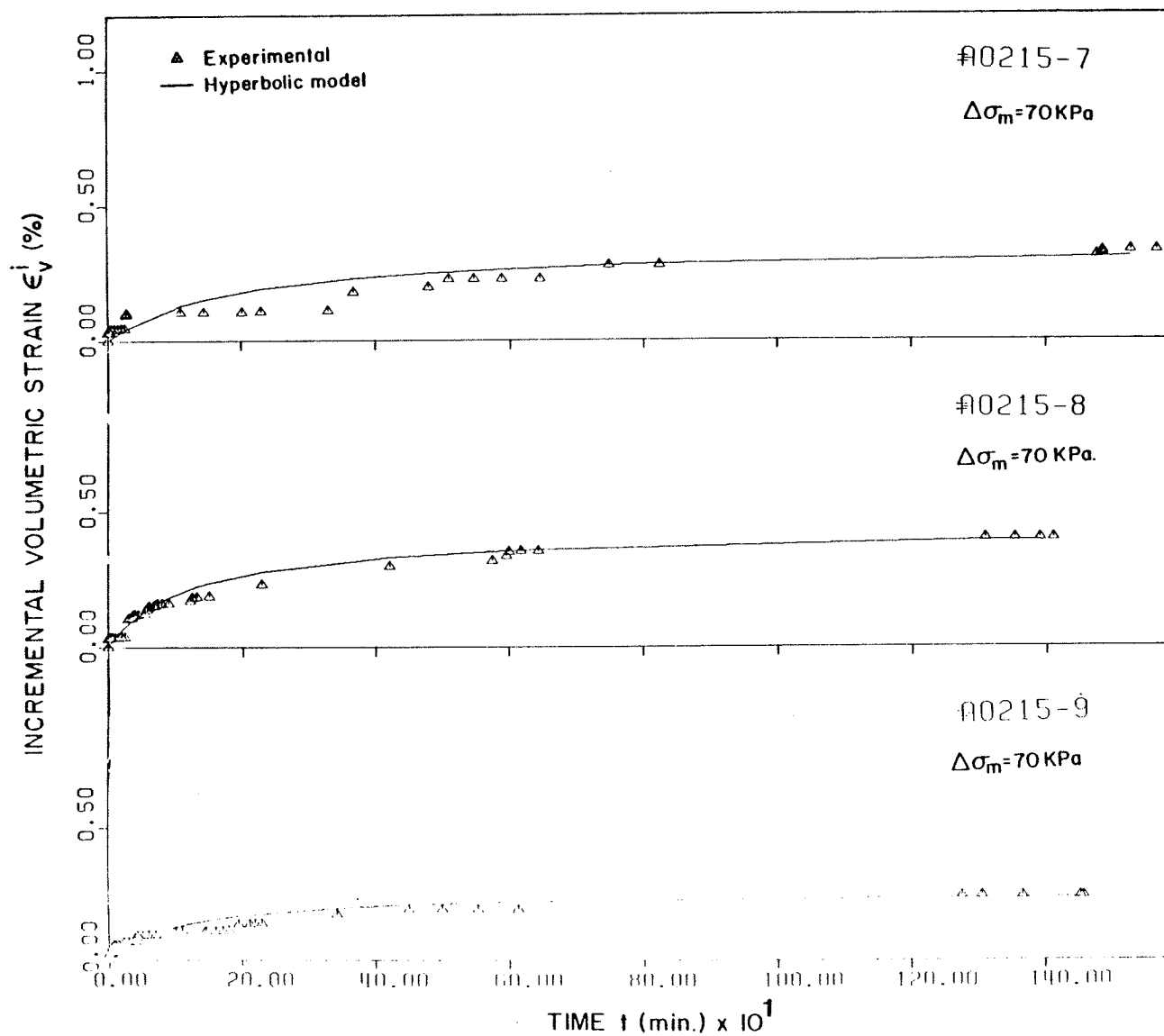


Figure I.4 The incremental volumetric strain versus time for the 2nd and 4th stress increments on Sample A0210.

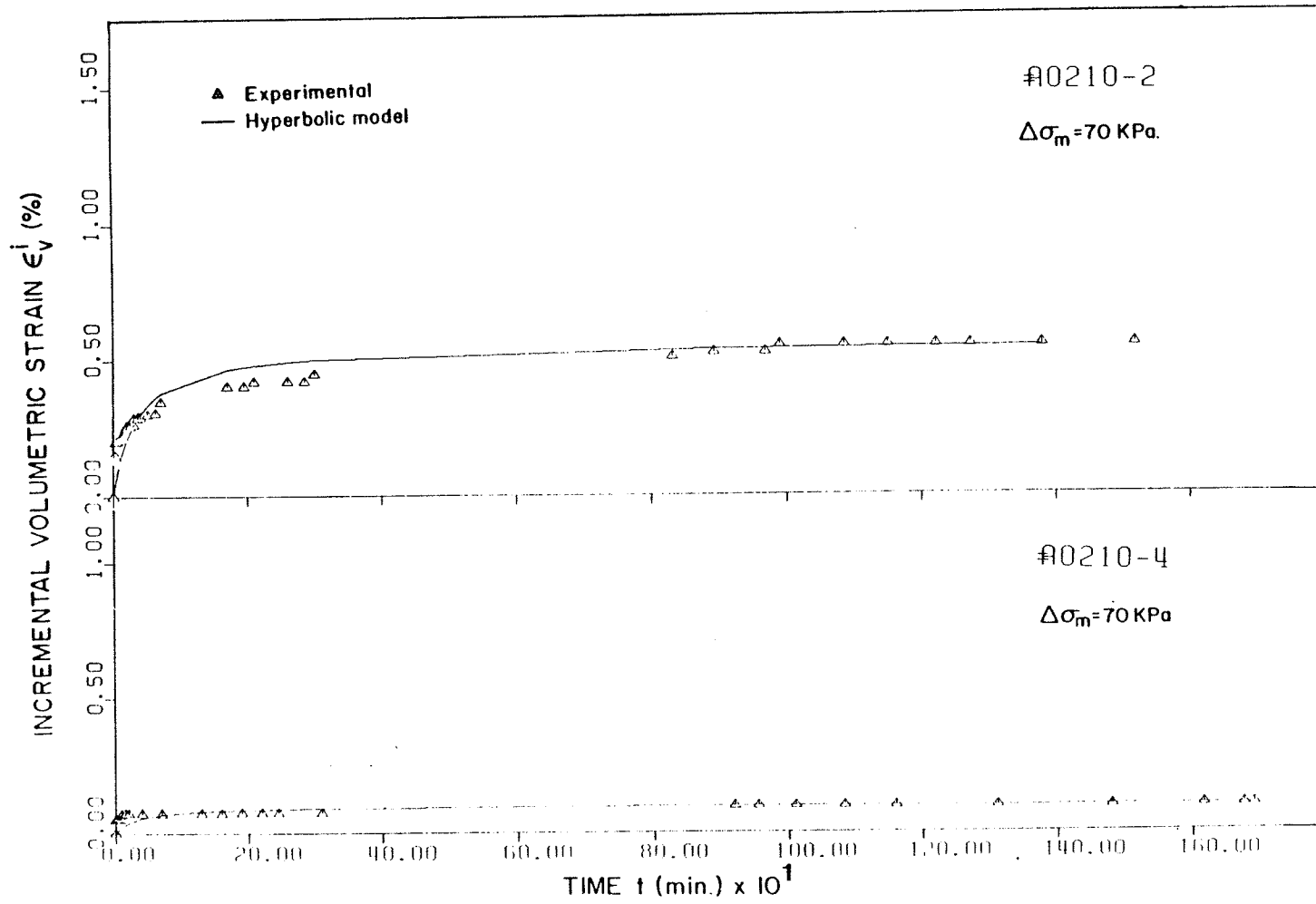


Figure I.5 The incremental volumetric strain versus time for the 5th,6th and 7th stress increments on Sample A0210.

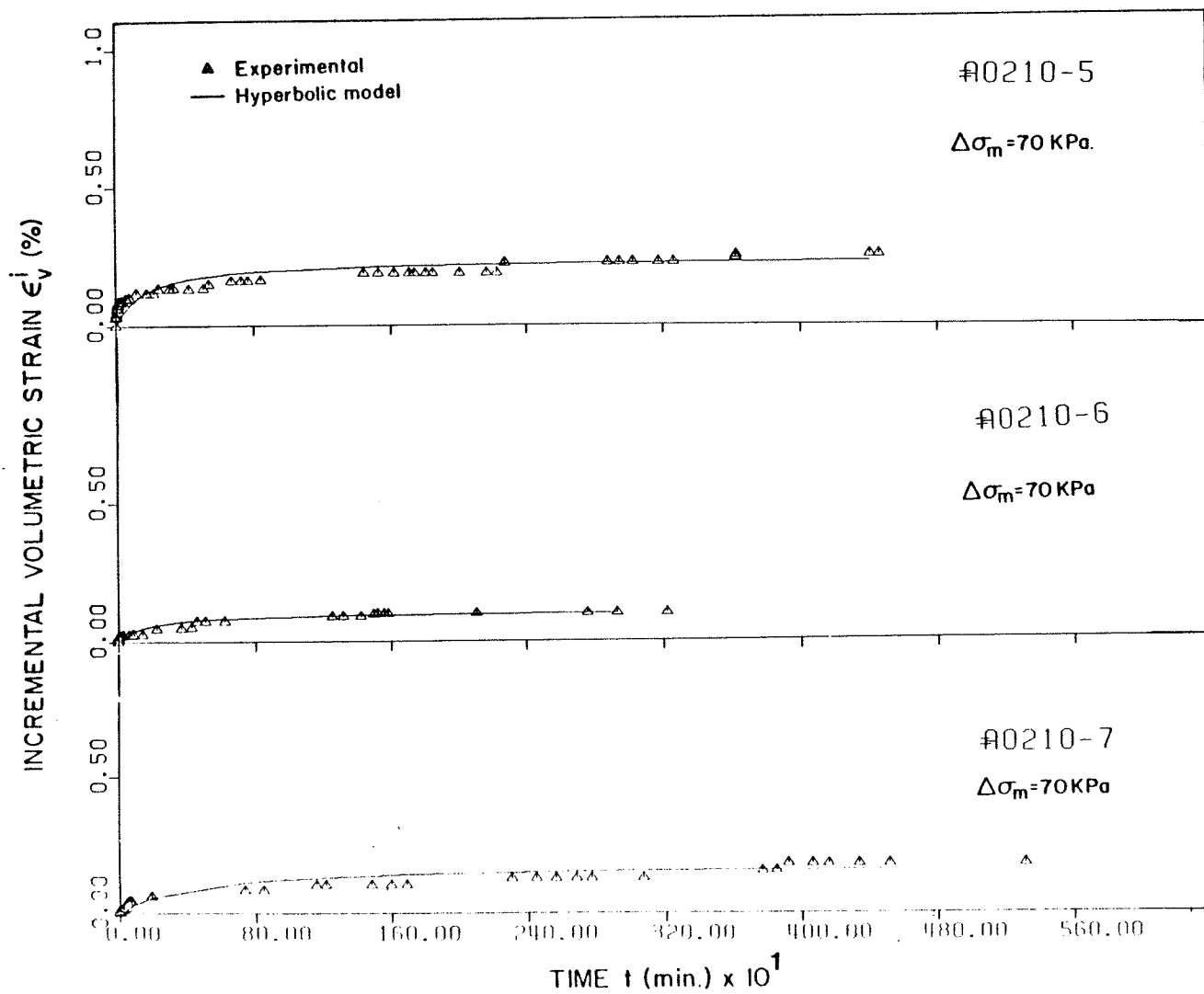


Figure I.6 The incremental volumetric strain versus time for the 8th,9th and 10th stress increments on Sample A0210.

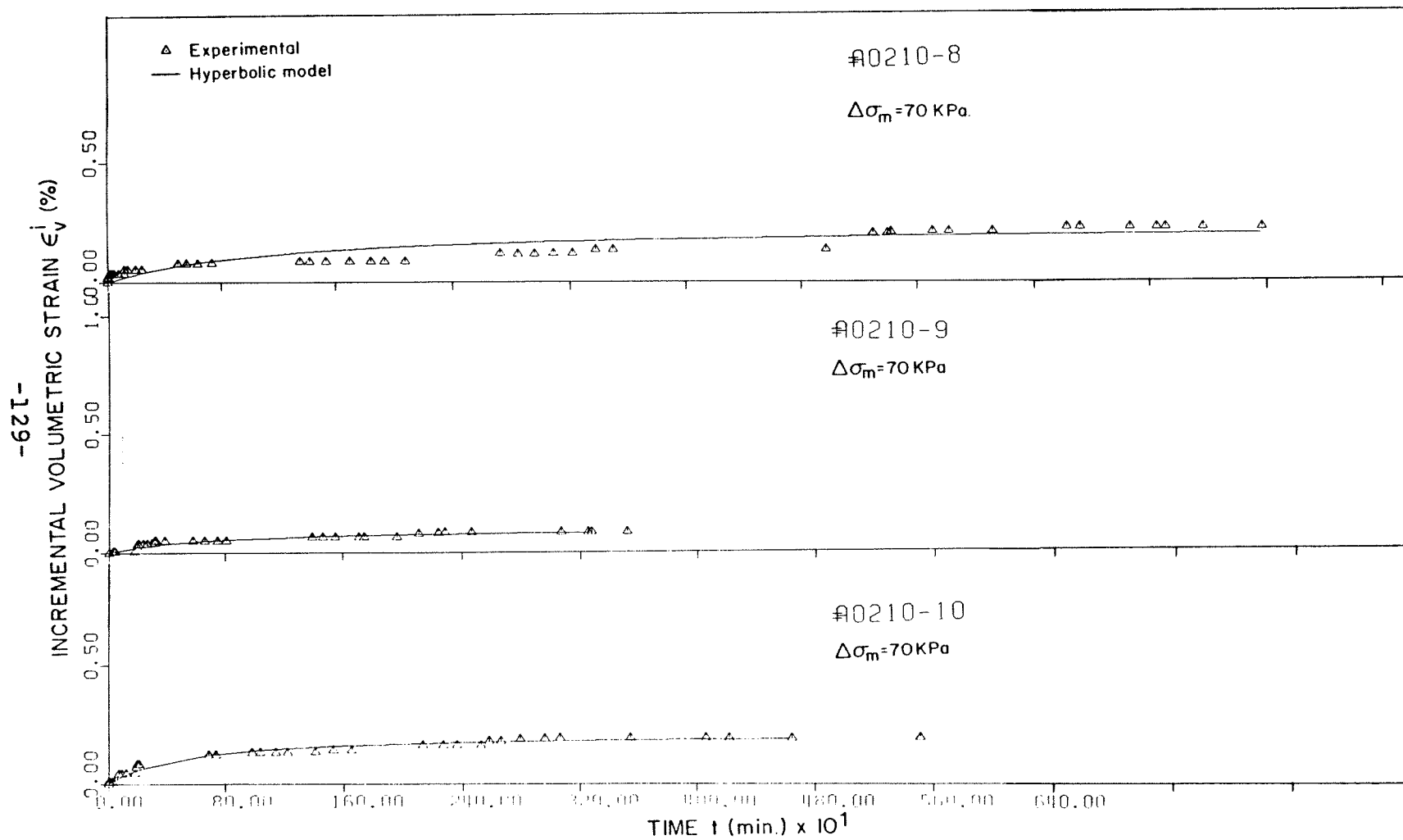


Figure I.7 The incremental volumetric strain versus time for the 3rd,4th,5th and 6th stress increments on Sample A0205.

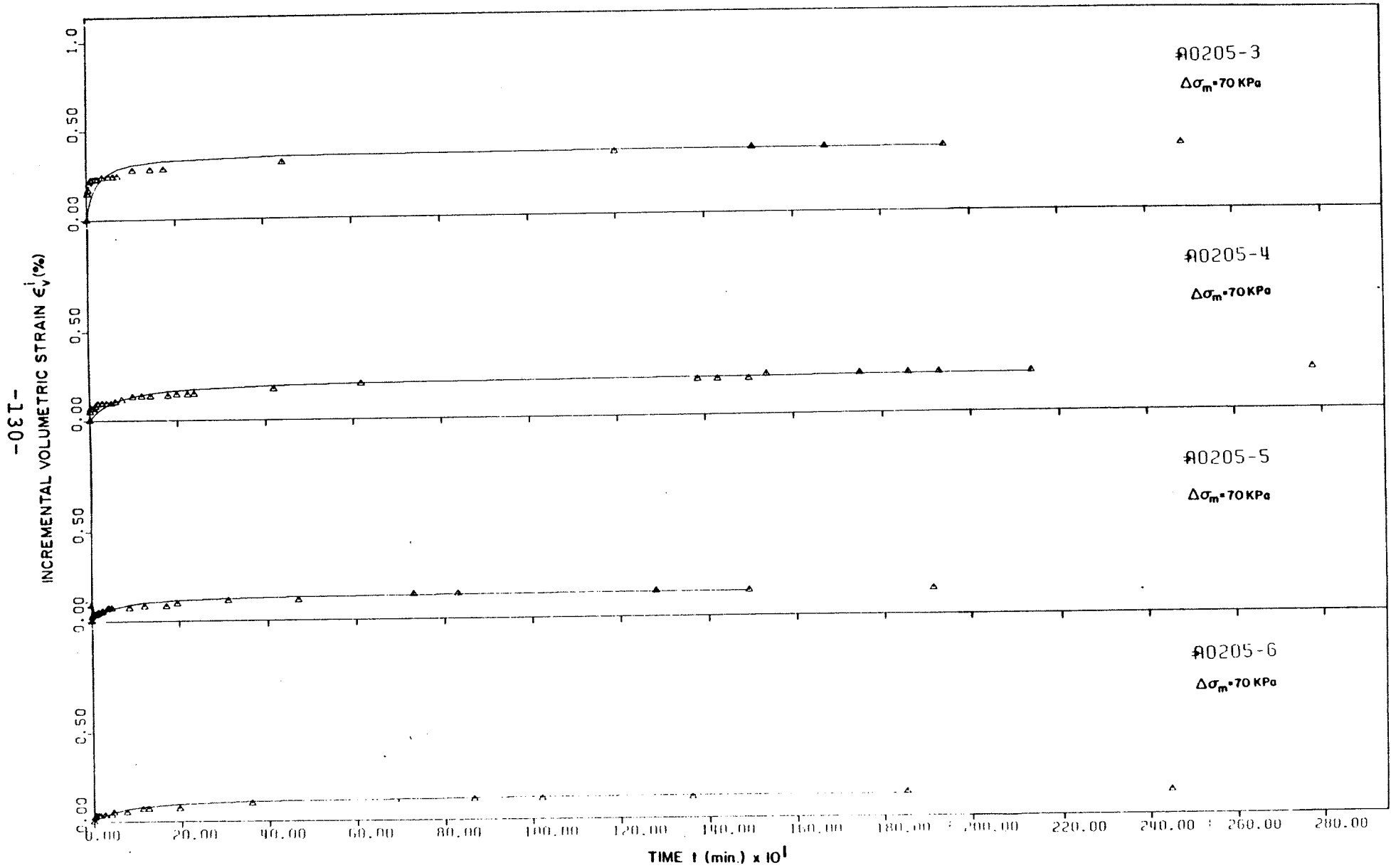


Figure I.8 The incremental volumetric strain versus time for the 9th and 7th stress increments on Sample A0205.

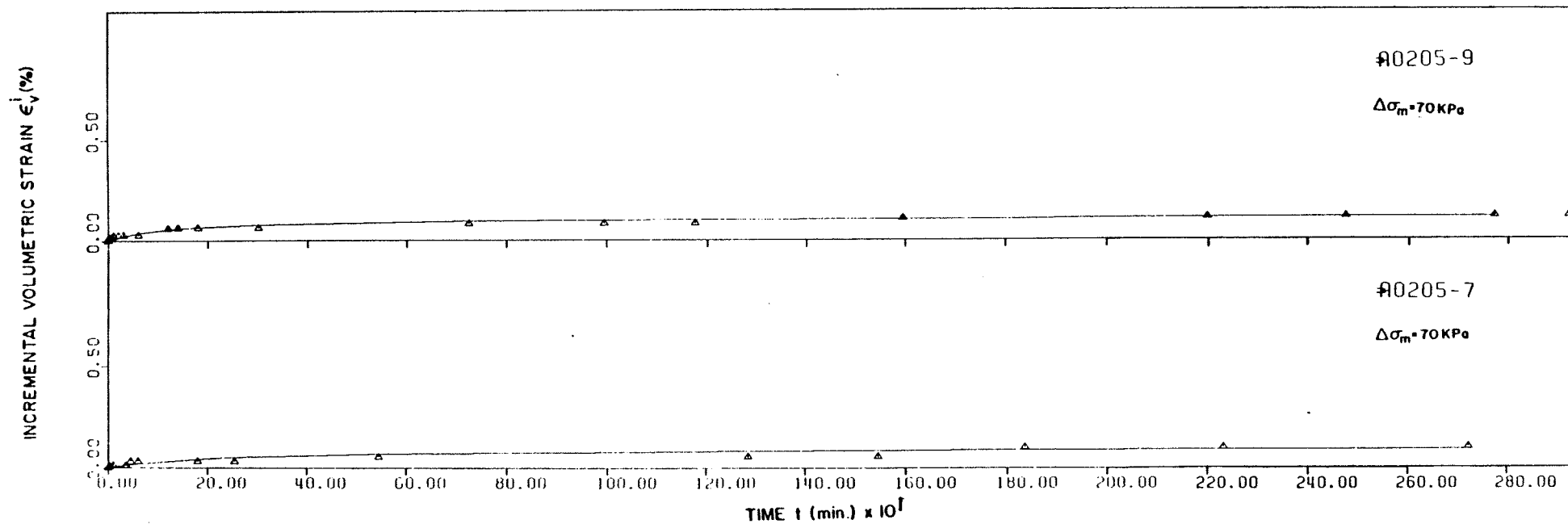


Figure I.9 The incremental volumetric strain versus time for the 8th and 10th stress increments on Sample A0205.

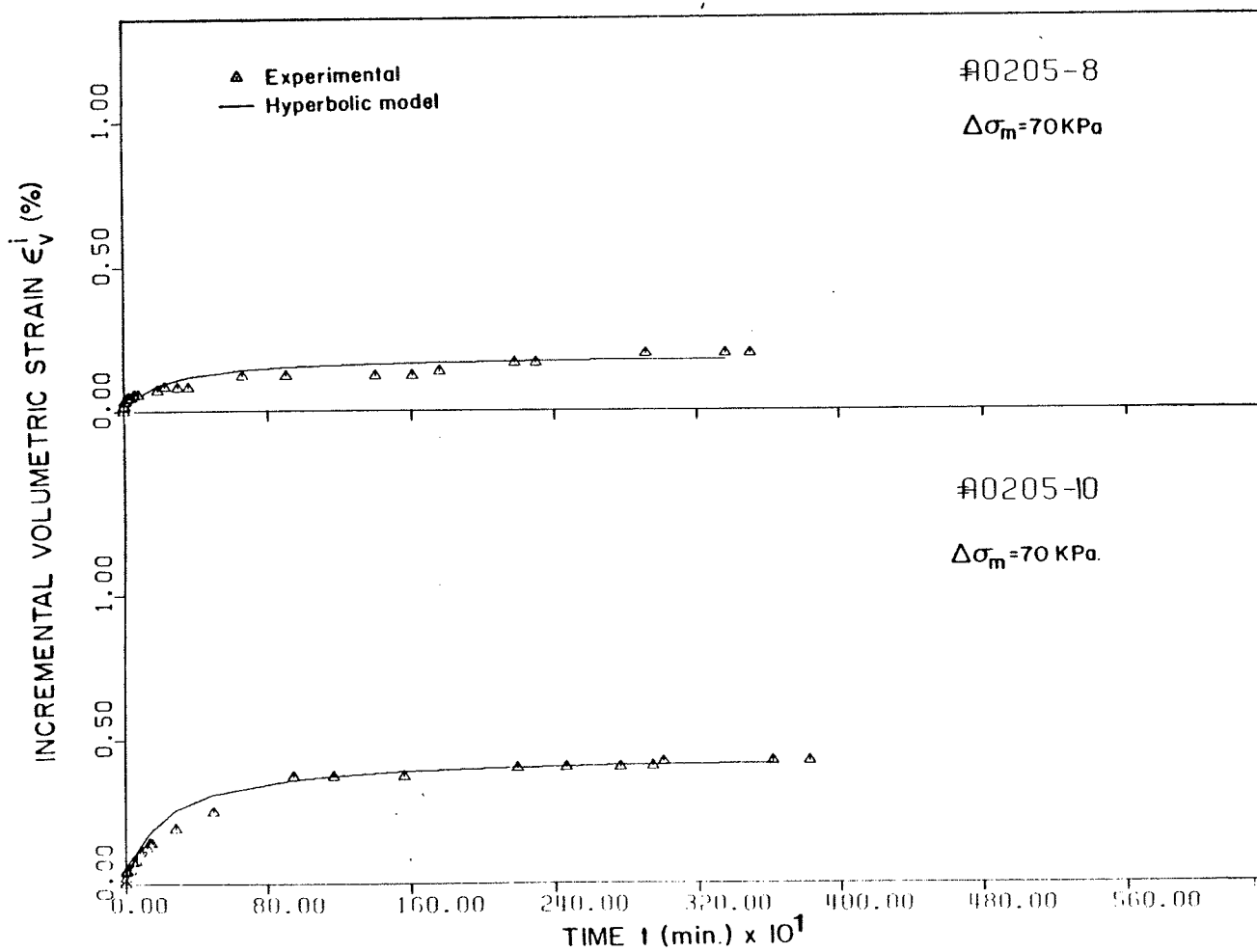


Figure I.10 The incremental volumetric strain versus time for the 1st and 2nd stress increments on Sample A0615.

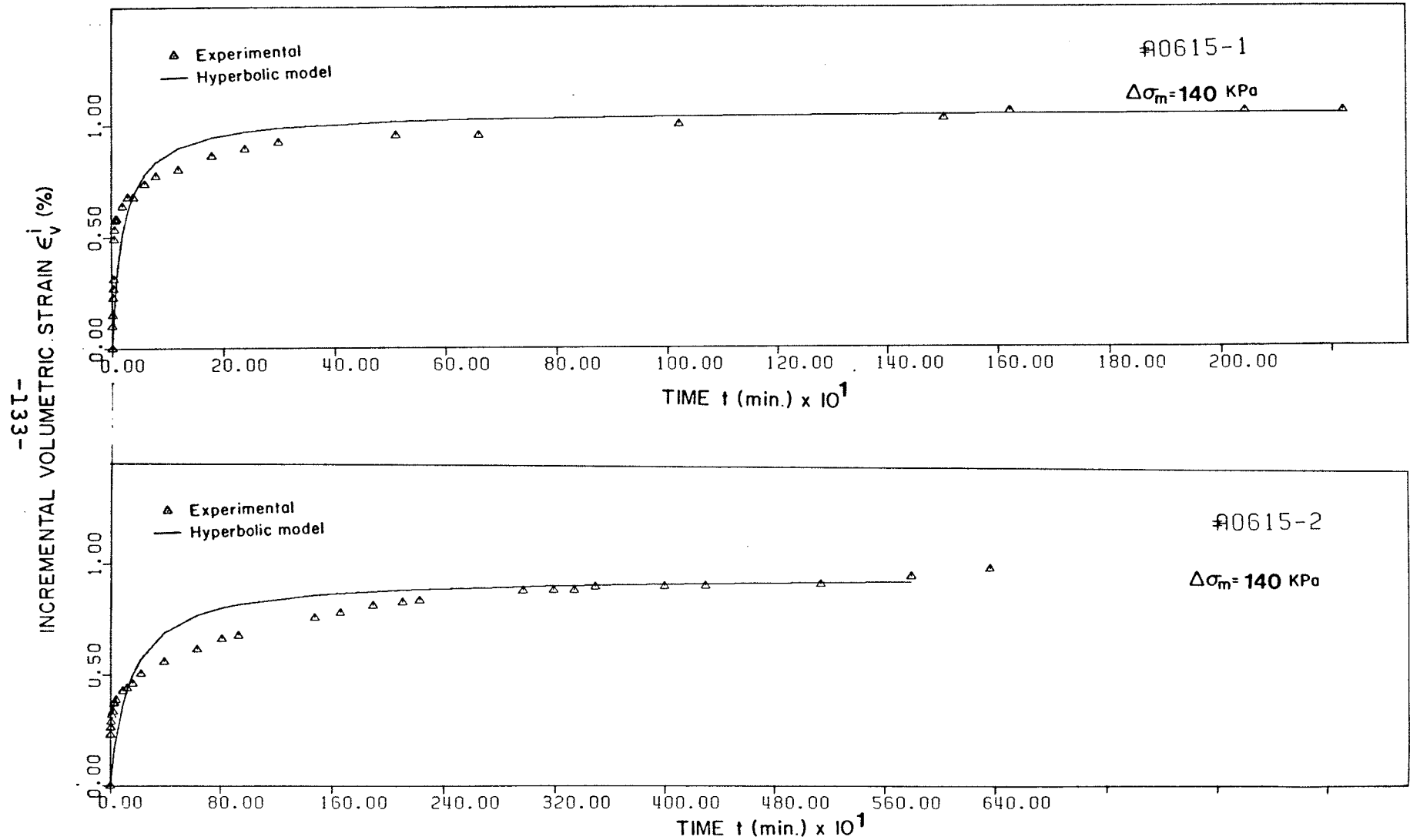


Figure I.11 The incremental volumetric strain versus time for the 3rd stress increment on Sample A0615.

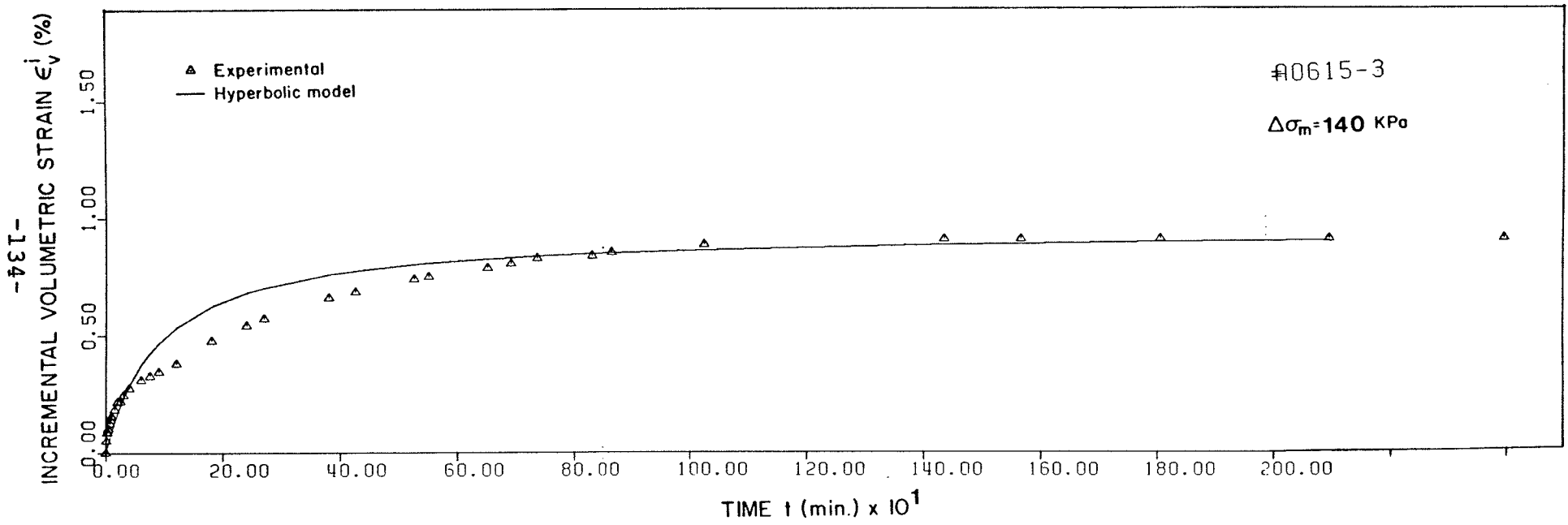
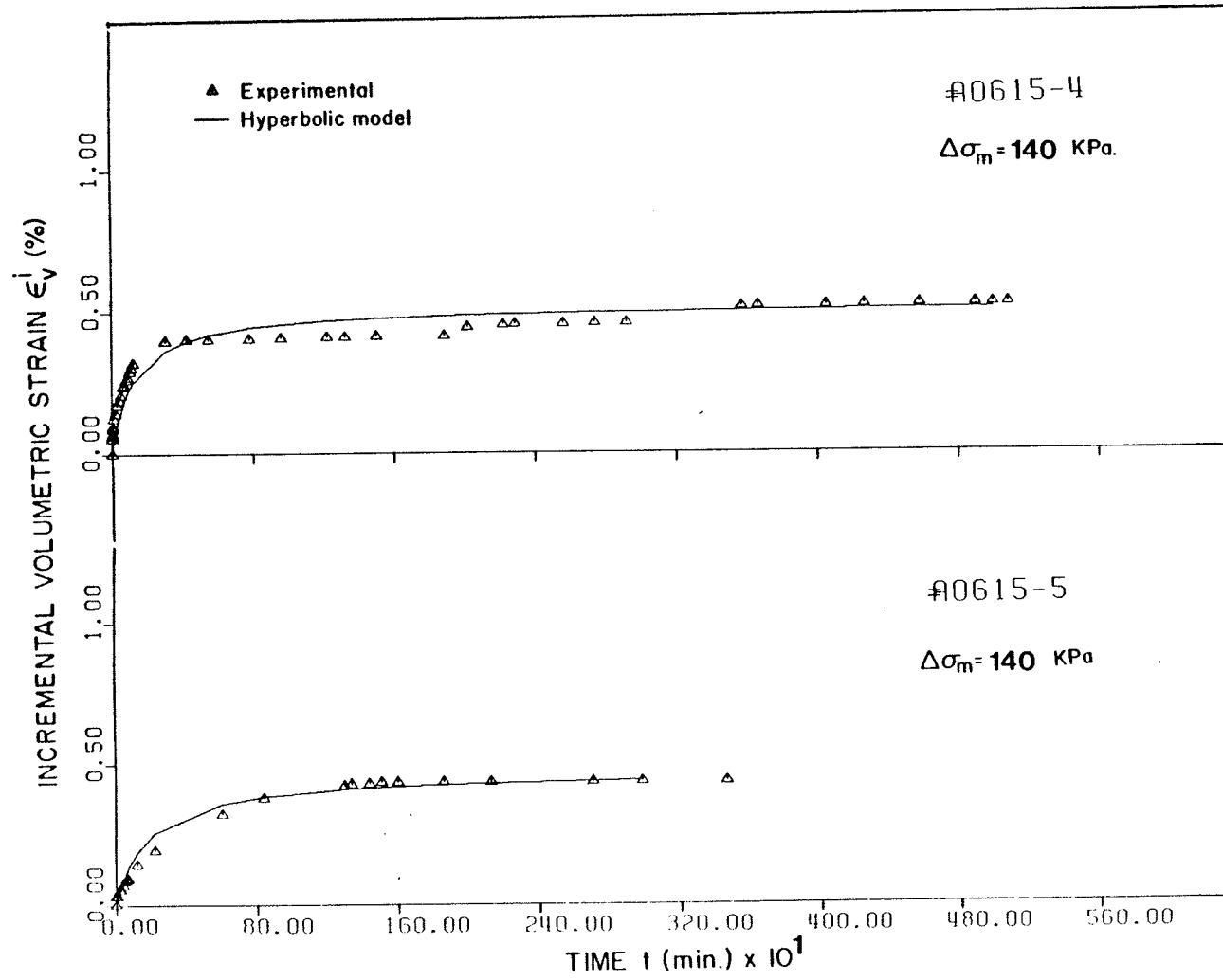


Figure I.12 The incremental volumetric strain versus time for 4th and 5th stress increments on Sample A0615.



APPENDIX II

CALIBRATION OF VOLUME CHANGE MEASUREMENT DEVICE

CALIBRATION OF VOLUME MEASUREMENT DEVICE

The volume changes (ΔV) which occur in the test specimen will alter the level of fluid (Δh) in the burette (volume measurement device).

$$\Delta V = A_b \times \Delta h$$

where A_b = cross-sectional area of the burette

The change of fluid level in the burette was monitored by the glass float attached to a displacement transducer.

The displacement transducer (LVDT) of 5.08 cm. (2 inches) maximum travel and a burette of 4.70 cm. (1.85 inches) were used. The calibration factors were found to be 0.122 v/cc. at -15°C and 0.114 v/cc at 25°C . The error of linear regression best fit curve was about 0.1 % of 30 cc. (± 0.015 cc) . For a voltmeter (LVDT) reading the corresponding volume change is

$$V = \text{voltmeter reading} / \text{LVDT calibration factor}$$

The calibration of float movement with compression of fluid was found to be temperature independent. The average total error which is the sum of errors of the linear regression and the float movement with compression of fluid was determined. The average total error for stress increments (σ) of 70 kpa was about ± 0.05 cc., but the error for the first

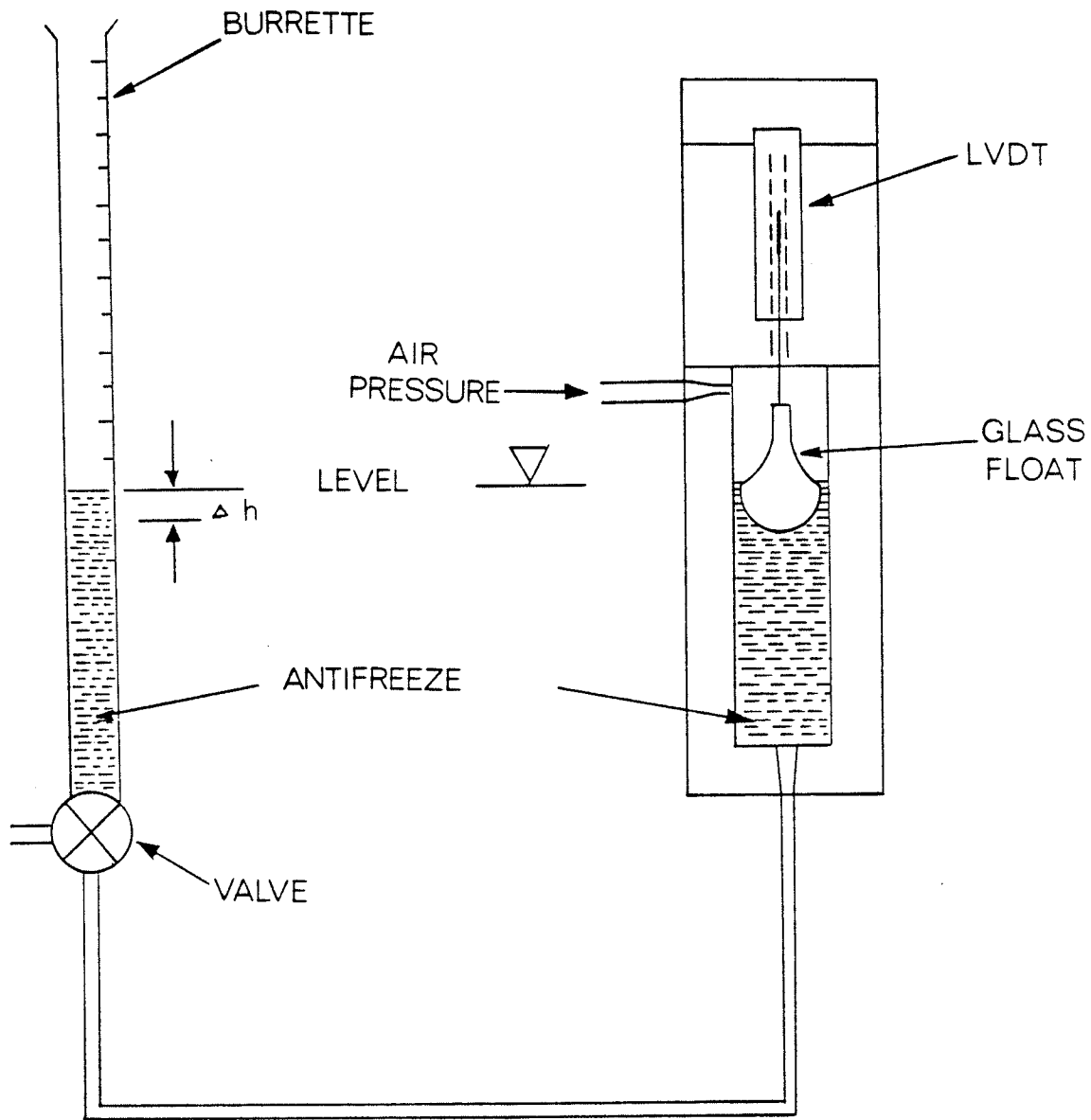
six stress increments was higher (± 0.06 cc). For stress increments of 140 kpa the average total error was approximately $+0.105$ cc. The average total error for stress increment of 350 kpa was found to be ± 0.135 cc., but the error for first increment was about ± 0.18 cc. and about ± 0.09 cc for second stress increment (700 kpa). For the stress increment of 700 kpa the average total error was about ± 0.29 cc.

The thermal expansion of the antifreeze was found to be approximately $0.6 \text{ cc} / ^\circ\text{C} / 2000 \text{ cc}$. The temperature fluctuation cause the fluid, as well as the apparatus, to expand or contract. During the test no reading was taken during the defrosting cycles of the environment chamber, therefore, the temperature effect was assumed to be negligible. But the temperature effect has to be taken into account especially if the test is going to be carried out in warmer temperature.

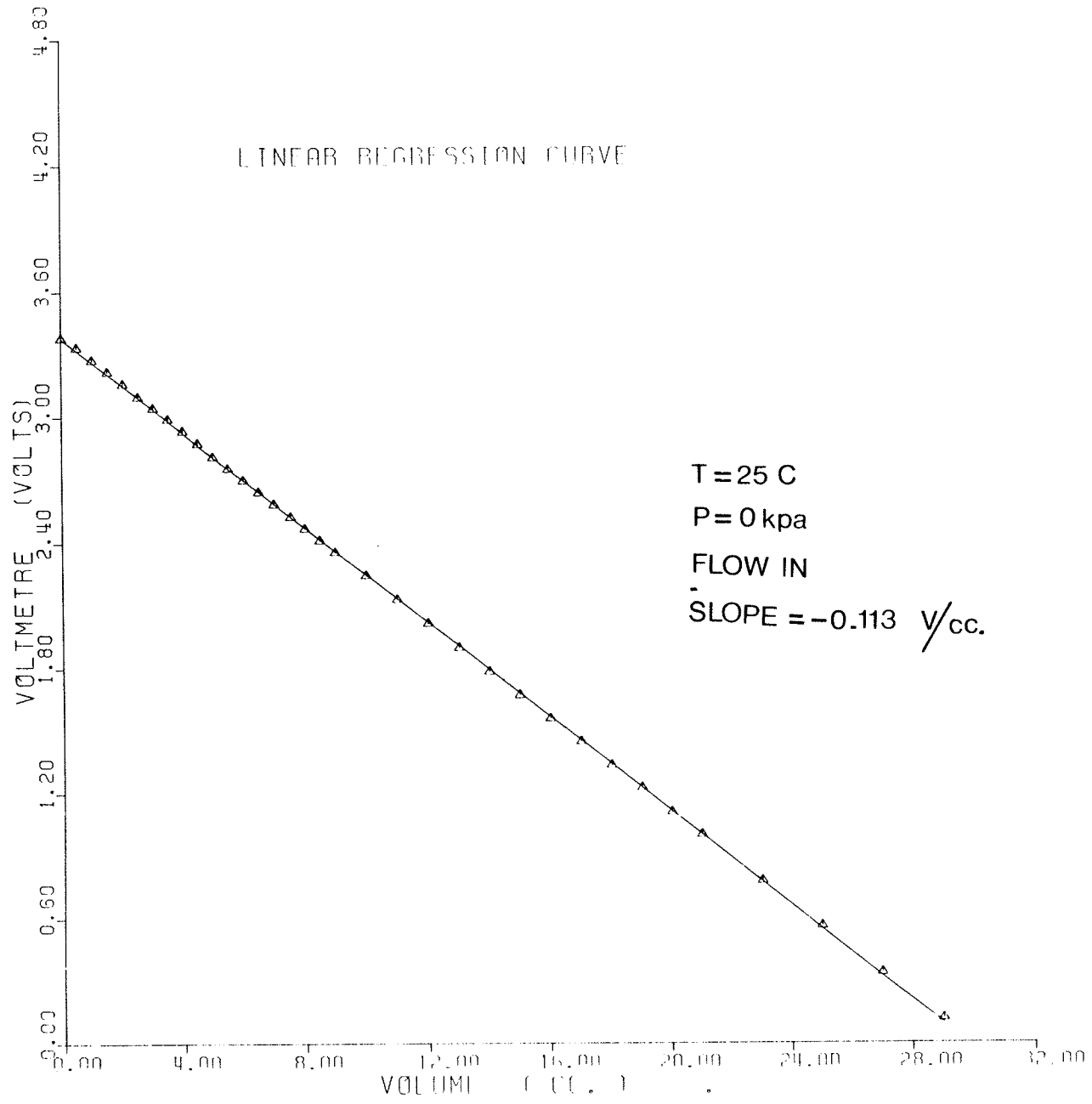
The initial volume change was calculated from the following

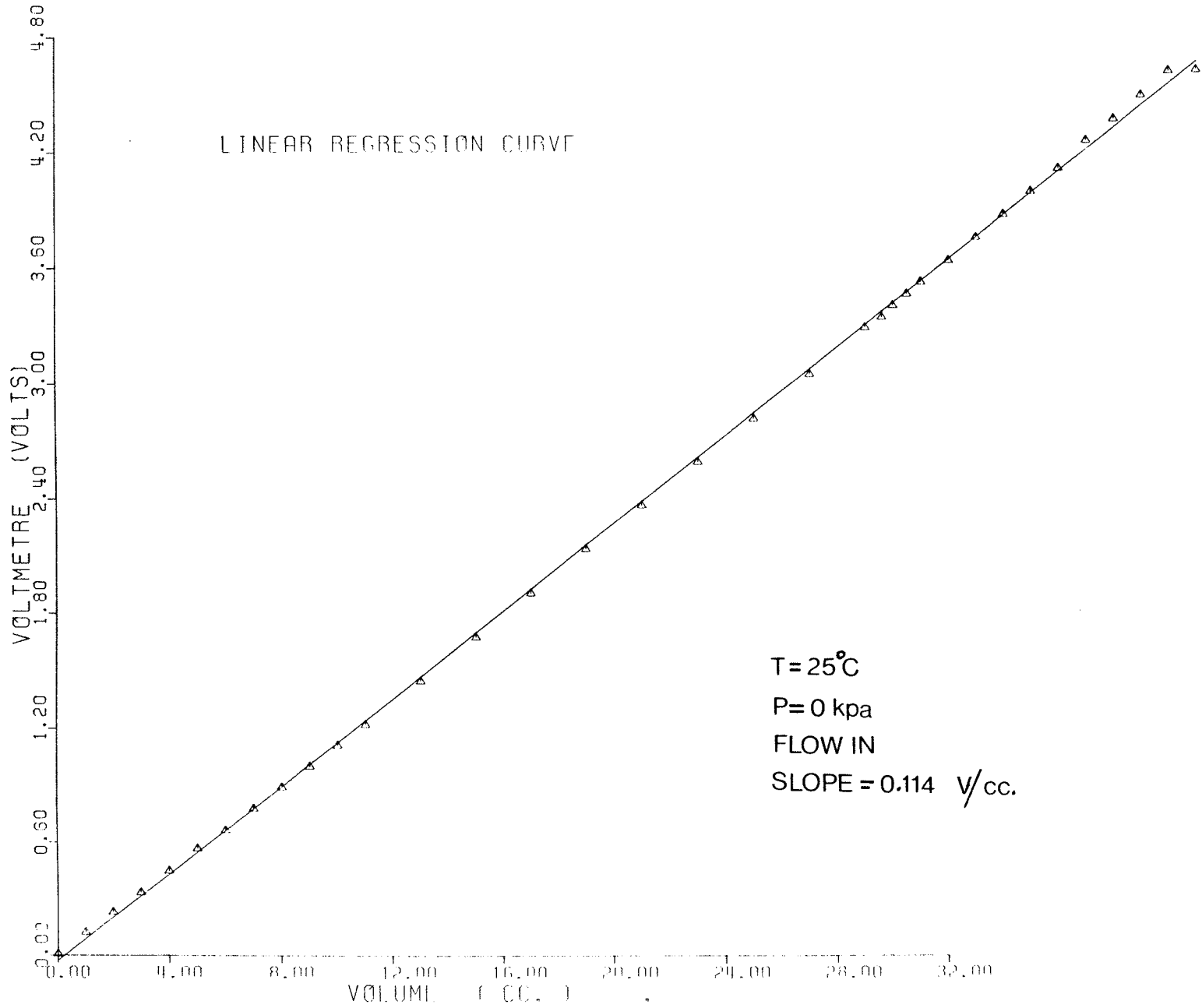
$$v_0 = (\text{LVDT reading (from test)} - \text{LVDT reading (from calibration)})$$

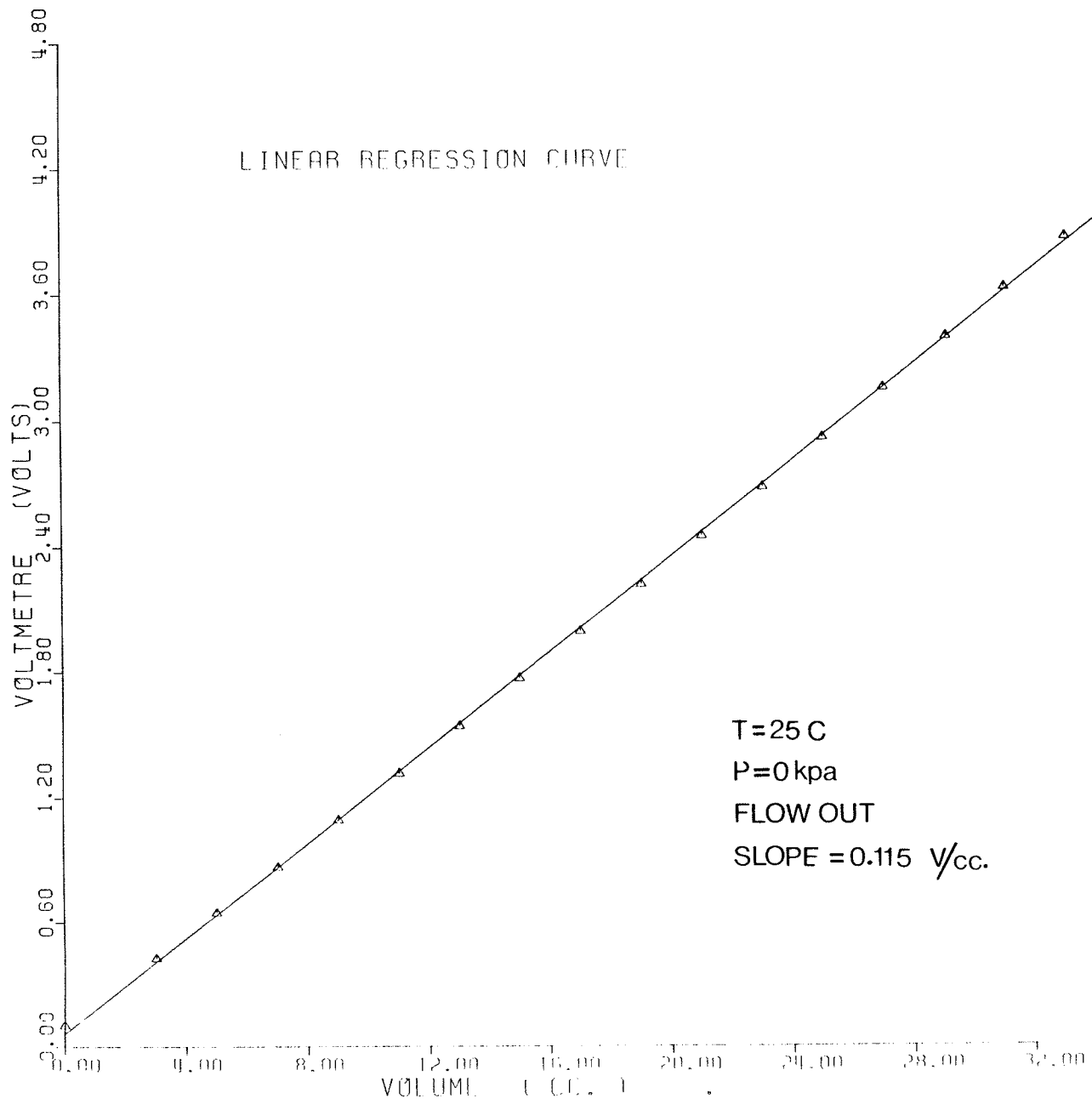
$$V_0 = v_0 / \text{LVDT calibration factor}$$

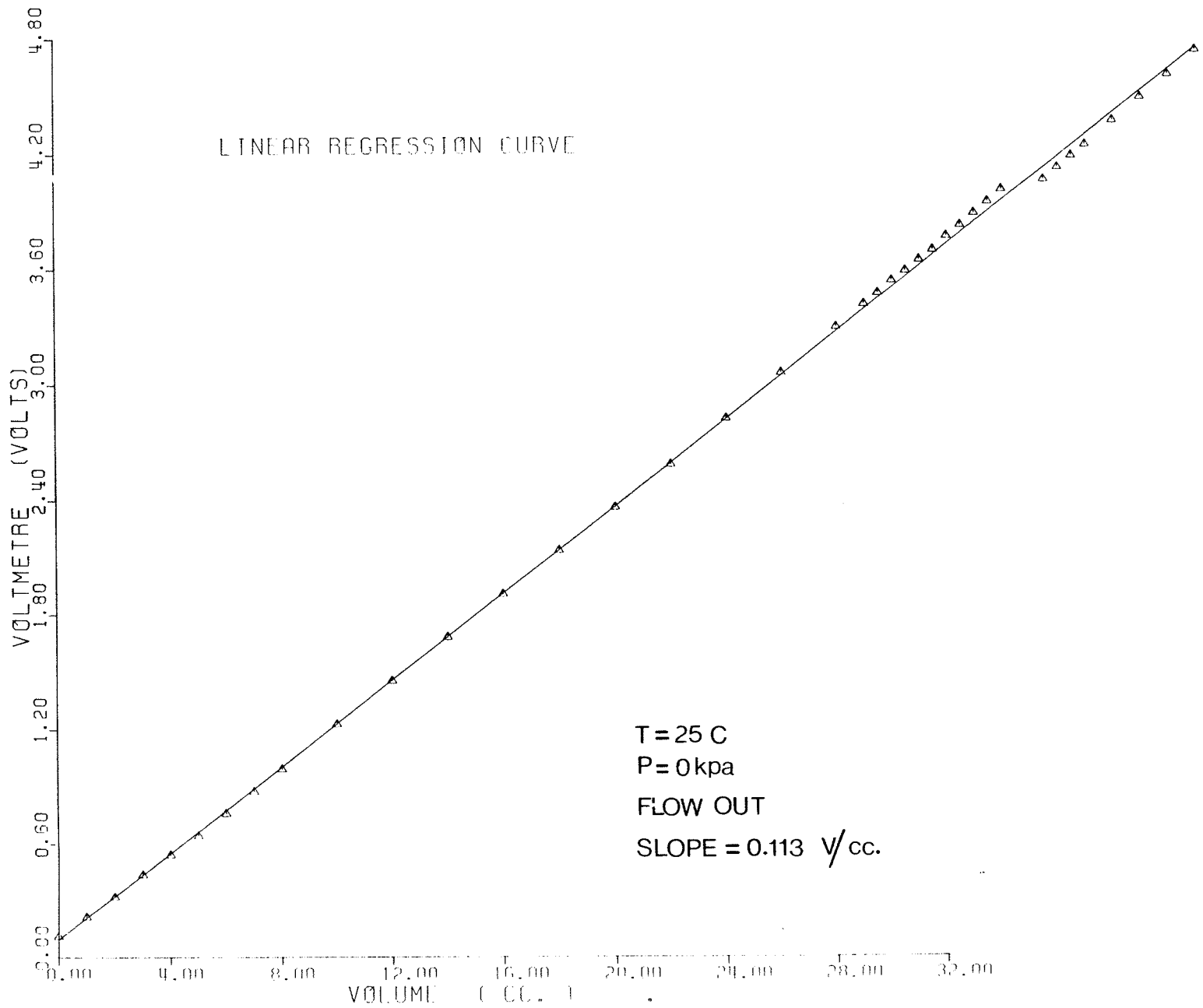


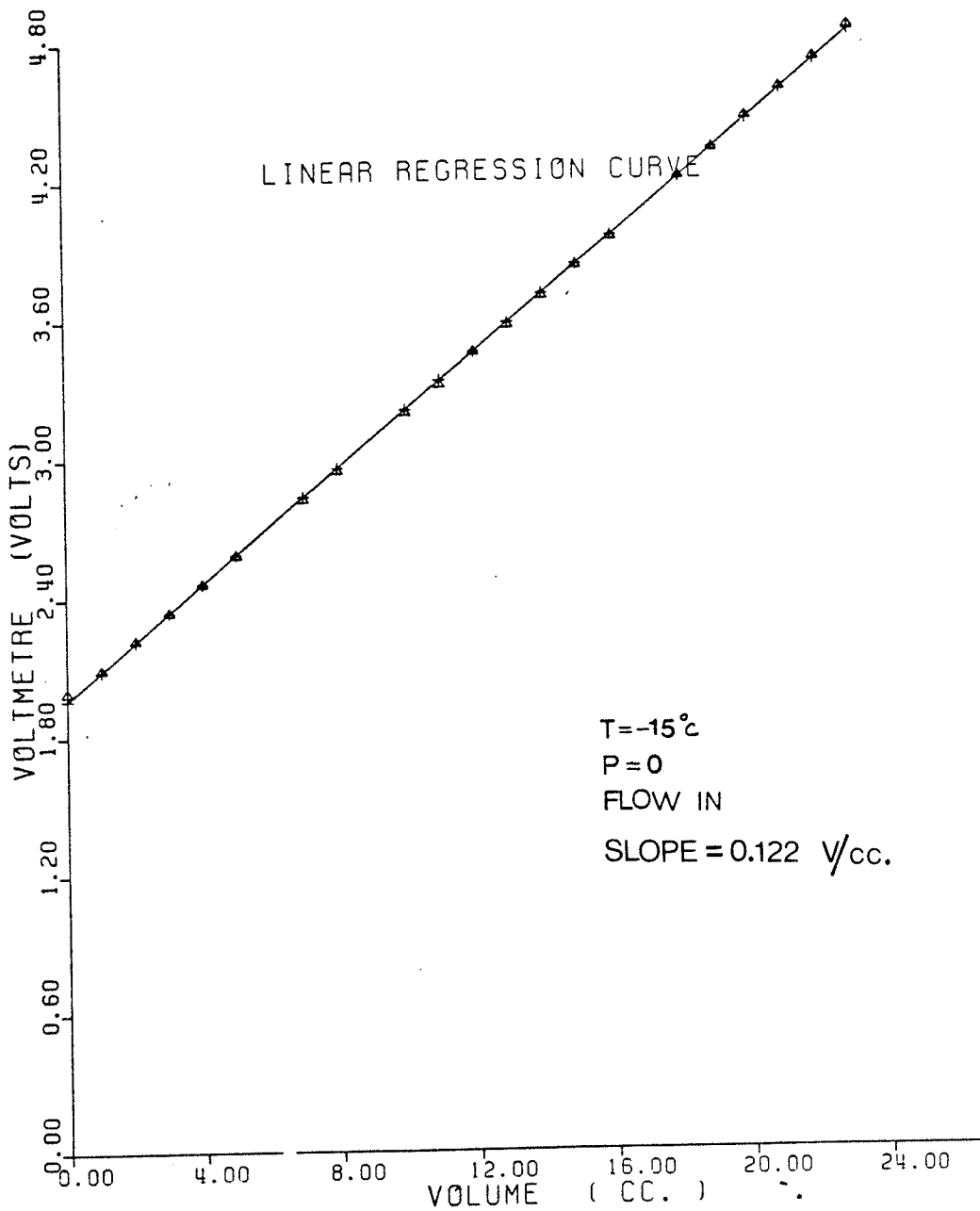
CALIBRATION OF VOLUME CHANGE MEASUREMENT DEVICE

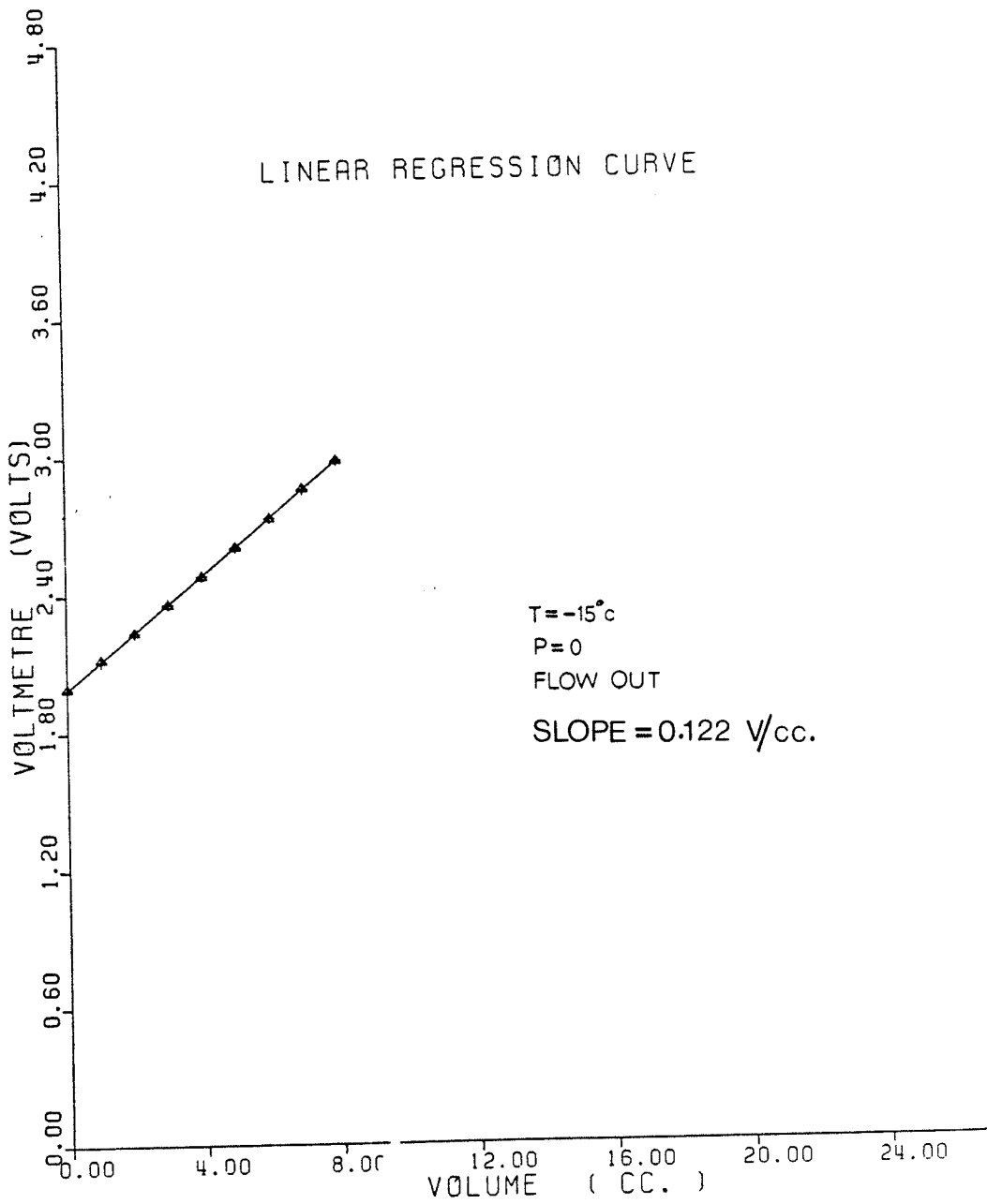


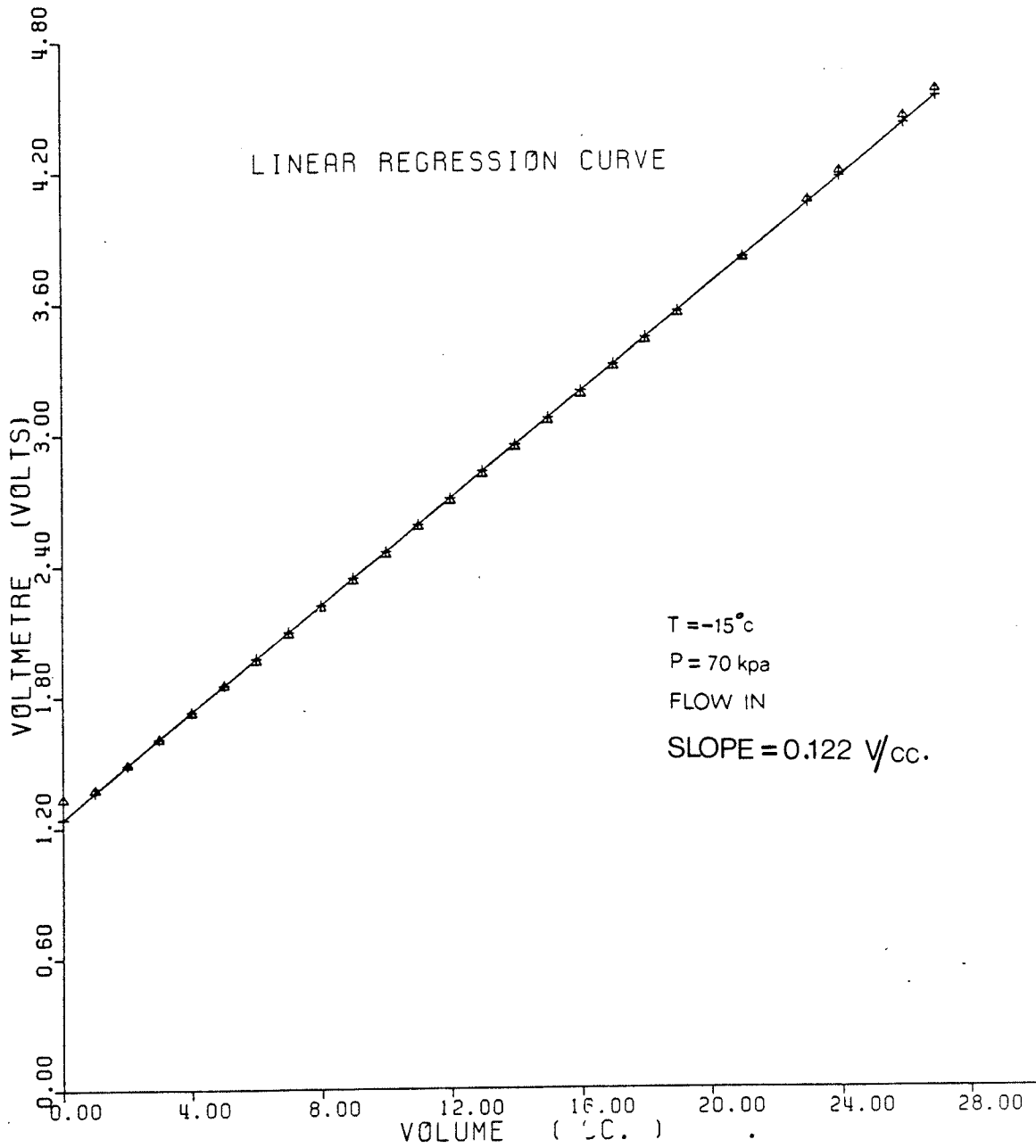


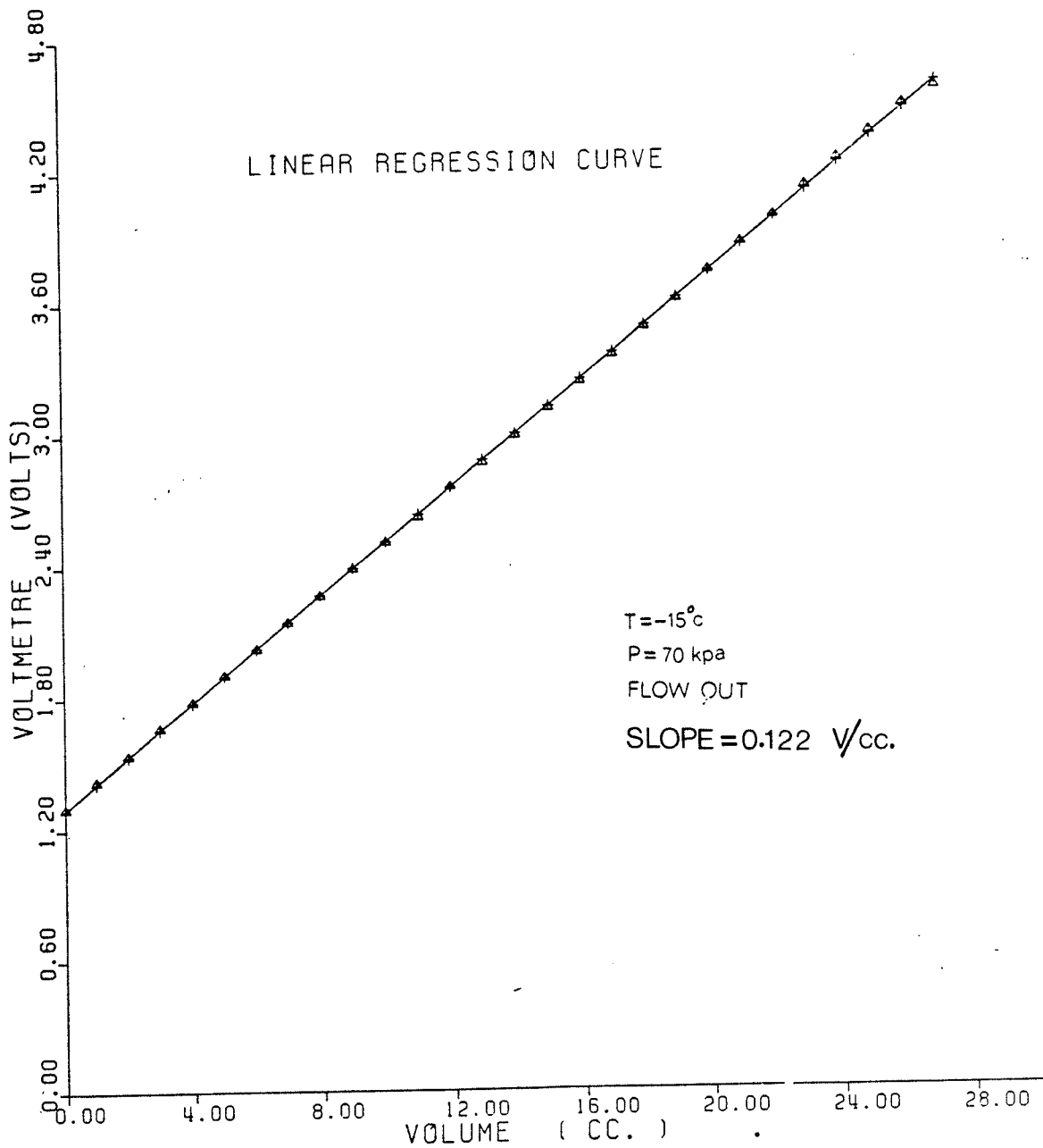


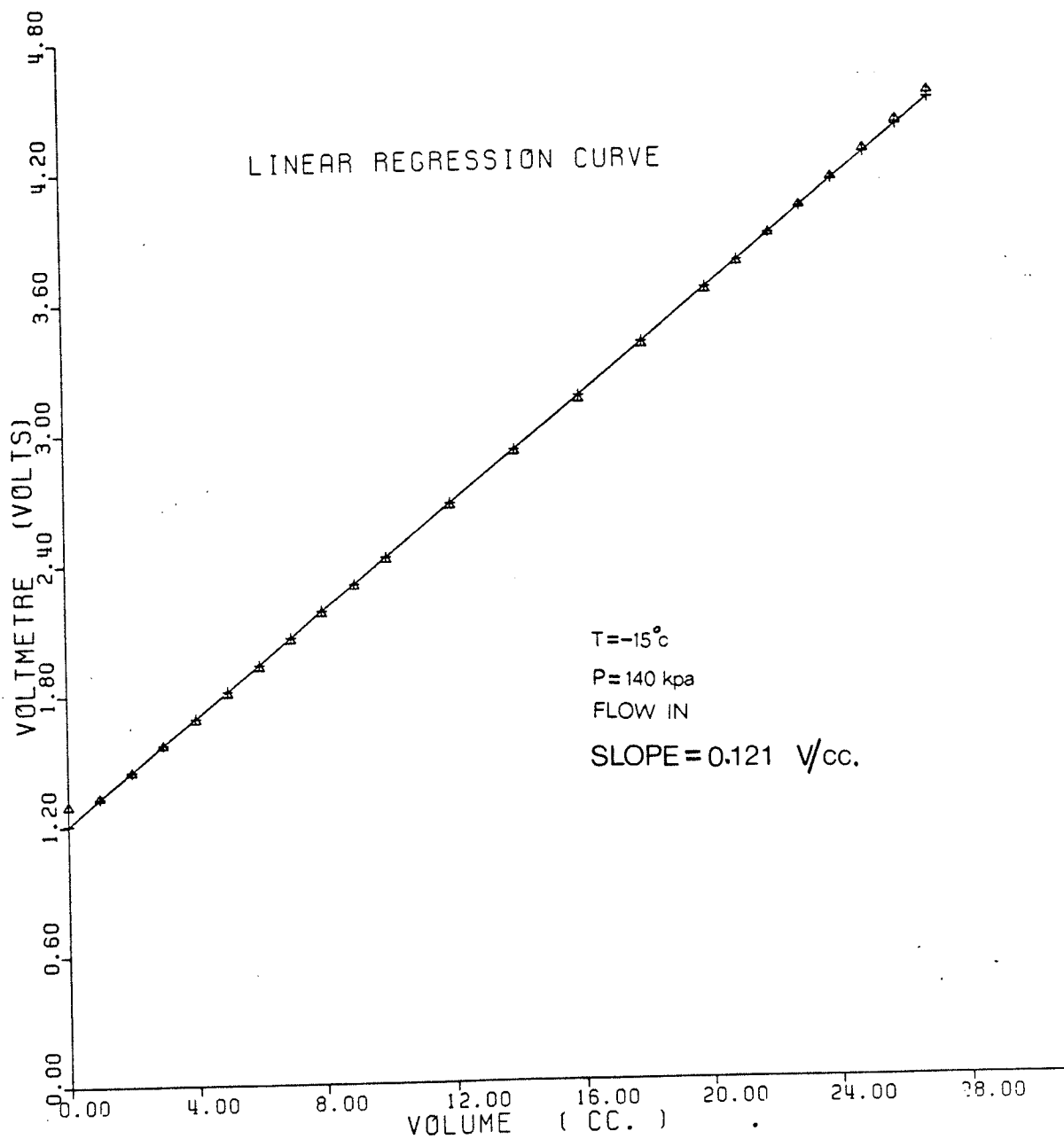


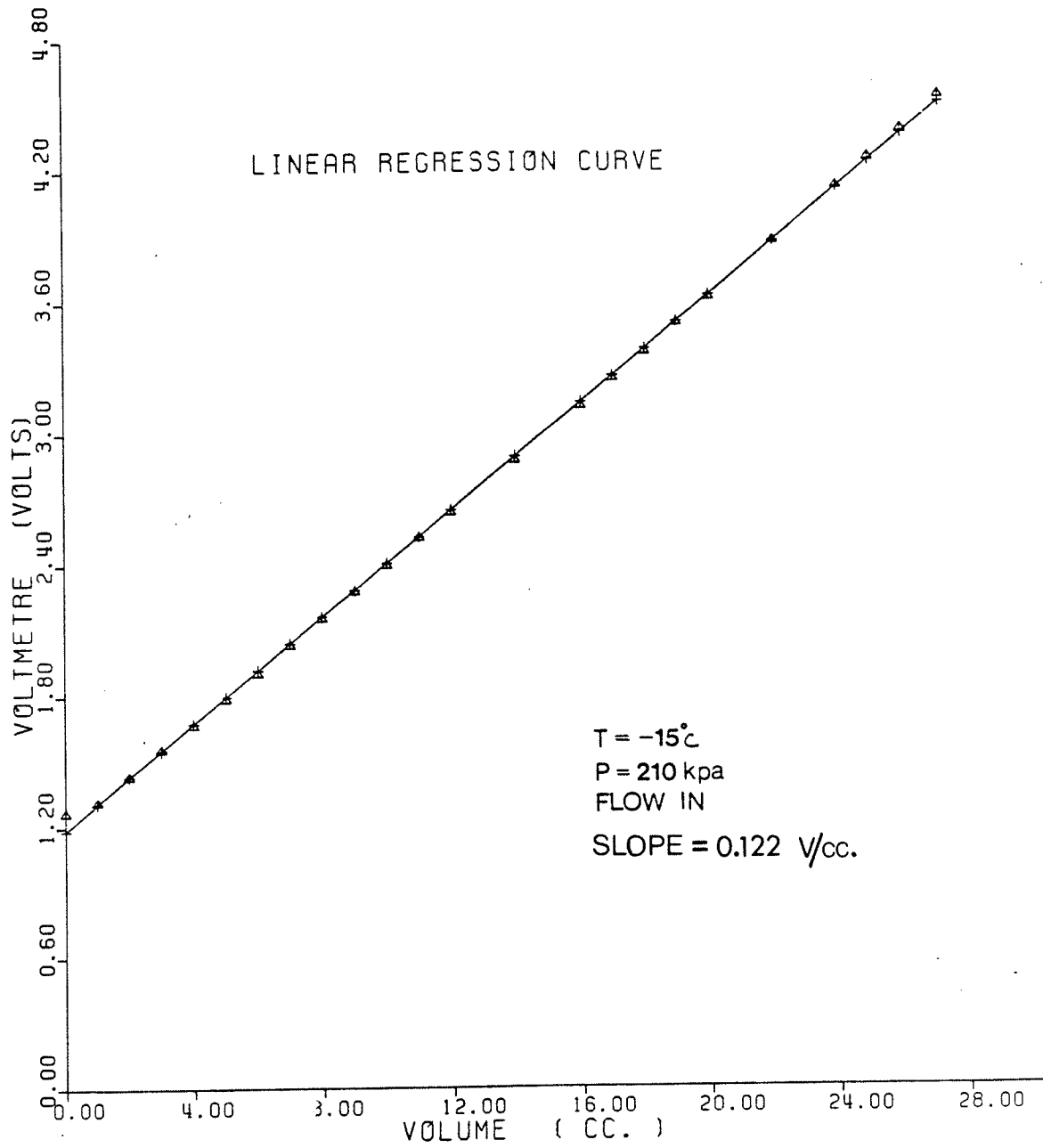


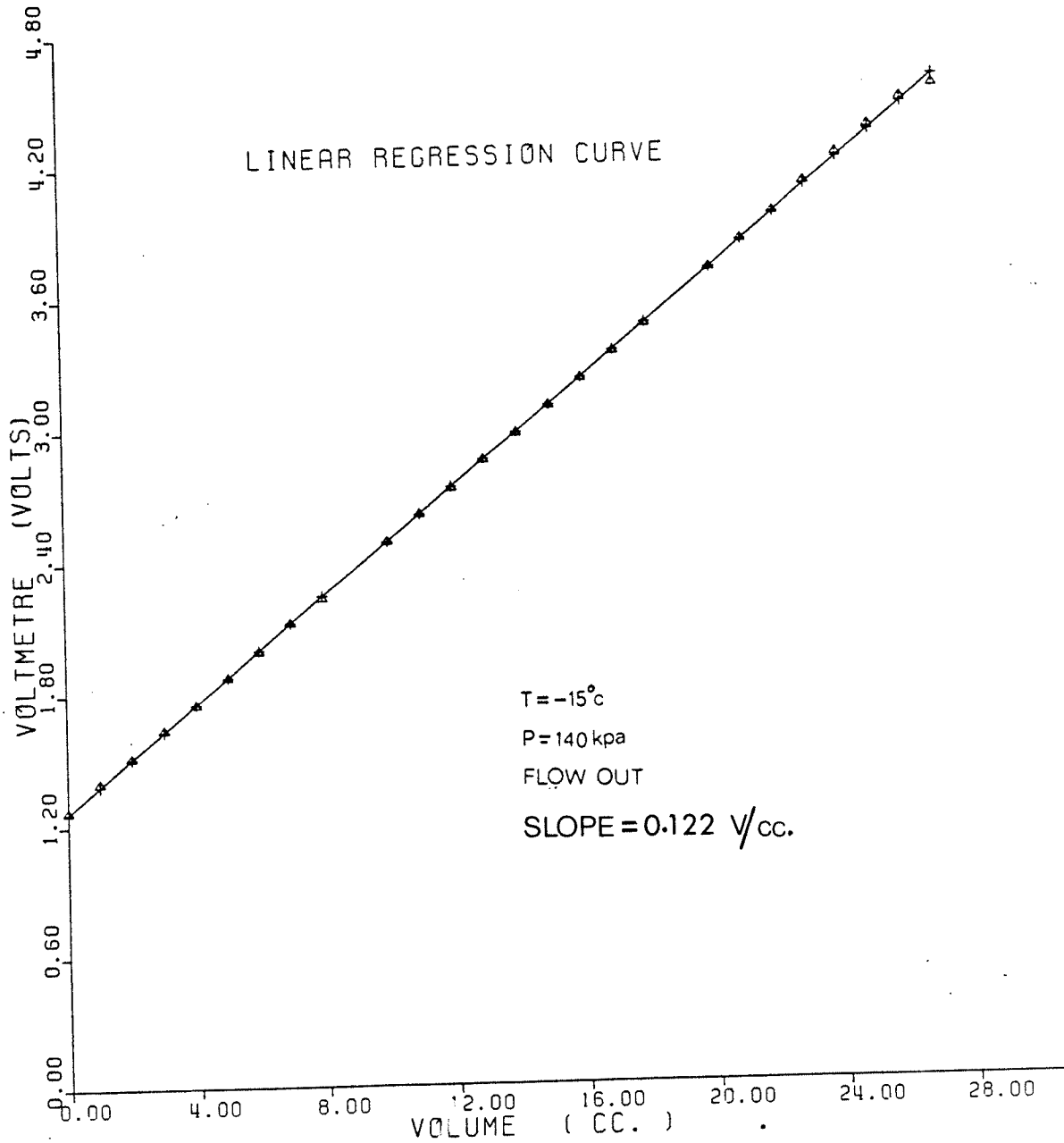


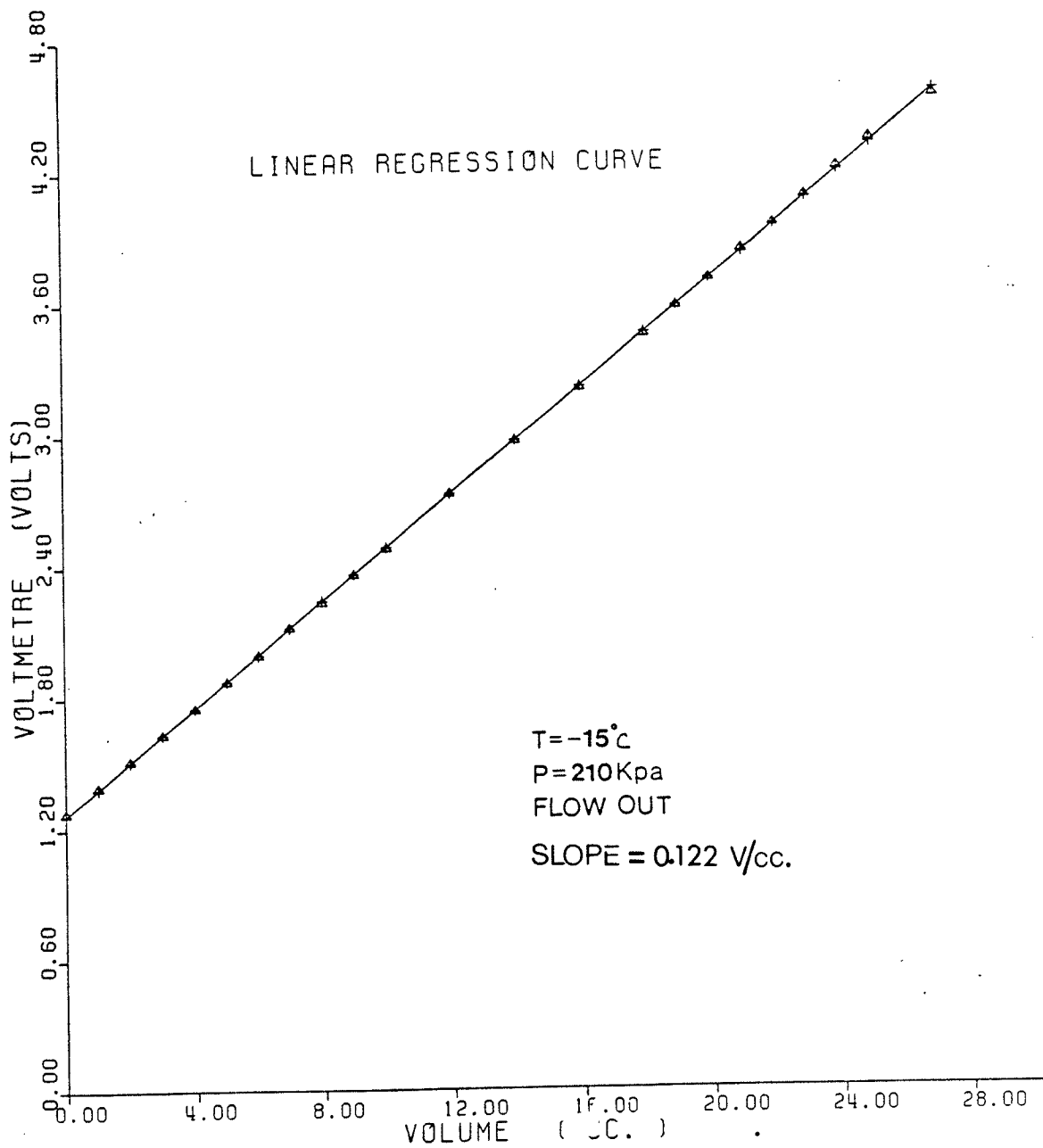


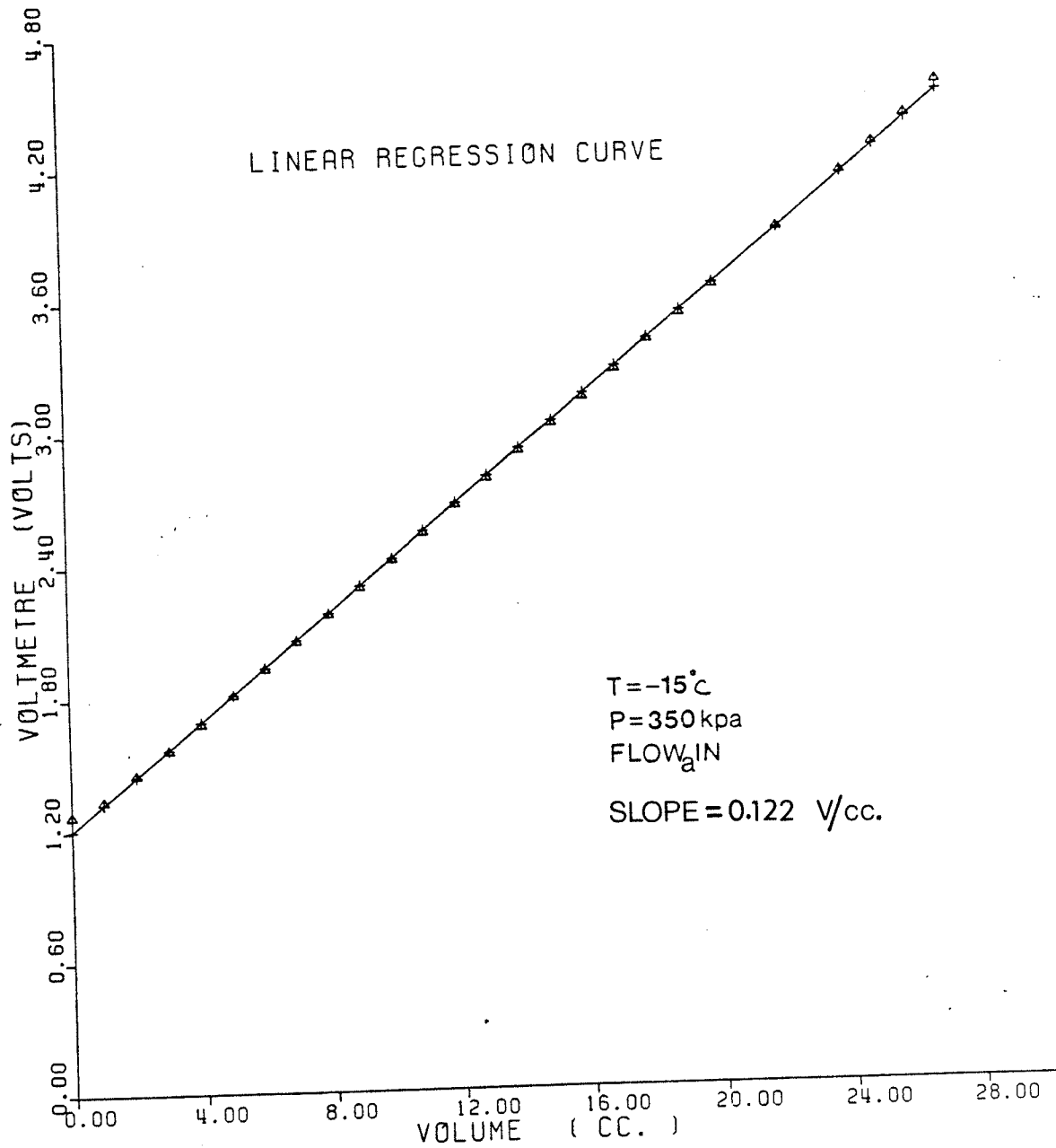


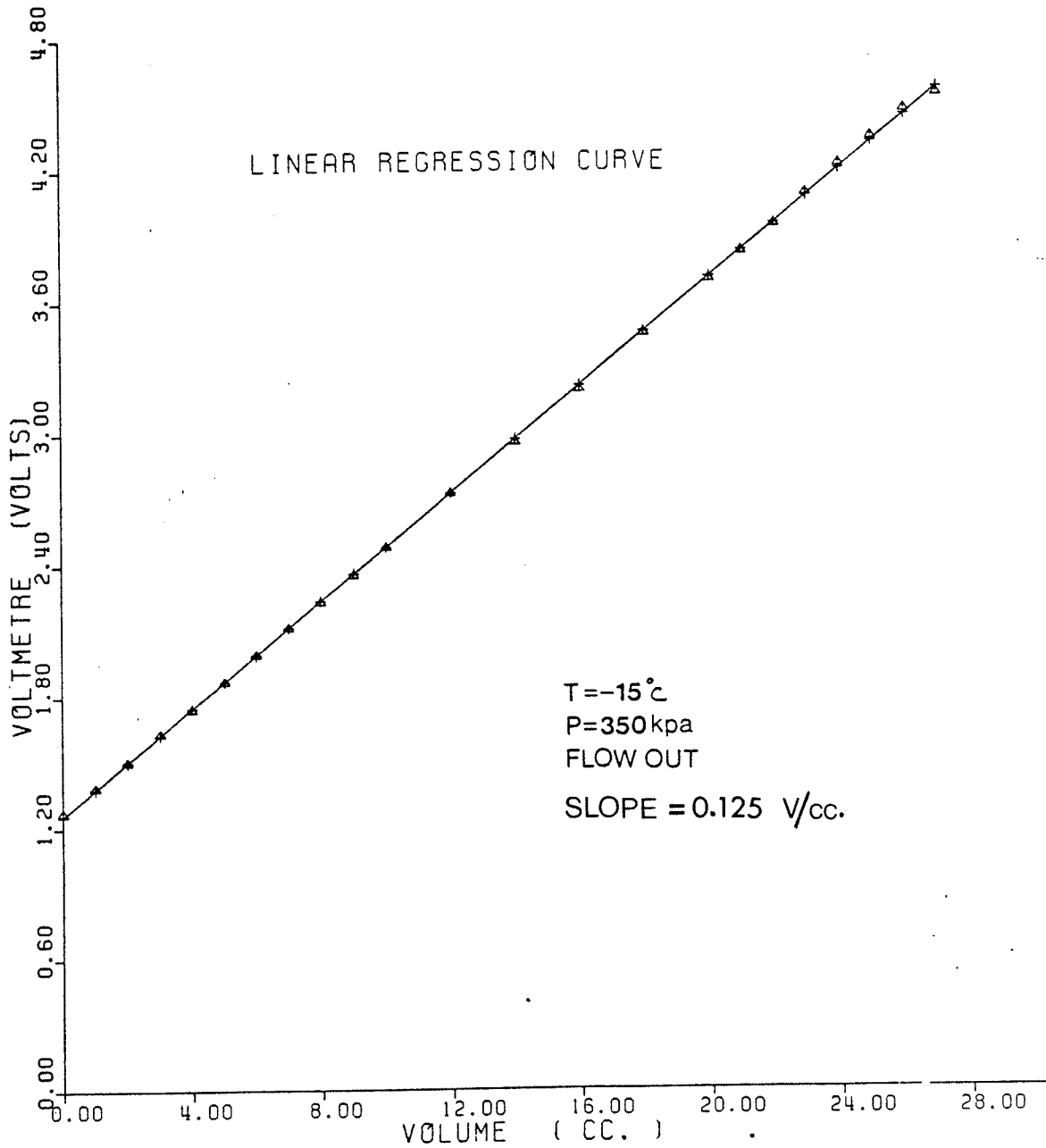


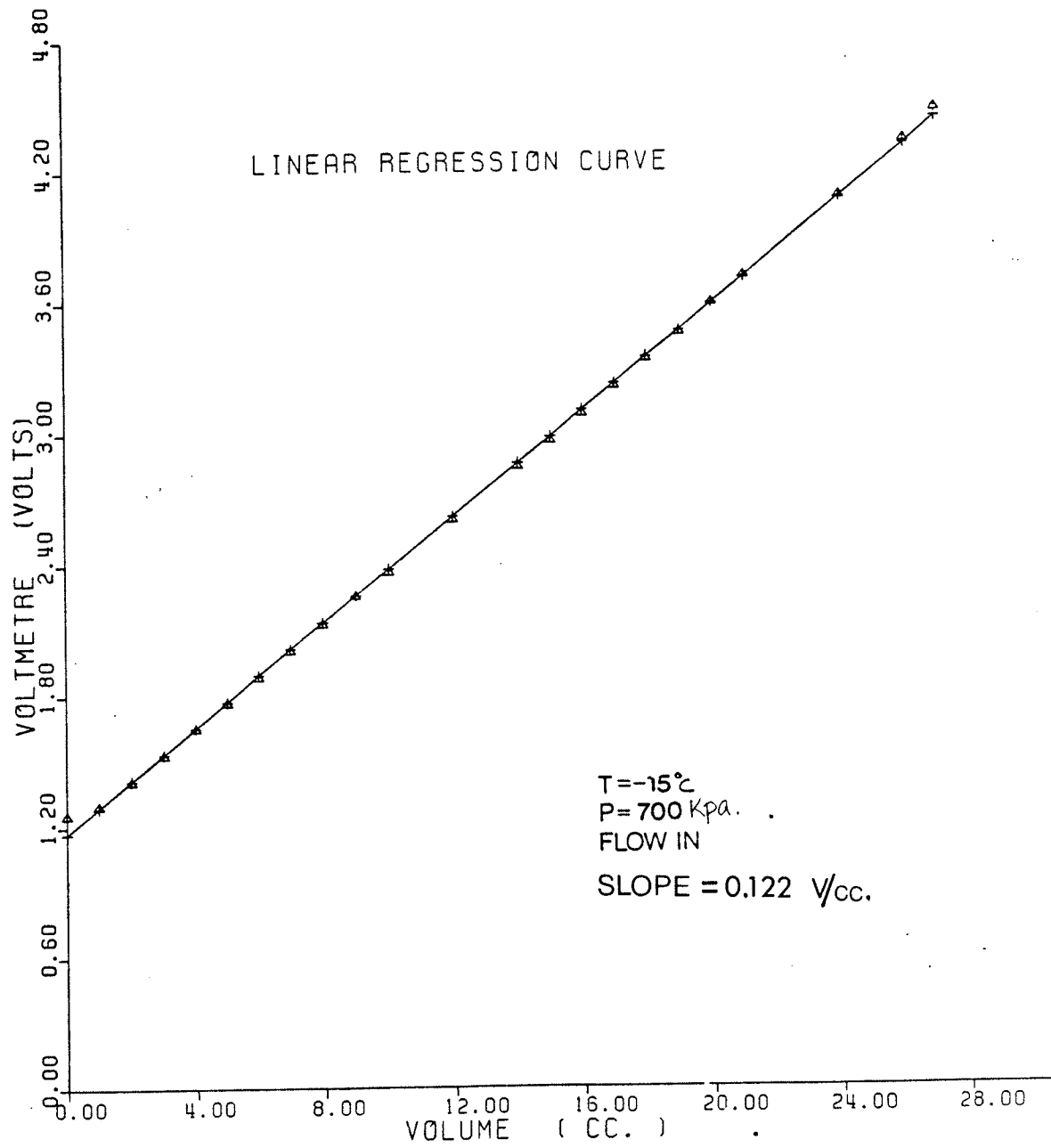


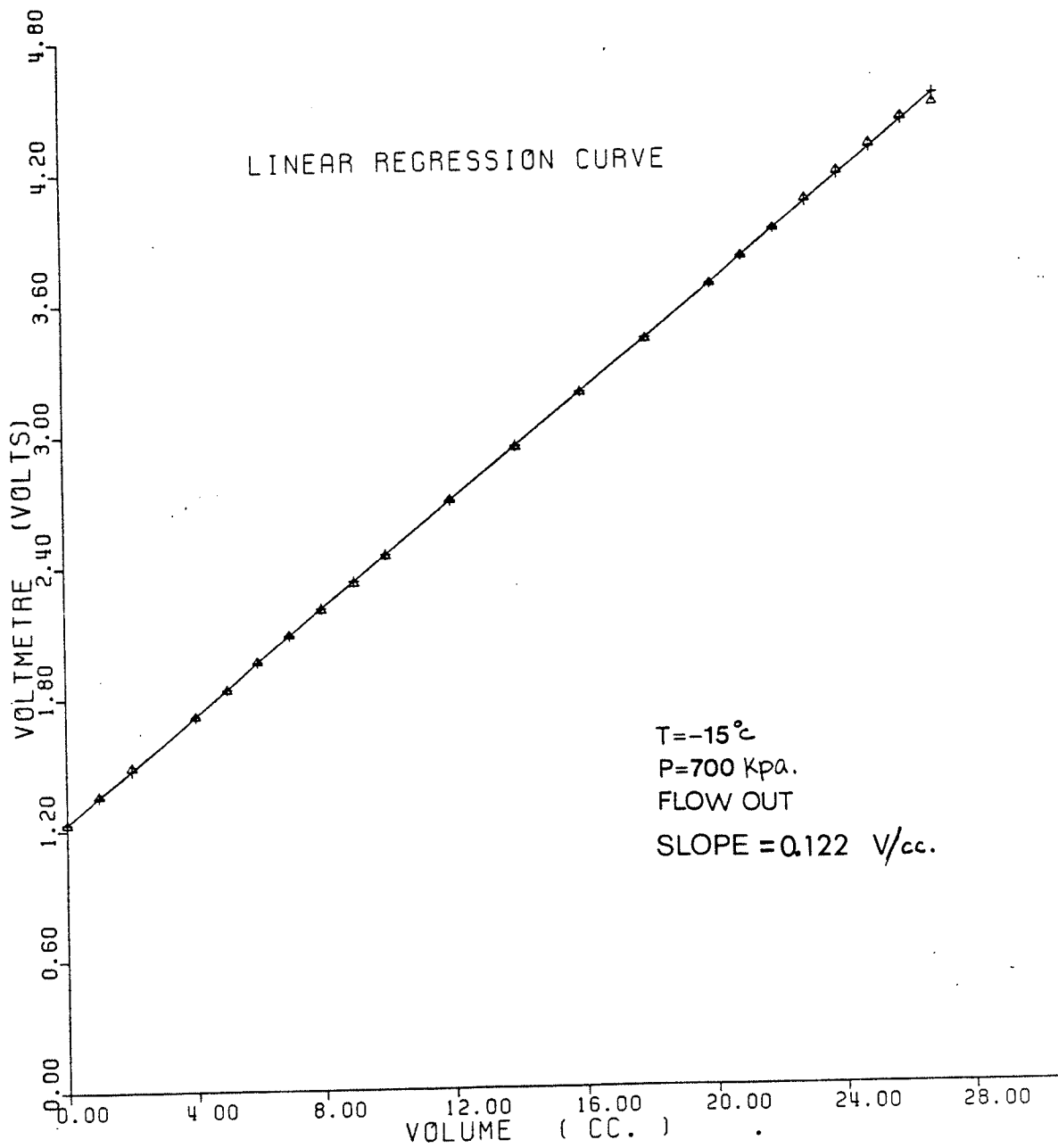


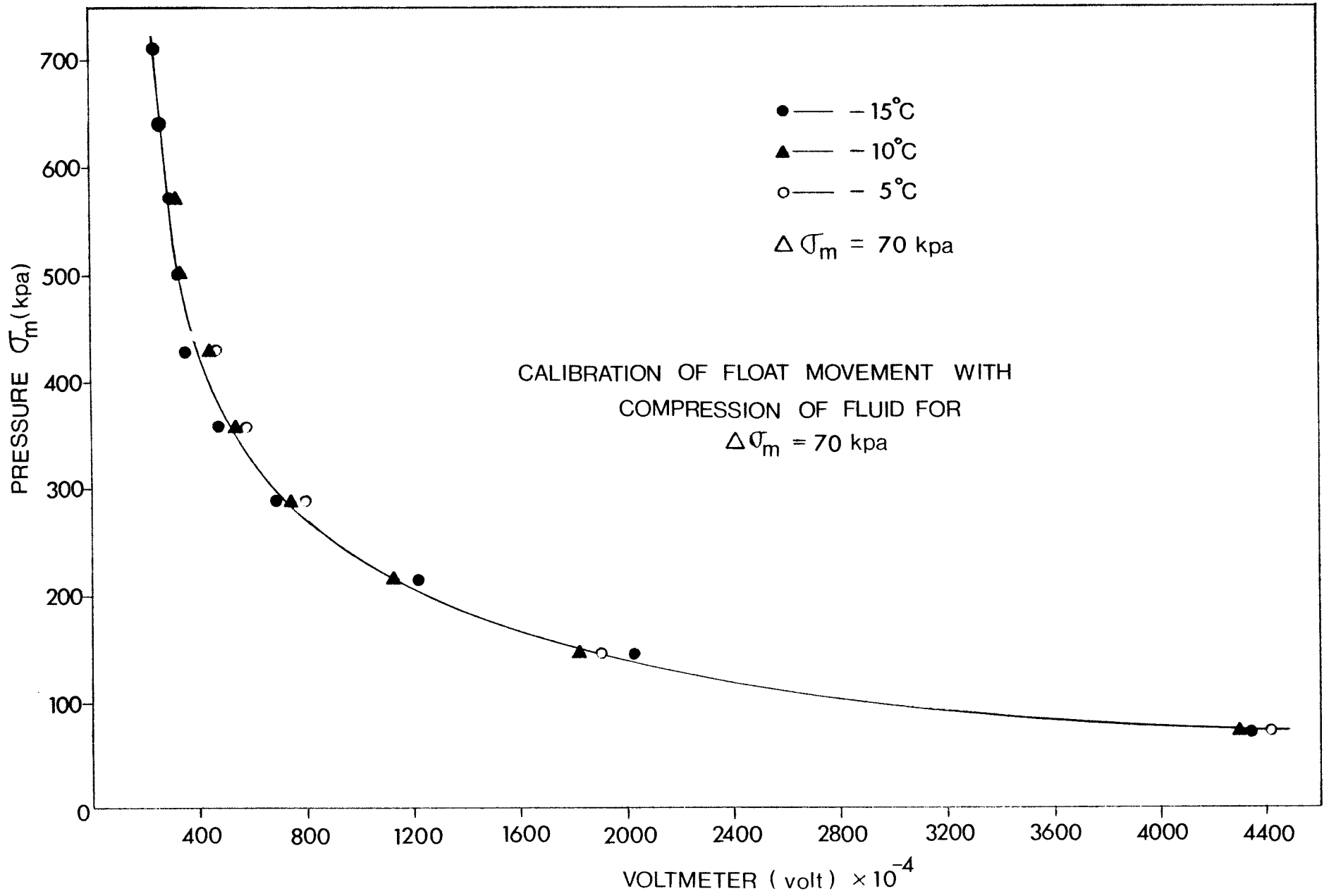


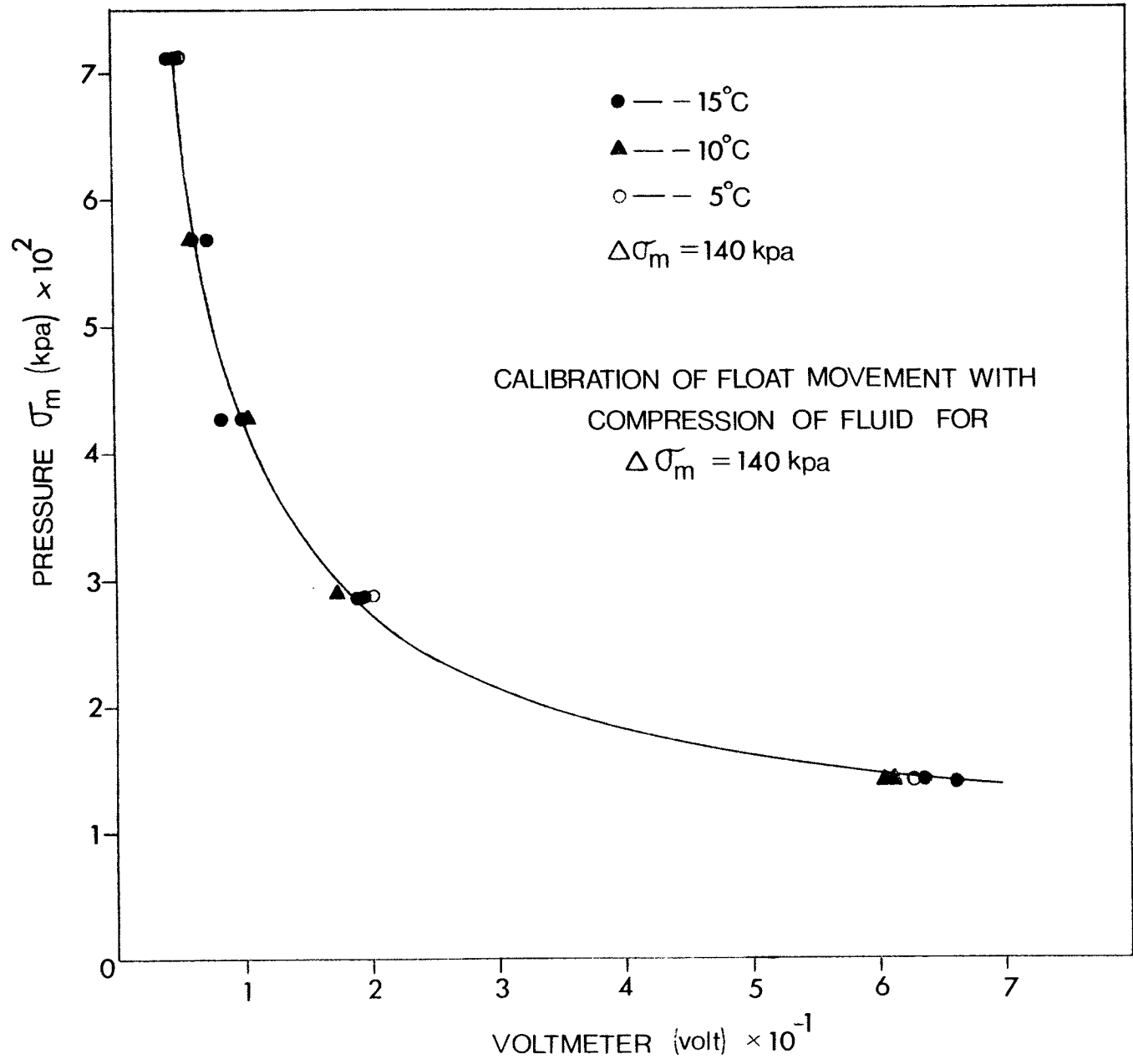


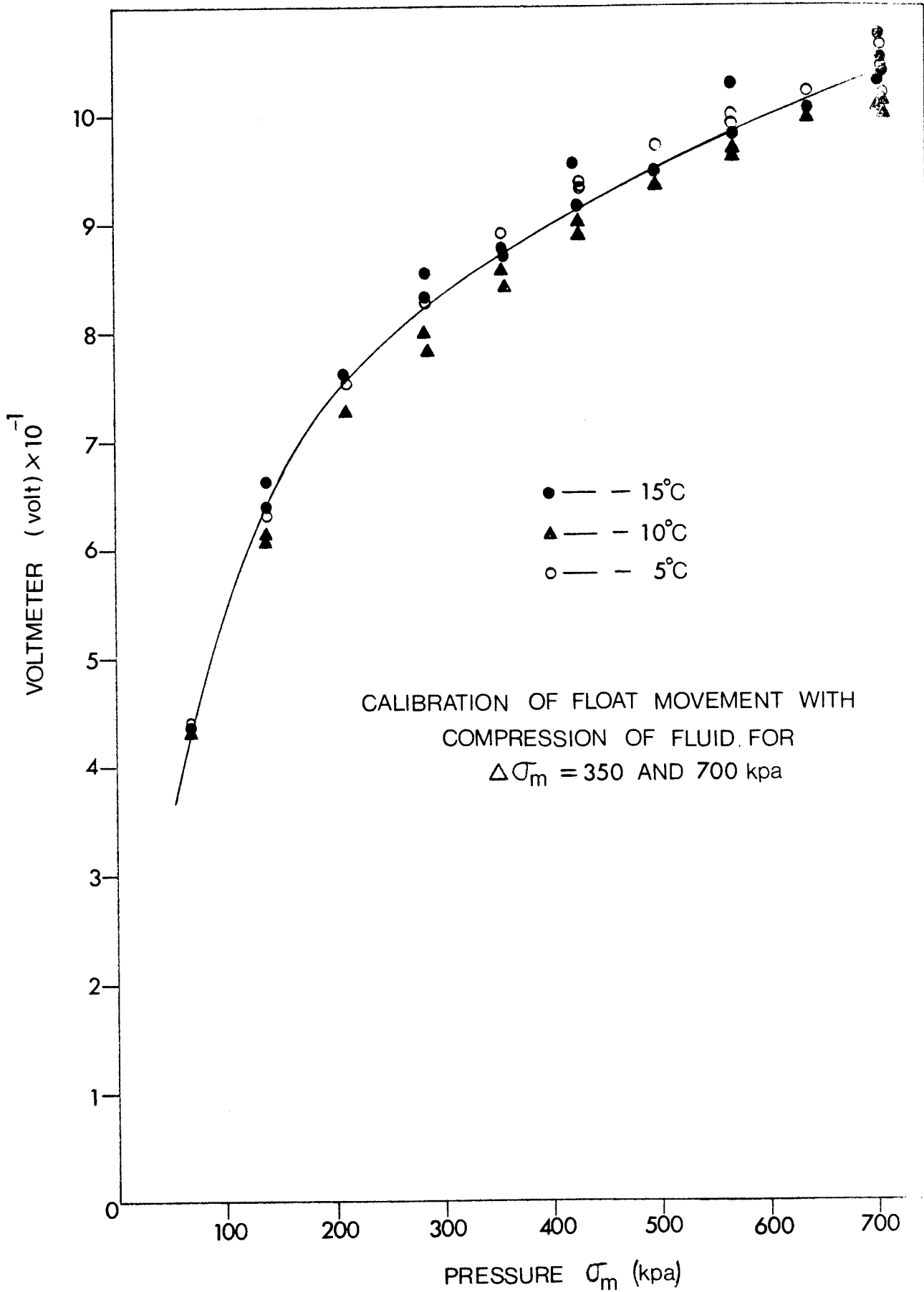












CALIBRATION OF FLOAT MOVEMENT AND COMPRESSION OF FLUID

DATE: 7th July 82

RATE OF TESTING: $\Delta\sigma = 70$ Kpa.

PRESSURE Kpa.	73	143	215	287	358	429	500	569	640	707
LVDI READING VOLT $\times 10^{-4}$	4349	1918	1128	748	526	429	325	308	254	244
SUM OF READING	4349	6267	7455	8503	8739	9168	9503	9811	10065	10309

TEMPERATURE: _____

NOTE: THE VALUES SHOWN IN THIS TABLE ARE THE MEAN VALUE.

THE INITIAL LVDI READING FROM THE TEST RESULTS ARE SUBTRACTED FROM THIS TABLE LVDI READING IN ORDER TO OBTAIN THE "ACTUAL" INITIAL READING.

RATE OF TESTING: $\Delta\sigma = 100$ Kpa

PRESSURE Kpa	143	284	430	569	705
LVDI READING VOLT $\times 10^{-4}$	6296	1902	1002	671	495
SUM OF READING	6296	8198	9200	9871	10366

RATE OF TESTING: $\Delta\sigma = 350$ Kpa

PRESSURE Kpa.	350	708		
LVDI READING VOLT $\times 10^{-4}$	8696	1622		
SUM OF READING	8696	15228		

RATE OF TESTING: $\Delta\sigma = 705$ Kpa.

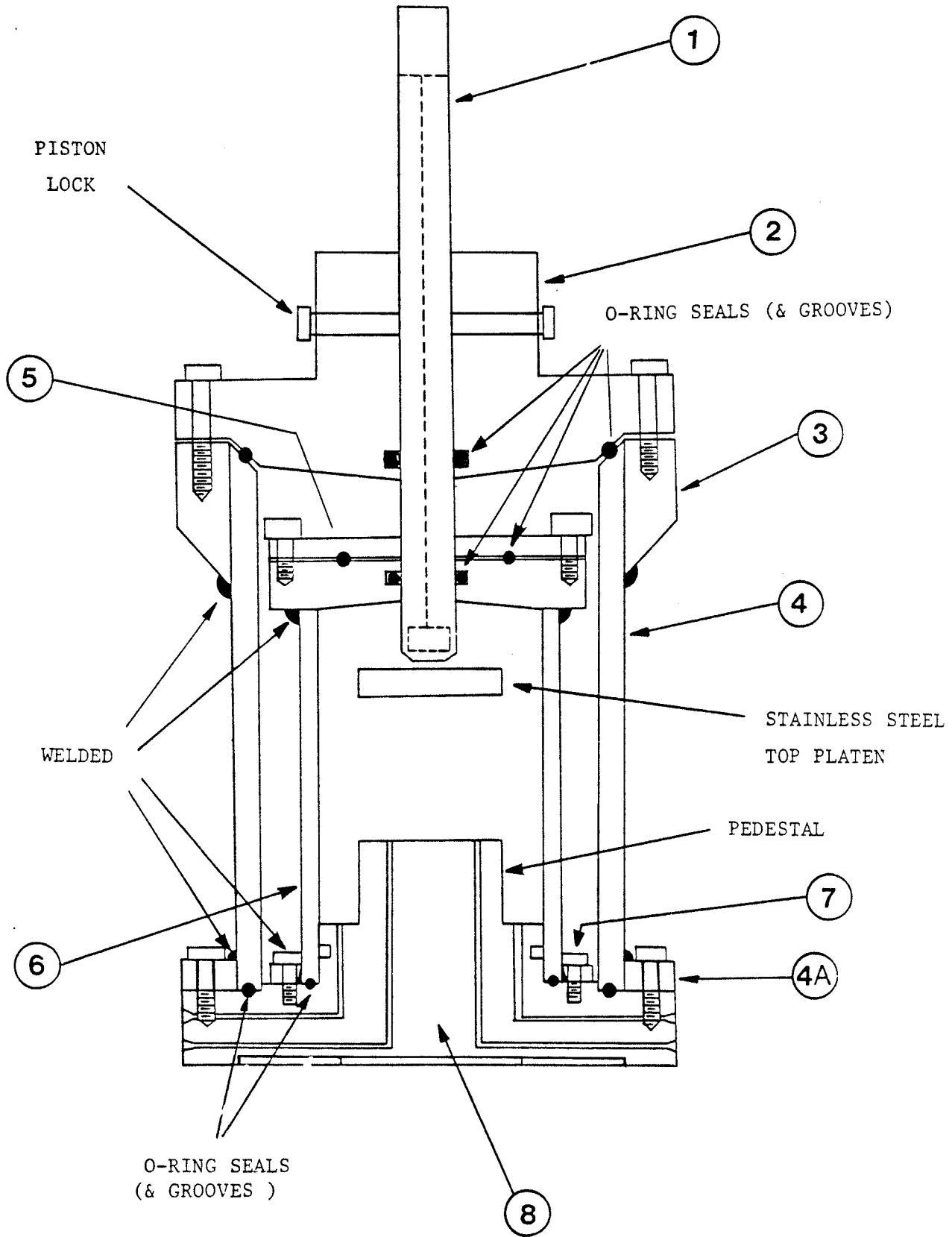
	705		
	10289		

APPENDIX III

DETAILS OF TRIAXIAL CELL AND VOLUME CHANGE

MEASUREMENT DEVICE

TRIAXIAL CELL ASSEMBLY

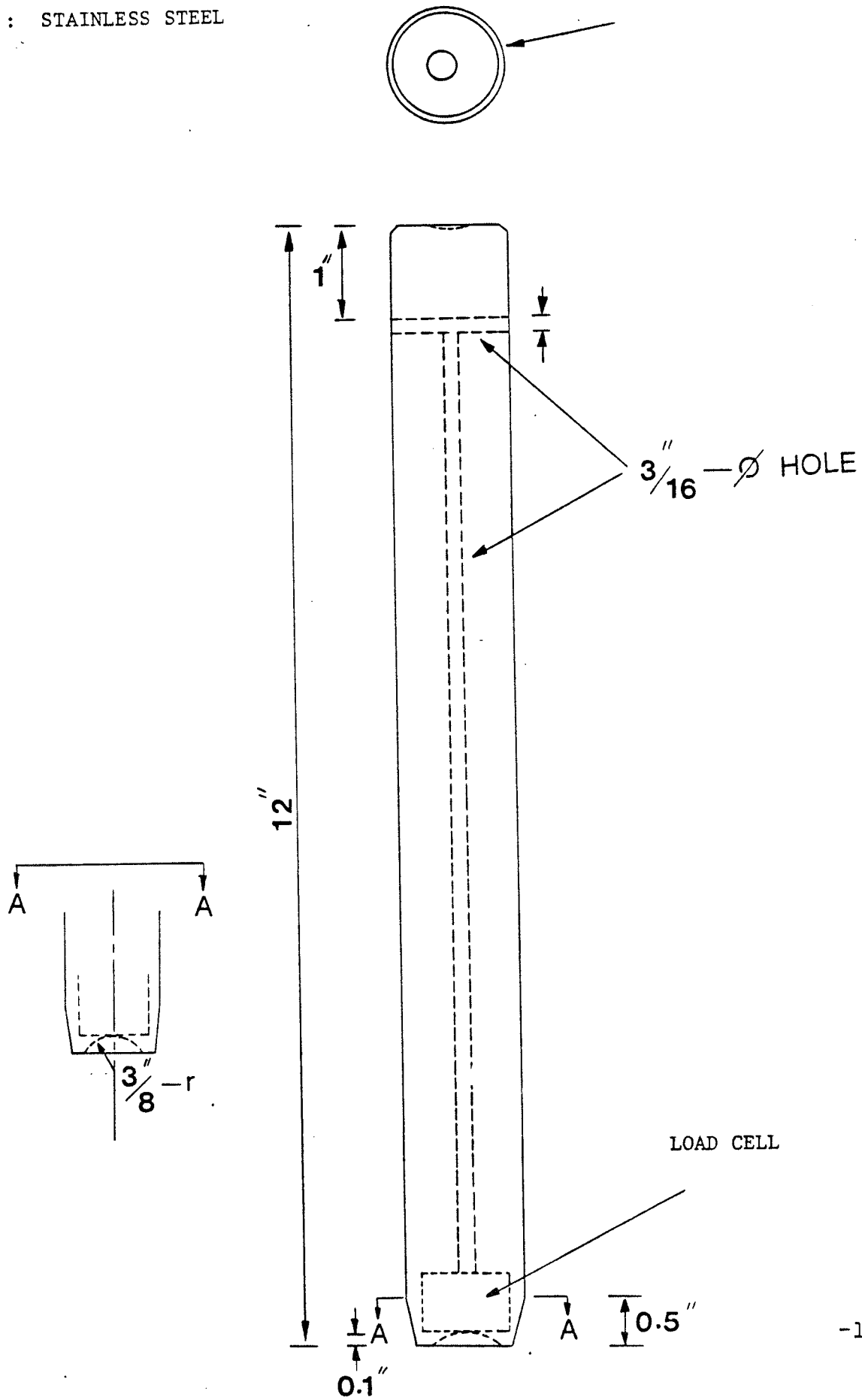


- ① ————— PISTON
- ② ————— OUTER CYLINDER TOP COVER
- ③ ————— OUTER CYLINDER SHOULDER (TOP)
- ④ ————— OUTER CYLINDER
- ④A ————— OUTER CYLINDER SHOULDER (BOTTOM)
- ⑤ ————— INNER CYLINDER TOP COVER
- ⑥ ————— INNER CYLINDER
- ⑦ ————— INNER CYLINDER SHOULDER (BOTTOM)
- ⑧ ————— CELL BASE

PART # 1 : PISTON

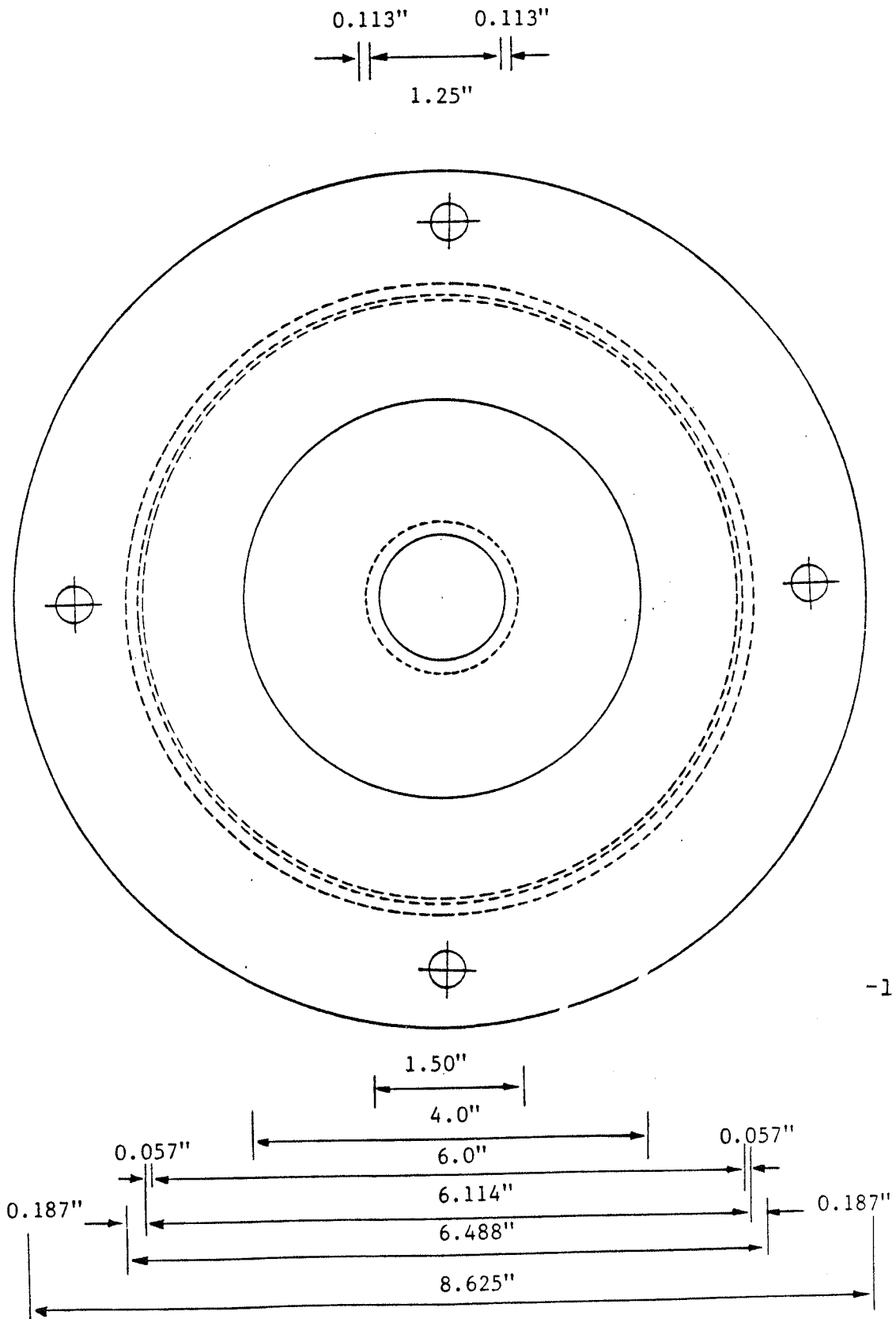
MATERIAL : STAINLESS STEEL

O.D. = 1.250" + 0.003 "



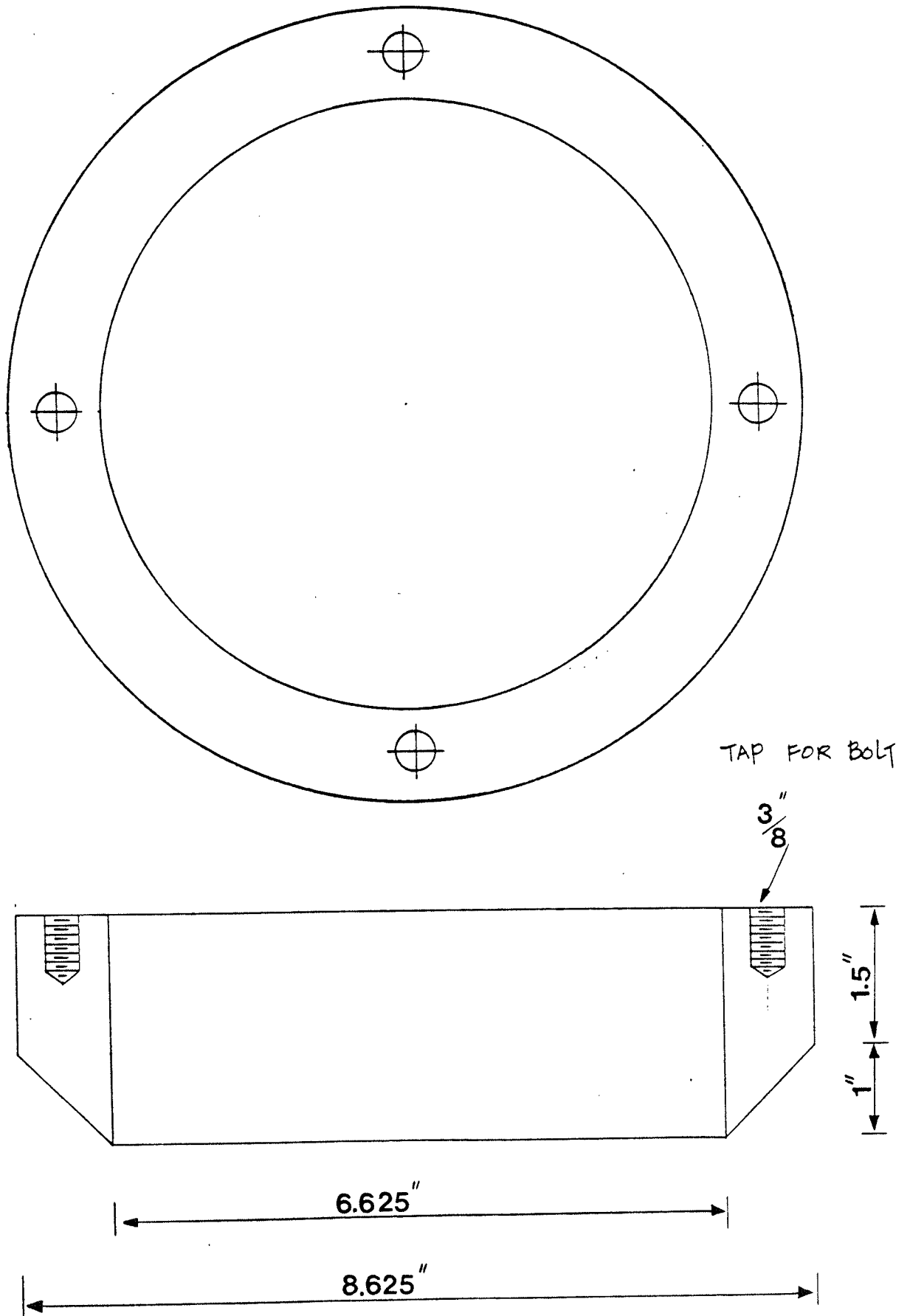
PART # 2 : OUTER CYLINDER TOP COVER

MATERIAL : ALUMINUM



PART # 3 : OUTER CYLINDER SHOULD (TOP)

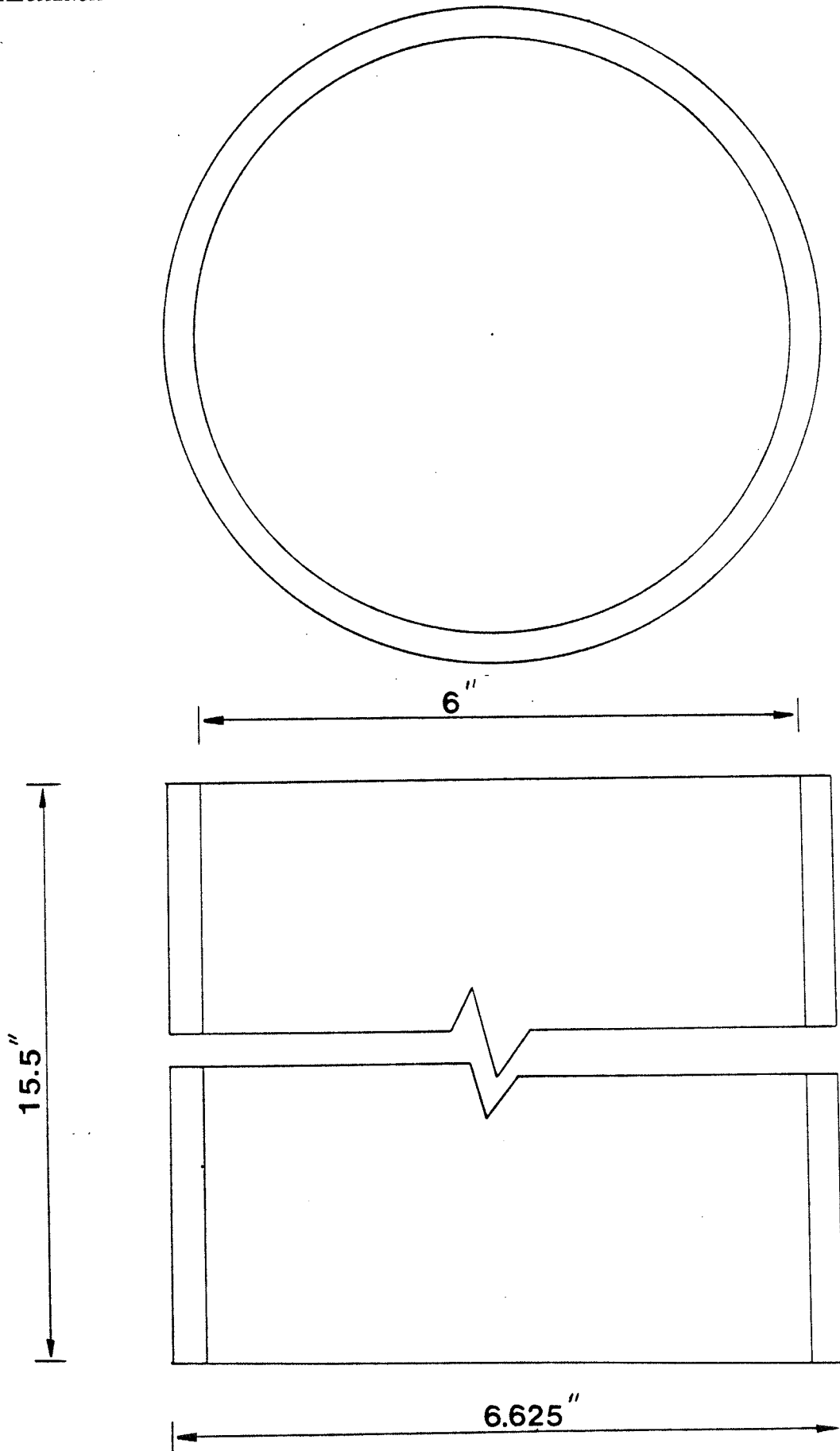
MATERIAL : ALUMINUM



PART # 4 : OUTER CYLINDER

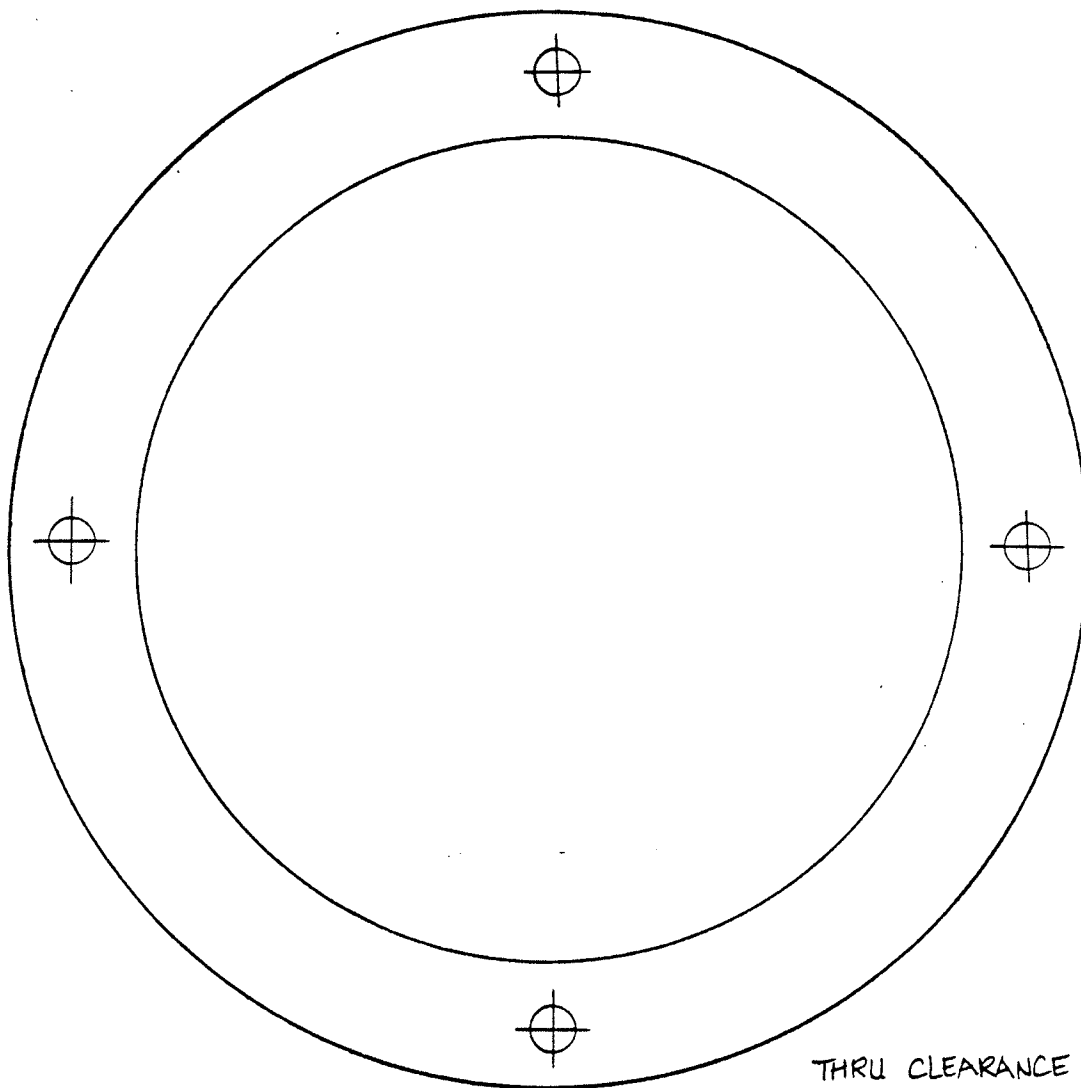
MATERIAL : ALUMINUM

NOTE: MACHINE O.D.
SO THAT PART
#3 FITS THIGHT
OVER PIPE.



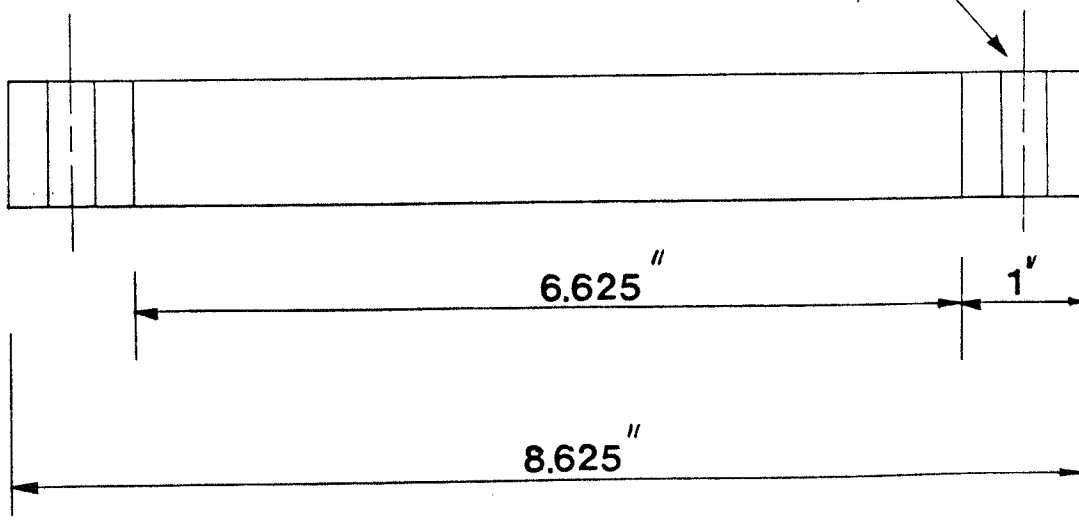
PART # 4A : OUTER CYLINDER SHOULDER (BOTTOM)

MATERIAL : ALUMINUM



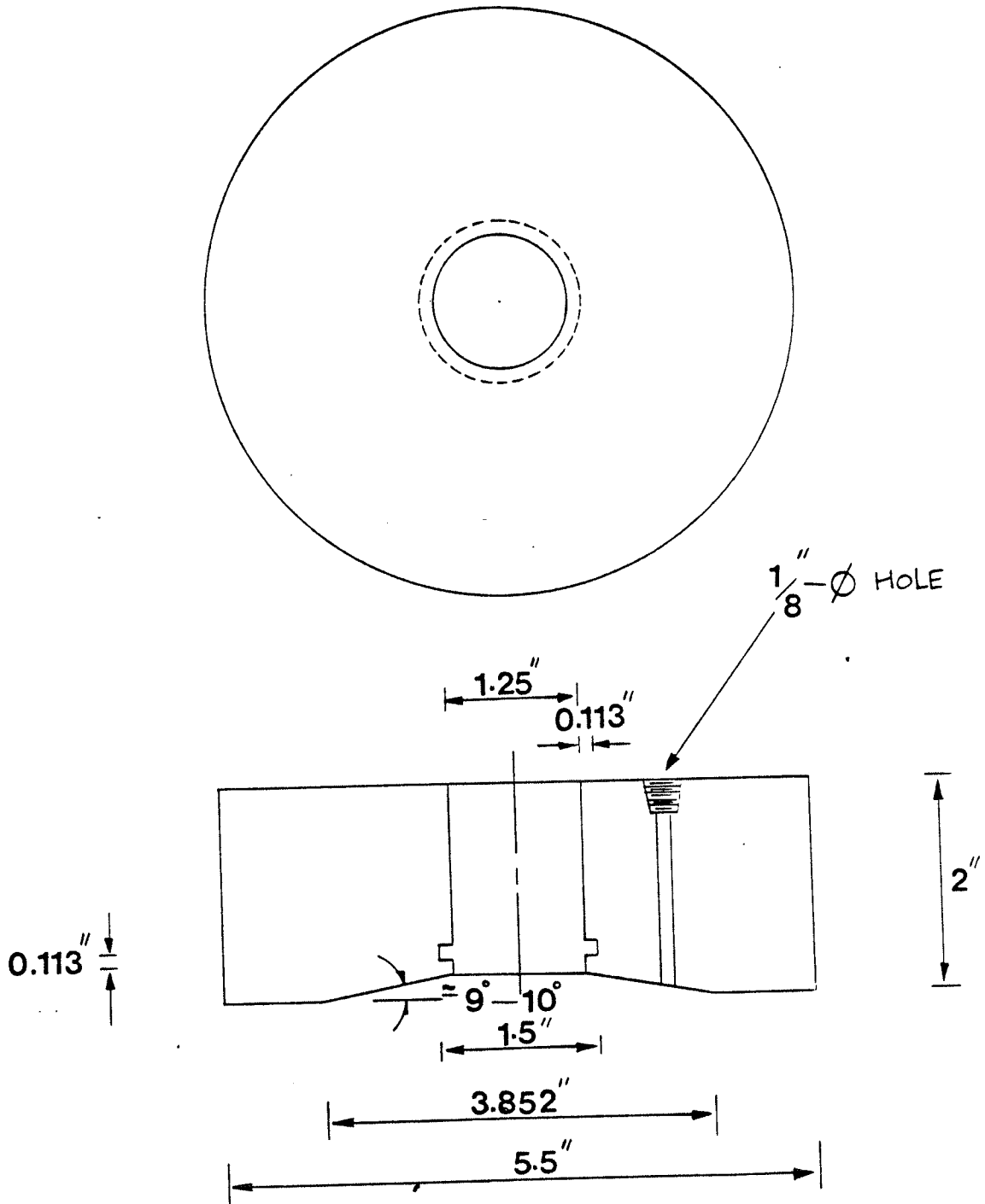
THRU CLEARANCE

$\frac{3}{8}$ " \varnothing HOLE



PART # 5 : INNER CYLINDER TOP COVER

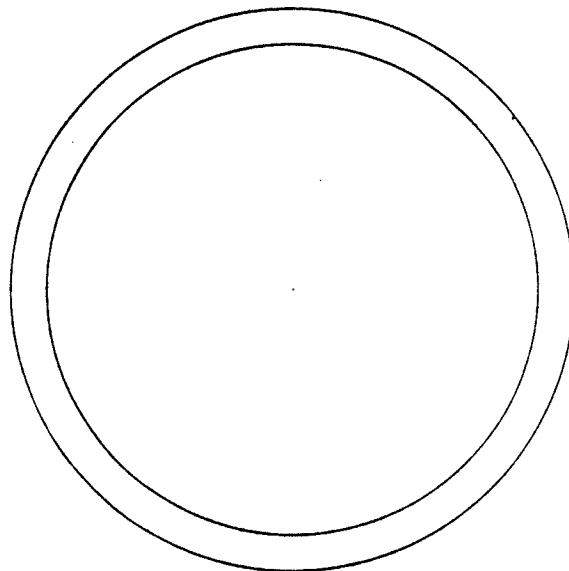
MATERIAL : ALUMINUM



PART # 6 : INNER CYLINDER

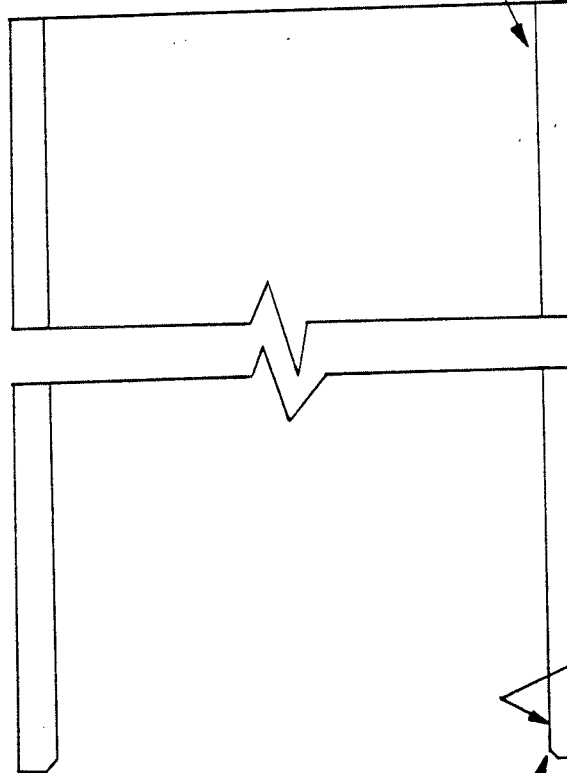
MATERIAL : ALUMINUM

3.85"



MACHINE O.D. & I.D.
TO FIT GROOVE.

12"



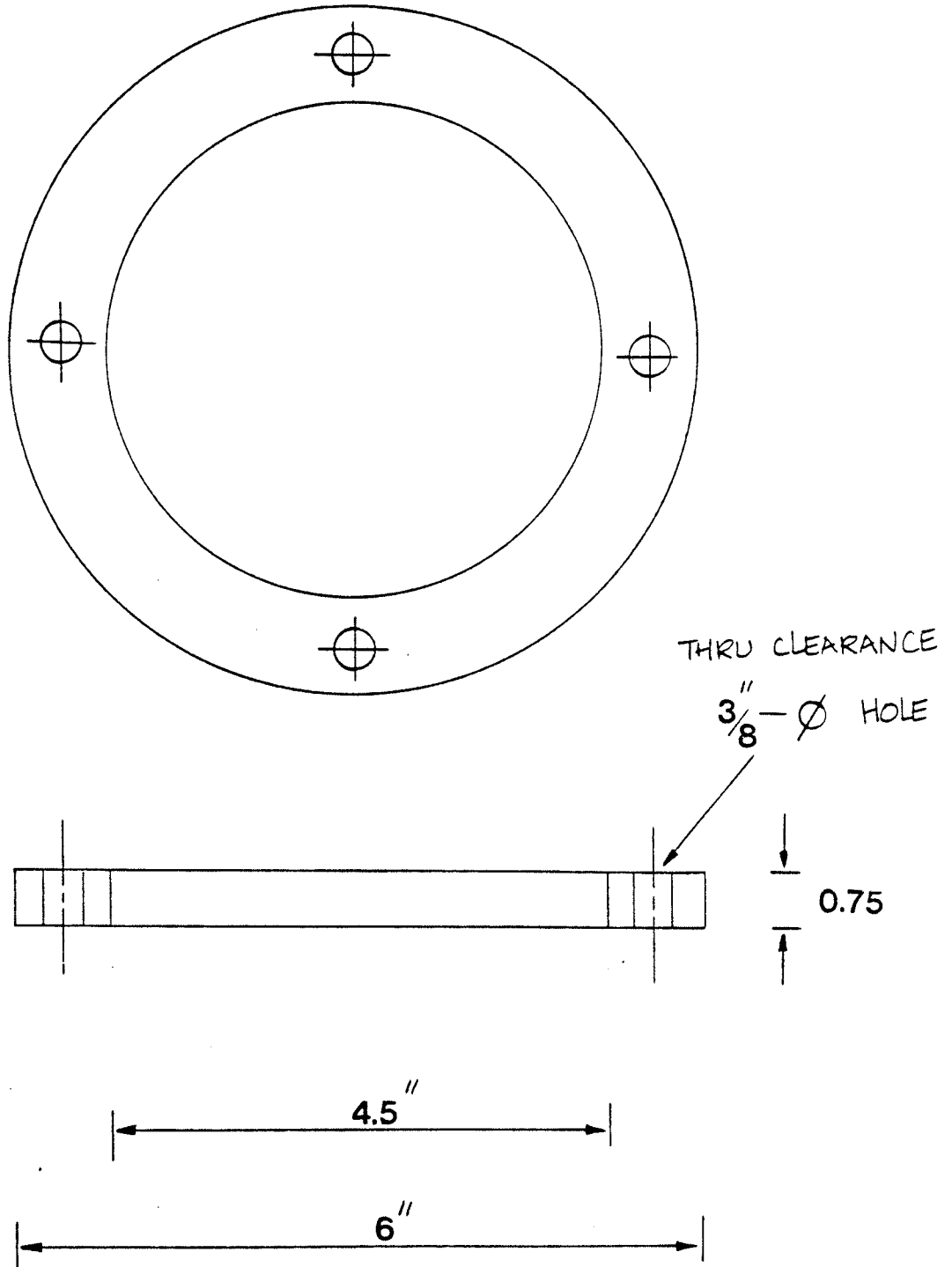
MACHINE I.D. TO
FIT PLUG

BREAK INSIDE EDGE
TO PASS OVER O-
RINGS.

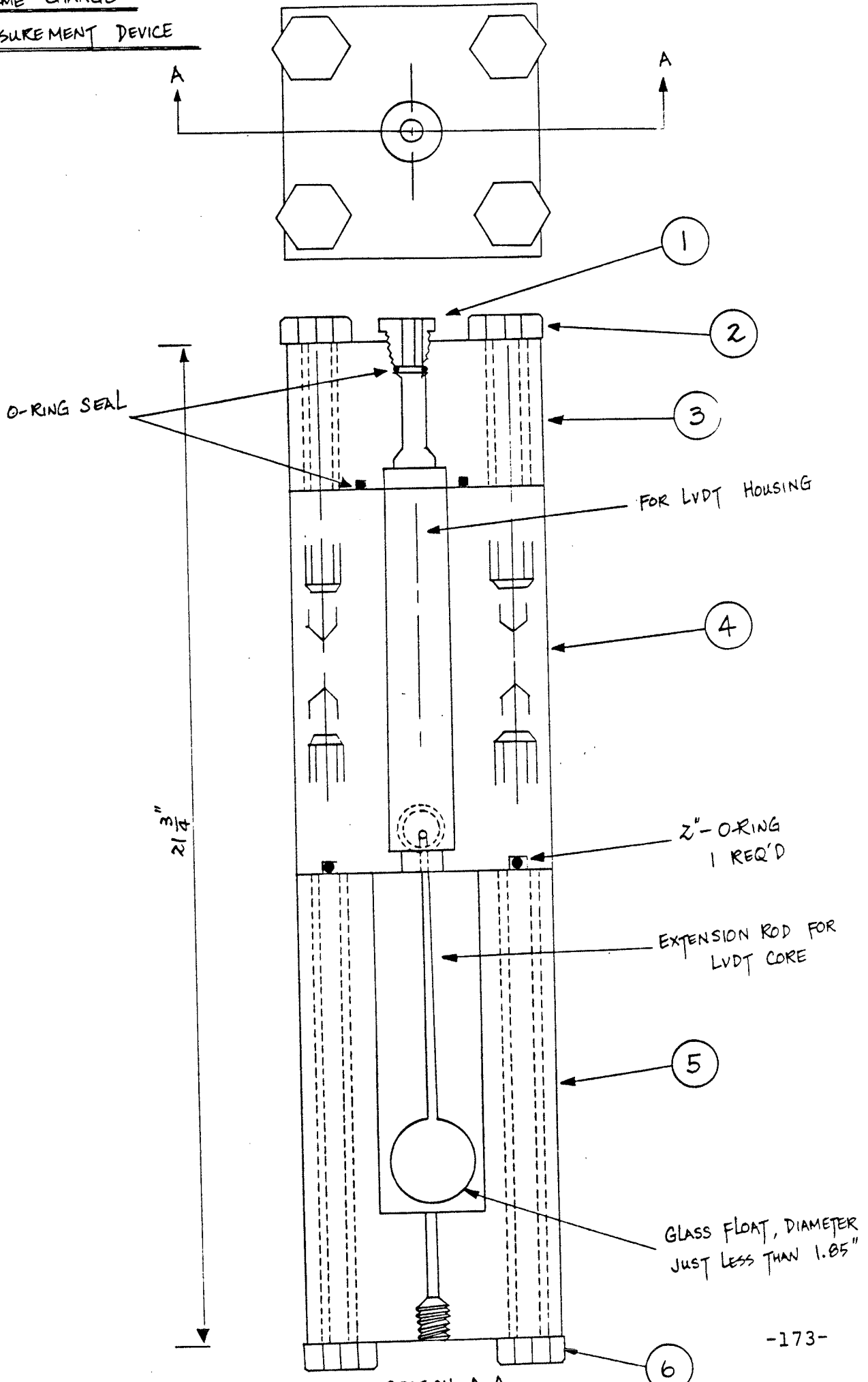
4.5"

PART # 7 : INNER CYLINDER SHOULDER (BOTTOM)

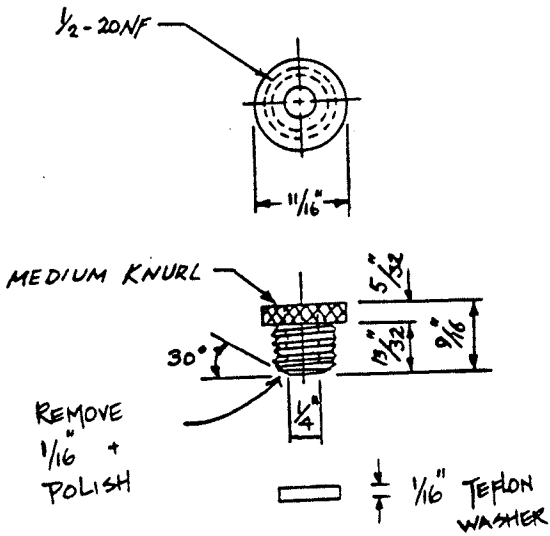
MATERIAL : ALUMINUM



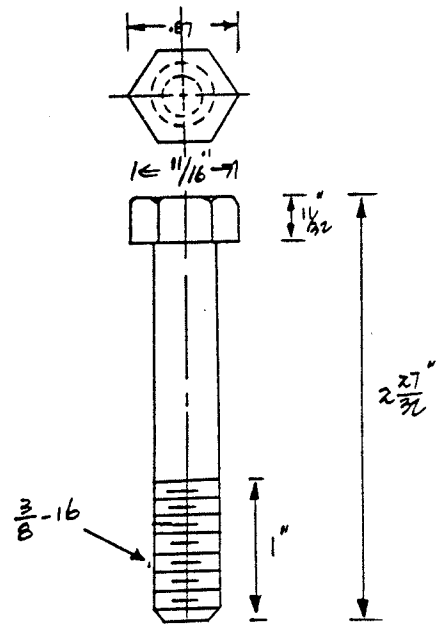
VOLUME CHANGE
MEASUREMENT DEVICE



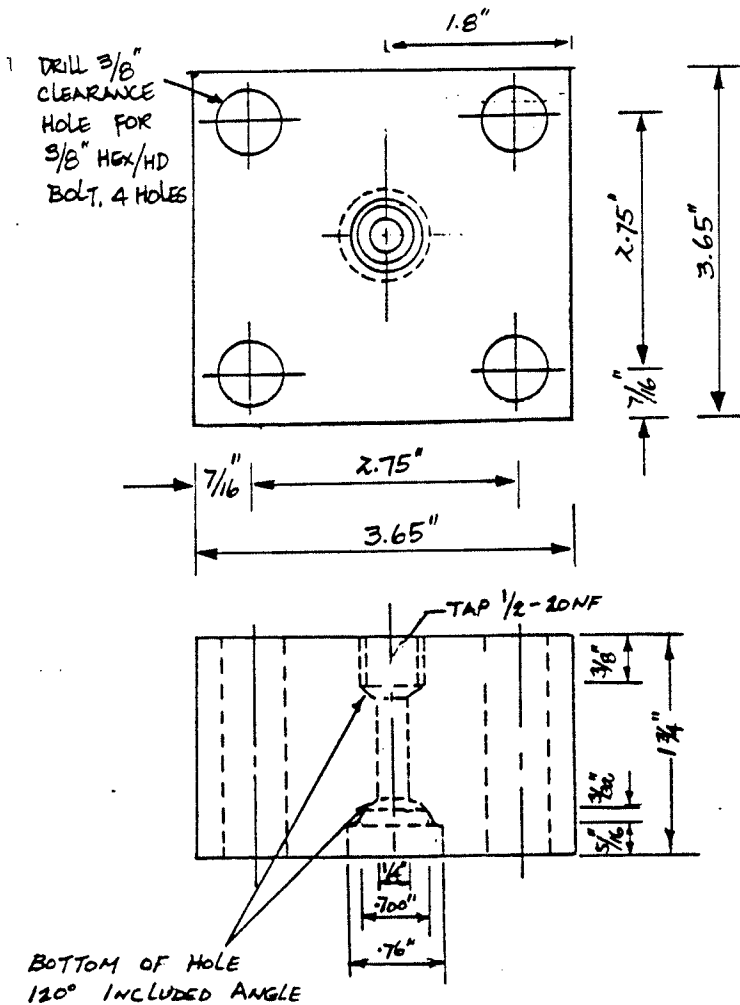
① MATERIAL: BRASS
1 REQ'D



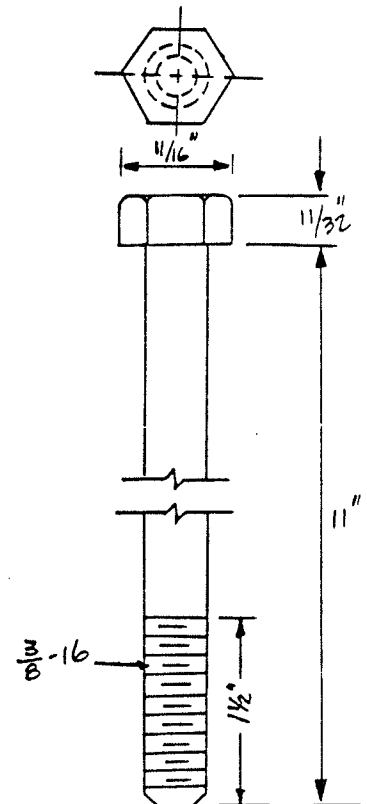
② MATERIAL: STEEL
4 REQ'D



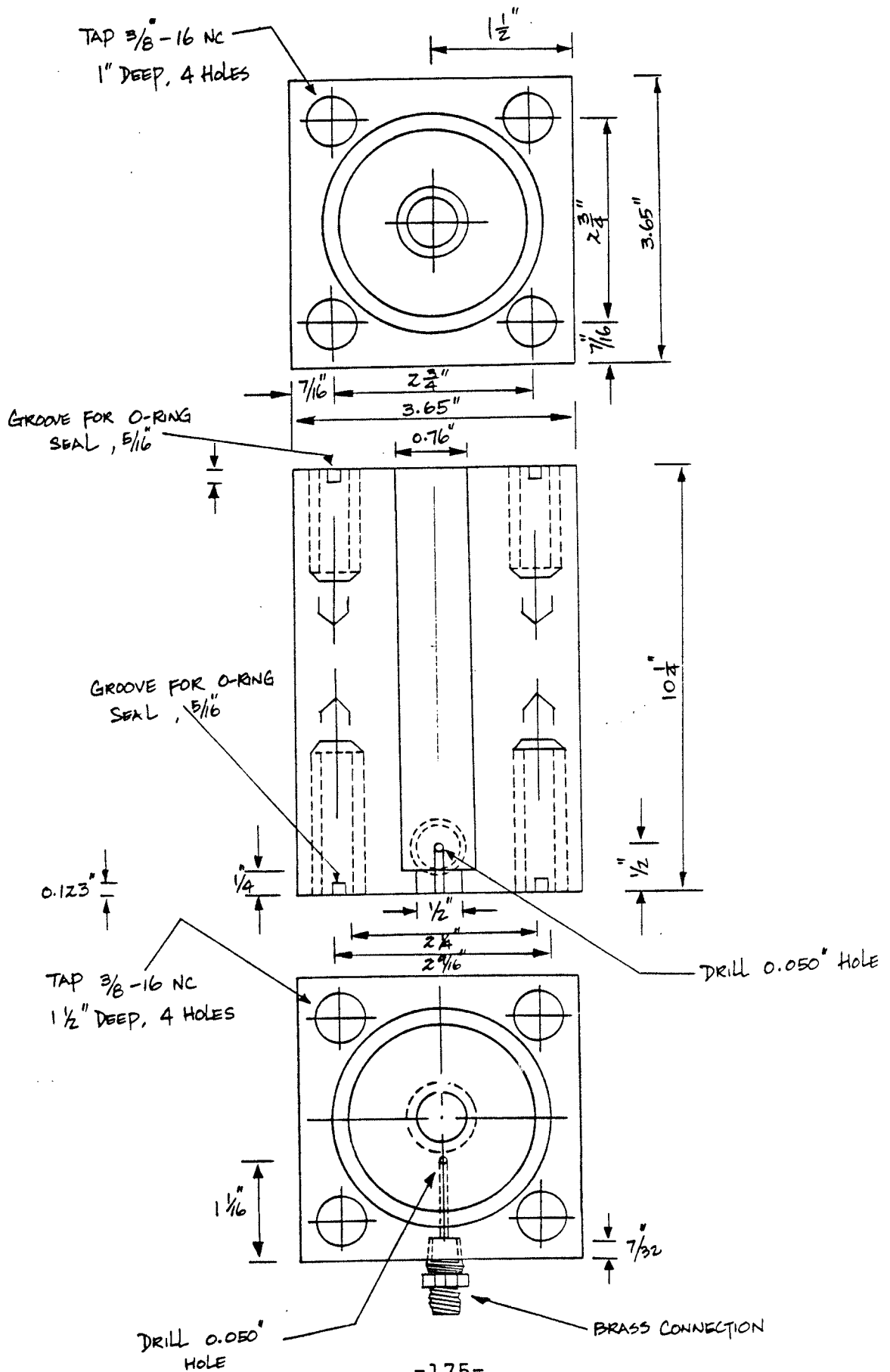
MATL: ALUMINUM
③ 1 REQ'D



⑥ MATERIAL: STEEL
4 REQ'D

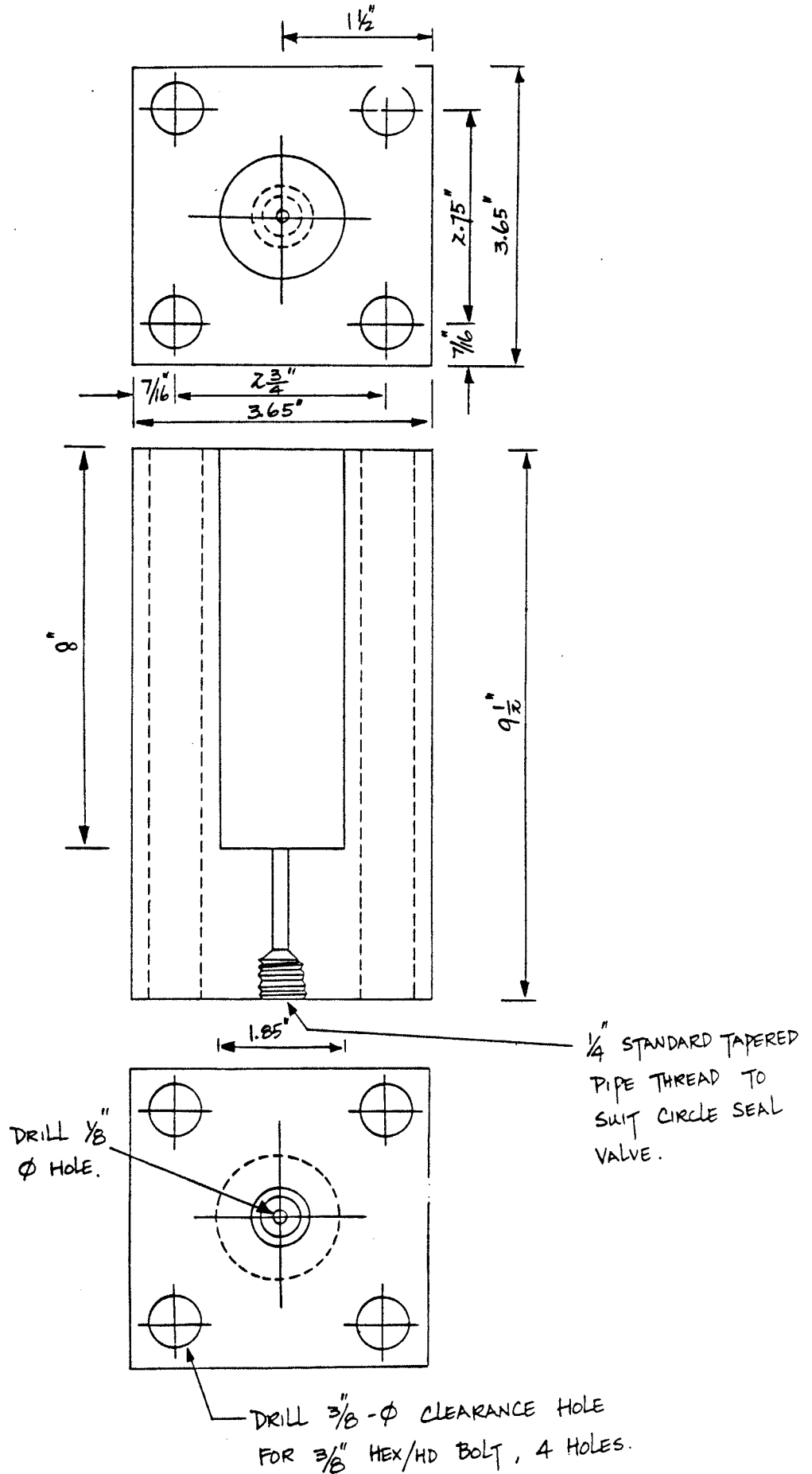


④ MATERIAL : ALUMINUM ; 1 REQ'D



5

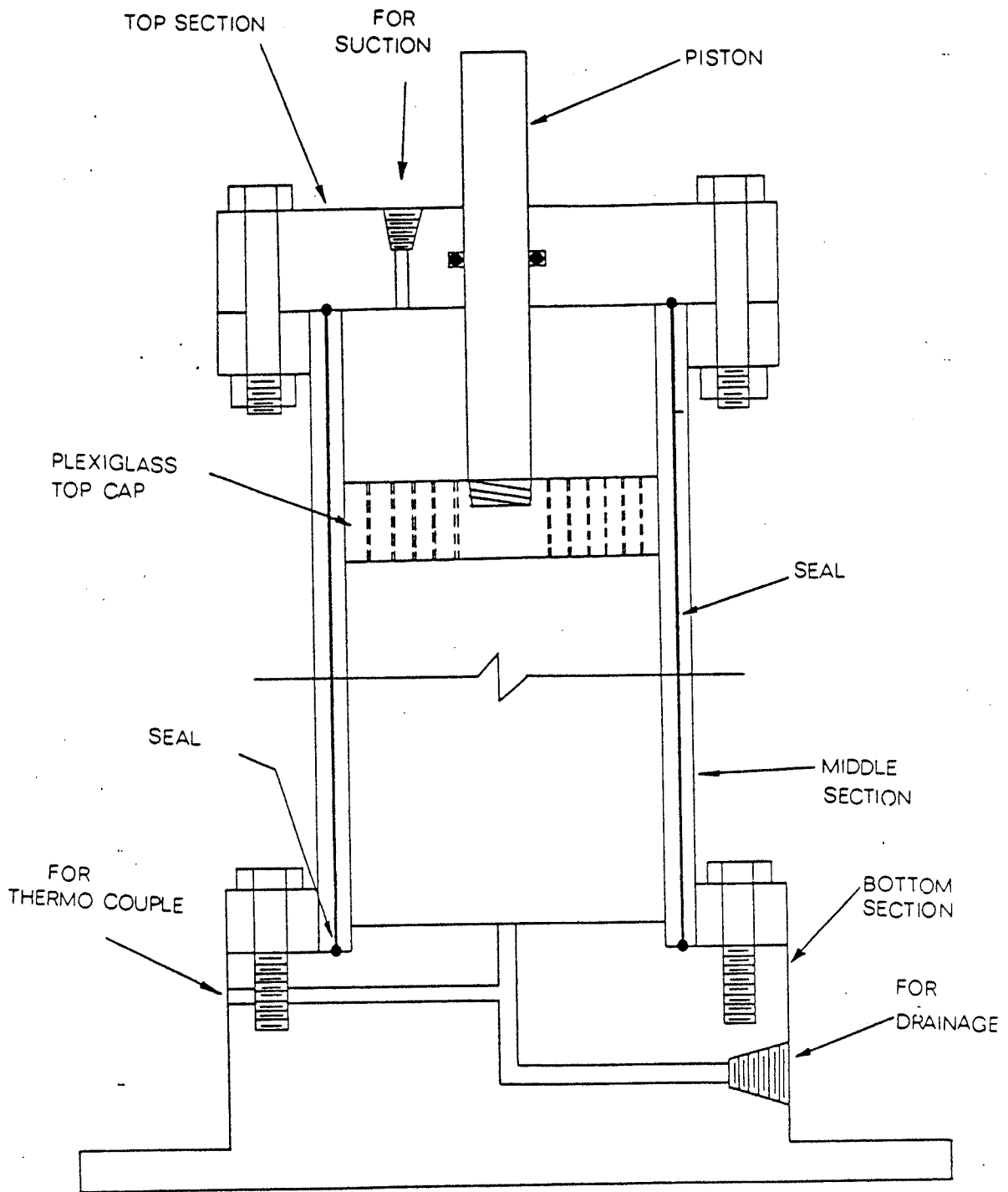
MATERIAL : ALUMINUM ; 1 REQ'D



APPENDIX IV

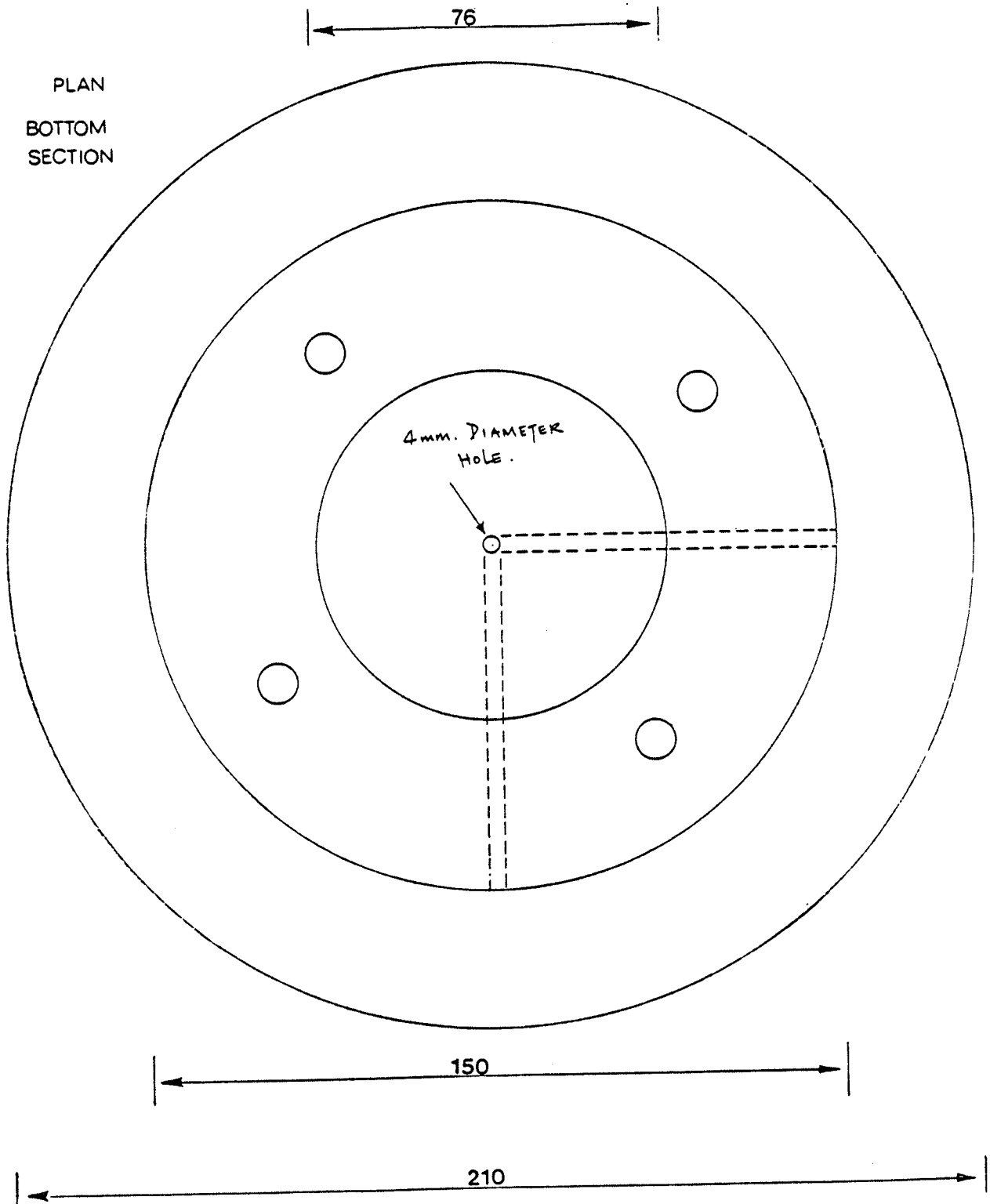
DETAILS OF PLEXIGLASS SPLIT MOULD

The unit used in this Appendix is in mm.

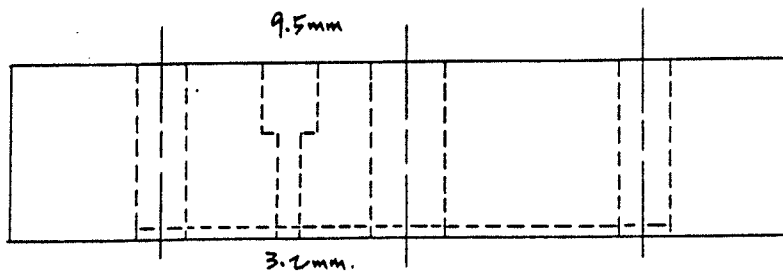
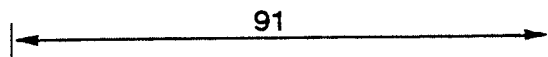
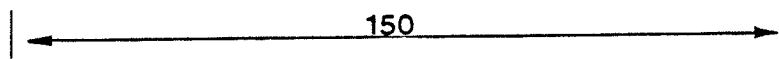
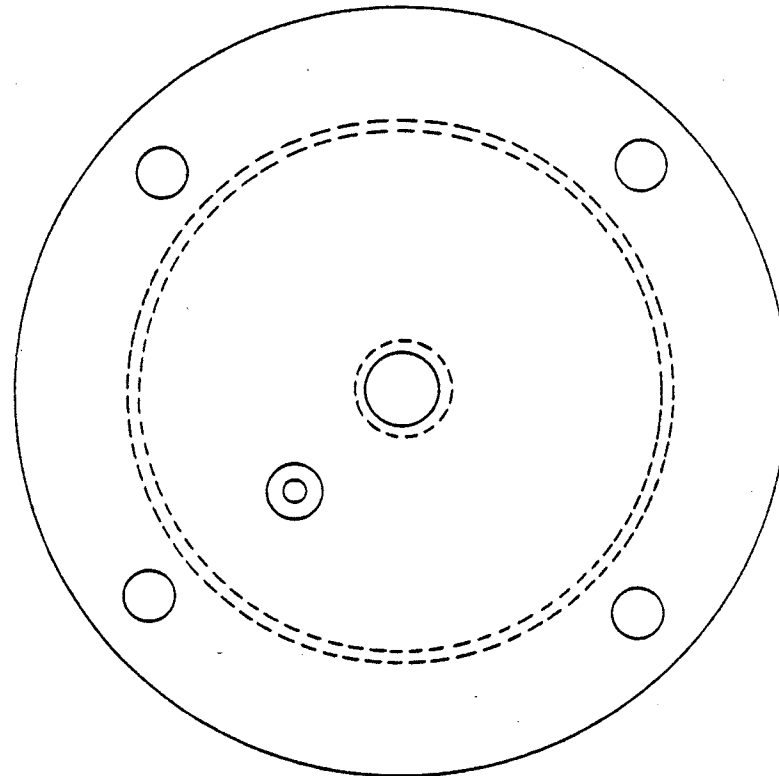


Plexiglass split mould.

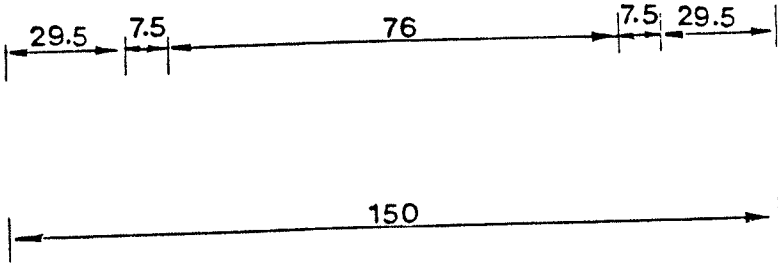
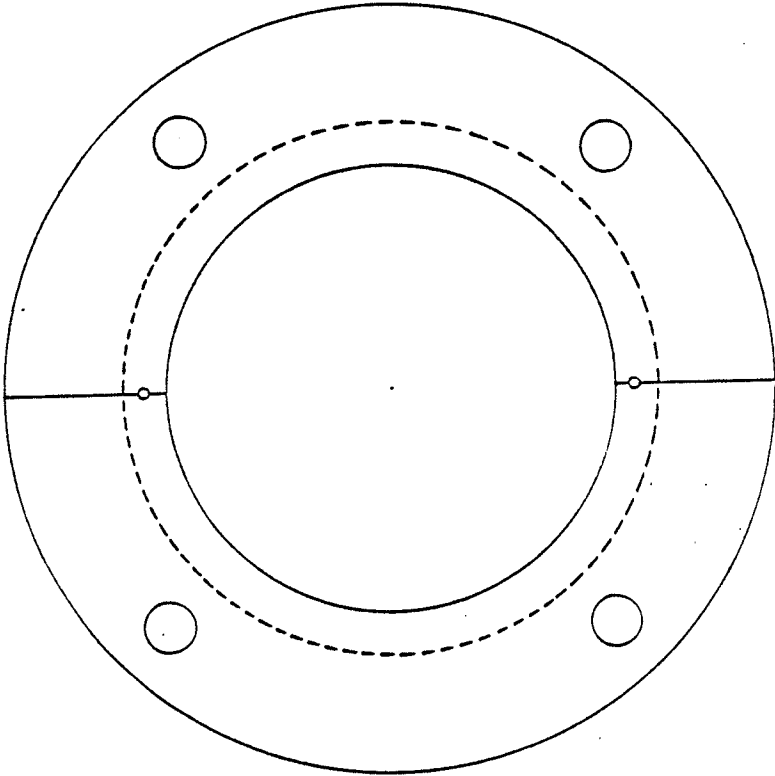
PLAN
BOTTOM
SECTION



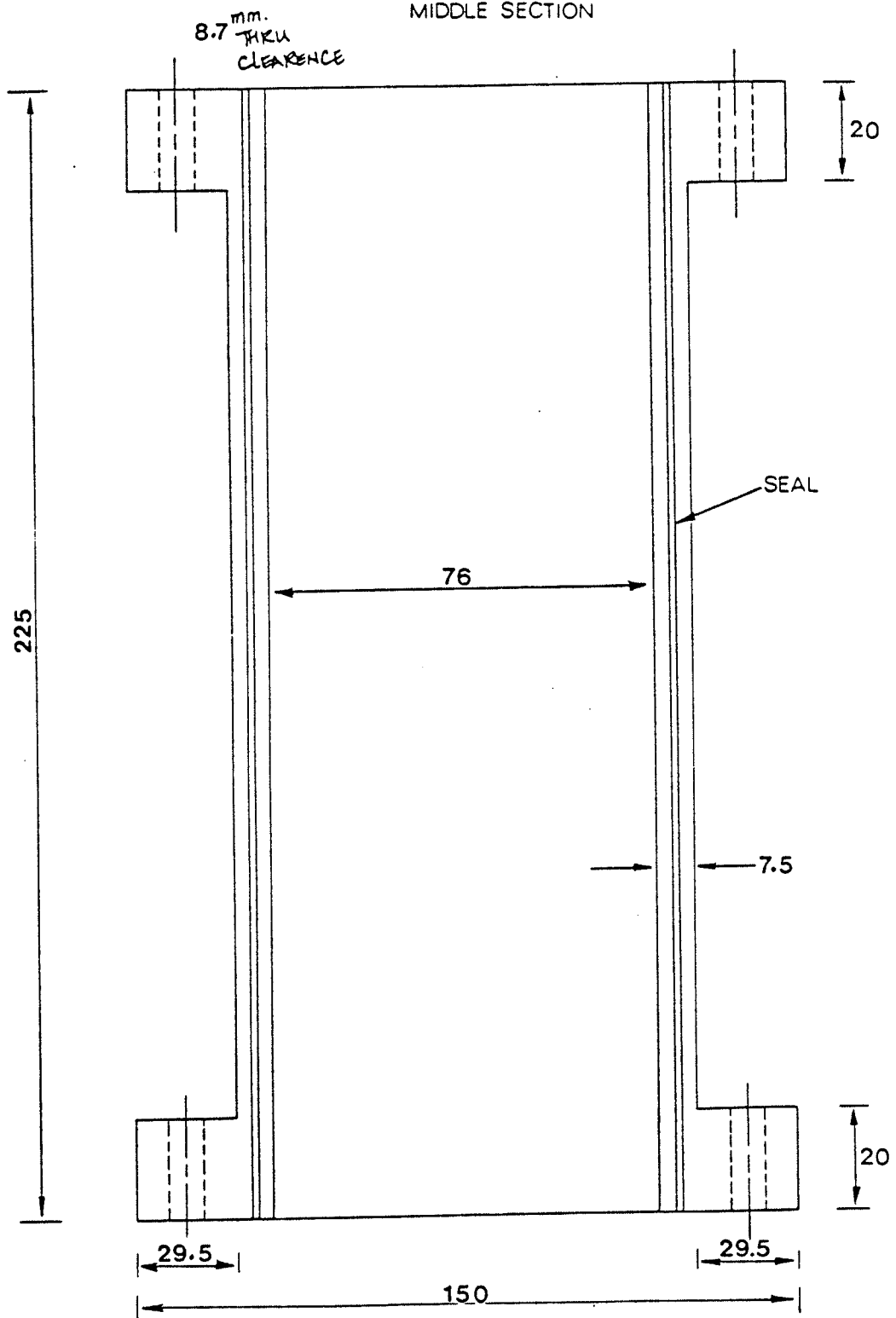
TOP
SECTION



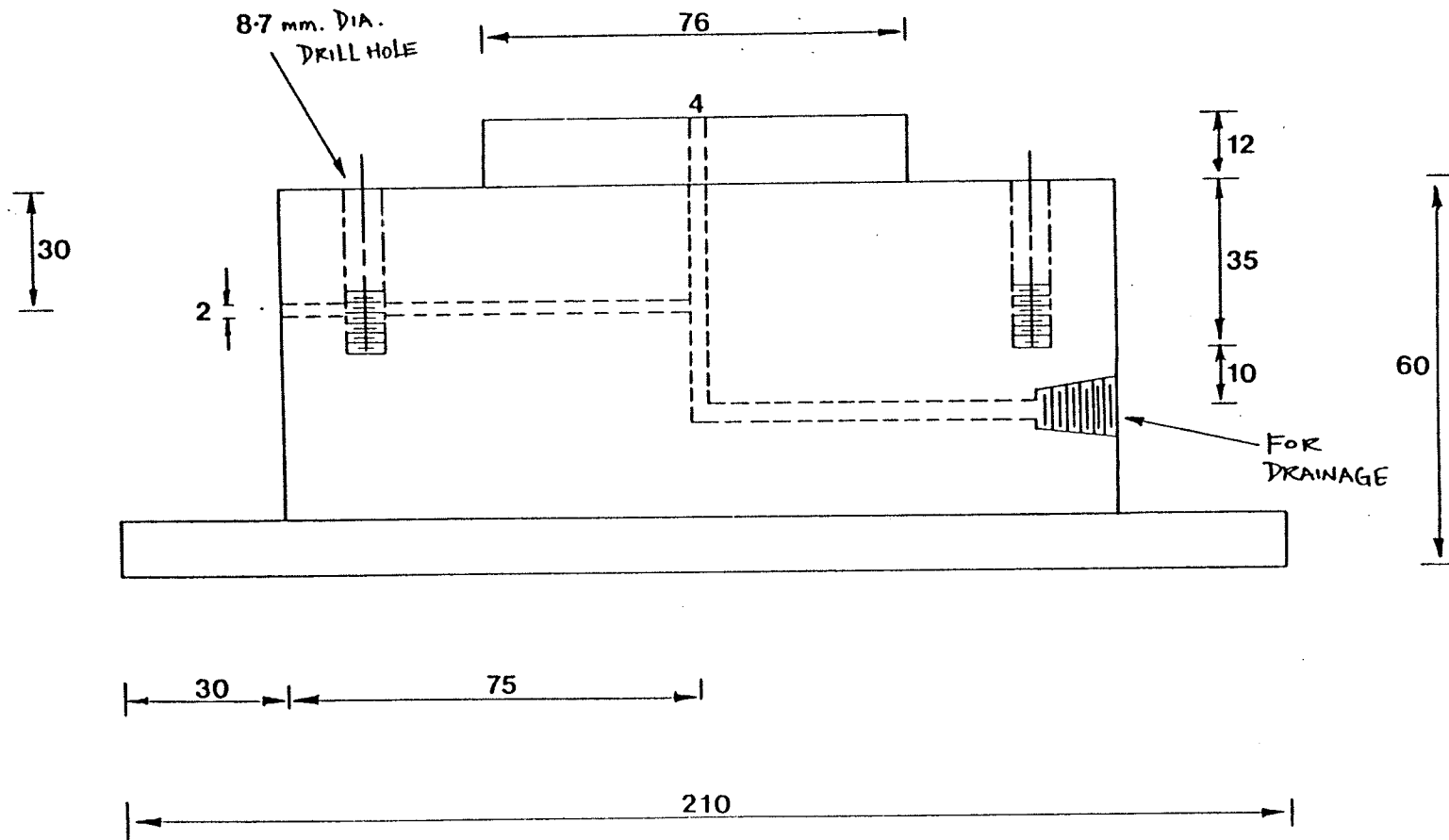
MIDDLE
SECTION



MIDDLE SECTION



-184-



BOTTOM SECTION

APPENDIX V

PROGRAMME LISTING FOR HYPERBOLIC REGRESSION ANALYSIS

APPENDIX V

DATA INPUT FOR HYPERBOLIC REGRESSION ANALYSIS PROGRAM

INTRODUCTION

The plotting program is written in standard FORTRAN and using the University of Manitoba computer system, calcomp 750/563 incremental drum plotter. The program can plot multiple curves on one figure or single curve on each figure with multiple files. Details of input, output informations and program listing are given in the following section.

PREPARATION OF INPUT INFORMATION

All data are using free format input. Input should be presented in the order shown below as integer, real or alphanumeric data. Data present on one card should be separated by a space. Data punch on one card should always be within 80 columns.

The order of input information is as follows :

	format
A) Number of data set (NSD)	Integer
B) User's choice of plotting (NPLOT)	Integer
set the value	
NPLOT = 1 for one curve on each figure	
= 2 for multiple curves on each figure	

C) Option of plotting (NOPT1)	Integer
set the value	
NOPT1 = 0 for individual curve	
= 1 for accumulating curve	
D) Testing number (5A4)	
column 1 - 20 alphanumeric data	
E) Number of curve for each data set	
(NC1)	Integer
F) Number of data point on each curve	
(NDC) (Maximum 10)	Integer
G) Mean pressure of each test (PR)	Real
H) LVDT calibration factor (COR)	Real
I) Initial reading of each stress increments	
(INI)	Real
J) Elapsed time (Q) (Maximum 300)	Real
K) Voltmeter reading (R) (Maximum 300)	Real
L) Unit weight (UWT)	Real

If the number of curve to be plotted in each data files is more than one ($NC > 1$), then repeat the data input from step G to step L. If the number of data set is more than one ($NSD > 1$), then repeat the data input from step B to step L.

OPERATIONAL PROCEDURE

The job and data control cards must be prepared and specified. The job control language (JCL) cards must be prepared as follows :

1.

```
//jobname job 'acc#,pswd,T=2m,L=5,I=20','username'  
/*D800 VPLOT  
// EXEC FORTHCLG,USERLIB='SYS3.VPLOTLIB'  
//FORT.SYSIN DD *
```

2. Program.

3.

```
//GO.FT01F001 DD DSN=&&FT01F001,UNIT=SYSDA,  
// DISP=(NEW,PASS),SPACE=(CYL,(2,2))  
//GO.VWORK DD DSN=&&VWORK,UNIT=SYSDA,  
// DISP=(NEW,PASS),UNIT=(CYL,(2,2))  
//GO.SYSIN DD *
```

4. Data.

5.

```
/*  
// EXEC VPLOT
```

/*

The parameter of the job card are specified according to the size of the data input. For example the values of time(T),line(L),input and output count (I/O) (I) can be specified as : T=30,i.e. 30 sec.for computer time. L=3,i.e. the line print is 3000 lines. I=10,i.e. the input and output count are 1000 units.

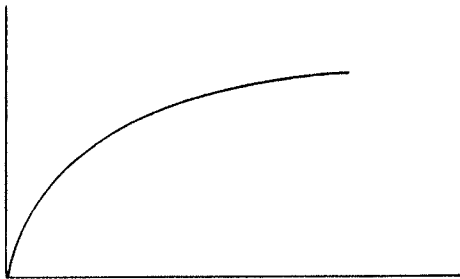
OUTPUT INFORMATION

The program will print out the following information :

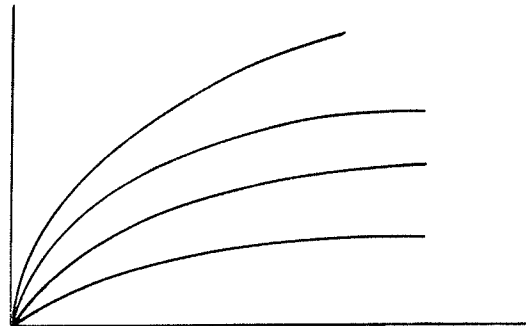
1. Number of data files.
2. User's choice of plotting.
3. Option of plotting .
4. Test sample number.
5. Number of curve in each data set.
6. Number of points in each curve.
7. Mean normal stress.
8. LVDT calibration factor.
9. Initial LVDT reading.
10. Unit weight of sample.
11. Table 1. The raw data
12. Table 2 . Hyperbolic function regressed data.
13. Table 3. Volume change at each stress, i.e., Time
 ,Vol change ,Vol Strain ,Strain Rate ,Creep Rate.
14. Table 4 The accumulated volume change.

The scale on x and y axes must be selected before the job is submitted. In the program, (XSCA) and (YSCA) represent the scale set on x and y axes. For example, XSCA = 2.0 means the scale selected on x-axis is 2.0 per every inch. The (XLEN) and (YLEN) represent the length specified on x and y axes. For example, XLEN = 20.0 means the maximum length on x-axis is 20.0 inches. There is no restriction in length for x-axis, but y-axis is restricted to 10 inches. Details of the complicate plotting must refer to the Calcomp Plotter Manual.

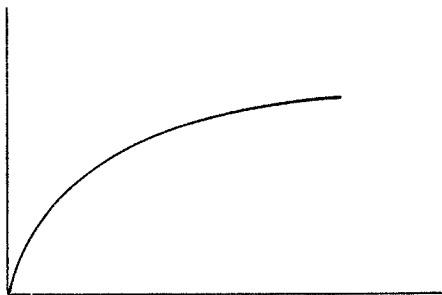
one curve



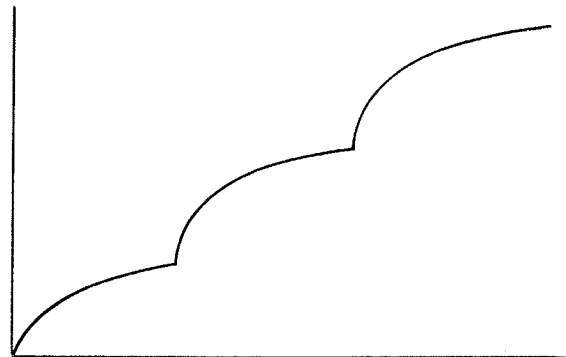
multiple curves



individual curve



accumulating curve



```

10.      DIMENSION A(2000),NDC(10),N1(10),V(2000),B(2),CA(2000),
11.      &COR(10),INI(10),PR(10),CN1(5),IBUF(4000)
12.      COMMON / CNTRL/ NP,COR1,INI1,XX2,YY2,NUMT,NUMD ,NPT
13. C
14. C *****
15. C
16. C THIS IS A SINGLE / OR MULTIPLE
17. C PLOTTING PROGRAM WITH MULTIPLE FILES
18. C
19. C *****
20. C
21. C NP = NO. OF POINT IN EACH CURVE
22. C NUMT = TOTAL NO. OF POINT IN THE DATA FILE
23. C NUMD = TOTAL NO. TO BE PLOTTED
24. C *****
25. C
26. C READ IN NUMBER OF DATA FILES , NSD.
27. C
28. C *****
29. C
30. C *****
31. C
32. C USER'S CHOICE OF PLOTTING
33. C SET THE VALUE OF NPLOT =
34. C 1 ----- FOR ONE CURVE ON EACH FIG.
35. C 2 ----- FOR MULTIPLE CURVE ON EACH FIG.*
36. C
37. C *****
38. C
39. C
40.      READ*,NSD
41.      WRITE (6,40) NSD
42.      READ*, NPLOT
43.      IF (NPLOT.EQ.1) GOTO 122
44.      WRITE (6,200)
45.      GOTO 130
46. 122 WRITE (6,190)
47. C
48. C *****
49. C
50. C OPTION OF PLOTTING
51. C SET YHE VALUE OF NOPT =
52. C 0 ----- FOR SINGLE PLOT
53. C 1 ----- FOR ACCUMULATING PLOT
54. C
55. C *****
56. C
57. 130 DO 110 JJ = 1,NSD
58.      READ*,NOPT1
59.      IF (NOPT1.LT.1) GOTO 137
60.      WRITE (6,25)
61.      GOTO 138
62. 137 WRITE (6,210)
63. 138 READ(5,35) (CN1(N),N=1,5)
64.      WRITE(6,45) (CN1(N),N=1,5)
65.
66. C
67. C *****
68. C
69. C READ IN NO. OF CURVE OF EACH DATA SET
70. C
71. C *****
72. C
73.      READ*,NC1
74.      WRITE (6,50) NC1
75.

```

```

76. C
77. C *****
78. C *
79. C READ IN NO. POINT IN EACH CURVE *
80. C *
81. C *****
82. C
83. C READ*(NDC(J),J=1,NC1)
84. C WRITE (6,55) (NDC(J),J=1,NC1 )
85. C
86. C *****
87. C *
88. C INITIALIZE THE POINTS OF MAXIMUM AND MINIMUM *
89. C *
90. C *****
91. C
92. C XO = 0.0
93. C X1 = 0.0
94. C YO = 0.0
95. C Y1 = 0.0
96. C
97. C *****
98. C *
99. C SET POINTER IN A ARRAY TO KEEP TRACK OF THE X & Y COORD. *
100. C X COORD. DATA IN X-ARRAY WILL START AT 1 ,NP+1,...ETC *
101. C Y COORD. DATA IN Z-ARRAY WILL START @ 1, NP+1,...ETC *
102. C *
103. C *****
104. C
105. C NS = 1
106. C DO 10 I = 1,NC1
107. C
108. C *****
109. C *
110. C COR IS THE LVDT CALIBRATION FACTOR. *
111. C THE FACTOR CONVERTS THE VOLTMETER READING ,VOLT, INTO MM. *
112. C *
113. C *****
114. C
115. C *****
116. C *
117. C *
118. C READ IN ISOTROPIC PRESSURE , PR *
119. C *
120. C *****
121. C
122. C READ*,PR(I)
123. C PRES = PR(I)
124. C WRITE (6,60) PRES
125. C READ*,COR(I)
126. C
127. C *****
128. C *
129. C INI IS THE INITIAL READING OF THE START IN CHANGE IN VOLUME. *
130. C *
131. C *****
132. C
133. C READ*,INI(I)
134. C COR1=COR(I)
135. C INI1=INI(I)
136. C WRITE (6,65) COR1
137. C WRITE (6,70) INI1
138. C NP = NDC(I)
139. C NPT = NP + 2

```

```

140.      N1(I) = NS
141.      IF ( NOPT1.GE.1 ) GOTO 11
142.      NS = N1(I) + NPT
143.      GOTO 12
144. 11  NS = N1(I) + NP
145. C
146. C *****
147. C
148. C CALL SUBROUTINE CORR TO READ IN THE TEST DATA
149. C AND DO THE VOLUME CHANGE CALCULATION
150. C
151. C *****
152. C
153. 12  CALL CORR( A(N1(I)), V(N1(I)),I ,NOPT1 ,CA(N1(I)) )
154. C
155. C *****
156. C
157. C CALL SUBROUTINE PMAX TO DETERMINE THE MAXIMUM AND MINIMUM
158. C VALUES OF ALL THE TEST DATA AFTER CALCULATION.
159. C
160. C *****
161. C
162.      CALL PMAX( A(N1(I)), V(N1(I)),XO,X1,YO,Y1)
163. 10  CONTINUE
164.      WRITE (6,75) XO,X1
165.      WRITE (6,80) YO,Y1
166.      IF (NOPT1.LT.1) GOTO 20
167. 15  NUMT = NS -1
168.      NUMD = NUMT + 2
169.      WRITE (6,85) NUMT,NUMD
170.      WRITE (6,90)
171.      WRITE (6,95)
172.      WRITE(6,96)
173.      WRITE (6,100) ( N, A(N), V(N),CA(N) , N = 1,NUMT )
173.1 C
173.2 C *****
174. C
175. C CALL PLOTTING PROGRAM
176. C
177. C *****
178. C
179. 20  CALL PLOTS(IBUF,4000)
180.      CALL PLOT(1.0,1.0,-3)
181.      CALL FACTOR(1.0)
182. C
182.1 C *****
183. C SELECT PROPER SCALE
184. C
185.      IF ( NOPT1.GE.1 ) GOTO 26
186.      IF ( X1.GT.3200 ) GOTO 22
187.      XSCA = 200
188.      XLEN = 10.0
189.      GOTO 21
190. 22  IF ( X1.GT.6400 ) GOTO 23
191.      XSCA = 800
192.      XLEN = 8.0
193.      GOTO 21
194. 23  IF ( X1.GT.10000 ) GOTO 24
195.      XSCA = 800
196.      XSCA = 12.0
197.      GOTO 21
198. 24  XSCA = 1920
199.      XLEN = 17
200. 21  IF ( Y1.LE.4.0 ) GOTO 29

```

```

201.      YSCA = 1.0
202.      YLEN = 8
203.      GOTO 30
205. 29   YSCA = 0.5
206.      YLEN = 4
207.      GOTO 30
208. 26   XSCA = 2400
209.      XLEN = 20
211.      YSCA = 0.8
212.      YLEN = 8.0
213. C
214. C *****
215. C *
216. C PLOTTING PROGRAM REQUIRES TWO MORE SPACES WHICH ARE NP+1,NP+2 *
217. C OR NUMT+1, NUMT+2 *
218. C *****
219. C
220. 30   B(1) = 0.0
221.      B(2) = XSCA
222. C
223. C *****
224. C *
225. C CALL SUBROUTINE AXIS AND SET TITLE ON COORDINATES *
226. C *
227. C *****
228. C
229.      CALL AXIS(0.0,0.0,21HACCUMULATED TIME MIN,-21,XLEN,0.0,B(1),B(2))
230.      B(1) = 0.0
231.      B(2) = YSCA
232.      CALL AXIS(0.0,0.0,19HVOLUMETRIC-STRAIN %,19,YLEN,90.,B(1),B(2))
233.      YY = YLEN + 0.5
234.      CALL SYMBOL(2.0,YY,0.14,24HVOLUME-CHANGE-TIME CURVE,0.0,24)
235.      XX = XLEN + 1
236.      CALL SYMBOL( XX,2.0,0.14,15H TEST NO. =,0.0,15 )
237.      CALL SYMBOL( XX,1.5,0.14,15HMEAN PRESSURE =,0.0,15 )
238.      XX = XX + 2
239.      CALL SYMBOL( XX,2.0,0.14,CN1,0.0,20 )
240.      IF ( NOPT1.GE.1 ) GOTO 1
241.      XX = XX + 2.0
242.      CALL SYMBOL( XX,1.5,0.14,4HKPA.,0.0,4 )
243. 1   IF ( NOPT1.GE.1 ) GOTO 2
244.      J = 1
245.      NP = NDC(J)
246.      CALL DRAW3( A(N1(J)), V(N1(J)), XSCA , YSCA , J )
247.      JK = J + 1
248.      CALL DRAW4( A(N1(J)),CA(N1(J)),XSCA,YSCA,JK)
249.      NXSP = XLEN * 4
250.      NYSP = YLEN * 4
251.      CALL GRID(0.0,0.0,0.25,0.25,NXSP,NYSP)
252.      IF (NPL0T.EQ.2) GOTO 4
253.      CALL PLOT(0.0,0.0,999)
253.1 4   J = J + 1
253.2   IF ( J.LE.NC1 ) GOTO 20
254.      CONTINUE
255.      IF (NPL0T.EQ.1) GOTO 110
256.      CALL PLOT(0.0,0.0,999)
257.      GOTO 110
258. 2   DO 31 N = 1,NUMT
259.      A(N) = A(N)
260.      V(N) = V(N)
261. C    CA(N) = CA(N)
262. 31   CONTINUE
263.      CALL DRAW1( A ,V ,XSCA,YSCA, JJ )
264. C    CALL DRAW2( A ,CA ,XSCA,YSCA, JJ )

```

```

265. C 3 NXSP = XLEN*4
266. C NYSP = YLEN*4
267. C CALL GRID(O.O,O.O,0.25,O.25,NXSP,NYSP)
268. IF (NPLOT.EQ.2) GOTO 110
269. CALL PLOT(O.O,O.O,999)
270. 35 FORMAT( 5A4 )
271. 40 FORMAT('1', 5X,30HNUMBER OF DATA FILES -----,5X,I2,/)
272. 190 FORMAT('O',5X,42HYOU ARE PLOTTING ONE CURVE ON EACH FIGURE.,/)
273. 200 FORMAT('O',5X,45HYOU ARE PLOTTING MULTIPLE CURVES ON EACH FIG.,/)
274. 25 FORMAT('1',5X,17HACCUMULATED PLOT.)
275. 210 FORMAT('1',5X,12HSINGLE PLOT.)
276. 45 FORMAT('O',5X,30HTEST SAMPLE NO. -----,5X,5A4 )
277. 50 FORMAT('O', 5X,30HNO. OF CURVE IN EACH DATA SET-,5X,I5 )
278. 55 FORMAT('O', 5X,10I8 )
279. 60 FORMAT('1', 5X,30HMEAN NORMAL STRESS -----,5X,F6.1,/)
280. 65 FORMAT('O', 5X,30HLVDT CALIBRATION FACTOR -----,5X,F10.8 )
281. 70 FORMAT('O', 5X,30HINITIAL LVDT READING -----,5X,I10 )
282. 75 FORMAT('O',5X,30HMINIMUM VALUE OF X -----,1X,F10.5,
283. &30HMAXIMUM VALUE OF X -----,1X,F10.1)
284. 80 FORMAT('O',5X,30HMINIMUM VALUE OF Y -----,1X,F10.5,
285. &30HMAXIMUM VALUE OF Y -----,1X,F15.8)
286. 85 FORMAT('O',5X,30HTOTAL NUMBER OF PLOT DATA-----,I6,4X,
287. &30HREQUIRE SPACE FOR PLOTTER -----,I6 )
288. 90 FORMAT('1',5X,10H TABLE 4 ,/ )
289. 95 FORMAT('O', T24,'TIME',T44,'VOLUME CHANGE',T71,'HYP.REG',/)
290. 96 FORMAT(' ',T23,'(MIN)',T49,'(CC.)',T72,'(CC.)',/)
291. 100 FORMAT('O', 5X,I5,8X,F10.2,10X,F15.4,8X,F15.4)
292. 110 CONTINUE
293. IF (NPLOT.EQ.1) GOTO 115
294. CALL PLOT(O.O,O.O,999)
295. 115 CALL PLOT(O.O,O.O,9999)
296. STOP
297. END
298. SUBROUTINE CORR( X, Y, I ,NOPT1 ,HY )
299. COMMON /CNTRL/NP,COR1,INI1,XX2,YY2 ,NUMT,NUMD,NPT
300. C
301. C *****
302. C
303. C THIS SUBROUTINE CONVERT LVDT-VOLT READING INTO MM *
304. C AND DO THE VOLUME CHANGE CALCULATION *
305. C *
306. C *****
307. C
308. C DIMENSION X(300),Y(300),CH(300),HY(300),R(300),Q(300),Y2(300),
309. C &Y1(300),VO(300),TI(300),CR(300),EINV(300)
310. C
311. C *****
312. C *
313. C READ IN X & Y COORDINATE *
314. C X = TIME OR STRESS *
315. C Y = VOLUME CHANGE *
316. C R & Q ARE RAW DATA OF THE TEST *
317. C Q IS THE ELAPSED TIME *
318. C R IS THE LVDT READING *
319. C *
320. C *****
321. C
322. C READ*( Q(II),II=1,NP)
323. C READ*( R(II),II=1,NP)
324. C READ*,UWT
325. C WRITE (6,56) UWT
326. C WRITE (6,15)
327. C WRITE (6,20)
328. C WRITE (6,21)

```

```

329.      WRITE (6,25) ( N, Q(N), R(N), N = 1,NP )
330. C
331. C *****
332. C *
333. C COR IS THE LVDT-CALIBRATION FACTOR *
334. C *
335. C INI IS THE INITIAL READING OF THE TEST *
336. C *
337. C *****
338. C
339.      DO 10 J=1,NP
340.      X(J) = Q(J)
341.      CH(J) = ABS(INI1 - R(J)) * COR1
342.      IF (CH(J).GE.10E-8) GOTO 1
343.      CH(J) = 0.0
344.      1 Y2(J) =( CH(J) / UWT )
345.      IF ( Y2(J).LE.10E-8.OR.X(J).LE.10E-8 ) GOTO 2
346.      Y1(J) = Y2(J) / X(J)
347.      GOTO 3
348.      2 Y1(J) = 0.0
349.      3 K = J - 1
350.      IF ( K.GT.0 ) GOTO 4
351.      VO(J) = 0.0
352.      TI(J)=0.0
353.      GOTO 6
354.      4 VO(J) = Y2(J) - Y2(K)
355.      TI(J) = X(J) -X(K)
356.      6 IF ( VO(J).LT.10E-8 ) GOTO 12
357.      CR(J) = VO(J) / TI(J)
358.      GOTO 10
359.      12 CR(J) = 0.0
360.      10 CONTINUE
361.      CALL HYRG( Q, Y2, HY )
362.      DO 11 J = 1,NP
363.      IF ( I.LE.1 ) GOTO 5
364.      X(J) = XX2 + X(J)
365.      Y(J) = YY2 + Y2(J)
366.      HY(J) = HY2 + HY(J)
367.      GOTO 11
368.      5 Y(J) = Y2(J)
369.      X(J) = X(J)
370.      HY(J) = HY(J)
371.      11 CONTINUE
372.      XX2 = X(NP)
373.      YY2 = Y(NP)
374.      HY2 = HY(NP)
375.      WRITE(6,40)
376.      WRITE (6,42)
377.      WRITE (6,43)
378.      WRITE (6,46) (N,Q(N),CH(N),Y2(N),Y1(N),CR(N),N = 1,NP )
379.      IF ( NOPT1.LE.0 ) GOTO 60
380.      WRITE (6,50)
381.      WRITE (6,54)
382.      WRITE (6,55)
383.      WRITE (6,45) ( N, X(N), Y(N) ,HY(N) , N = 1,NP )
384.      15 FORMAT('1', 5X,9H TABLE 1)
385.      20 FORMAT('0', T8,'NO.',T20,'ELAPSED TIME',T38,'LVDT READING',/)
386.      21 FORMAT(' ',T24,'(MIN)',T41,'(VOLT)',/)
387.      25 FORMAT('0', 5X,15,7X,F10.2,10X,F10.1)
388.      40 FORMAT('1', 5X,42HTABLE 3 VOLUME CHANGE AT EACH STRESS CC.,/)
389.      45 FORMAT( '0',5X,15,5X,F10.2,10X,F10.4,5X,F10.4 )
390.      42 FORMAT('0',T8,'NO.',T17,'TIME',T25,'VOLUME',T34,'VOL STR',
391.      & T43,'STR RATE',T54,'CREEP RATE',/)
392.      43 FORMAT(' ',T17,'(MIN)',T26,'(CC)',T36,'(%)',T44,'(%/MIN)',

```

```

393.      & T55, '(%/MIN)', /)
394.      46 FORMAT('O', 5X, I4, 3X, F8. 2, 3X, F7. 4, 3X, F6. 4, 3X, E8. 2, 3X, E8. 2 )
395.      50 FORMAT('1', 5X, 44H TABLE 4 ACCUMULATED TIME AND VOLUME CHANGE, /)
396.      54 FORMAT('O', T8, 'NO', T20, 'ELAPSED TIME', T39, 'VOL STRAIN', T53, 'HYP.
397.      & REG', /)
398.      56 FORMAT('O', 5X, 30HUNIT WEIGHT (KN/100CU.M) -----, 5X, F10.6)
399.      55 FORMAT(' ', T24, '(MIN)', T42, '(%)', T57, '(%)', /)
400.      60 RETURN
401.      END
402.      SUBROUTINE PMAX( X, Y, XO, X1, YO, Y1)
403.      COMMON / CNTRL/ NP, COR1, INI1, XX2, YY2, NUMT, NUMD ,NPT
404.      DIMENSION X(NPT), Y(NPT)
405. C
406. C *****
407. C *
408. C THIS PROGRAM IS TO DETERMINE THE MAXIMUM AND MINIMUM *
409. C VALUES OF ALL CORRECTED DATA *
410. C *
411. C AMIN1 AND AMAX1 ARE THE IBM BUILD-IN FUNCTION *
412. C XO, YO ARE THE MINIMUM VALUES *
413. C X1, Y1 ARE THE MAXIMUM VALUES *
414. C *
415. C *****
416. C
417.      DO 10 J=1, NP
418.      XO = AMIN1(XO, X(J))
419.      X1 = AMAX1(X1, X(J))
420.      YO = AMIN1(YO, Y(J))
421.      Y1 = AMAX1(Y1, Y(J))
422. 10 CONTINUE
423.      RETURN
424.      END
425.      SUBROUTINE HYRG( T, VOLCH, TSD )
426.      COMMON / CNTRL/ NP, COR1, INI1, XX2, YY2, NUMT, NUMD ,NPT
427.      DIMENSION T(300), VOLCH(300), XCAST(300), YRSDS(300), ESDS(300), HYRG0010
428.      &TSD(300) ,TT(300), TTSD(300), CSR(300) HYRG0020
429. C
430. C *****
431. C *
432. C THIS IS A HYPERBOLIC FUNCTION APPROXIMATION PROGRAM. *
433. C LEAST SQUARE CURVE FITTING METHOD IS USED TO OBTAIN *
434. C THE HYPERBOLIC REGRESSION CURVE *
435. C *
436. C *****
437. C
438. C *****
439. C *
440. C THIS PROGRAM CAN BE USED WITH MULTIPLE FILES *
441. C *
442. C RF = FAILURE RATIO *
443. C N = NO. OF DATA POINT IN EACH DATA SET *
444. C SMX = SUM OF XI = SUM OF T(I) *
445. C SM2X = SUM OF SQUARE OF XI = SUM OF T(I)*T(I) *
446. C SMY = SUM OF YI = SUM OF VOLCH(I) *
447. C SXY = SUM OF ( XI * YI ) = SUM OF ( T(I) * VOLCH(I)) *
448. C T(I) = TIME *
449. C VOLCH = VOLUME CHANGE *
450. C *
451. C *****
452. C
453.      L = 1 HYRG0040
454.      N = NP
455.      DO 20 I = 1, N HYRG0080
456.      IF ( T(I).LE.O.O ) XCAST(I)=O.O

```

```

457.      IF ( VOLCH(I).EQ.O.O) GOTO 15
458.      EDSD(I) = T(I) / VOLCH(I)
459.      XCAST(I) = T(I)
460.      YRSDS(I) = EDSD(I)
461.      GOTO 20
462. 15    EDSD(I) = O.O
463.      YRSDS(I) = O.O
464. 20    CONTINUE
465.      K = 1
466.      MM = 1
467. 30    CALL SUM(N, XCAST, K, 1, SMX)
468.      CALL SUM(N, XCAST, K, 2, SM2X)
469.      CALL SUM(N, YRSDS, K, 1, SMY)
470.      CALL SUMXY(N, XCAST, YRSDS, K, SMXY)
471.      Q = N - K + 1
472.      D = (Q * SM2X) - (SMX * SMX)
473.      AN = (SMY * SM2X) - (SMX * SMXY)
474.      BN = (Q * SMXY) - (SMY * SMX)
475.      A = AN / D
476.      B = BN / D
477.      G = 1.O / A
478.      US = 1.O / B
479.      WRITE (6,120)
480.      WRITE (6,150)
481.      WRITE (6,160)
482.      WRITE (6,170)
483.      DO 70 I = 1, N
484.      TSD(I) = ((G * ( T(I))) / (1.O + (B * G * T(I))))
485. 70    CONTINUE
486.      DO 80 I = 1, N
487.      WRITE (6,180) T(I), VOLCH(I), TSD(I)
488. 80    CONTINUE
489.      WRITE (6,190) A
490.      WRITE (6,200) B
491.      WRITE (6,210) G
492.      ULTS = 1.O / B
493.      WRITE (6,220) ULTS
494.      DO 81 I = 2, N
495.      K = I - 1
496.      TT(K) = T(I) - T(K)
497.      TTSD(K) = TSD(I) - TSD(K)
498.      CSR(K) = TTSD(K)/TT(K)
499. 81    CONTINUE
500.      RETURN
501. 120   FORMAT ( / )
502. 150   FORMAT ('1',T40, 'TIME', T53, 'VOL.CHANGE', T68, 'VOL.CHANGE')
503. 160   FORMAT (T38, '(OBSERVED)', T53, '(OBSERVED)', T68, '(HYP.REGN)')
504. 170   FORMAT (T41, 'MIN',T57, '(%)', T72, '(%)', / / )
505. 180   FORMAT ('O', 30X, F15.2, 2F15.4)
506. 190   FORMAT ( / / / /, 45X, 'INTERCEPT A(=1/GD)=' , F10.5, / / )
507. 200   FORMAT (45X, 'SLOPE B=' , F8.5, / / )
508. 210   FORMAT (45X, 'PARAMETER GD=' , F15.3, / / )
509. 220   FORMAT (45X, 'ULTIMATE VOL.CHANGE=' ,F10.4, / / )
510.      END
511.      SUBROUTINE SUM(N, X, J, L, SM)
512.      DIMENSION X(100)
513.      SM = O.O
514.      DO 10 I = J, N
515.      SM = SM + X(I) ** L
516. 10    CONTINUE
517.      RETURN
518.      END
519.      SUBROUTINE SUMXY(N, X, Y, J, SXY)
520.      DIMENSION X(100), Y(100)

```

```

HYRGO090
HYRGO100
HYRGO110

HYRGO120
HYRGO130
HYRGO140
HYRGO170
HYRGO180
HYRGO190
HYRGO200
HYRGO210
HYRGO220
HYRGO230
HYRGO240
HYRGO250
HYRGO260
HYRGO270
HYRGO280
HYRGO440
HYRGO470
HYRGO480
HYRGO490
HYRGO500
HYRGO510
HYRGO520
HYRGO530
HYRGO540
HYRGO550
HYRGO560
HYRGO570
HYRGO580
HYRGO590
HYRGO600

HYRGO670
HYRGO710
HYRGO720
HYRGO730
HYRGO740
HYRGO750
HYRGO760
HYRGO770
HYRGO780
HYRGO790
HYRGO800
HYRGO810
HYRGO820
HYRGO830
HYRGO840
HYRGO850
HYRGO860
HYRGO870
HYRGO880
HYRGO890

```

```

521.      SXY = 0.0
522.      DO 10 I = J, N
523.      SXY = SXY + (X(I) * Y(I))
524. 10   CONTINUE
525.      RETURN
526.      END
527.      SUBROUTINE DRAW1( X, Y, XSCA, YSCA, JJ )
528.      COMMON / CNTRL/ NP,COR1,INI1,XX2,YY2,NUMT,NUMD ,NPT
529.      DIMENSION X(NUMD),Y(NUMD)
530. C
531. C THE PROGRAM IS TO PLOT THE DATA BY USING THE SUBROUTINE
532. C FLINE OR SMOOT OR ANY SELECTED PROGRAM.
533. C SEE CALCOMP PLOTTING MANUAL
534. C
535.      X(NUMT+1) = 0.0
536.      X(NUMT+2) = XSCA
537.      Y(NUMT+1) = 0.0
538.      Y(NUMT+2) = YSCA
539.      PRINT*,NUMT,NUMD
540.      J = JJ + 1
541.      CALL FLINE( X, Y,NUMT, 1, 0, J )
542. C   CALL SMOOT(0.0,0.0,0.0)
543.      RETURN
544.      END
545.      SUBROUTINE DRAW2 ( X , Y, XSCA, YSCA, JJ )
546.      COMMON / CNTRL/ NP,COR1,INI1,XX2,YY2,NUMT,NUMD ,NPT
547.      DIMENSION X(NUMD),Y(NUMD)
548.      J = 1
549.      X(NUMT+1) = 0.0
550.      X(NUMT+2) = XSCA
551.      Y(NUMT+1) = 0.0
552.      Y(NUMT+2) = YSCA
553.      CALL FLINE( X , Y , NUMT , 1 , 0 , J )
554.      RETURN
555.      END
556.      SUBROUTINE DRAW3( X, Y, XSCA, YSCA, J )
557.      COMMON / CNTRL/ NP,COR1,INI1,XX2,YY2,NUMT,NUMD ,NPT
558.      DIMENSION X(NPT),Y(NPT)
559. C
560. C THE PROGRAM IS TO PLOT THE DATA BY USING THE SUBROUTINE
561. C FLINE OR SMOOT OR ANY SELECTED PROGRAM.
562. C SEE CALCOMP PLOTTING MANUAL
563. C
564.      X(NP+1) = 0.0
565.      X(NP+2) = XSCA
566.      Y(NP+1) = 0.0
567.      Y(NP+2) = YSCA
568.      J = J + 1
569.      CALL FLINE( X, Y, NP, 1, -1, J )
570. C   CALL SMOOT(0.0,0.0,0.0)
571.      RETURN
572.      END
573.      SUBROUTINE DRAW4 ( X , Y, XSCA, YSCA, J )
574.      COMMON / CNTRL/ NP,COR1,INI1,XX2,YY2,NUMT,NUMD ,NPT
575.      DIMENSION X(NPT),Y(NPT)
576.      X(NP+1) = 0.0
577.      X(NP+2) = XSCA
578.      Y(NP+1) = 0.0
579.      Y(NP+2) = YSCA
580.      CALL FLINE( X , Y , NP , 1 , 0 , J )
581.      RETURN
582.      END

```

```

HYRG0900
HYRG0910
HYRG0920
HYRG0930
HYRG0940
HYRG0950

```

Example

```
1. //GEOPLOT JOB ', , , T=2M, R=256, L=15, I=25, C=0', 'ED YONG'  
2. /*D800 VPLOT  
3. // EXEC FORTHCLG, USERLIB='SYS3.VPLOTLIB'  
5. //FORT.SYSIN DD *
```

PROGRAMME

```
1. //GO.FT01F001 DD DSN=&&FT01F001, UNIT=SYSDA, DISP=(NEW, PASS),  
2. // SPACE=(CYL, (2, 2))  
3. //GO.VWORK DD DSN=&&VWORK, UNIT=SYSDA, DISP=(NEW, PASS),  
4. // SPACE=(CYL, (2, 2))  
5. //GO.SYSIN DD *  
1. 2  
2. 0  
3. A0210-1  
4. 1  
5. 48  
6. 10  
7. 0.0008183  
8. 42872  
9. 0 0.5 3 3.5 4 4.5 5 6 7 8 9 10 11 12 13 14 15  
10. 16 17 19 20 24 29 36 42 98 116 136 169 179 244 264  
11. 334 346 388 424 486 556 586 616 1236 1396 1348 1386  
12. 1463 1623 1688 1786  
13. 42872 44069 42572 42104 41905 41840 41767 41760 41614 41596  
14. 41534 41482 41333 41326 41306 41297 41187 41125 41122 41109  
15. 41078 40906 40900 40700 40654 40168 40166 40155 40160  
16. 40160 40025 40023 39790 39789 39789 39788 39705  
17. 39701 39700 39700 39502 39504 39506 39508 39508 39506  
18. 39509 39504  
19. 6.3477  
20. 0  
21. A0205-1  
22. 1  
23. 24  
24. 10  
25. 0.0008183  
26. 35798  
27. 0 3 18 23 28 38 48 113 188 293 323 533 618 1083  
28. 1243 1353 1498 1593 1713 1863 1998 2123 2638 2793  
29. 35798 35630 35243  
30. 35240 35236 35059 34958 34655 34276 33886 33793 33474 33366  
31. 33123 33123 33123 32954 32947 32948 32948 32840 32837 32823  
32. 32825  
33. 6.2699  
34. /*  
35. // EXEC VPLOT  
36. /*
```

APPENDIX VI

PROGRAMME LISTING FOR LINEAR REGRESSION ANALYSIS

APPENDIX VI

DATA INPUT FOR LINEAR REGRESSION ANALYSIS PROGRAMME

PREPARATION OF INPUT INFORMATION

All data are using free format input. Input should be presented in the order shown below as integer or real. Data present on one card should be separated by a space. Data punch on one card should always be within 80 columns.

The order of input information is as follows :

	Format
1. Number of data set (NSET)	Integer
2. Test number (TEST)	Real
3. Number of data points (N)	Integer
4. Option for linear regression (OPT)	Real
0 -- For ordinary linear regression	
1 -- For line pass through origin	
5. Observed data (OBX) and (OBY)	Real
(Input x and y) (Maximum 150)	

OUTPUT INFORMATION

The program will print out the following informations :

1. Number of data set .
2. Test number .
3. Number of data points .
4. Option of regression .

5. Data of observed (OBX) and (OBY), regressed (Y) and DIFF

Note: $DIFF = (OBY - \text{regressed } (Y))$

6. The intercept on y-axis.

7. Error number.

Note: Error no. = error / sum of y.

error = sum of DIFF

The operational procedures and plotting procedures are the same as given in the Appendix V.

```

10.      DIMENSION OBX(150),OBY(150),RGY(150),DIFF(150),B(2),IBUF(4000)
20.      COMMON / CNTRL / NP ,NPT
30. C
40. C   NSET = NO. OF DATA SET
50. C   TEST = TEST NO.
60. C     N = NO. OF POINTS
70. C   OPT = OPTION FOR REGRESSION ANALYSIS
80. C   OPT = 0   FOR ORDINARY LINEAR REGRESSION
90. C     = 1   FOR LINE PASSING THRU ORIGIN
100. C
110.      READ*,NSET
120.      WRITE (6,130) NSET
130.      L = 1
140. 10  READ*,TEST,N,OPT
150.      WRITE (6,140) TEST
160.      WRITE (6,141) N
170.      WRITE (6,142) OPT
180.      READ*,(OBX(I),OBY(I),I = 1,N )
190.      WRITE (6,150)
200.      WRITE (6,160)
210.      WRITE (6,170)
220.      XSUM = 0.0
230.      DO 20 I = 1,N
240.        XSUM = XSUM + OBX(I)
250. 20  CONTINUE
260.      YSUM = 0.0
270.      DO 30 I = 1,N
280.        YSUM = YSUM + OBY(I)
290. 30  CONTINUE
300.      XSQS = 0.0
310.      DO 40 I = 1,N
320.        XSQS = ( XSQS + ((OBX(I)**2)))
330. 40  CONTINUE
340.      XYSUM = 0.0
350.      DO 50 I = 1,N
360.        XYSUM = ( XYSUM + ((OBX(I) * OBY(I))))
370. 50  CONTINUE
380.      IF (OPT-1) 60,70,70
390. 60  X = N
400.      DEN = (( X * XSQS ) - ( XSUM**2))
410.      AN = (( YSUM * XSQS) - ( XYSUM * XSUM))
420.      BN = (( X * XYSUM ) - ( XSUM * YSUM ))
430.      A = AN / DEN
440.      BB = BN / DEN
450.      GOTO 80
460. 70  A = 0.0
470.      BB = XYSUM / XSQS
480. 80  ERROR = 0.0
490.      YYSUM = 0.0
500.      DO 90 I = 1,N
510.        RGY(I) = ( OBY(I) * BB ) + A
520.        DIFF(I) = ( OBY(I) - RGY(I) )
530.        ERROR = ERROR + ABS(DIFF(I))
540.        YYSUM = YYSUM + OBY(I)
550. 90  CONTINUE
560.      ERNOM = ERROR / YYSUM
570.      DO 100 I = 1,N
580.        WRITE (6,180) OBX(I), OBY(I), RGY(I), DIFF(I)
590. 100 CONTINUE
600.      WRITE (6,190) A, BB
610.      WRITE (6,200) ERROR, ERNOM
620.      NP = N
630.      NPT = NP + 2
640.      CALL PLOTS(IBUF,4000)

```

```

650.      CALL PLOT(1.0,1.0,-3)
660.      CALL FACTOR(1.0)
670.      XSCA = 4.0
680.      XLEN = 8.0
690.      YSCA = 0.6
700.      YLEN = 8
710.      B(1) = 0.0
720.      B(2) = XSCA
730.      CALL AXIS(0.0,0.0,20HVOLUME ( CC. )      .,-20,XLEN,0.0,B(1),B(2))
740.      B(1) = 0.0
750.      B(2) = YSCA
760.      CALL AXIS(0.0,0.0,18HVOLTMETRE (VOLTS),18,YLEN,90.,B(1),B(2))
770.      YSY = YLEN - 1
780.      CALL SYMBOL(1.5,YSY,0.14,38HLINEAR REGRESSION CURVE AT -15,      KP
781.      &,0.0,23)
790.      CALL DRAW1( OBX,OBY,XSCA,YSCA )
800.      CALL DRAW2( OBX,RGY,XSCA,YSCA )
810. C      NXSP = XLEN * 4
820. C      NYSP = YLEN * 4
830. C      CALL GRID(0.0,0.0,0.25,0.25,NXSP,NYSP)
840.      CALL PLOT(0.0,0.0,999)
850.      L = L + 1
860.      IF ( L.LE.NSET ) GOTO 10
870.      CALL PLOT(0.0,0.0,9999)
880.      STOP
890. 130  FORMAT('1',5X,25HNUMBER OF DATA SET      =,15, / )
900. 140  FORMAT(5X,25HTEST SAMPLE NO.      =,F8.5, / )
910. 141  FORMAT(5X,25HNUMBER OF POINTS      =,15, / )
920. 142  FORMAT(5X,25HOPTION FOR PLOTTING      =,F5.0, / )
930. 150  FORMAT( T31,'VALUES',T46,'VALUES',T61,'VALUES',T76,'DIFF')
940. 160  FORMAT( T31,'OF X',T46,'OF Y',T61,'OF Y')
950. 170  FORMAT( T59,'REGRESSION', / / )
960. 180  FORMAT( 20X, 4F15.3, / )
970. 190  FORMAT( / / ,20X,'INTERCEPT =' ,T41,F14.3,T59,'SLOPE',T67,F14.3, / )
980. 200  FORMAT(20X,'SUM OF ERROR =' ,T41,F14.3,T59,'ERROR NORM =' ,
990.      &T67,F14.3, / )
1000. 210  FORMAT(1H1, / / / / / / )
1010.      END
1020.      SUBROUTINE DRAW1( X,Y,XSCA,YSCA )
1030.      COMMON / CNTRL / NP , NPT
1040.      DIMENSION X(NPT),Y(NPT)
1050.      X(NP+1) = 0.0
1060.      X(NP+2) = XSCA
1070.      Y(NP+1) = 0.0
1080.      Y(NP+2) = YSCA
1090.      CALL FLINE( X,Y,NP,1,-1,2 )
1100.      RETURN
1110.      END
1120.      SUBROUTINE DRAW2(X,Y,XSCA,YSCA)
1130.      COMMON / CNTRL/ NP, NPT
1140.      DIMENSION X(NPT),Y(NPT)
1150.      X(NP+1) = 0.0
1160.      X(NP+2) = XSCA
1170.      Y(NP+1) = 0.0
1180.      Y(NP+2) = YSCA
1190.      CALL FLINE( X, Y, NP, 1, 0, 3 )
1200.      RETURN
1210.      END

```

Example

```
1. //GEO PLOT JOB ' , , , T=2M,R=512K,L=5,I=20,C=0' , 'ED YONG'  
2. // MSGLEVEL=(1,1)  
3. //*D800 VPLOT  
4. // EXEC FORTHCLG,USERLIB='SYS3.VPLOTLIB',SIZE=512K  
5. //FORT.SYSIN DD *
```

PROGRAMME

```
1. //GO.FT01F001 DD DSN=&&FT01F001,UNIT=SYSDA,DISP=(NEW,PASS),  
2. // SPACE=(CYL,(2,2))  
3. //GO.VWORK DD DSN=&&VWORK,UNIT=SYSDA,DISP=(NEW,PASS),  
4. // SPACE=(CYL,(2,2))  
5. //GO.SYSIN DD *  
1. 1  
2. 15 40 0  
3. 0.0 0.0027 0.635 0.1241 1.270 0.2450 1.905 0.3663  
4. 2.540 0.4877 3.175 0.6089 3.810 0.7309 4.445 0.8527  
5. 5.080 0.9756 5.715 1.0987 6.350 1.2226 6.895 1.3469  
6. 7.620 1.4717 8.255 1.5967 8.890 1.7223 9.525 1.8474  
7. 10.160 1.9736 10.795 2.0998 11.430 2.2262 12.065 2.3528  
8. 12.700 2.4799 13.335 2.6076 13.970 2.7359 14.605 2.8646  
9. 15.240 2.9942 15.875 3.1243 16.510 3.2547 17.145 3.3852  
10. 17.180 3.5168 18.415 3.6482 19.050 3.7800 19.685 3.9125  
11. 20.320 4.0460 20.955 4.1801 21.590 4.3146 22.225 4.4496  
12. 22.860 4.5853 23.495 4.7208 24.130 4.8565 24.765 4.9919  
13. /*  
14. // EXEC VPLOT  
15. /*
```